Drug sensitivity and drug resistance in *Trypanosoma brucei* and *Leishmania*: the aquaporins

Ali Hassan S Alghamdi

Institute of Infection, Immunity and Inflammation

College of Medical, Veterinary and Life Sciences

This thesis is submitted in fulfilment of the requirements for the

Degree of Doctor of Philosophy

Institute of Infection, Immunity and Inflammation of the

School of Life Sciences

University of Glasgow

October 2020

Abstract

Neglected parasitic diseases (NPD) include some of the worst human infections and are caused by pathogens including *T. brucei* (human African trypanosomiasis or sleeping sickness), *T. cruzi* (American trypanosomiasis or Chagas disease), *Leishmania spp* (leishmaniasis), which cause large disease burdens, as well as high mortality and morbidity rates in afflicted countries. In the absence of effective vaccines against any trypanosomatid diseases, chemotherapy is the main mechanism to combat them. Many anti-protozoal drugs are inherently cytotoxic but derive their selectivity from preferential uptake by the pathogen rather than by the host. Conversely, loss of the specific drug transporters is a main cause of drug resistance. Identification of parasite-specific targets and uptake mechanisms is critical for the development of new therapeutic agents. In this project, the aim of the research is to understand the roles of kinetoplastid aquaporins (AQPs) in trypanosomatid parasites with respect to drug resistance and transport.

The observed cross-resistance between melarsoprol and pentamidine (MPXR) of the parasite threatens the status of the latter as a viable drug. There is clear consensus that a membrane transporter protein, *T. brucei* aquaglyceroporin-2 (TbAQP2), is implicated in the uptake of both drugs and therefore appears a likely basis for MPXR emergence. What has remained, unclear is weather the TbAQP2 protein is acting as transmembrane transporter, while situated in the *T. brucei* flagellar pocket, with pentamidine being a permeant, or if the protein simply acts as a receptor for pentamidine to then be internalised together via receptor-mediated endocytosis or the natural turnover of TbAQP2.

Investigations on TbAQP2 were conducted to determine how the structure of TbAQP2 allows it to transport pentamidine. In *T. brucei*, AQP2 and AQP3 are closely related, but AQP2 has unusual selectivity filter amino acids residues in and around the pore (NSA/NPS/IVLL), compared to the latter (NPA/NPA/WGYR) in AQP3, and it also lacks the “aromatic/arginine (a/R)” motif. Using site-directed mutagenesis approaches, the TbAQP2 and TbAQP3 selectivity filter residues were therefore swapped with the goal of determining the effects of each amino acid on the uptake of drugs by *Trypanosoma brucei*. The results showed that the selectivity filter differences

between TbAQP2 and TbAQP3 are largely responsible for their differences in pentamidine sensitivity and transport rates. Moreover, the TbAQP2 pore width was constricted using amino acids of different sizes, in order to test whether size restrictions at the cytoplasmic end of TbAQP2, *i.e.* below the selectivity filter, would impact on pentamidine transport. Through a combination of drug sensitivity determinations and uptake assays, the results of the introduction of different-sized amino acids at selected positions showed that it is likely that the effect depended on the residue size at the cytoplasmic end of the TbAQP2 pore. In addition, the potential correlation between the *T. brucei* endocytosis rate and the rate of pentamidine uptake was investigated in order to distinguish between pentamidine uptake by transporters and via endocytosis. The combined evidence of the observed results strongly suggests that pentamidine is not taken up by endocytosis, and does not induce endocytosis of TbAQP2. To conclude, the obtained results highlight a clear, direct role for the TbAQP2 membrane transporter in pentamidine uptake, with the drug most likely traversing the protein's channel to enter the cell.

The *Leishmania major* AQP1 was also investigated for the uptake of heavy metals antimony and arsenic. For this aim, *Lm*AQP1 was cloned and expressed into the *Tb*AQP1-3 null and *Lm*AQP1 null cell lines, which were then tested for changes in sensitivity to antimony and arsenic. The results show that LmAQP1 is able to sensitise cells to heavy metals. These findings could help to confirm and advance the understanding of a role of *Leishmania* AQP1 in the sensitivity and resistance to first-line antimonial drugs such as Glucantime and Pentostam.

Table of Contents

List of figures

List of tables

Publications and presentations

Publications:

Jane C. Munday, Stefan Kunz, Titilola D. Kalejaiye, Marco Siderius2, Susanne Schroeder, Daniel Paape, **Ali, H. Alghamdi.**, Zainab Abbasi, Sheng Xiang Huang, Anne-Marie Donachie, Samia William, Abdel Nasser Sabra, Geert Jan Sterk, Sanaa S. Botros, David G. Brown, Charles S. Hoffman, Rob Leurs, Harry P. de Koning. (2020) Cloning and functional complementation of ten *Schistosoma mansoni* phosphodiesterases expressed in the mammalian host stages. *PLOS Neglected Tropical Diseases*.

Alghamdi, A. H., Munday, J. C., Campagnaro, G. D., Gurvic, D., Svensson, F., Okpara, C. E., Kumar, A., Quintana, J., Martin Abril, M. E., Milić, P., Watson, L., Paape, D., Settimo, L., Dimitriou, A., Wielinska, J., Smart, G., Anderson, L. F., Woodley, C. M., Kelly, S., Ibrahim, H. M. S., Hulpia, F., Al-Salabi, M. I., Eze, A. A., Sprenger, T., Teka, I. A., Gudin, S., Weyand, S., Field, M., Dardonville, C., Tidwell, R. R., Carrington, P. O., Boykin, D. W., Zachariae, U. & De Koning, H. P. (2020). Positively selected modifications in the pore of TbAQP2 allow pentamidine to enter *Trypanosoma brucei*. *eLife*, *9*, e56416.

Presentations:

Alghamdi, A. H., Fredrik Svensson & De Koning, H. P (2017) Introduction of a large amino acid (tryptophan) at the cytoplasmic end of the AQP2 pore displayed reduced sensitivity to pentamidine (and melarsoprol) uptake (**Poster presentation**), British Society for Parasitology (BSP) spring meeting, University of Dundee. 3rd-5th April 2017.

Alghamdi, A. H., & De Koning, H. P (2018) Site-directed mutagenesis of specific amino acid residues supports the model of conductance of pentamidine through the TbAQP2 channel (**Poster presentation**), SULSA Antimicrobial Resistance Conference, Technology and Innovation Centre, Glasgow. 26th-27th April 2018.

Alghamdi, A. H. & De Koning, H. P. (2019) Site-directed mutagenesis of specific amino acid residues supports the model of conductance of pentamidine through the TbAQP2 channel (**Oral presentation**), Research Update Meeting (RUM), the University of Glasgow, 15th March 2019.

Alghamdi, A. H. & De Koning, H. P. (2019) Mutagenesis of leucine residues at the cytoplasmic end of the TbAQP2 pore affects the protein's ability to transport pentamidine. (**Poster presentation**), British Society for Parasitology (BSP) spring meeting, the University of Manchester, 15th-17th April 2019.

Acknowledgement

Praise be to Allah, the Almighty, for His blessings and for giving me the strength and courage to complete this thesis. His continuous grace and mercy was with me throughout my life particularly during the tenure of my research.

I would like to express my deep and sincere gratitude to my research supervisor Prof. Harry De Koning for the continual support throughout my PhD study and related research, for his patience, motivation and assistance in writing up this thesis. Without his help and intellect, completion of this thesis would not have been possible. Admittedly, I would not have imagined having a better supervisor and mentor for my PhD study.

I would, also, like to express my deepest and sincere sense of gratitude to Prof. Mohamed E. Wagih for his invaluable advice, guidance and care throughout this research. I am indebted to him for enlightening me the first glance of research and thereafter. He, indeed, gave me the confidence to dream big. I am extremely grateful for all what he has offered me.

I am very grateful to my cosupervisor, Prof. Julian Dow, and my assessors, Prof. Matthias Marti and Prof. Michael Barrett, for their insightful comments and encouragement and not to mention, the hard questions which incanted me to widen my research from various perspectives.

My sincere thanks also go to the members of the Harry de Koning group including Khalid, Ibrahim, Manal, Amani, Lola, Marzuq, Tahani, Maha, Hamzah and Mustafa for their support, advice and, the stimulating discussions and the time we have had together in the last few years. To Aidan, Anna, Inês, Annemiek, my students during my PhD work, thank you for all the help they offered. I am extending my thanks to all the level-5 and level-6 people at the Institute of Infection, Immunity and Inflammation, for all the help and support they offered me. Without their supportive help it would not have been possible to conduct this research. I am deeply grateful to Dr. Jane Munday for her kind help, great contribution and not to mention giving me the opportunity to follow up her research. Big thanks are also due to Dr. Daniel Paape who helped me greatly at the beginning of this project.

Most importantly, this journey would not have been possible without the support I received from my family. My sincere thanks from the bottom of my heart go to my dear mother for her love, prayers caring, support and sacrifices throughout my life. I am so blessed to have a great mum like her in my life. I would, also, like to express my undying gratitude to my lovely wife, Abrar, and my daughter, Sama, for their love, patience, prayers, and support while living in the UK. I am very lucky and so happy to have both of you in my life. Very special thanks also go to my brothers and sisters for their love, prayers, support and encouragement throughout my life in general and my studies, in particular. My family members know how they mean to me and words alone cannot express my appreciation of them all. I am so proud and happy to have them as my family.

Last but not the least, I would like to thank the sponsor, Albaha University, for giving me the opportunity to pursue my PhD study in UK.

Dedication

This work is dedicated to the loving memory of my late Father, Hassan Aifan, may Allah have mercy on him. He was very proud of my achievements, and this would have pleased him, beyond measure.

I equally dedicate my work to my great mother, Azah Ali Gerboa, whose support, encouragement and unending love were instrumental in getting this research work completed.

Author's Declaration

I declare that this thesis and the results presented here are my own work, except where otherwise stated and acknowledged. This work contains no material submitted to obtain any other degree at any institution or University.

Ali Hassan Alghamdi

Definitions/Abbreviations

°C	degree celsius
AAT	African Animal trypanosomiasis
ABC	ATP-binding cassette
BBB	blood-brain barrier
bp	Base pairs
BSF	Bloodstream form
CCCP	Carbonyl cyanide m-chlorophenyl hydrazone
CNS	central nervous system
dH_2O	distilled water
DRC	Democratic Republic of Congo
E. coli	*Escherichia coli*
EC_{50}	50% effective concentration
FBS	Foetal bovine serum
g	Gravity force
gDNA	Genomic DNA
h	Hour
HAPT1	High Affinity Pentamidine Transporter
HAT	Human African Trypanosomiasis
HMI-9	Hirumi's medium 9
IC_{50}	50% inhibitory concentration
ISG75	Surface Molecule Invariant Surface Glycoprotein 75
Kb	Kilobase
Km	Michaelis-Menten constant
KO	Double Knockout

L	Litre
LAPT1	Low Affinity Pentamidine Transporter
LB	Luria broth
LDL	Low-Density Lipoprotein
*Lm*AQP1	*Leishmania major* aquaporin-1 gene
LS	Long slender
M	Molar concentration
MDR1	Multi-drug resistant transporter 1
MFST	Major Facilitator Superfamily Transporter
mg	Milligram
min	Minute
ml	Millilitre
mM	Millimolar
MMP	Membrane potential
MPXR	Melarsoprol and pentamidine cross resistance
mRNA	Messenger-ribonucleic acid
MRPA	Multidrug resistance protein A
NECT	Nifurtimox-Eflornithine Combination Therapy
ng	Nanogram
nM	Nanomolar
NPDs	Neglected Parasitic Diseases
NTDs	Neglected Tropical Diseases
ORF	Open reading frame
P2	Amino purine transporter
PAT	Potassium Antimony Tartrate

PBS	Phosphate-buffered saline
PCF	Procyclic form
PCF	Procyclic form
PCR	Polymerase chain reaction
PMF	proton-motive force
pmol	Picomol
PSG	Promastigote secretory gel
QRT-PCR	Quantitative Reverse Transcription PCR
RNA	Ribonucleic acid
RNAi	RNA interference
rpm	Revolutions per minute
s	Second
SBIII	Trivalent antimonials
SbV	Pentavalent antimonials
SDS	Sodium Dodecyl Sulphate
SEM	Standard error of mean
SNP	Single Nucleotide Polymorphism
SS	Short Stumpy
T. b. b	*Trypanosoma brucei brucei*
*Tb*427	*Trypanosoma brucei* strain 427
*Tb*AQP1	*Trypanosoma brucei* aquaporin-1gene
*Tb*AQP2	*Trypanosoma brucei* aquaporin-2 gene
*Tb*AQP3	*Trypanosoma brucei* aquaporin-3 gene
TbAT1	*Trypanosoma brucei* adenosine transporter
Tet	Tetracycline

TM	Trans-membrane
UTRs	Untranslated regions
UV	Ultraviolet light
Vmax	Maximal velocity
VSG	variant surface glycoprotein Vmax
WHO	World Health Organization
WT	Wild type
ΔG0	Gibbs free energy
µg	Microgram

Chapter 1 General introduction

1.1. Kinetoplastid parasites and disease

By definition, Kinetoplastids are a group of flagellated, unicellular, and motile protozoans whose specific characteristic is the presence of a kinetoplast. The kinetoplast is located in a single large mitochondrion, and is a term originally coined by Alexeieff in 1917 (Maslov et al., 2001). The Kinetoplastida belong to the larger group of phylum Euglenozoa, along with Diplomonads and Euglenids. Based on their morphological criteria, there is a division of Kinetoplastida into two major groups namely the biflagellate Bodonina and the uniflagellate Trypanosomatina (Dolezel et al., 2000).

Trypanosoma species cause Chagas disease and sleeping sickness while *Leishmania* species cause leishmaniasis are among the most common human diseases (Stuart et al., 2008). Substantial morbidity is the major outcome associated with these diseases, especially in the world's subtropical areas and amongst the poorest populations. These diseases, together with other bacterial, viral, and parasitic infections, are regarded to be NTDs (neglected tropical diseases) based on the consideration that there is inadequate donor funding tailored towards their control and are too often left untreated (Fidalgo & Gille., 2011).

1.2. African Trypanosomiasis

Human African Trypanosomiasis (HAT) and Animal African Trypanosomiasis (AAT), known more commonly as sleeping sickness and nagana, respectively, are vector-borne diseases which pose serious health problems to people and animals throughout sub-Saharan Africa (SSA) causing physical suffering, food security issues and large economic losses (Bacchi, 2009; Holt et al., 2016). HAT is the result of infection by subspecies of the protozoan parasite *Trypanosoma brucei*, but AAT can also be caused by other species such as *T. vivax*, *T. congolense*, *T. suis*, and *T. evansi* (Birhanu, 2015; Giordani et al., 2016). The parasite is spread by an insect vector, which in this case is the tsetse fly of the genus *Glossina* spp. (Kennedy, 2013).

1.2.1. Life cycle of *Trypanosoma brucei*

The complex life cycle of *T. brucei* (Figure 1.1) begins when the infected tsetse fly injects metacyclic trypomastigotes into a mammalian host skin and pass into the bloodstream during the fly blood meal. Within the bloodstream, *T. brucei* remains extracellular and enters a haemolymphatic stage, differentiating into a bloodstream long slender (LS) form that proliferates in both blood and lymph (Langousis & Hill, 2014). To evade detection in the bloodstream, the protozoan parasite uses antigenic variation through its dense variant surface glycoprotein (VSG) coat (Pinger et al, 2017). The coat has a stochastic switching expression pattern from a genomic repertoire of over 1000 VSG sequences, making a mounted host immune response difficult to achieve (Hutchinson et al, 2007). Early on in infection in mice, *T. brucei* has been shown to accumulate and replicate within adipose tissue, and evidence has revealed that parasites from within the adipose tissue are capable of infecting other naïve mice (Trindade et al., 2016). As the infection progresses, parasites in the blood breaches vessel walls, enabling access to extravascular tissue including the central nervous system (CNS) (Langousis & Hill, 2014). As the level of parasitaemia rises in the body, a quorum-sensing signal triggers non-reversible differentiation of LS forms, through a transition form, into non-dividing short stumpy (SS) forms of the parasite that are pre-adapted for survival inside a tsetse fly (Langousis & Hill, 2014; Seed & Wenck, 2003). It is thought the transition to non- dividing form is also a deliberate method of prolonging host survival until tsetse fly uptake by controlling parasitaemia in any given host (Seed & Wenck, 2003). Upon the next blood meal of a tsetse fly, SS and LS trypanosomes are taken up into the midgut of the tsetse fly. The role of the dermis and subcutis layers of the skin as a reservoir of vector-borne infection has often been overlooked. However, research from animal models has shown that sufficiently abundant populations of live, extravascular T. brucei residing in this organ play an important role in maximal parasite transmission (Capewell et al., 2016).

The new surrounding environment, with different pH, temperature and nutrient availability (Silvester et al, 2017) triggers changes in parasite gene expression and morphology leading to differentiation from the SS form to procyclic forms that proliferate in the tsetse fly midgut (Rico et al, 2013) whilst LS forms die out in the

midgut (Ooi & Bastin, 2013). Procyclic trypomastigote then migrate the length of the tsetse fly, first passing the proventriculus from where the procyclic trypomastigote asymmetrically divides, producing longer and shorter daughter cells. The latter is the epimastigote form of the trypanosome, which traverses to the salivary gland. On the other hand, the longer form appears to die shortly after being produced (Sharma et al., 2008). Upon arrival at the salivary gland, the epimastigote proliferates through two simultaneous cycles. The first involves symmetric division into daughter cells which bind to the gland epithelium and allows for the gland to be compromised for current and future infections. Meanwhile, the second form involves asymmetric division, giving rise to the infective metacyclic form of the parasite that is able to infect the host upon the next blood meal (Rotureau et al., 2012).

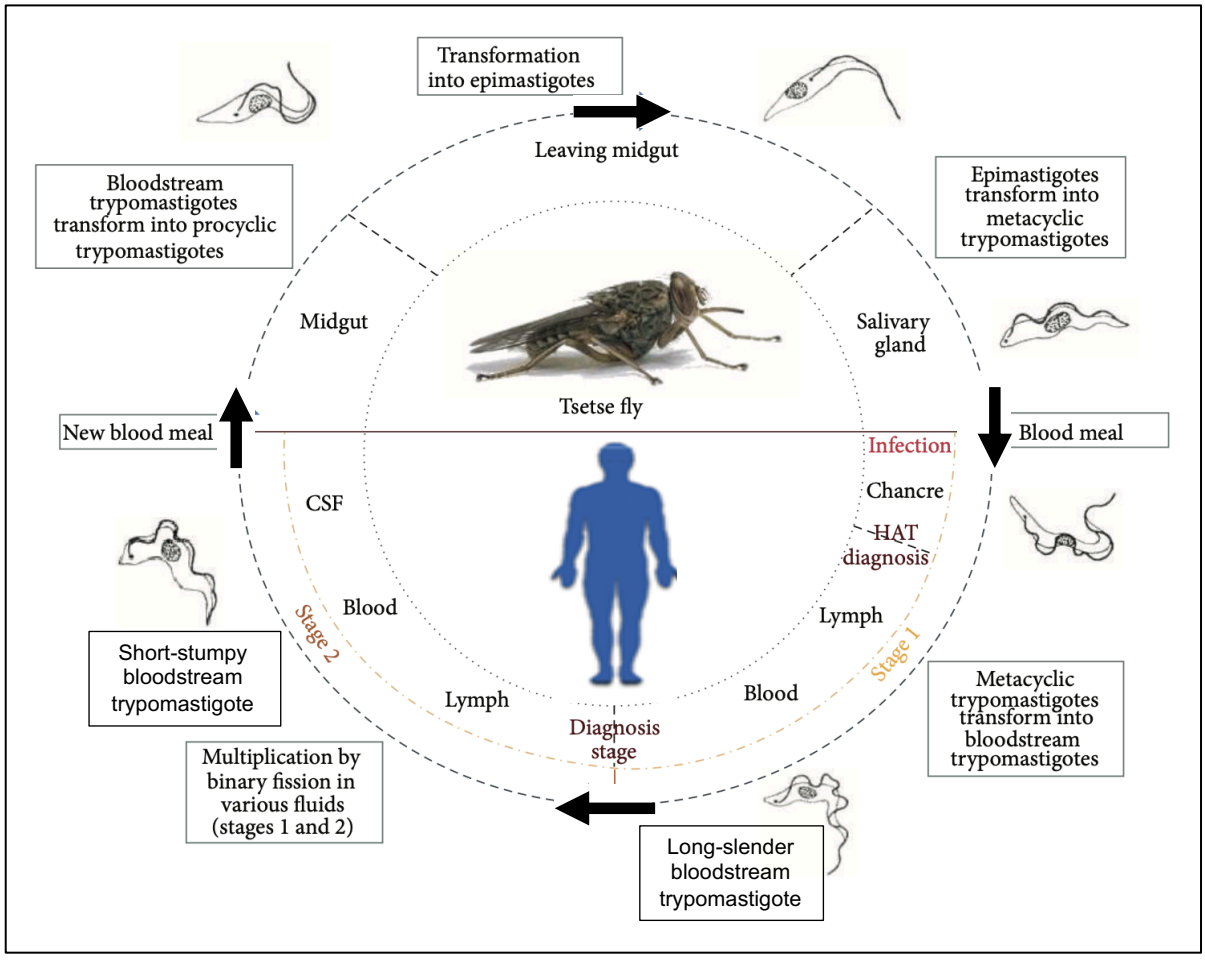

Figure 1.1: Life cycle of *Trypanosoma brucei*, the causative parasite of African trypanosomiasis. The figure highlights the important steps involved in the life cycle of the parasite in both tsetse fly and human stages. (Adapted from Bonnet et al., 2015)

1.2.2. Morphology of *Trypanosoma brucei*

The African trypanosome has two main morphologies: the trypomastigote and the epimastigote (Figure 1.2) which follow the same basic cellular architecture: a single copy set of organelles including a flagellum and flagellar pocket, a kinetoplast, a mitochondrion and a nucleus. Throughout the life cycle, the flagellar pocket is a crucial part of the cell as it remains the exclusive site for all endo- and exocytosis. Many of the cell organelle structures, including the kinetoplast, mitochondrion and nucleus, in all *T. brucei* cell forms appear to be skewed towards the posterior and central parts of the cell. (Matthews, 2005).

At the posterior of the cell body the kinetoplast and the nucleus are hallmark features of the trypomastigote form (Figure 1.2A). The flagellum allows LS trypomastigote to be motile in the mammalian blood and spread to other areas of the body, including the CNS (Matthews, 2005). However, as the parasite differentiates into a non-dividing SS form in the mammalian bloodstream, the flagellum length decreases, which is possibly a sign of pre-adaptation to the tsetse fly, giving preference to environmental sensory functions over motility, akin to the *Leishmania* amastigote whilst in macrophages (Gluenz et al., 2010). As procyclic forms establish in the vector midgut, and differentiate into longer mesocyclic forms, the flagellum once again becomes a useful feature for propelling and migrating cells across the midgut (Ooi & Bastin, 2013; Langousis & Hill, 2014). Reaching the proventriculus, the mesocyclic form undergoes significant cell nucleus repositioning in the process to become epimastigotes (Schuster et al., 2017).

The epimastigote morphology resembles cells with kinetoplasts that are anterior to the nucleus, effectively switching positions as it undergoes changes in cell length, width, as well as flagellar length (Ooi & Bastin, 2013). The asymmetric division by the proventricular epimastigote form, leading to both short and long forms, provides striking differences in all of these features (Figure 1.2B). However, this does not appear to be a hindrance, as it has thought the poorly motile short epimastigotes with short flagella are compensated by facilitated delivery to the SG by elongated

epimastigotes forms that are instead highly motile with long flagella (Van den Abbeele et al., 1999).

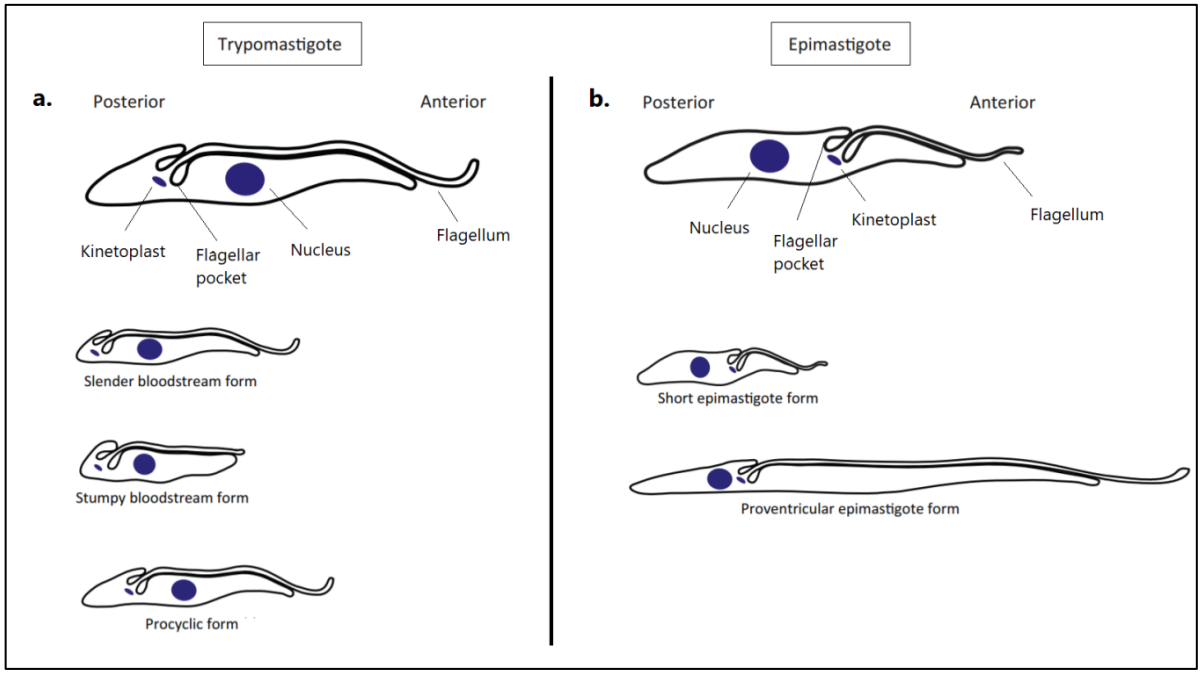

Figure 1.2: Trypomastigote and epimastigote morphologies of *Trypanosoma brucei*.
The figure shows the forms of the parasite that have the trypomastigote morphology, including the long slender bloodstream form, the short stumpy bloodstream form, the procyclic form and the mesocyclic form (mesocyclic is not shown in the legend) (a). The epimastigote forms that include the proventricular long epimastigote form and the short epimastigote form created as a result of asymmetric divison (b). Key cell organelles and structures, as well as relative subcellular locations within each form, are shown (adapted from Sunter & Gull, 2016, not drawn to scale).

1.2.3. Epidemiology of African trypanosomiasis

An encouraging decline has been observed in the numbers of new individuals contracting HAT over the last two decades, and in 2018, WHO reported only 977 cases of HAT (Franco et al., 2020). However, HAT mostly occurs in more rural areas of Africa where efforts towards disease detection and surveillance are poorer (Franco *et al*, 2014b) and interventions must be continued to combat the disease as just under 50 million people are estimated to remain at risk (Franco et al., 2020). The two subspecies of *T. brucei* that cause HAT, *Trypanosoma brucei gambiense* and *Trypanosoma brucei rhodesiense*, still remain active in spreading HAT in Africa but only occur in highly selective foci where the parasite, host, reservoir, and vector co-exist (Franco et al., 2014a).

T. b. gambiense causes a chronic form of the disease in both western and central Africa, with the worst affected countries including the Democratic Republic of Congo (DRC) and Guinea (Figure 1.3A; WHO, 2020d). Animal reservoirs play a minimal role in the transmission of *T. b. gambiense* HAT. Instead, hotspots of transmission via anthroponosis tend to be areas where there is humid forest, woodland, savannas and mangroves, or where these areas have been exploited by humans for agriculture such as coffee and cocoa plantations, as these are favourable habitations for tsetse fly vectors like *Glossina palpalis gambiensis* and *Glossina palpalis palpalis*. Here, proximate human-fly contact is at its greatest (Franco et al., 2014a). HAT control programmes like targeted screening of human populations for the infection have made a significant impact towards declining numbers of HAT cases in these regions of Africa. However, there are many rural areas that are hard to reach, leading to misrepresentation of numbers affected by the disease. This can be a result of regions in Africa with difficult terrain or with security threats that are more difficult to cover through programmes, resulting in less than 10% of the population being screened in endemic regions (Barrett et al., 2003; Franco et al., 2014a; Franco et al., 2014b; Steinmann et al., 2015).

On the other hand, HAT caused by the subspecies *T. b. rhodesiense* has an acute form of progression, and exclusively affects eastern and southern African countries like Malawi and Zambia (Figure 1.3B; WHO, 2020d). Notably, an overlap of *T. b. gambiense* infection in Uganda exists, making human co-infection possible (Figure 2.3) (Kennedy, 2013). *T. b. rhodesiense* disease is predominantly transmitted as a zoonosis and wildlife ranging from giraffes to impalas, as well as livestock such as cattle, play an important role as reservoirs that spread the parasite via vectors like *Glossina morsitans* that are found in East Africa. As a zoonosis, spread of the disease has proven more difficult to control, particularly as contact with domestic animals increases with human dependency on activities such as livestock husbandry (Franco et al., 2014a; Kennedy & Rodgers, 2019).

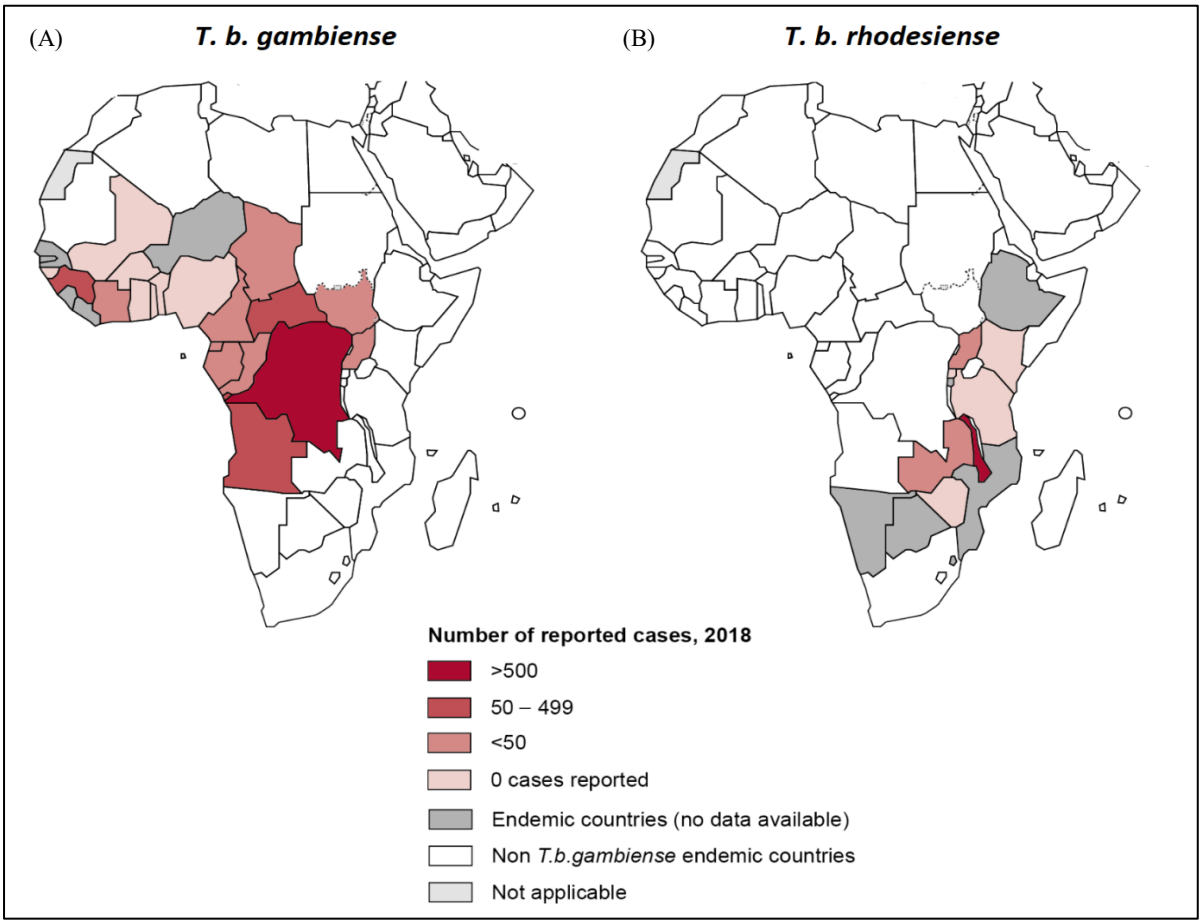

Figure 1.3: Map of Africa showing distribution of human African trypanosomiasis in 2018. (A) Countries in Africa coloured based on the number of reported cases of HAT caused by subspecies *T. b. gambiense*. Areas with most reported cases include the Democratic Republic of the Congo, Angola, the Central African Republic and Guinea (B) countries in the world coloured based on the number of reported cases of HAT caused by subspecies *T. b. rhodesiense*. Areas with most reported cases include Malawi, Zambia and Uganda (adapted from WHO, 2020d).

1.2.4. Clinical manifestations

The course of overall clinical manifestation of HAT that a patient may experience is dependent on the form of disease; exhibited by either *T. b. gambiense* or *T. b. rhodesiense* forms. Initial clinical manifestations in rhodesiense HAT involve a lesion (e.g. an ulcer) appearing at the site of the tsetse fly bite. As bloodstream forms of the parasite proliferate in the bloodstream, patients can experience headaches and enlarged lymph nodes, and on the skin, reddish rashes may begin to appear with both forms of the disease (Rodgers, 2009; MacLean et al., 2010). As previously mentioned, stages of the *T. brucei* life cycle in the host include a breach to the blood vessels into extravascular tissue including in organs such as the heart and liver,

and the effects of parasite invasion and proliferation manifest, including cardiovascular inflammation and fibrosis (Blum et al., 2007) as well as hepatomegaly (Kennedy & Rodgers, 2019). Even if the parasite has yet to cross the blood-brain barrier (BBB), neurological symptoms can appear in the earlier stages of the disease as well, though the underlying mechanisms for this warrant further research (Kennedy & Rodgers, 2019).

The later development of the disease, otherwise termed the encephalitic stage, concerns the disruption of a wide range of neural activities, caused as *T. brucei* progresses into the CNS after crossing the BBB. This can ultimately lead to meningoencephalitis (inflammation of the brain), as well as disruption to sensory processes (particularly visual features), as well as involuntary muscle twitching and seizures caused by irregular and disrupted nerve signalling (Bentivoglio et al., 1994). There are also characteristic sleeping disorders that give the disease the label 'sleeping sickness', which refers to daytime hypersomnia and night-time insomnia experienced by patients feeling continuously fatigued. Unless treated, or a rarer asymptomatic form of *T. b. gambiense* disease has occurred, patients with HAT almost always experience death from recurring symptoms (Kennedy & Rodgers, 2019).

Though these clinical presentations are common for both forms of HAT, important differences exist depending on the causative species of the disease. As previously mentioned, the *T. b. rhodesiense* form of HAT has an acute progression compared to the chronic *T. b. gambiense* form, and thus HAT duration in patients living in East and South Africa ranges typically from a few weeks to months whereas those *in T. b. gambiense* endemic areas have slow onset trypanosomiasis ranging from months to years. In the case of *T. b. rhodesiense* infection, shorter disease duration goes hand-in-hand with quicker progression to second-stage symptoms (Rodgers, 2009), though studies show geographical differences in clinical presentation here, such as less frequent presentations of *T. b. rhodesiense* second stage neuropathy in patients from Uganda compared to patients in Tanzania (Kuepfer et al., 2011).

1.2.5. Treatments available

A wide range of trypanocidal chemotherapy has been explored as early as the 19th century (Steverding, 2010). However, treatment options in the 21st century consist of only few approved drugs: suramin, pentamidine, eflornithine and nifurtimox-eflornithine combination therapy (NECT), melarsoprol, and fexinidazole. Clinical choice of treatment is dependent on the stage of HAT disease progression, and whether the disease takes the *rhodesiense* or *gambiense* form (Legros et al., 2002). However, despite the fatality of HAT, none of these options provide the ideal solution for HAT treatment, with either no means of oral administration, underlying toxic effects, low efficacy, a lack of knowledge on specific intracellular drug targets, as well as resistance to some of these existing drugs, particularly melarsoprol (Kennedy, 2013; de Koning, 2020).Treatment options reaching the end of the development pipeline are few and far between; until recent approval of fexinidazole in 2018 (Deeks, 2019) the last approved drug dates back to the 1970s. This reflects the real challenge faced with research and development for getting newer, more effective trialled therapies on the ground (Steverding, 2010).

1.2.5.1. Suramin

Suramin has been used as a first-line treatment for the haemolymphatic early stages of HAT caused by T. b. rhodesiense since the 1920s. It is administered intravenously, with five injections given to the patient every 3 to 7 days, usually over a 4 weeks treatment course (Barrett et al., 2007). The large size and negative charge of suramin prevents passive cell transport into the parasite (de Koning, 2020). Instead, the negative charge allows suramin to bind to the bloodstream trypanosomes glycolytic enzymes by means of electrostatic interactions, and in circulation almost all of the drug is bound to serum proteins (Barrett et al., 2007; Nok, 2003; Morgan et al., 2011). Multiple bodies of evidence have previously pointed towards the compound entering by a receptor-mediated endocytosis mechanism (Alsford et al., 2012; Pal et al., 2002), and it is more recently apparent that the major mediator in this process is the surface molecule invariant surface glycoprotein 75 (ISG75), as well as major facilitator superfamily transporter (MFST). In turn, there is a high selectivity and rapid accumulation of suramin in the cell (Zoltner et al., 2015). It is

thought that once inside the trypanosome cell, suramin can inhibit positively charged glycolytic enzymes, as well as interfere with cytokinesis of parasite cells. Suramin can also interfere with multiple metabolic pathways, including low-density lipoprotein (LDL) uptake and disruption of lysosomes (Nok, 2003; Thomas et al., 2018). A most recent study has shown that in addition to complex changes to metabolic pathways, a major collapse in cellular ATP levels found in suramin treated cells likely causes cell death (Zoltner et al., 2020).

Perhaps unique amongst HAT treatment options, suramin has shown very rare treatment failure when used for early stage *rhodesiense* HAT, and there are almost no reports of drug resistance from the field (Barrett et al., 2007). However, administration of suramin comes with the risk of a wealth of adverse effects in some patients. Neurotoxic effects have been observed even at lower concentrations of drug administration (Barrett et al., 2007), as well as side effects including renal failure, anaphylactic shock, fatigue and bone marrow toxicity (Barrett et al., 2007; Kennedy, 2013).

1.2.5.2. Pentamidine

Pentamidine is an aromatic diamidine used as an alternative for early-stage HAT treatment. Though it is more commonly used against *gambiense* infection, it can also be used as a second-line treatment for *rhodesiense* disease (Kennedy, 2013) as well as against antimonial-resistant *Leishmania* (Chakravarty & Sundar, 2010). Pentamidine is administered intramuscularly to affected HAT patients, typically with seven to ten injections at doses of 4 mg kg^{-1} given on a daily basis (Barrett et al., 2007; de Koning, 2020).

The drug enters parasite cells through multiple transport channels. Partial transport is achieved by the aminopurine transporter P2, often referred to as *Trypanosoma brucei* AT1 (*Tb*AT1), which has been evidenced by reduced pentamidine sensitivity after knockout of the encoding gene (*TbAT1*) (Matovu et al., 2003), as well as partial inhibition of pentamidine transport by adenine, a known substrate of *Tb*AT1 (Carter et al., 1995). The bulk of pentamidine transport is facilitated by the presence of two other channels, a High Affinity Pentamidine Transporter (HAPT1) and a Low Affinity Pentamidine Transporter (LAPT1), discovered in 2001. This has been further

supported by competitive inhibition work using radiolabelled [^{3}H]-pentamidine with increasing concentrations of unlabelled pentamidine substrate, causing significant biphasic uptake inhibition in *tbat1*-null mutants (de Koning, 2001; Matovu et al., 2003). The former channel, HAPT1, has since been identified as *Trypanosoma brucei* aquaglyceroporin 2 (*Tb*AQP2) located at the flagellar pockets of *T. brucei* cells (Munday et al., 2014).

Though the exact mode of action of the drug is yet to be fully elucidated, recent research suggests pentamidine involvement in loss of kinetoplast DNA in trypanosome cells, as well as disruption mitochondrial membrane transport gradients (Thomas et al., 2018).

The high potency for pentamidine in killing *T. brucei* cells has been demonstrated, with low nanomolar 50% effective growth-inhibitory concentration (EC_{50}) levels, matched only by the toxic melaminophenyl arsenical, melarsoprol (Baker et al., 2013). It has been established for some time now that intracellular concentrations of more than 1 mM pentamidine can be measured before parasite cell death (de Koning & Jarvis, 2001). However, like suramin, use of pentamidine can come with side-effects including abnormal glucose metabolism, as well as renal and GI disruption (Kennedy & Rodgers, 2019).

1.2.5.3. Eflornithine and NECT Therapies

Though both suramin and pentamidine have proven effective in the treatment of those affected by early-stage HAT, diagnosis of the disease is often too late, corresponding with when the parasite progresses into the later meningoencephalitic stages (Wastling & Welburn, 2011). Both suramin and pentamidine are ineffective at treating later stages of the disease, which is thought to be the result of difficulty in the drugs crossing the BBB to reach *T. brucei* cells. Even where possible, suramin and pentamidine either do not accumulate in sufficient quantities in the CNS or become trapped in capillary endothelia respectively, leading to little to no patient response against the developing infection (Sanderson et al., 2007; Sanderson et al., 2009).

Eflornithine is the one of the more recent registered and approved monotherapies for HAT, which being discovered back in the mid-1980s (De Koning, 2020). At the

start of the 2000s, eflornithine was most often used for the *gambiense* form of the disease, to treat later stages with a usual course comprising a dosage of 150 mg kg^{-1} of body weight (for adults) or 100 mg kg^{-1} body weight (for children) slow intravenous infusions for 6 hours for 2 weeks (Burri & Bun, 2003).

Eflornithine works by inhibiting ornithine decarboxylase, which plays a vital role in *T. brucei* polyamine synthesis and in turn, cell multiplication and differentiation (Priotto et al., 2007). Though initially developed for the treatment of cancers, the drug is thought to be particularly effective against *gambiense* infection as parasite versions of the enzyme are more stable and cannot gather polyamines from their external environment (De Koning, 2020). However, the short half-life of eflornithine makes administration difficult. Additionally, monotherapy treatment of eflornithine is often poorly tolerated, and causes toxicity in patients, for example in the bone marrow (Brun *et* al., 2010).

With a push for efforts to find efficacious and safer alternatives, *T. b. gambiense* infections are now preferably treated in patients using a nifurtimox-eflornithine combination therapy (NECT). This involves giving 400 mg kg^{-1} eflornithine intravenously on a 7 day course, combined with nifurtimox, an oral drug usually used in the treatment of American trypanosomiasis (Chagas' disease), at a dose of 15 mg kg^{-1} for 10 days (Priotto et al., 2009). Nifurtimox has the added benefit as a powerful oxidative agent against eflornithine-treated trypanosomes with a weakened oxidative stress defence because of the reduced synthesis of trypanothione (Babokhov et al., 2013).

NECT has shown a range of key benefits that has led to it replacing eflornithine monotherapy, as evidenced from initial trials in both Uganda (Checchi et al., 2007) and the DRC (Priotto et al., 2009): 4-fold fewer infusions required (and therefore shorter hospitalisation and costs), reduced bone marrow toxicity is experienced from lower eflornithine doses, and combinations can delay emergence of future trypanosome drug resistance (Priotto et al., 2007; Priotto et al., 2009). NECT appears to be as efficacious in *gambiense* treatment as eflornithine monotherapy, however both eflornithine and NECT are ineffective against the *rhodesiense* form of infection due to a higher ornithine decarboxylase turnover than in the *gambiense*

form (Burri & Brun, 2003; Babokhov et al., 2013; Kennedy, 2013), leaving a more dangerous HAT treatment as the only treatment option.

1.2.5.4. Melarsoprol

Melarsoprol is an organic melaminophenyl arsenical drug, introduced as a second-stage HAT treatment in the late 1940s due to its ability to penetrate the BBB. To this day, it remains first-line treatment for second-stage *T. b. rhodesiense* infection (Babokhov et al., 2013; De Koning, 2020), and although also effective for *gambiense* forms of the disease in Central and West African countries, the development of NECT therapy in 2009 provides a much safer and equally effective method of patients being treated in recent times, as explained above. The typical regime for affected patients currently involves the administration of melarsoprol intravenously to patients at 2.2 mg kg^{-1} every 24 hours for 10 days (Brun et al., 2010).

After penetrating the patient BBB and reaching trypanosomes, melarsoprol enters the trypanosome cell via more than one transport channel. By studying resistant strains of *T. brucei*, Carter and Fairlamb (1993) established one of these as the adenosine *Tb*AT1/P2 transporter, and clinical isolates and laboratory strain studies of the African trypanosome have demonstrated the additional importance of the *Tb*AQP2 transporter, exhibiting HAPT1 activity, in melarsoprol uptake and trypanosome susceptibility to the drug (Bridges et al., 2007; Baker et al., 2012; Graf et al., 2013). Hence, both *Tb*AT1/P2 and TbAQP2 play pivotal roles in both melarsoprol and pentamidine influx.

Once in the *T. brucei* cell, the specific mode of melarsoprol remains unclear. Cunningham et al. (1994) showed that a melarsoprol derivative formed from subsequent intracellular reactions can disrupt activity of the antioxidant enzyme trypanothione reductase, most likely leading to toxicity to the parasite (Fairlamb & Horn, 2018). However, specific pathways are yet to be established, as well as other mechanisms such as underlying causes behind cell lysis of trypanosome cells that are observed in treated patients (Fairlamb & Horn, 2018).

The current regime of melarsoprol treatment has proven particularly effective against *rhodesiense* forms of the disease, with cure rates as high as 96% one year after treatment in a study looking at *T. b. rhodesiense* foci in Tanzania and Uganda

(Kuepfer et al., 2012). Melarsoprol also has a high potency like pentamidine (i.e. low EC_{50}). However, there are a number of drawbacks to melarsoprol use. Most striking is that 5-10% of patients exhibit post-treatment reactive encephalopathy (PTRE), which is fatal for around half of them. PTRE in itself is thought to be caused by major cytokine recruitment to neural regions in response to rapid lysis of *T. brucei* cells from melarsoprol treatment (Kennedy & Rodgers, 2019; De Koning 2020). However, melarsoprol can also lead to other adverse effects, such as cardiotoxicity, peripheral neuropathy and mild to severe skin rashes in the patient (Kennedy & Rodgers, 2019).

1.2.5.5. Fexinidazole

A new treatment option for first-stage and second-stage *T. b. gambiense* infection recently received approval from the European Medicines Agency (Deeks, 2019). It is the first treatment to receive approval for use since the 1970s, having entered phase 1 clinical trials around a decade ago (Torreele et al., 2010). Fexinidazole appears to overcome two main obstacles of other current alternative treatments. Firstly, it is the first all-orally administered drug for gambiense HAT, making the treatment more widely available to remote and rural areas where gambiense HAT is prevalent (Deeks, 2019). Secondly, adverse effects from the drug are described as minimal (WHO, 2019).

Fexinidazole and its primary sulfoxide and sulfone metabolites are nitroimidazoles, which represent a group of compounds that bind DNA and inhibit nucleic acid and protein synthesis (Mital, 2009; Torreele et al., 2010). Effective treatment involves one dose administered orally each day over ten days (Lindner et al., 2020).

Though a 21st century success in relation to treatments against HAT, further work with fexinidazole is needed refine the treatment and overcome some linked drawbacks, including higher treatment failure rates observed in patients with more severe CNS involvement in late second-stage gambiense HAT (European Medicines Agency, 2018).

1.2.5.6. Acoziborole

On the back of fexinidazole, focus has intensified on bringing more oral therapies for HAT through the development pipeline. The Drugs for Neglected Disease initiative has developed a promising benzoxaborole named acoziborole (Dickie et al., 2020). Through initial murine model studies, the orally administered drug has shown potential to cure second stage (Nare et al., 2010) HAT in a single dosing, and the success of initial clinical trials with acoziborole has now pushed the progression of trials to phase II/III since 2016. Efficacy and safety of the candidate drug is currently being assessed for HAT patients across a number of SSA countries, and trials are due for completion by the end of 2020 (Drugs for Neglected Diseases Initiative, 2020).

1.2.6. Drug resistance

Since Ehrlich's early observations in the early 1900s, the underlying mechanisms behind African trypanosome drug resistance has been area of great research interest (Baker et al., 2013). By the very definition of a parasite, African trypanosomes are typical examples of host nutrient and ion scavengers, using transporters to take up substrates important for cell survival and viability from the host. Examples of such transporter substrates that get taken up by *T. brucei* transporters include adenine, adenosine and glucose (Schmidt et al., 2018), but also important trypanocidal agents, including: melaminophenyl arsenicals like melarsoprol, diamidines like pentamidine, eflornithine that cannot enter the cell by other means, such as passive diffusion (Baker et al., 2013; Schmidt et al., 2018). The study of transporters is therefore critical to elucidate how resistance and sensitivity to current trypanosome treatments has, or could, emerge (Munday et al., 2015).

1.2.6.1. Resistance to melarsoprol and pentamidine

The fact of melarsoprol-resistant HAT has been apparent for approximately half a century (Fairlamb & Horn, 2018), which only reflects the decades of over-dependence on the arsenical for treating second-stage form of the disease (Munday et al., 2015). Melarsoprol treatment failure rates were around 5% in the 1990s. However, at the turn of the 21st century, refractoriness has accelerated, ranging

from 20%-30% in South Sudan, Angola and Northern Uganda and even up to 50% in the DRC (Fairlamb & Horn, 2018). On the other hand, field treatment failures for the drug pentamidine are rare. In most exceptions to this, cases are instead the result of misdiagnoses of the second-stage disease, to which pentamidine is not effective. Despite this, pentamidine-resistant strains can, and have been, generated *in vitro* (Bridges et al., 2007; Delespaux & De Koning, 2007).

One of the clearest and most well-identified patterns from *T. brucei* drug resistance work is that of melarsoprol and pentamidine cross resistance (MPXR). The phenomenon has since been associated with the reduced uptake of both drugs from MPXR-resistant trypanosome cells, either through genetic changes to, or loss of, key transporter proteins (Baker et al., 2013).

The first transporter protein implicated in this manner was the *Tb*AT1/P2 transporter that has unusual specificity for adenine and adenosine (Carter & Fairlamb, 1993; de Koning & Jarvis, 2001). *Tb*AT1/P2 has a role to play in both melarsoprol (Carter & Fairlamb, 1993) and pentamidine (Carter et al., 1995; De Koning, 2001) uptake. For example: knockout of the encoding gene, *TbAT1*, has been shown to decrease both melarsoprol and pentamidine sensitivity in *T. brucei* cells *in vitro* (Matovu et al., 2003; Bridges et al., 2007); heterologous expression of *Tb*AT1 in *Saccharomyces cerevisiae* confers melarsoprol sensitivity, amongst other melaminophenyl arsenicals (Mäser et al., 1999) and *T. b. gambiense* clinical isolates have been identified that possess mutant versions of *TbAT1,* exhibiting reduced pentamidine sensitivity (Graf et al., 2013). However, the levels of resistance reported from these studies, for example resistance factors of 2.3 (melarsoprol) and 2.4-fold (pentamidine) (Matovu et al., 2003), do not match the high resistance levels achieved with MPXR strains *in vitro,* indicating other transporters are involved in creating the high resistance profile of MPXR (Baker et al., 2013).

Since then, two other transporters have been linked with the transport of both melarsoprol and pentamidine; namely *Tb*AQP2 (previously known as HAPT1) and LAPT1 (De Koning, 2001). The former shows a high affinity (K_m: ~36 nM) and low capacity for pentamidine transport, whilst the latter displays a low affinity (K_m: ~56 µM) and high capacity for pentamidine transport (De Koning, 2020). An *in vitro* study found a highly adapted pentamidine and melarsoprol *tbat1*-null strain, B48, had lost

HAPT1 activity (implying additional loss or disruption to the *Tb*AQP2 transporter as well as *Tb*AT1) and had, as a result, become 130-fold resistant to pentamidine, whilst LAPT1 activity was retained unchanged. In this study, melaminophenyl arsenicals similar to melarsoprol showed similar patterns of resistance (Bridges et al., 2007). This shows a marked difference of the impact on resistance with the combined functional removal of *Tb*AT1 and *Tb*AQP2 transporters. Support for the critical role that *Tb*AQP2 plays in melarsoprol and pentamidine uptake has been demonstrated in other bodies of work, for example in a double-gene-knockout study of *AQP2* and neighbouring gene *AQP3* (*aqp2-3* null). Here, increases of 15-fold resistance to pentamidine and 2-fold resistance to melarsoprol were observed when compared with wild-type *AQP2* expressed in a *AQP1-3 null* background cells as a reference (Alsford et al., 2012). Additionally, RNAi library screening has shown re-introduction and expression of *TbAQP2* to *aqp2-aqp3* null cells controlled both pentamidine and melaminophenyl arsenical sensitivity (Baker et al., 2012). From the same study, the specific role of *Tb*AQP3 was not as apparent as *Tb*AQP2 which seemed to be the deciding factor between normal sensitivity and MPXR (Baker et al., 2012).

1.2.6.2. Resistance to suramin

Despite being one of the oldest anti-HAT treatments still in use, the evidence for suramin treatment failure in the field remains scarce. Along with pentamidine as a fellow first-stage treatment, suramin failure is reported in patients with misdiagnosed second-stage HAT, as the drug cannot reach the parasite after it crosses the BBB (De Koning, 2020). Inducible resistance of factors 20-140 have been shown *in vivo* after selection with the drug, but the phenotypic effect is short-lived and normal suramin sensitivity levels are restored once the parasite re-enters the tsetse fly stages (Scott et al., 1996). However, use of transcriptomics and reverse genetics has recently revealed that *T. brucei* cell lines selected with high suramin doses can develop resistance from a switch in expression of their outer membrane VSG coat to a particular glycoprotein called VSG^{Sur}. The resistance developed is over 90-fold, and takes a matter of days to achieve in bloodstream forms *in vitro* (Wiedemar et al., 2018).

1.2.6.3. Eflornithine resistance

Similar to pentamidine and suramin, reports of field eflornithine treatment failures are rare, but underlying mechanisms to understand future risks of resistance have been explored (Vincent et al., 2010). Eflornithine-resistant procyclic trypomasigotes were first observed to have a reduced uptake and accumulation of eflornithine compared to wild-type cells, implicating a potential transporter as part of an underlying mechanism (Bellofatto et al., 1987; Philips & Wang, 1987). Indeed, deletion of the gene encoding the amino acid transporter TbAAT6 was identified in 2010 with two separate resistant *T. brucei* lines, which concurred with findings from RNA interference analysis (Alsford and Horn, 2008) that removal of *TbAAT6* from wild-type lines, and re-expression from resistant lines ultimately determined eflornithine sensitivity (Vincent et al., 2010).

1.3. Leishmaniasis

Leishmaniasis is a neglected tropical disease caused by at least 21 species of an obligate intracellular parasite of the genus *Leishmania*. The parasite relies upon a sand fly vector as a form of transmission between human and mammal hosts, and to complete an essential stage of its life cycle development (Rodrigues et al., 2014). *Leishmania* species are classified into two subgenera based on their location in the vector's intestine: *Leishmania* (found in both the Old and New Worlds) and *Viannia* (restricted to the New World) (Stevens et al., 2001). In tropical and subtropical areas across the globe, *Leishmania* spp. infect humans and mammals with two major forms of disease: cutaneous (CL) and visceral leishmaniasis (VL), as well as rarer forms such as mucocutaneous leishmaniasis (MCL) (Barrett & Croft, 2012). Though leishmaniasis was discovered in the early 20th century by William Leishman and Charles Donovan, the parasite’s reliance on a vertebrate host to complete its life cycle has shaped the evolution and spread of the disease ever since early human activity (Steverding, 2017).

1.3.1. Life cycle of *Leishmania*

Completion of the complex digenetic *Leishmania* life cycle (Figure 1.4) requires both a female sand fly and mammalian host (Handman, 1999). The life cycle of the *Leishmania* parasite begins with the regurgitation of infectious metacyclic promastigotes into a mammal's skin by an infected female sand fly. There is little understanding of how the regurgitation of gut content occurs during blood-feeding, however it is indicated that it happens as a result of the blockage produced by the promastigote secretory gel (PSG) (Rogers, 2012). Consequently, parasite inoculation involves the transmission of several components, including vector saliva, released parasite proteophosphoglycans, exosomes, and the insect gut microbiota. Together these facilitate the establishment and survival of the parasite by modulating the host immune response at the bite site (Gomes & Oliveira, 2012; Rogers, 2012; Atayde et al., 2015; Dey et al., 2018).

It has been shown that once in the wound metacyclic promastigotes are either directly phagocytised by skin macrophages (primary target cells) or engulphed by neutrophils ("trojan" cells). The activation signals originate from components of the alternative complement pathway of the host (C3bi and C3b), which promote parasite uptake by macrophages via CR3 and CR1 receptors (Peters & Sacks, 2006). When the *Leishmania* parasites are ingested by neutrophils, the parasite activates the programmed cell death of the polymorphonuclear cells which are then ingested by macrophage cells (Ritter et al., 2009; Dey et al., 2018). Irrespective of the infection route, once inside macrophages the metacyclic promastigotes enter the phagolysosome, which is a hostile environment for the parasite. Next, the metacyclic parasite transforms to the amastigote stage and multiplies by binary division to infect other macrophage cells.

When the *Leishmania* amastigote is returned by the sand fly within its blood meal, it transforms into procyclic promastigotes (first replicative stage). Following this, promastigotes replicate in the gut of the sand fly until they transform into non-dividing motile nectomonads; these then escape the peritrophic matrix via the posterior opening and attach to midgut microvilli in the anterior midgut. Nectomonads then develop into leptomonads (second replicative stage) in the sand fly's anterior midgut

and then differentiate into metacyclic promastigotes, they can then produce Promastigote Secretory Gel (PSG) which alters the feeding behaviour of the fly (Rogers et al., 2002). Infected sand flies usually have difficulty with feeding because of the action of PSG stimulating regurgitation after the blood meal is mixed in their gut, this ensures transmission of the metacyclic-promastigote. Multiple blood feeds are known to be fundamental in *Leishmania* transmission by inducing sand fly infectiousness, this is achieved by enhancing *Leishmania* amplification. It is of interest that the ingestion of a second uninfected blood meal triggers "reverse differentiation" of the metacyclic promastigotes into retroleptomonad promastigotes, these then rapidly multiply and progressively differentiate back to metacyclic promastigotes (Serafim et al., 2018).

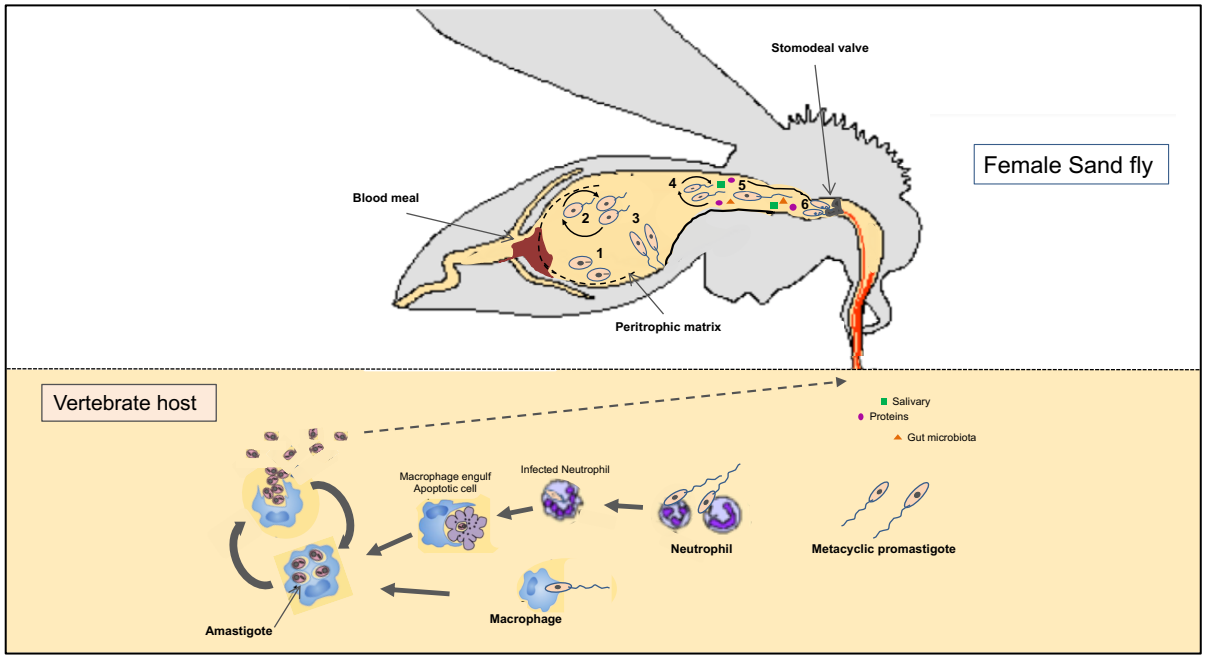

Figure 1.4: The *Leishmania* life cycle.
Metacyclic promastigotes enter the mammalian host skin when a sand fly bites a mammalian host during a blood meal. The parasites become internalised by means of phagocytosis by several host cells, including tissue-resident macrophages. Within, they are then delivered to a phagolysosome where they transform into intracellular amastigotes that proliferate leading to lysis of the cell, either reinvading other phagocytes or being taken up in the next sand fly bite. The first stage as showed in the diagram involves the sand fly feeding on a vertebrate mammal, and introduction of different vector's components from vector to facilitate the migration of metacyclic promastigotes. Afterwards the vector's components multiply within the mammal's host cells inform of amastigotes as showed in process 1. The life cycle continues as another sand fly feeds on the infected blood to continue the development to procyclic promastigotes stage as showed in process 2 in the diagram. As labelled in the diagram, process 3 involves the development of the parasite life cycle to long motile nectomonads. Process 4 on the other hand illustrates escape of the necomonads and their attachment to the midgut microvilli, which are later transformed to Leptomondas. Process 5 in the diagram involves the transformation of the Leptomonads to infective metacyclic promastigotes and 6 shows transformation to haptomonads. The Leptomonads

as illustrated in the diagram play an imperative role in the production of Promastigote Secretory Gel (PSG) which fills the thoracic midgut of the sand fly. Once inside the sand fly, amastigotes transform into procyclic promastigotes that proliferate in the midgut, and then move to the anterior of the sand fly where they become the infective and highly motile metacyclic promastigotes ready to infect another host (Dostalova and Volf, 2012; Serafim *et al*, 2018; Kaye & Scott, 2011).

1.3.2. Morphology

Over the span of its life cycle, the single-celled *Leishmania* parasite possesses two main cell morphologies as it traverses between vectors and hosts – a promastigote and amastigote morphology. The architecture of the cell is mostly conserved throughout both, for example, single copies of organelles; a flagellar pocket; a kinetoplast (containing mitochondrial DNA) anterior to the nucleus; and the attachment of the kinetoplast to the flagellar basal body (Ogbadoyi et al., 2003; Ambit et al., 2011; Sunter & Gull, 2017). However, notable differences lie in the cell's shape, flagellum length and distance between the nucleus and kinetoplast. Whilst the promastigote is elongated, has an extended flagellum protruding from the basal body at its anterior end, and a segregated nucleus and kinetoplast, the amastigote is ovoid, has a rudimentary flagellum and its nucleus proximal to the kinetoplast (Gluenz et al., 2010; Sunter & Gull, 2017) (Figure 1.5).

Precise morphologies in promastigote and amastigote forms translate directly into important functions for the parasite during different stages of the life cycle. During the time spent within the sand fly, the *Leishmania* procyclic promastigote uses its elongated cell shape with a long, motile flagellum to propel itself across different parts of the sand fly's digestive tract, and to attach to the midgut epithelium (Bates, 2008). Meanwhile, the much-reduced size of the amastigote relative to the promastigote reduces overall exposure to hostile conditions within the phagolysosome of host phagocytes (Sunter & Gull, 2017). The amastigote's short flagellum highlights the lack of a need for high motility through the host; however, there is evidence to suggest that this feature holds a sensory function within the macrophage (Gluenz et al., 2010).

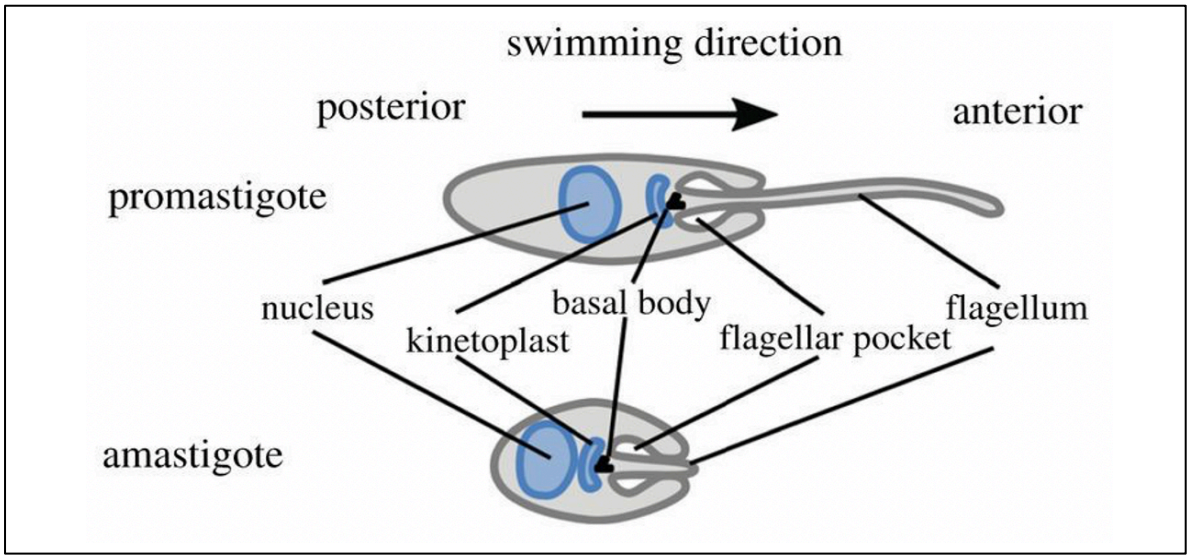

Figure 1.5: Schematic comparing the morphology of *Leishmania* promastigote and amastigote forms.
Showing from the posterior end of the parasite cell to the anterior end. Key cell organelles and structures, as well as relative subcellular locations within each form, are shown (Sunter & Gull, 2017).

1.3.3. Epidemiology of leishmaniasis

Leishmaniasis remains a global threat to many people around the world; from over 89 countries known to have had the disease, 12 to 15 million people become infected by the leishmaniases at any given time (Georgiadou et al., 2015; Torres-Guerrero et al., 2017). Meanwhile, 700,000 to 1 million new cases are collectively reported every year (WHO, 2020a) and over 350 million remain at risk of contracting one form or another (Torres-Guerrero et al., 2017). In areas where the leishmaniases are endemic, as high as 9% of the entire healthy population can test positive for the disease (Bari, 2006).

Over 10 years ago, it was reported that 90% of new cases of VL were located to Brazil, Sudan, South Sudan, as well as India and neighbouring countries (Blackwell et al., 2009). These regions remain hotspots of burden of VL today, but this now also includes Ethiopia, which has experienced a substantial increase in cases over the past decade (Tadese et al., 2019) (Figure 1.6A). The two major species of the parasite that cause VL are *Leishmania (Leishmania) donovani* and *Leishmania (Leishmania) infantum*. In almost all cases, *L. donovani* infection remains exclusive to Africa, Asia and Europe. In India it is alternatively labelled ‘Kala-Azar’ or ‘Black

Fever', because of a blackening of skin that is associated with this disease there, and spreads as an anthroponosis. On the other hand, *L. infantum* infection extends to both the Old World and Latin America and spreads as a zoonosis (Ready, 2014), resulting from the well-studied domestic dog as the natural reservoir, but also including other important reservoirs such as cats and opossums (Ready, 2014; Roque & Jensen, 2014). There are now been reports of human immunodeficiency virus (HIV) that co-infects leishmaniasis patients in over 35 countries. Increased risk of developing VL in areas that are HIV endemic comes as no surprise, given that HIV severely compromises the immune system. Indeed, patients who are co-infected often have high parasite load, a sign that the compromised immune system has become overwhelmed (Sundar et al., 2019).

Clinical CL is more common and more widely distributed than VL (Georgiadou et al., 2015), impacting almost all Latin American countries including Brazil, Peru, Colombia and Costa Rica, as well as Algeria, North Sudan and Ethiopia in Africa, and Iran and Syria in the Middle East (WHO, 2020b) (Figure 1.6B). Although there has been a decline in reported CL cases in Saudi Arabia, the country still stands as the fourth most endemic for the disease in western Asia (Alvar et al., 2012; Abuzaid et al., 2017). Over 20 species of *Leishmania* can cause CL, and the predominant aetiological agents in the Old World are the species *Leishmania major* and *Leishmania tropica*, whilst in the Americas, this applies to the complexes *Leishmania mexicana* and *Leishmania braziliensis* (Torres-Guerrero et al., 2017). Whilst it is understood that *L. tropica* related disease spreads as an anthroponosis, and *L. major* disease as a zoonosis, there is no defined natural reservoir at present for the latter, though the domestic dog has been the most extensively studied and associated (Roque & Jensen, 2014; Bamorovat et al., 2018). Another cutaneous form, MCL, is found in Bolivia, Brazil, Peru and Ethiopia which collectively accounts for over 90% of known cases (WHO, 2020a) and is caused by species such as *L. braziliensis* and *Leishmania amazonensis* with show more regional distribution patterns (Torres-Guerrero et al., 2017).

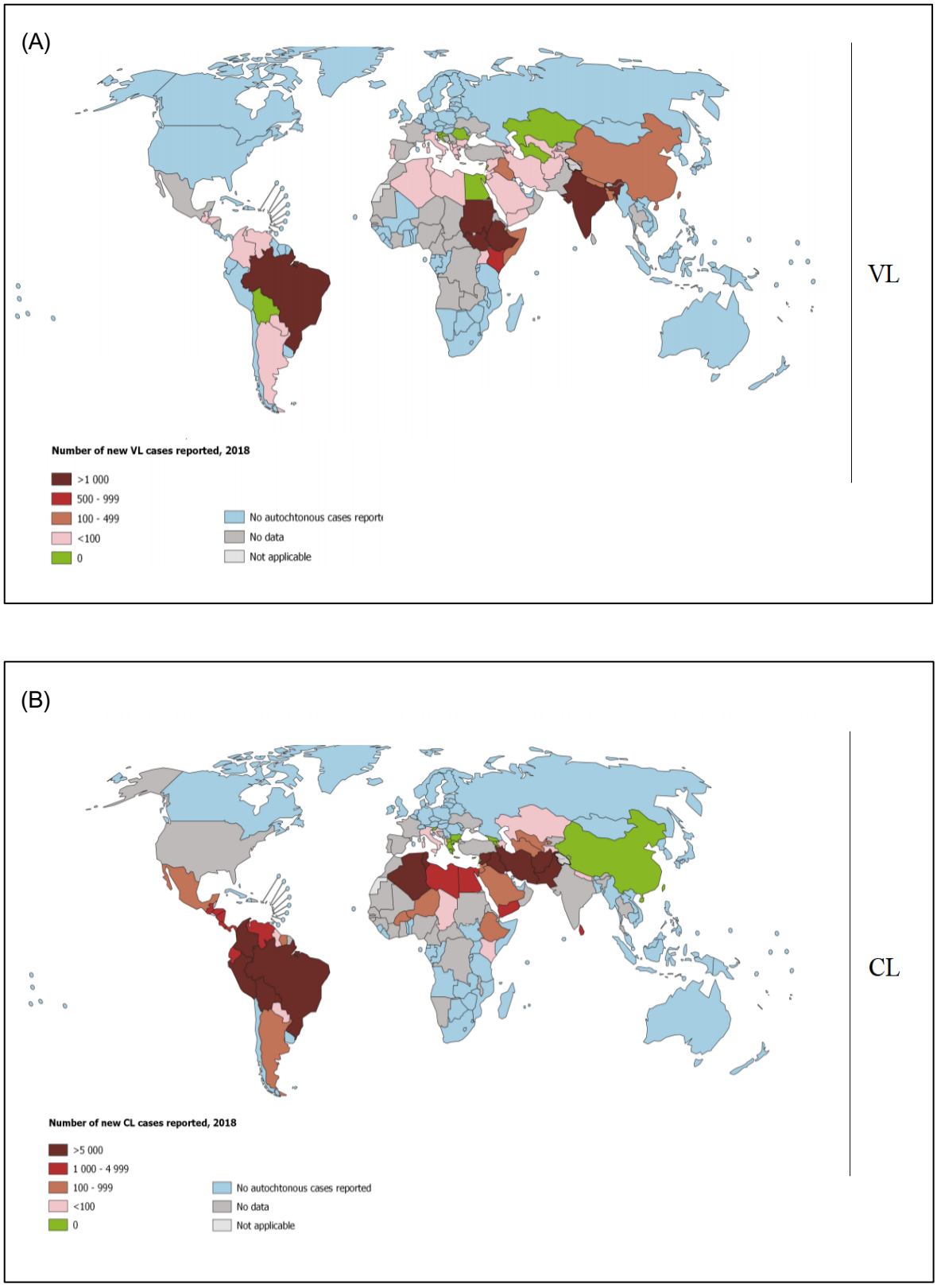

Figure 1.6: Maps showing endemicity status of leishmaniasis in 2018.
(A) Countries in the world coloured based on the number of new cases of visceral leishmaniasis (VL). Areas with highest endemicity include Brazil, Sudan, South Sudan, Ethiopia and southern Asia (B) countries in the world coloured based on the number of new cases of cutaneous and mucocutaneous leishmaniasis (CL). Areas with highest endemicity include: Central and South America, North Africa and the Middle East (adapted from WHO, 2020b).

The spread and persistence of the leishmaniases is exacerbated by a range of political and socioeconomic factors. Conflict outbreaks in Afghanistan (Ahmad, 2002) and Syria (Al-Salem et al., 2016), poor housing and irregular garbage collections in Latin American countries (which in turn promote sand fly resting grounds and breeding) as well as delays in access to healthcare in India (Okwor & Uzonna, 2016) have all been shown to contribute towards increased incidence of the leishmaniases.

1.3.4. Clinical manifestations

The leishmaniases can range from asymptomatic to clearly visible clinical presentations (Figure 1.7). Manifestations are normally distinguished between the two most common forms CL and VL, as well as the rarer MCL form.

Figure 1.7: Different clinical presentations of the leishmaniases.
(*Left panel*) Child affected by visceral leishmaniasis, with a striking protruding abdomen, (*middle panel*) a man afflicted with mucocutaneous leishmaniasis, with almost total destruction to the mucous membranes of his nose and mouth (*right panel*) human skin with an ulcer lesion, characteristic of cutaneous leishmaniasis (Stanford University, 2008).

1.3.4.1. Cutaneous Leishmaniases

CL, caused by species such as *L. major* and *L. tropica*, leads to lesions on exposed areas of the skin, and are typically ulcers (WHO, 2020a) as shown in Figure 1.7 (right panel). The type of lesion can vary depending on the causative species of *Leishmania* and host immune response to infection (Torres-Guerrero et al., 2017). For example, *L. tropica* infection leads to a manifestation of large, scaly oriental sores on many

areas of the skin, which are commonly identified in Middle Eastern, North African and Central Asian countries (Cairns, 1968). In comparison, Chiclero's ulcer, which appears exclusive to the ear region, is the result of infection by *L. mexicana* that are endemic to areas like Mexico (Andrade-Narváez et al., 2001) and Ecuador (Calvopiña et al., 2013). In any case, self-healing of the lesion eventually leaves depressed scarring (WHO, 2020c). The approximate incubation period of CL varies based on parasite species from weeks to months (Weiss et al, 2009) with *L. major* usually taking less than 4 months to present symptoms, and *L. tropica* infection usually manifesting after between 2 to 8 months (WHO, 2020c). A large proportion of those asymptomatic for CL in endemic regions are able to control the infection, though the underlying mechanisms behind this are yet to be fully elucidated (Bahrami et al., 2018).

Particularly in the Americas, MCL can also occur where the nasal and oral cavities become partially or fully eroded as pictured in Figure 1.7 (middle panel). This form of the disease, which disfigures the host, either takes place after resolution of previous CL lesions, or a co-existing presentation on the skin. MCL appears to be primarily the consequence of *L. braziliensis* infection (Handler et al., 2015).

1.3.4.2. Visceral Leishmaniasis

In the case of VL, the disease itself gains its name because of the causative parasite's ability to progress away from the skin and infect, survive, and proliferate in several of the host's visceral organs, most of all the liver and spleen. VL is therefore fatal if left untreated. Pathogenesis ensues from parasite proliferation within the viscera, ultimately causing hepatosplenomegaly (enlargement of the spleen and liver) which gives rise to the presentation of a distended abdomen as shown in Figure 1.7 (left panel) (McCall et al., 2013). Other features include pancytopenia (destruction of blood cells) thought to be the result of causative *Leishmania* species triggering over-activation of the host macrophage and T-cell response (Gagnaire et al., 2000), as well as polyclonal hyper-gammaglobulinemia (a marked increase in production of immunoglobulins in the bloodstream) (Makaritsis et al., 2009). VL has an incubation period of around 3 to 8 months (Weiss et al., 2009).

In some cases, both during and after a course of VL infection, a complication called post-kala-azar dermal leishmaniasis (PKDL) can develop. This is particularly the case in *L. donovani* endemic regions like Sudan and India, and affects 5%-60% of patients whereby papular, micropapular or nodular lesions appear as a rash, spreading from the mouth area to other areas of the body if the patient's case of PKDL is more severe. The lesions are created as a result of an inflammatory reaction to the parasite, but interestingly lack plasma cells unlike lesions with CL (Zijlstra et al., 2003). Incidence of asymptomatic VL has been vastly underestimated in the past, mainly due to remaining poorly understood. Carriers can be diagnosed by means of PCR or leishmaniasis skin testing, which estimated that a large number of people in VL endemic areas are asymptomatic. One such example is Sudan where asymptomatic *L. donovani* and *L. infantum* VL infections form around 30% of all cases (Singh et al., 2014).

1.3.5. Treatments available

Due to the variety of clinical manifestations and the number of causative *Leishmania* parasite species causing the disease, there is no one general first choice of treatment for leishmaniasis. Instead, treatment options must be considered in line with the challenges that disease forms pose in each affected area (Moore & Lockwood, 2010). The options to treat both major forms of the disease, CL and VL, are limited by several factors, for example: local availability of the drug, efficacy rates impacted by levels of resistance at the regional level, and side effects that can range from mild to adverse depending on the patient (Miranda-Verastegui et al., 2009; Moore & Lockwood, 2010). Leishmaniasis being mostly a disease of developing countries, cost of the medication can also be an important factor.

1.3.5.1. Pentavalent antimonials (Sb^v)

For over 60 years, antimonial drugs (Sb^v), such as sodium stibogluconate (SSG) and meglumine antimoniate (MA), have been used as first line of treatments for all forms of leishmaniasis (Haldar et al., 2011). The standard treatment prescribed for affected VL patients is either a daily intravenous (SSG) or intramuscular injection (MA) of 20 mg kg^{-1} body weight for up to 30 days, whilst for CL patients antimonials

are administered intralesionally (1-5ml of Sb^{v} every 3 to 7 days) and systemically (20 mg kg^{-1} for 20 days) (Sundar & Chakravarty, 2015).

There have been three models proposing the mechanism of action for Sb^{v} activity, including a stage-specific thiol-mediated process of reducing Sb^{v} to the more lethal trivalent antimony Sb^{III} in amastigotes once engulfed within macrophages. In turn, Sb^{III} would target, bind and inhibit trypanothione reductase and zinc-finger proteins to kill the cell from within by compromising the cell to oxidative damage and metal toxicity. The second model proposes that Sb^{v} may directly inhibit macromolecular synthesis by disturbing intracellular metabolic pathways, though this model has not evidenced a specific target in the process of disruption. The third model suggests that Sb^{v} may activate innate and adaptive immune responses by the host by influencing host effector and signalling pathways that can lead to eventual parasite cell death. One such example is generation of host reactive oxygen species and nitrogen oxide within infected macrophage cells by means of the PI3K-PKC-Ras/Raf and P13K/Akt pathways respectively (Haldar et al., 2011).

To this day, Sb^{v} compounds are the treatment of choice in many areas of the world affected by CL and VL, particularly developing countries in Africa and South America, as well as central and some southern Asian countries including Bangladesh, Nepal and most of India (Haldar et al., 2011; WHO, 2020b). Despite this, the efficacy of the chosen SSG drug for patients in India has gradually declined over the last few decades, with the greatest apparent loss in the eastern state of India, Bihar, where cure rates between 1994-1997 were as low as 35% (Sundar et al., 2000; Rijal et al, 2003).

Success of Sb^{v} treatment to CL conditions is not as clear cut, as sensitivity levels to Sb^{v} sensitivity vary greatly, correlating with mixed CL patient response to treatment (Haldar et al., 2011). However, a 28 day course of Sb^{v} remains highly recommended against *L. braziliensis* infection in America, achieving 75% cure rates for those with mild to moderate MCL, and to prevent disfiguration from mucosal lesions from an earlier onset of CL (Torres-Guerrero et al., 2017).

Though Sb^{v} remains one of the more popular choices of leishmaniasis treatment across affected nations, with exceptions to Bihar, the drug is by no means ideal due

to adverse effects like high toxicity (such as nephrotoxicity and cardiotoxicity), poor tolerability presented by some patients and high recurrence rates in patients who relapse (Elmahallawy & Agil, 2015).

1.3.5.2. Amphotericin B

The polyene antifungal drug Amphotericin B (AmB) has been a major treatment for cases of VL, and was the only 'rescue treatment' for patients who didn't respond successfully to Sb^v or relapsed, at the beginning of the 2000s (Alves et al., 2018). It was previously used in its conventional form, sodium deoxycholate, but due to its high toxicity, alternative formulations were desired. Fortunately, a lipid-associated formulation has been developed since then, known as liposomal amphotericin (L-AmB), and successfully contains the drug until it reaches target parasite cells, making it a preferred option in order to significantly reduce exposure, and thus toxic effects, particularly to the kidneys (Aguirre & Hamid, 2015). L-AmB therapy has been the recommended choice of VL treatment by the National Program of Nepal, after increasing rates of local VL treatment failure with Sb^v as well as areas of India like Bihar where Sb^v drug resistance is already firmly established (Torres-Guerrero et al., 2017) whilst conventional AmB appears to be reserved mostly for teaching and district hospitals (Alves et al., 2019), and L-AmB remains unaffordable for the many affected (Barrett & Croft, 2012). Whilst conventional AmB is administered intravenously at 0.75-1 mg kg^{-1} either daily or on alternating days for 15-20 days, patients co-infected with HIV on L-AmB therapy courses can afford extended courses of periodic infusions up to total doses of 40 mg kg^{-1}, which provide less chances of patient relapse without significantly increasing the risk of adverse effects (Sundar & Chakravarty, 2010).

Similar to their action on fungal cell membranes, AmB is understood to bind to ergosterol in *Leishmania* cell membranes and increase permeability of the cell to metabolites, by forming pores (Saha et al., 1986). L-AmB has been shown to be rapidly taken up by parasite-loaded phagocytes that are located in vital organs, effectively killing the parasite 'from within' and preventing further development of disease to the viscera (Adler-Moore & Proffitt, 2003).

With this mode of action, L-AmB has proven to be highly effective at treating VL, with over 95% efficacy shown from a study in India using the treatment, regardless of slight variations in dose regimens (Thakur et al., 1996). Though data on L-AmB treatment is less available for other forms of leishmaniasis, it does appear to also be highly effective in systemic forms of particular forms of CL and treatment of MCL in the New World (Alvar et al., 2006; Cunha et al., 2015). Despite this effectiveness, the drug is not usually administered except where challenges are faced with Sb^{v} administration, given the high costs to buy sufficient quantities to effectively treat the disease. In addition, clinical studies indicate that VL patient response rates to L-AmB are lower in East Africa and South America than India (Barrett and Croft, 2012).

1.3.5.3. Paromomycin

Paromomycin is an aminoglycoside antibiotic identified in the 1960s as a potential treatment for leishmaniasis. However, it only became clinically available in the mid-2000s after patient response rates were found to be over 90% for topical treatment of Old World CL (Asilian & Davami, 2006) and comparable with efficacy rates of AmB in VL treatment, passing phase III trials (Sundar et al., 2007).

During phase III trials, a treatment course consisting of 15 mg kg^{-1} paromomycin for 21 days with intramuscular administration delivered 95% efficacy, and is now the licensed dose for VL patients in India, and standard for VL treatment in the surrounding regions (Sundar et al., 2007). However, similar efficacy could not be replicated with paromomycin in East Africa and the World Health Organisation (WHO) now recommends combination therapies with Sb^{v}, allowing for shorter VL treatment courses to Sb^{v} monotherapy with similar levels of efficacy (Uliana et al., 2018).

The mechanism of paromomycin against *Leishmania* cells is similar to those described against bacteria such as *Staphylococcus* strains (Ibrahim et al., 2019); it plays a major inhibitory role on protein synthesis at the ribosome by binding to the 30S ribosomal subunit and disrupting polypeptide chain initiation and elongation from subsequent mRNA misreading (Sundar & Chakravarty, 2008). This mechanism

has also been supported by proteomic studies based on paromomycin-resistant *L. donovani* (Jhingran et al., 2009).

So far, paromomycin is one of the cheapest anti-leishmanial treatments, costing as little as $10 per course (Barrett & Croft, 2012) and without major, non-reversible side effects (Sundar & Chakravarty, 2008). However, it has little efficacy for systemic treatment of CL or MCL, with the exception of New World CL in Brazil (Sundar & Chakravarty, 2015). Therefore, it seems likely that current recommended combination regimens with Sb^v for VL treatments will be the only way it is used for the future.

1.3.5.4. Miltefosine

The alkyl phospholipid, miltefosine, became the first orally available VL treatment in 2002 when registered in India, two decades after being identified for possessing anti-leishmaniasis properties in the 1980s with *L. donovani* (Barrett & Croft, 2012; Uliana et al., 2018). A 94% VL cure rate was found from one phase III trial with a 28 day treatment course (Sundar et al., 2002). Since, it has also shown promise as an orally administered CL treatment in some regions. However, there is large geographical variation in response rates, for example a phase II-III clinical trial in Brazil reported a 71.4% cure rate for *L. guyanensis* New World CL compared to a 53.6% cure rate with Sb^v treatment (Chrusciak-Talhari et al., 2011), whilst a phase III trial in Colombia reported a 69.8% cure rate for *L. braziliensis* and *L. panamensis* New World CL compared to 85.1% cure rate with Sb^v treatment (Vélez et al., 2010). The treatment was also shown to be non-inferior to Sb^v treatment for *L. major* Old World CL from Iran.

Current recommendations point to the same 28 day treatment course with a dosage dependent on the individual patient's body weight: daily doses of 2.5 mg kg^{-1} for 2-11 year olds, 50 mg for patients over 12 years of age but less than 25 kg, 100 mg for patients between 25 kg and 50 kg and 150 mg for patients over 50 kg (Dorlo et al., 2012).

As a drug that is also used to target human cancers, miltefosine has multiple targets and effects on *Leishmania* cells that influence cell multiplication. The drug targets an enzyme called phosphocholine cytidylyltransferase, preventing intracellular

phosphatidylcholine biosynthesis pathways. The presence of phosphatyidylcholine is critical for cell survival, with the miltefosine intervention instead resulting in the triggering of apoptosis (Braga, 2019). Apoptotic programmed cell death also seems to be triggered by miltefosine causing overexpression of methionine aminopeptidase 2 (MAP2) in *Leishmania* cells treated *in vitro* (Kumar et al., 2017). Another target appears to be the replication machinery of the *Leishmania* cell, with RNA synthesis being downregulated by over 96%, triggering a 'domino effect' on protein and DNA synthesis in the cell (Braga, 2019).

The discovery of miltefosine has been praised as a success on the path to a wider range of accessible options for treating leishmaniasis. However, it hasn't completely met expectations on the ground, with inefficient drug supply chains and limited access to the drug from availability of the drug and high price tags, making it inaccessible for patients most in need but living in poverty (Sunyoto et al., 2018). Miltefosine also involves a much longer course of treatment in comparison to other treatment options, and has been shown to exhibit teratogenicity (defects to, or death of, an embryo or foetus). Additionally, phase IV trials have also revealed toxic side effects in the gastro-intestinal (GI) tract, kidneys and liver (Singh et al., 2016).

1.3.5.5. Pentamidine

Pentamidine is a diamidine drug synthesised in the late 1930s, and became a treatment of Sb^{v}-refractory VL in India in the early 1940s for patients who did not respond to treatment. After the 1980s, the frequency of pentamidine use for VL treatment declined due to poor efficacy rates, combined with patient relapses and high frequency of adverse reactions including cardiotoxicity, diabetes mellitus onset and disruption to metabolic processes (Sundar & Chakravarty, 2015; Uliana et al., 2018).

Pentamidine, however, still has a role in treating particular CL forms, particularly in South America with New World CL (Barrett & Croft, 2012). Studies from South America have reported 90% (Suriname) and 95% (Colombia) cure rates against *L. guyanensis* and *L. panamensis* infections respectively (Soto et al., 1994; Lai et al., 2002). Pentamidine has also shown to be effective for treating MCL lesions in Brazil, reporting 90-94% cure rates for affected patients with treatment courses of 2 - 4 mg

kg^{-1} given on alternate days usually over a week to two weeks (Sundar & Chakravarty, 2015).

Electron microscopy of pentamidine-treated *Leishmania* cells, in addition to *L. mexicana* diamidine-resistant strain studies suggest pentamidine works by accumulating in the mitochondria of *Leishmania* and thereby causing disintegration of the mitochondrion and its membrane potential (MMP) (Basselin et al., 2002). Disintegration of the kinetoplast is also observed through electron microscopy, which a study suggests may be due to the accumulation of pentamidine leading to disruption of kinetoplast DNA replication (Yang et al., 2016).

1.3.6. *Leishmania* drug resistance

Pathogen resistance to drug treatments is normally the result of changes to uptake, efflux, the way a drug is metabolised, or interactions between drugs and their target (Baker et al., 2013). The use of current anti-leishmaniasis drugs is constantly under threat from an underlying emergence of *Leishmania* drug resistance, particularly in the Indian sub-continent where VL treatment refractory rates have been the most apparent. Whilst in many affected countries, Sb^v remain the preferred drugs for the range of clinical forms, use of Sb^v as well as other second-line treatments are met with increasing treatment failure, compromising future dependence on the existing line of treatments (Ponte-Sucre et al., 2017).

1.3.6.1. Resistance to pentavalent antimonials (Sb^v)

Antimonial-resistant *Leishmania* has been studied over the sixty-year course of Sb^v treatment of VL. Reports of resistance first came in Bihar in India, where treatment failure rates were ~30% in the 1980s. Although WHO recommendations to increase both dosage and duration of the Sb^v treatment course to 20 mg kg^{-1} for 20 days had a modest short-term impact on helping to revive cure rates, a progressive decline was monitored in the region (Croft et al., 2006), with Sundar *et al*. (2000) reporting treatment failure rates as high as ~65% in North Bihar in one study. In neighbouring regions and countries, there is variation in the patient response; whilst some areas are largely unaffected, such as 2% failure rates reported in Uttar Pradesh, patient refractoriness in the Nepalese Terai regions were near 24% (Rijal et al., 2003).

Treatment failure is strongly associated with the emergence of *L. donovani* resistance in Bihar *in vitro*, where a three-fold lower sensitivity has been shown in *L. donovani* amastigote stage isolates in non-responsive patients compared with patients who responded to treatment (Lira et al., 1999).

Historically, the emergence of Sb^{v} resistance in sub-continental India has been a result of widespread misuse of the drug. It had become easily accessible to many in the population without qualified medical diagnosis for guidance on Sb^{v} use. Additionally, regimens that had an increasing dose progression or with intervals were previously recommended and thought to boost chances of treatment success. Pronounced Sb^{v} treatment failure in newly treated patients appears to be almost exclusive to sub-continental India and surrounding regions, with the anthroponotic nature of VL transmission in this area accelerating the spread of drug resistance once acquired by the parasite (Haldar et al., 2011).

Various cellular processes have been pinpointed as possible underlying causes for Sb^{v} resistance, including: reduced conversion of Sb^{v} into its trivalent more active and toxic form Sb^{III}; increased levels of thiols such as trypanothione that have been shown to protect *Leishmania* cells from oxygen radical attack caused by antimonials, and overexpression of ATP-binding cassette (ABC) and of multidrug resistance protein A (MRPA) transporters that boost efflux and sequestration of Sb^{v} metabolites respectively and lower drug accumulation inside the cell (Mandal et al., 2007; Singh et al., 2014; Ponte-Sucre et al., 2017). Another *Leishmania* transporter, aquaglyceroporin 1 (AQP1), has been implicated in the facilitated uptake of Sb^{III} in *Leishmania* species. *In vitro*, greater *Leishmania* cell sensitivity and resistance to Sb^{III} can be altered with over-expression or deletion of the encoding gene, *AQP1*, respectively (Gourbal et al., 2004; Richard et al., 2004), and in VL and PKDL *L. donovani* field isolates, down-regulation of AQP1 RNA levels have been found to correlate with reduced accumulation of Sb^{III} and drug resistance in the area (Mandal *et al*, 2010).

1.3.6.2. Resistance to amphotericin B

Reports of *Leishmania* treatment failure and resistance to the antifungal drug AmB have been relatively rare, posing a low threat over the last 60 years of use as an

anti-leishmaniasis agent (Ponte-Sucre et al., 2017). Despite this, there are some sparse cases of treatment failure that have been identified. For example, *L. donovani* isolates from a patient who relapsed in a non-endemic region of India were reported to exhibit *in vivo* drug tolerance (Srivastava et al., 2011) and an immunosuppressed patient in Switzerland was identified with L-AmB primary treatment failure. Cases from non-endemic regions may be the result of increasing migration and travel globally (Eichenberger et al., 2017) though future AmB resistance in endemic areas is equally probable. One factor that may exacerbate this is single-shot minimal dosage L-AmB regimens supported by WHO, widely used across India which have the effect of facilitatating selection of less AmB sensitive forms of the parasite (Ponte-Sucre et al., 2017).

Several mechanisms have been linked with AmB resistance from laboratory studies. One study showed that *L. donovani* isolates selected for 8-fold AmB resistance circumvented AmB binding cell membranes from loss of ergosterol. Instead, the sterol was replaced with the precursor cholesta-5,7,24-trien-3ß-ol, thereby decreasing AmB action on membrane permeability (Purkait et al., 2012). Secondly, the efflux transporter multi-drug resistant transporter 1 (MDR1), was shown to have been 3-fold overexpressed in resistant promastigotes, with treatment of a MDR1 inhibitor beforehand partially reversing the AmB resistance phenotype (Purkait et al., 2012). Separate studies have also identified that mutations to the gene sterol 14α-demethylase can result in ergosterol loss and changes to sterol metabolism (Mwenechanya et al., 2017). Resistant parasites also appear to upregulate a range of defence mechanisms against AmB oxidative stress (Sundar et al., 2019).

1.3.6.3. Resistance to miltefosine

Miltefosine has been a promising drug alternative to replace traditional Sb^{v} in the Indian sub-continent for nearly two decades, with high initial cure rates of around 94% (Ponte-Sucre et al., 2017). However, in as little as a decade, increasing patient relapses in India, Nepal and Bangladesh reflect a cure rate decline down to 85% in these areas (Rahman et al., 2011; Sundar et al., 2012; Rijal et al., 2013). Low efficacy rates have been more recently identified for VL treatment in Kenya and Sudan with standard miltefosine monotherapy regimens (Wasunna et al., 2016). Risk of resistance to the drug is compounded by the long elimination half-life of

miltefosine in the body (~120 h), causing long-lingering low concentrations of the drug that promote parasite resistance selection whilst being largely ineffective for parasite cell death. This problem is exacerbated where patients don't comply with the full medication regimen (Ponte-Sucre et al., 2017; Sundar et al., 2019).

Miltefosine resistance can be induced *in vitro*, with the first evidence emerging from a paper in 2003. Here, defects to internal protein-dependent phospholipid translocation of the drug were suggested as a possible causative resistance mechanism (Pérez-Victoria et al., 2003). The proteins implicated as part of the translocation machinery have now been identified as the *L. donovani* miltefosine transporter (*Ld*MT) and the *L. donovani* subunit for *Ld*MT (*LdRos3*), which appear to both be required for *Leishmania* miltefosine uptake and sensitivity (Pérez-Victoria et al., 2006). Both *in vitro* and *in vivo* assays have demonstrated that mutations or deletions to encoding genes that compromise the function of *Ld*MT and *Ld*RoS3 lead to high-fold increases in miltefosine resistance levels by *L. donovani* cells (Ponte-Sucre et al., 2017). It is also now clear that *Ld*MT function, whilst essential, does not fully account for wild-type or drug-induced levels of sensitivity or resistance respectively. To this end, additional mechanisms, such as overexpression of ABC transporters MDR1, ABCG4 and ABCG6 increase efflux of miltefosine, reducing accumulation of the drug in the parasite to achieve sufficient potency (Pérez-Victoria et al., 2006; Sundar et al., 2019).

Though recent studies using 'omics' technology have revealed that *Leishmania* miltefosine resistance is in fact multifaceted and beyond the scope of just *Ld*MT and ABC efflux transporters, the roles that other components play are yet to be elucidated (Ponte-Sucre et al., 2017).

1.3.6.4. Resistance to pentamidine

Historically, pentamidine had been used to successfully combat VL in the North Bihar region, with cure rates of 99%. In the short space of time of only two decades, however, treatment failures up to ~30% were reported. This led pentamidine to be abandoned in the surrounding region as a second-line treatment in favour of more effective currently used treatments such as miltefosine (Chakravarty & Sundar, 2010). As a first-line treatment it is now almost exclusively used for specific forms

of CL and MCL in the New World, and for this it has retained a relatively high efficacy (Barrett & Croft, 2012). Its current limited use in South America for *Leishmania* species that spread by zoonotic transmission has fortunately reduced the possible risk and burden of acquired drug resistance on treatment failures with new world leishmaniasis (Croft et al., 2006). However, the situation in India suggested from early on that selection against pentamidine could be easily achieved by the parasite, especially by anthroponotic transmission and widespread use (Uliana et al., 2017).

Early work showed that pentamidine resistance can be quickly obtained in multiple parasite species *in vitro*, including: *L. major* (Ellenberger & Beverley 1986) *L. mexicana* (Basselin et al., 2002) and *L. amazonensis* (Coelho et al., 2008). A study using *L. mexicana* showed that the resistance phenotype corresponds with a substantially lower intracellular pentamidine accumulation than wild-type lines, particularly within the mitochondria as shown by fluorescent labelling (Basselin et al., 2002). This may be partly due to alterations made to AT-rich regions of kinetoplast DNA in resistant lines that are understood to be necessary for pentamidine binding (Basselin et al., 1998). As a result of a higher proportion of pentamidine in the cytosol as opposed to organelles, more of the drug is available for efflux (Basselin et al., 2002; Bray et al., 2003). Reduced accumulation was suggested to be at least partly the result of reduced uptake by a transport-carrier mechanism (Basselin et al., 1996; 2002) which is supported by observed 18-fold and 75-fold reduced uptake rates of pentamidine in *L. donovani* and *L. amazonensis* promastigote clones respectively (Croft et al., 2006). However, the exact mechanism for resistance remains unclear, although one proposed involves reduced uptake through a *Leishmania* high-affinity plasma membrane transporter, driven by reduced MMP rather than a change to the transporter itself. This has been supported by findings that the membrane transport carrier remains unaltered despite resistance, and that the use of MMP inhibitors is able to reduce wild-type cell pentamidine uptake (Basselin et al., 2002; Bray et al., 2003). Moreover, the expression of a pentamidine transporter, TbAQP1, in *L. mexicana* promastigotes, increased rates of uptake as well as pentamidine sensitivity (Munday et al., 2014).

Efflux of pentamidine in resistant lines of *L. major and L. infantum* promastigotes and amastigotes are likely mediated by the ABC transporter pentamidine resistance

protein 1, PRP1, that was identified through functional cloning. Overexpression by transfection of *PRP1* conferred resistance to pentamidine in both promastigotes and amastigotes (Coelho et al., 2003; Coelho et al., 2007). Though a specific mechanism for efflux is not established, it has suggested that PRP1 may transport pentamidine into vesicles that then exit the cell via exocytosis from the flagellar *pocket (Coelho et al., 2007). However, the role of PRP1 in pentamidine resistance* does not appear to be shared in all *Leishmania* species, for example in *L. amazonensis* (Coelho et al., 2008).

1.4. Trypanosomatid aquaporins: as new drug targets

The presence of aquaporins (AQP), which are integral membrane protein transporters, is critical in playing the role tailored towards facilitating the regulated and rapid movement of non-polar solutes such as water in and out the cells (Borgnia et al., 1999; Gourbal et al., 2004). AQPs belong to the Major Intrinsic Protein (MIPs), a super-family of integral membrane proteins present throughout the kingdoms of viruses, bacteria, plantae, animalia, archaea, fungi, and protista (Thomas et al., 2010). With aquaporin monomers comprising six transmembrane helical segments and two short helical segments covering cytoplasmic and extracellular vestibules bound by a narrow aqueous pore, they have a similar basic structure (Verkman, 2013). It is possible to functionally classify these small channels of integral membrane protein into two primary sub-groups namely the aquaglyceroporins (which are responsible for the transportation of different small, uncharged solutes as well as water) and orthodox aquaporins (which chiefly serve as water specific channels). Uncharged solutes transported by aquaglyceroporins include methylglyoxal, dihydroxyacetone, urea, polyols, glycerol, and metalloids such as antimony (SbIII) and trivalent arsenic (AsIII) (Bhattacharjee et al., 2009).

It has been determined that the success of kinetoplastid parasites such as *Trypanosoma brucei* and *Leishmania major* is dependent on their respective abilities to meet the diverse challenges presented by different environments both in insects and mammals. Following the nature of trypanosomatid parasites to be frequently traveling between the mammalian and insect hosts, they are often exposed to the risk of facing severe osmotic challenges (Rohloff & Docampo, 2008). Therefore,

there is an interface that exists between the kinetoplastid cells and its respective environment, which is in part constituted of numerous membrane transporter proteins and glycoproteins, and this serves in overcoming diverse unavoidable biological barriers. Several aquaporins have been identified in trypanosomatid parasites (Chen et al., 2005; Beitz et al., 2006; Montalvetti et al., 2004; Figarella et al., 2007). In comparison, it has been generally determined that parasite AQPs have a higher level of transporting water than mammalian and *E. coli* aquaporins. Aquaglyceroporins of protozoan parasites have also been reported to be bifunctional and thus serve to improve the conduction of glycerol and water at reasonable rates (Beitz et al., 2005).

1.4.1. Role of AQPs in drug response in *Trypanosoma brucei*: Human African Trypanosomiasis (HAT)

In the *T. brucei* genome there exist three aquaglyceroporins, namely *Tb*AQP1, *Tb*AQP2 and *Tb*AQP3 (Uzcategui et al., 2004; Beitz, 2005). These aquaglyceroporins are differentially involved in the regulation of the localization and abundance of the different AQPs depending on the unique developmental stages of *T. brucei* (Baker et al., 2012). In the case of *Tb*AQP1, it is localized in the flagellar membrane, whereas the localization of *Tb*AQP3 occurs in the pellicular membrane, independent of the developmental stage (Bassarak et al., 2011; Baker et al., 2012). Interestingly, the situation is different when it comes to the case of *Tb*AQP2, whose redistribution occurs over the pellicular membrane in insect stage form but it is located to the flagellar pocket in bloodstream forms (Baker et al., 2012). The characterized AQPs from *T. brucei* are aquaglyceroporins, and as a result, they are explicitly responsible for the transportation of water in addition to other small molecules that are uncharged as trivalent metalloids, urea, and glycerol (Uzcategui et al., 2004; 2013). Unlike the cases of other aquaglyceroporins, TbAQP2 has been implicated in the transportation of larger compounds such as melarsoprol (398 Da) and pentamidine (340 Da). Both melarsoprol (398 Da) and pentamidine (340 Da) are trypanocides, which are three-fold larger than glycerol, widely considered as the largest substrate of TbAQP2 (Baker et al., 2012). The arsenical and diamidine resistant parasites are reported to be cross-resistant and have shown reduced uptakes of both drugs in HAT.

Many studies have found that there is that the TbAT1 (purine transporter 2 - P2) and TbAQP2 transporters (Baker *et al*, 2013; Figure 1.8) are implicated in determining the rate of uptake of pentamidine and melarsoprol, as well as in the emergence of MPXR in *T. brucei* (Mäser et al., 1999; Munday et al., 2014; Munday et al., 2015b; Carter & Fairlamb, 1993; Baker et al., 2012, 2013).

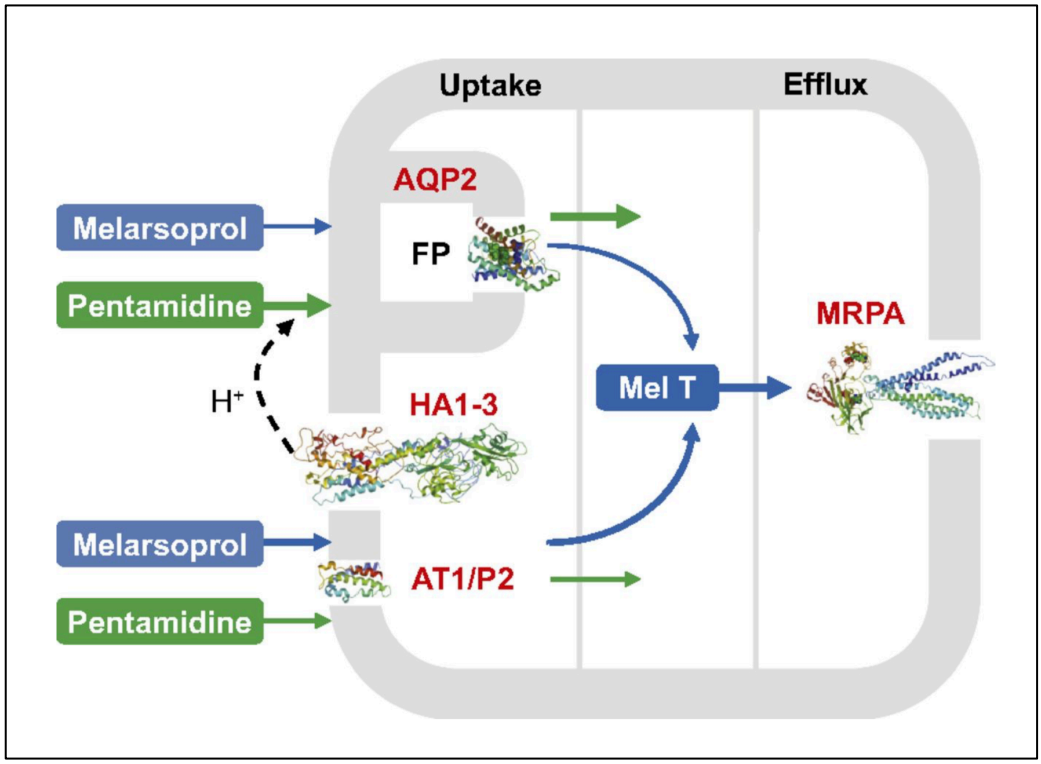

Figure 1.8: A depiction of the model explaining the pentamidine and melarsoprol transport in *T. brucei*.

There is the linkage of four *T. brucei* transporters to the pentamidine susceptibility and melarsoprol control. The entrance of both drugs into the cell occurs through AQP2 (Tb927.10.14170) and AT1/P2 (Tb927.5.286b). HAI-3 (Tb927.10.12500-10, with only two of them reflected through annotation in the reference genome) has been specifically associated with the susceptibility of pentamidine. It is suggested that there is requirement for pentamidine symport via AQP2 for the generation of the proton motive force (De Koning, 2001). MRPA (Tb927.8.2160) is the channel through which the efflux of the Mel T, a toxic melarsoprol-trypanothione adduct. AQP2 and AT1/P2 channels are responsible for the transportation of the drugs with different efficiencies, indicated by the weight arrows in the figure. (Baker et al., 2013).

There is a close relation between *Tb*AQP2 and *Tb*AQP3, which have close sequence similarity and are adjacent to each other on the chromosome. In comparison to *Tb*AQP3, *Tb*AQP2 is characterized by unusual selectivity filter amino acids residues in comparison with *Tb*AQP3. The *Tb*AQP2 exhibits unusual selectivity pore amino

acids residues, (NSA/NPS/IVLL) in the pore, unlike the latter which has the usual motifs (NPA/NPA/WGYR) (Baker et al., 2012; Figure 1.9). *Tb*AQP2 also does not have the aromatic/arginine (a/R) motif in comparison with *Tb*AQP3 (Baker et al., 2012). Aquaporins usually have a selectivity filter which usually defined by two constrictions in the channel: one formed by extremely conserved of two of "NPA" motifs within the half helices, the other one is usually narrower, created by an "aromatic arginine" (ar/R) motif (de Groot et al., 2001; Sui et al., 2001). These two regions have been suggested as filters that block solutes larger than water and charged molecules from moving through. The two NPA motifs in the narrow central constriction of the pore, according to crystallographic studies, contribute to a monomeric pore structure that enables selective, bi-directional, and single-file transport of water in classical AQPs (Sui et al., 2001) and water and glycerol in aquaglyceroporins (Jensen et al., 2001). The aromatic-arginine region, which is narrower than the central NPA constriction and acts as a selectivity filter on the extracellular side of the AQP channel, blocks the entry of molecules larger than water (de Groot & Grubmu; 2005, 2001). (The selectivity filter of *Tb*AQP2 and *Tb*AQP3 will be further discussed in Chapter 3).

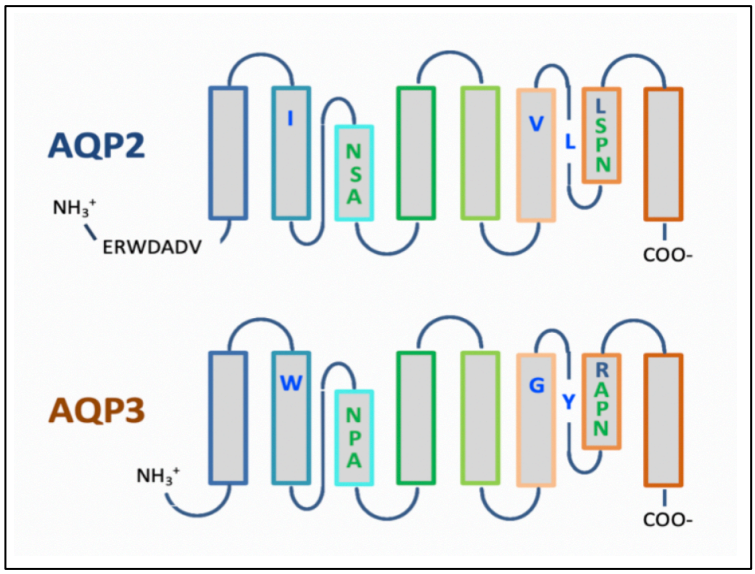

Figure 1.9: Schematic representation of AQP2 (Tb927.10.14170) and AQP3 (Tb927.10.14160). The selectivity filter residues are indicated; the unique NSA/NPS/IVLL in AQP2 and the classical NPA/NPA/WGYR in AQP3 (adapted from Baker et al., 2012).

It has been demonstrated that the genetic knockout of *Tb*AQP2 results in MPXR, while the re-expression of this gene causes a full reversal of the phenomenon. However, the expression or deletion of *Tb*AQP3 did not have any measurable effects on the uptake of (or sensitivity to) pentamidine or melaminophenyl arsenicals. Therefore, these findings show that *Tb*AQP2 is undeniably a genetic determinant of MPXR. Thus, owing to the unique selectivity of its filter functions, TbAQP2 is not only a water channel but also a potential drug transporter (Baker et al., 2012). The area of dispute remains the specific translocation mechanism for the *Tb*AQP2-mediated internalisation of pentamidine. The study by Song *et al*. (2016) challenged the drug uptake model through the uniquely permissive aquaglyceroporin by positing the argument that instead of traversing the pore of TbAQP2, there is the mere binding of pentamidine to an aspartate residue (Asp265) above the selectivity filter and close to the pore's extracellular end, followed by the process of endocytosis (Song et al., 2016). Based on this understanding, it is necessary to conduct further studies with the specific aim tailored towards determining the *Tb*AQP2-mediated drug transport mechanisms in the trypanosomes.

1.4.2. Role of AQPs in drug response and resistance in *Leishmania spp.*: Leishmaniasis

Drugs containing pentavalent antimony, such as meglumine antimonate (Glucantime) and stibogluconate (Pentostam), are used as the first treatment choice against all leishmaniasis forms. There have been reports of clinical resistance from diverse parts of the world when it comes to this class of drugs (Guerin et al., 2002). As membrane support proteins, aquaglyceroporins play critical functions in the life cycle of parasites as they serve roles in controlling transmembrane nutrient (or waste product) flux, alleviating osmotic stress, and releasing metabolites (Verkman et al., 2014; Brochu et al., 2003; Gourbal et al., 2004; Frezárd et al., 2014; Nilsen et al., 2016). One of markers that is commonly linked to antimonial resistance and most frequently identified in *Leishmania* is AQP1 (Marquis et al., 2005; Decuypere et al., 2005; Mandal et al., 2010; Maharjan et al., 2008; Kazemi-Rad et al., 2013). Pentavalent antimonials [Sb^{V}] chiefly serve as pro-drugs and in order for the drugs to be in its active form, they are usually reduced to trivalent antimony [Sb^{III}] (Ephros

et al., 1999). Shaked *et al*. (2001) acknowledges that the process of how pentavalent antimony is reduced to a trivalent compound in the parasites is still not known, and also, it has not yet been determined how the entry of antimonials mechanisms into macrophages and from there into the phagolysosomes takes place.

However, Gourbal, *et al*. (2004) suggested that the first Sb^{III} facilitator that has been identified in *Leishmania* is aquaglyceroporin 1 (LmAQP1) (Figure 1.10) and determined that it embodies a direct relationship to both the resistance and uptake of antimonite [Sb^{III}] (Gourbal et al., 2004; Marquis et al., 2005). The level of expression of AQP1 in cultured promastigotes and intra-macrophage amastigotes *in vitro* was found to correlate with the levels of susceptibility exhibited in different *Leishmania* species; AQP1 of *L. major* was reported to facilitate the highest level of sensitivity to Sb (III) (Mandal et al., 2015). It was found that five different aquaporins are expressed by the genome of *Leishmania major* species: LmAQP1, LmAQPα, LmAQPß, LmAQPγ, and LmAQPδ. LmAQP1 showed a strong degree of similarity to human AQP9 and to bacterial aquaglyceroporin GlpF, while the remaining water-transporting proteins (LmAQP α-δ) operated as classic aquaporins, reflecting similarity to the ones that are found in plants (Figarella et al., 2007; Biyani et al., 2011; Maurel et al., 2015).There has been proof supporting the permeability of LmAQP1 to glycerol and how it effectively functions as a route of drug-delivery for antimonial compounds as well as performing a critical role in osmotaxis (Figarella et al., 2007).

In promastigotes there is the exclusive localisation of LmAQP1 to the flagellum, while in amastigotes, its presence is within the contractile vacuoles, the rudimentary flagellum, and the flagellar pocket. LmAQP1 serves a significant physiological role in osmotaxis, volume regulation, and the transportation of solutes and water. Resistance to Sb^{III} could be increased when one of the two *Lm*AQP1 alleles in *L. major* is disrupted (Marquis et al., 2005). There are significantly lower levels of LmAQP1 mRNA in As (III) or Sb (III) resistant *Leishmania tarentolae* and *L. major* cells, which is an indication of how drug resistance is caused by the downregulation of LmAQP1 (Marquis et al., 2005). Later there was a corroboration of these findings in the field isolates from Nepal (Decuypere et al., 2005) and India (Mandal et al., 2010). The drug resistance and cellular physiology of *Leishmania* were amongst the

major roles played by the LmAQP1. As a result of all findings, there is the need for further work to be conducted with the specific goal focused on understanding the role performed by Leishmania particularly as drug transporter.

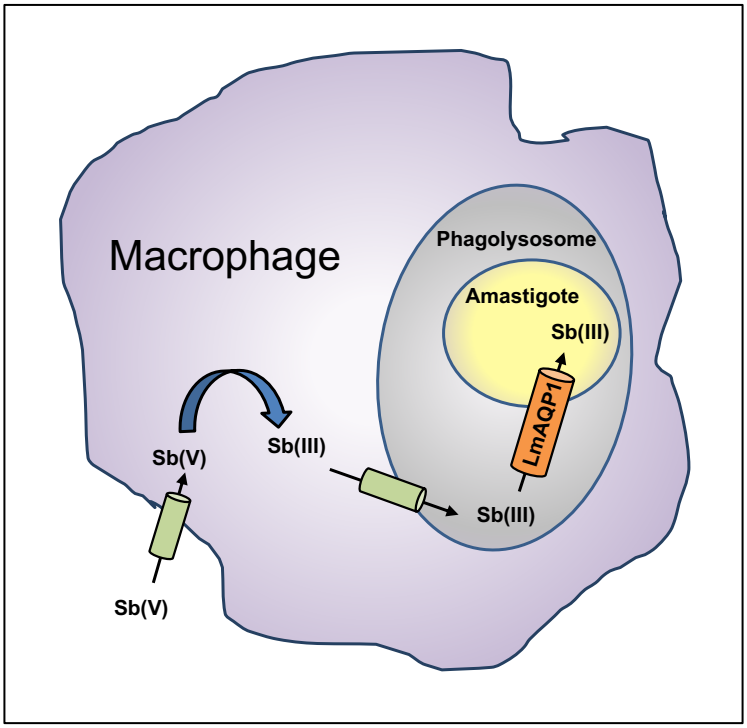

Figure 1.10: Representation of proposed antimonial transport mechanism diagrammatically for an infected macrophage in *Leishmania*.
The figure shows a potential mechanism of antimonial transport an infected macrophage in Leishmania. There is transportation of pentavalent antimony [Sb (V)] into the macrophage, which is then subsequently reduced to trivalent antimony [Sb (III)] prior to its transportation into the phagolysosome. Finally, the transportation of Sb (III) into the cytoplasm of the parasite is facilitated by LmAQP1 (adapted from Mandal et al., 2013).

1.5. Objectives and aims of the project:

Neglected parasitic diseases (NPD) include some of the worst human infections and are caused by pathogens including *T. brucei* (human African trypanosomiasis or sleeping sickness), *Leishmania spp* (leishmaniasis), which lead to large disease burden, high mortality and morbidity rates in afflicted countries. In the absence of effective vaccines against any trypanosomatid diseases, chemotherapy takes the centre stage to combat them. Many anti-protozoal drugs are inherently cytotoxic but derive their selectivity from preferential uptake by the pathogen rather than

the host. Conversely, loss of the specific drug transporters is a main cause of drug resistance.

Identification of parasite-specific targets and uptake mechanisms is critical for the development of new agents. Within two decades of discovery, significant advancement has been achieved with regard to mammalian AQPs. However, knowledge about AQPs from other living systems, especially in protozoa is lagging far behind. Therefore, further exploration of parasite AQP structures and functions, including their regulatory mechanisms, will eventually reveal their real potential for novel chemotherapeutic approaches and/or transmission intervention(s). The general aim of my research is to understand the roles of kinetoplastid AQPs in trypanosomatid parasites with respect to drug resistance and transport. For *Leishmania* AQP1 there have been credible reports of its involvement in antimony (stibogluconate, pentostam) resistance and for *T. brucei* spp the hypothesis is that AQP2 is involved in pentamidine and melaminophenyl sensitivity. In both cases, mutations in the AQPs are believed to be responsible, at least in part, for resistance to the drugs.

The first and largest aim of my project was to determine how the structure of TbAQP2 allows it to transport pentamidine, whereas the closely related TbAQP3 does not. The working hypothesis was that the pore of TbAQP2 was wider than that of TbAQP3 and that the cation filter in the form of a pore-located arginine must be one of the determining factors, the hypothesis was tested by conducting mutational and functional analyses of *Tb*AQP2 including:

- Swapping residues of *Tb*AQP2 and *Tb*AQP3, particularly in the selectivity filters with the goal of determining their effects on the uptake of pentamidine drug by *Trypanosoma brucei*.
- Investigating the effect of the size of amino acids at the cytoplasmic end of the *Tb*AQP2 pore to test the hypothesis that bulky residues would block the passage of pentamidine.
- Testing whether the constructed variants of *Tb*AQP2 exhibited different abilities to transport, and sensitise to, pentamidine and melaminophenyl-arsenicals.

- To determine the degree of their functional effectiveness as aquaglyceroporins, especially the ability to transport glycerol.
- To investigate whether the alternative hypothesis, of pentamidine uptake via endocytosis of a pentamidine-AQP2 complex, is compatible with all available data.

The second and last aim of my project is to get insight in the role of *Leishmania major* AQP1 in drug transport. Here, the hypothesis is that Sb(III) traverses the pore of AQP1 and that loss of functionality of this aquaporin contributes to antimonial resistance, which is a first-line treatment of leishmaniasis but is not used against any of trypanosomiasis. For this, a systematic examination on the LmAQP1 was achieved by:

Cloning, functional expression, and characterisation of *Lm*AQP1 in appropriate trypanosomatidae cells, with the aim of obtaining insights in the explicit role that AQP1 plays in drug transportation.

Chapter 2 Materials and methods

2.1. Materials

2.1.1. Media and growth chemicals

T. b. brucei bloodstream was cultured in Hirumi's modified Iscove's (HMI-9) powder, obtained from Gibco (Life Technologies, Paisley, United Kingdom). Heat-inactivated Fetal Bovine Serum (FBS) was obtained from PAA Laboratories (Linz, Austria). Sodium bicarbonate ($NaHCO_3$) and ß-mercaptoethanol were obtained from BDH and Sigma respectively (Dorset, United Kingdom).

Leishmania promastigotes were cultured in Eagle's Minimal Essential Medium (HOMEM) purchased from Gibco (Paisley, United Kingdom). Penicillin/Streptomycin antibiotic was also purchased from Gibco.

2.1.2. Radiolabelled compounds

Three radiolabelled drugs were used throughout the project, which enabled the characterisation of our transporters of interest. [^{3}H]-pentamidine was custom-made by GE Healthcare Life Sciences (Cardiff, UK) with a specific activity of 88 Ci/mmol. [^{3}H]-suramin; 20 Ci/mmol, and [^{3}H]-glycerol; 40Ci/mmol were both obtained from American Radiolabeled Chemicals, Inc (Arc Drive, St. Louis, USA).

2.1.3. Chemicals and compounds

Most chemicals and compounds, as well as antibodies, were obtained from Sigma. However, Potassium chloride, Sodium dihydrogen phosphate hydrate and (4-(2-hydroxyethyl)-1- piperazineethanesulfonic acid (HEPES) were all purchased from BDH Prolabo Chemicals (United Kingdom). Scintillation fluid [Optiphase HiSafe III] was purchased from Perkin-Elmer. 2-Thiouridine and 4-thiouridine were both obtained from Carbosynth Limited (Berkshire, United Kingdom).

The pGEM-T Easy sub-cloning vector, Go-Taq polymerase and dNTPs were all obtained from Promega (Madison, WI, USA). All primers used in the study were synthesized by Sigma-Aldrich Limited (Dorset, UK). The Q5 Site-Directed Mutagenesis Kits (#E0554S), High-fidelity proofreading polymerase Phusion and

Restriction enzymes were acquired from New England Biolabs (Hitchin, United Kingdom). The ultra-pure agarose was sourced from Invitrogen (Paisley, United Kingdom). All the extraction kits for plasmid, gel, DNA and RNA were obtained from Macherey-Nagel (Düren, Germany).

The Nanodrop ND 1000 spectrophotometer was obtained from ThermoFisher Scientific (UK), and was used to measure the concentrations of DNA and RNA in solution. The XL1-Blue competent cells of *E. coli* were supplied by Agilent Technologies (United Kingdom), while the 5-alpha competent cells of *E. coli* were supplied by New England BioLabs. A Neubauer haemocytometer was sourced from Weber Scientific (Teddington, Middlesex, United Kingdom).

2.2. Methods

2.2.1. Parasite cultures

2.2.1.1. Culturing of *T. b. brucei* bloodstream forms (BSF)

T. b. brucei 2T1 cells (Alsford et al., 2005) were used for all the work as control cell line. The *tbaqp2/tbaqp3* null cells (Baker et al., 2012) and *tbaqp1-2-3* null cells (Jeacock et al., 2017) (both obtained from David Horn, University of Dundee, UK) are derived from the 2T1 strain of *T. b. brucei* (Alsford & Horn, 2008). The *CRK12* RNAi cell line (Monnerat et al., 2013) was obtained from Dr. Tansy Hammarton (University of Glasgow, UK) and is also based on the 2T1 cell line; RNAi expression was induced with 1 µg/ml tetracycline in the medium. All experiments were performed with bloodstream form (BSF) trypanosomes grown *in vitro* in HMI-9 medium supplemented with 10% FBS and 2 mM ß-mercaptoethanol (pH 7.4) at 37 °C and 5% CO_2 as described (Bridges et al., 2007) and maintained in the log-phase of growth. Cultures were routinely grown in 10 ml of this medium, being seeded at 1 × 10^5 cells/ml and passed to fresh medium at reaching approximately 1.5 – 2 × 10^6 cells/ml. The 2T1 strain was grown in the media under two selective pressure of antibiotics (0.5 µg/ml phleomycin) and (0.2 µg/ml of puromycin) to maintain the tetracycline repressor (TetR) constructs for selection of correct integration. The

CRK12 RNAi cell line was routinely grown in the media with two antibiotics (phleomycin 0.5 ug/ml & hygromycin .2.5 ug/ml). All the AQP mutant cell lines were routinely maintained with a selection antibiotic (2.5 µg/ml hygromycin) and were induced with 1 µg/ml of tetracycline for 24 hours prior to the sensitivity and transporter assays to ensure expression of the test construct. For transport experiments 150 or 200 ml of culture was seeded, again at ~5×10^4 cells/ml, in large, vented tissue culture flasks and incubated until the culture reached late-log phase.

The growth curves of bloodstream form trypanosomes were performed in the HMI-9 standard medium. Dilution of a preliminary culture was made to achieve a density of 1×10^5 cells/ml. Counting of cells was done using a haemocytometer in triplicate, every 4 h for CRK12 RNAi and every 24 h for 2T1 and all mutant cell lines.

2.2.1.2. Culturing of *L. major* promastigotes

Wild type *L. major* strain LV39, *L. major* AQP1 null mutant (Plourde et al., 2015) (kind gift from Professor Marc Ouellette, Laval University, Quebec, Canada), and our mutant cell lines (*L. major* AQP1 null + *L. major* AQP1) were used in this project. The promastigotes of *L. major* strains were cultured in HOMEM medium obtained from Gibco (Paisley, United Kingdom) with 10% FBS and 1% Streptomycin antibiotic at a pH of 7.4. The culturing was performed in non-vented plastic flasks 25 cm^2 at temperature of 25 ºC according to Al-Salabi *et al*. (2003). Every 3 days, the growing cells were passaged and exposed to antibiotics whenever necessary. The selection of antibiotics included: Hygromycin at 100 µg/ml for *L. major* AQP1 null, and Neomycin (G418) at 50 µg/ml for mutant cells.

To perform the growth curves of *Leishmania* promastigotes strains, 1×10^5 cells/ml were seeded in HOMEM medium added with the required antibiotics. Using a haemocytometer, the cells were counted in triplicate every 24 hours.

2.2.1.3. Establishing stabilates

Stabilates were made from cells in the log phase. For *T. brucei*, for each cryovial 0.5 ml of log phase culture was added to 0.5 ml of HMI-9 supplemented with 10% FBS and 30% glycerol (resulting in a final concentration of 15% glycerol). For *L.*

major, 0.8 ml of log phase culture was added to 0.8 ml of HOMEM supplemented with 10% FBS and 30% of glycerol per cryovial (resulting in a final concentration of 15% glycerol). The cryovials were stored at -80 ºC for a period of 24-48 hours before transferring them to a liquid nitrogen storage tank.

2.2.1.4. Preparation and recovery of stabilates

Stabilates were recovered by removing cryovial tubes from the liquid nitrogen where they were stored and defrosting the cells rapidly in the hood at room temperature. For *T. brucei*, the cells were first transferred from stabilate into 5 ml of pre-warmed media, followed by centrifugation at 1300 x *g* for 5 min at room temperature. This process enabled the removal of glycerol which may otherwise affect the recovery of cells. The supernatant was very carefully decanted off, and the pellet re-suspended and transferred into a vented flask with 5 ml of fresh HMI-9/10% FBS. Flasks were then incubated in a 5% CO_2 atmosphere at a temperature of 37 ºC during the study. For *Leishmania* spp, the cells were transferred into non-vented plastic flasks containing 5 ml pre-warmed (25 ºC) HOMEM medium with 10% FBS. The flasks were then incubated horizontally at 25 ºC. Cells were renewed after about 20 passages by taking another stabilates from the liquid nitrogen storage tank.

2.2.2. Bacterial cultures

2.2.2.1. Bacterial components and culturing

XL1-Blue competent cells (Agilent Technologies®, UK), and 5-alpha competent cells (New England BioLabs, E0554S) of *E. coli* were used for plasmid amplification throughout the project. The XL1-Blue competent cells were used for routine cloning, while the NEB 5-alpha competent cells were used after site-directed mutation, in order to obtain high efficiency transformation. Both types of *E. coli* cells were cultured overnight at 37 ºC, either in LB broth (Appendix 1) (shaking incubator) or on LB agar (Appendix 1) (incubator).

2.3. Molecular techniques

2.3.1 Genomic DNA Extraction

Genomic DNA from *T. brucei and L. major cells* was extracted using the Nucleospin Tissue kit (Macherey-Nagel) according to the manufacturer's instructions. Briefly, 5 ml of cell culture was transferred to a 15-ml tube and centrifuged for 10 min at 1000 x *g*. The medium was discarded by inversion and the rim of the tube was cleaned with tissue paper. The cell pellet was then resuspended in 200 µl of buffer T1, followed by addition of 20 µl of Proteinase solution from the kit. 200 µl of buffer B3 was added and the tube was vigorously vortexed and incubated at 70 ºC for 10 minutes. 210 µl of absolute ethanol was then added to the mixture, vortexed and then transferred onto the NucleoSpin® tissue column followed by centrifugation at 11,000 x *g* for 1 min. The column was washed with 500 µl of buffer BW, centrifuged and then washed again with 600 µL of buffer B5 and centrifuged at 11,000 x *g* for 1 min. The column was then transferred to a new 1.5 ml tube and incubated at 70 ºC for 5 min. Finally, the DNA was eluted with 50 µl of elution buffer at room temperature for 20 min and the eluate collected by centrifugation at 11,000 x *g* for 2 min. The DNA concentration was measured on the NanoDrop ND 1000 spectrophotometer (ThermoFisher Scientific), and the samples were stored at -20 ºC until use.

2.3.2. Primer design

All the primers used in the study for PCR amplification for the purpose of screening and cloning were designed to flank the gene of interest with 18 to 25 nucleotide regions using the CLC Genomic workbench software (version 7.0, developed by CLC bio). Restriction sites were introduced in the primer 3' flank whenever it was necessary, preceded by six random nucleotides, so that the PCR product could be directly digested by restriction enzymes, and ligated into the relevant vector. For a point mutation, NEBaseChanger tools were used in the production of primer series and an annealing temperature for the anticipated mutation.

2.3.3. Polymerase chain reaction (PCR)

Prior to the amplification of a DNA fragment, the annealing temperatures were usually optimized for each pair of primers by evaluating 12 PCR reactions using different annealing temperatures ranging from 50 ºC to 70 ºC (Gradient PCR) (Appendix 2). All PCR reactions were performed on G-Storm thermocyclers (Gene Technologies).

Q5 Hot Start High-Fidelity (NEB) was used to generate the desired mutations. The 25 µl PCR mixtures contained 12.5 µl 2× Q5 Hot Start High-Fidelity Master Mix, 1.25 ul of each primer (taken from a 10 µM stock solution), 1 ul template DNA (conc. 1–25 ng/µl), and 9 ul nuclease-free water. The cycling conditions included an initial denaturation for 30 s at 98 ºC, followed by 24 cycles of denaturation for 10 s at 98 ºC, annealing for 20 s at 61 ºC, an extension for 4:05 min at 72 ºC, and a final extension at 72 ºC for 2 min.

The GoTaq polymerase (Promega) was used for routine PCR screening. The 50 µl PCR mixtures contained 10 µl Go Taq Reaction buffer (5 x), 5 ul MgCl2 (25 mM), 1ul dNTPs mix (10 mM), 1 ul of each primer (taken from a 10 µM stock solution), 0.5 ul template DNA (conc. ~200 ng/µl), and 31 ul distilled water. The cycling conditions included an initial denaturation for 3 min at 95 ºC, followed by 34 cycles of denaturation for 40 s at 95 ºC, annealing for 30 s at melting temperatures (Tm) based on the gradient PCR, an extension for 1 min at 72 ºC, and a final extension at 72 ºC for 10 min.

The High-fidelity Phusion polymerase (NEB) was employed when high fidelity amplification was required to amplify the gene of interest (GOI) from a genome. The 50 µl PCR mixtures contained 10 µl Phusion GC buffer (5 x), 2 ul dNTPs mix (10 mM), 2 ul of each primer (taken from a 10 µM stock solution), 0.5 ul template DNA (conc. ~200 ng/µl), and 33.3 ul distilled water. The cycling conditions included an initial denaturation for 30 s at 98 ºC, followed by 34 cycles of denaturation for 10 s at 98 ºC, annealing for 20 s at melting temperatures (Tm) based on the gradient PCR, an extension for 30 s at 72 ºC, and a final extension at 72 ºC for 10 min.

2.3.4. Plasmids constructions

2.3.4.1. Generation of AQP2 mutants

All mutations in the *Tb*AQP2 gene were introduced to the backbone WT pRPa$^{GFP\text{-}AQP2}$ vector (Baker et al., 2012), by Site-Directed Mutagenesis Kit (New England BioLabs), according to manufacturer's instructions.

To generate the named *Tb*AQP2 mutations into WT pRPa$^{GFP\text{-}AQP2}$ vector, the primer pairs (itemised in Table 2.1) were used and amplified by PCR using Q5 site-directed mutagenesis kit protocol (New England BioLabs, E0554), following the manufacturer's instructions. The plasmids were then introduced into NEB 5-alpha Competent *E. coli* cells by transformation, exactly as described in the Q5 Site-Directed Mutagenesis Standard Protocol (E0554). Briefly, NEB 5-alpha Competent *E. coli* cells were thawed on ice in an Eppendorf tube, for approximately 15 min. 5 µl of the Kinase, Ligase & DpnI (KLD) mix were added to the tube for assembling. The tube was gently flicked 4-5 times to mix. The mixture was placed on ice for 30 min, followed by a heat shock for 30 s at 42 ºC. The mixture was then placed on ice for 5 min. A volume of 950 µl of Super Optimal broth with Catabolite (SOC) repression medium was added into the mixture, which was then incubated at 37 ºC for 1 h with shaking at 250 rpm. The tubes were carefully flicked and a volume of 50-100 µl was spread onto a selection plate and incubated at 37 ºC overnight. The next day, colonies from the overnight transformation were screened by PCR using GoTaq polymerase (PCR mixture and programme conditions in section 2.3.3), with HDK529 and HDK209 primers (Table 2.2) to confirm the presence of the AQP2 gene. Positive colonies with the correct band size were incubated overnight in LB containing 100 µg/ml ampicillin, at 37 ºC. The plasmid extraction kit (Macherey-Nagel) was used to purify the plasmid DNA from the culture according to the manufacturer's instructions. Using the primers of HDK1011 and HDK430 (both present in the plasmid; table 2.2), the whole gene sequence checked by Sanger Sequencing by Source BioScience (Nottingham, UK) to check for additional unwanted mutations, the presence of the correct mutation(s) and correct cassette for integration. Plasmids

produced (Figure 2.1) were digested with *Asc*I (NEB, Hitchin, UK) prior to transfection into the *tbaqp2*/*tbaqp3* null cells and *tbaqp1-2-3* null cells.

Table 2.1: Primers used to create mutations in *Tb*AQP2.

Mutation	Primer	Sequence 5`-3` (altered base(s) underlined)	Generated Plasmid	Original Template
L84W	HDK1276	AAACTTCGTCTGGATATATATCGCTAAGGG	pHDK210	pRPa$^{GFP-AQP2}$
	HDK1277	CCCAGAAATTCAGCCACG		
L118W	HDK1274	CACCGCAGTGTGGCTGCTCTGTG	pHDK208	pRPa$^{GFP-AQP2}$
	HDK1275	GAAATGAGTTCAGCAAAAATTG		
L218W	HDK1272	CACGATGGCTTGGTATGTTTCACTG	pHDK209	pRPa$^{GFP-AQP2}$
	HDK1273	ACAGCCACACCAATACCA		
L84W/ L118W	HDK1276	AAACTTCGTCTGGATATATATCGCTAAGGG	pHDK227	pHDK208
	HDK1277	CCCAGAAATTCAGCCACG		
L84M	HDK1364	AAACTTCGTCATGATATATATCGCTAAGG	pHDK234	pHDK210
	HDK1367	GAAATGAGTTCAGCAAAAATTGGATAAAATATAC		
L118M	HDK1365	CACGATGGCTATGTATGTTTCAC	pHDK235	pHDK208
	HDK1367	GAAATGAGTTCAGCAAAAATTGGATAAAATATAC		
L218M	HDK1366	CACCGCAGTGATGCTGCTCTGTG	pHDK236	pHDK209
	HDK1367	GAAATGAGTTCAGCAAAAATTGGATAAAATATAC		

Table 2.2: Primers for confirmation of pRPa$^{GFP\text{-}AQP2\ mutant}$ constructs used before and after transfection.

Primer name	Direction	Position	Sequence (5' – 3')
HDK529	Forward	*Tb*AQP2 gene	CAGCTGCGAACTGACGGAAGTTGGT
HDK209	Reverse	*Tb*AQP2 gene	AAGCTTCGTAGTGTCCAACTGTGCAC
HDK1011	Forward	located 143 bp upstream of the open reading frame (ORF) of the gene of interest (GOI) in the plasmid backbone	TGCCCGACAACCACTACCTG
HDK430	Reverse	located 83 bp downstream of the open reading frame (ORF) of the gene of interest (GOI) in the plasmid backbone	GGATCCCGTGAGCCTGGTTGACGAAG
HDK713	Forward	located 989 bp upstream of the *Asc*I site in the plasmid backbone	ATGCAAGCTAGGCCACACCT
HDK991	Reverse	located 90 bp downstream of the *Asc*I site in the plasmid backbone	CCGAACGACCGAGCGCAGCG
HDK535	Reverse	located 338 bp downstream of the *Asc*I site in the plasmid backbone	CGGACAGGTATCCGGTAAGC

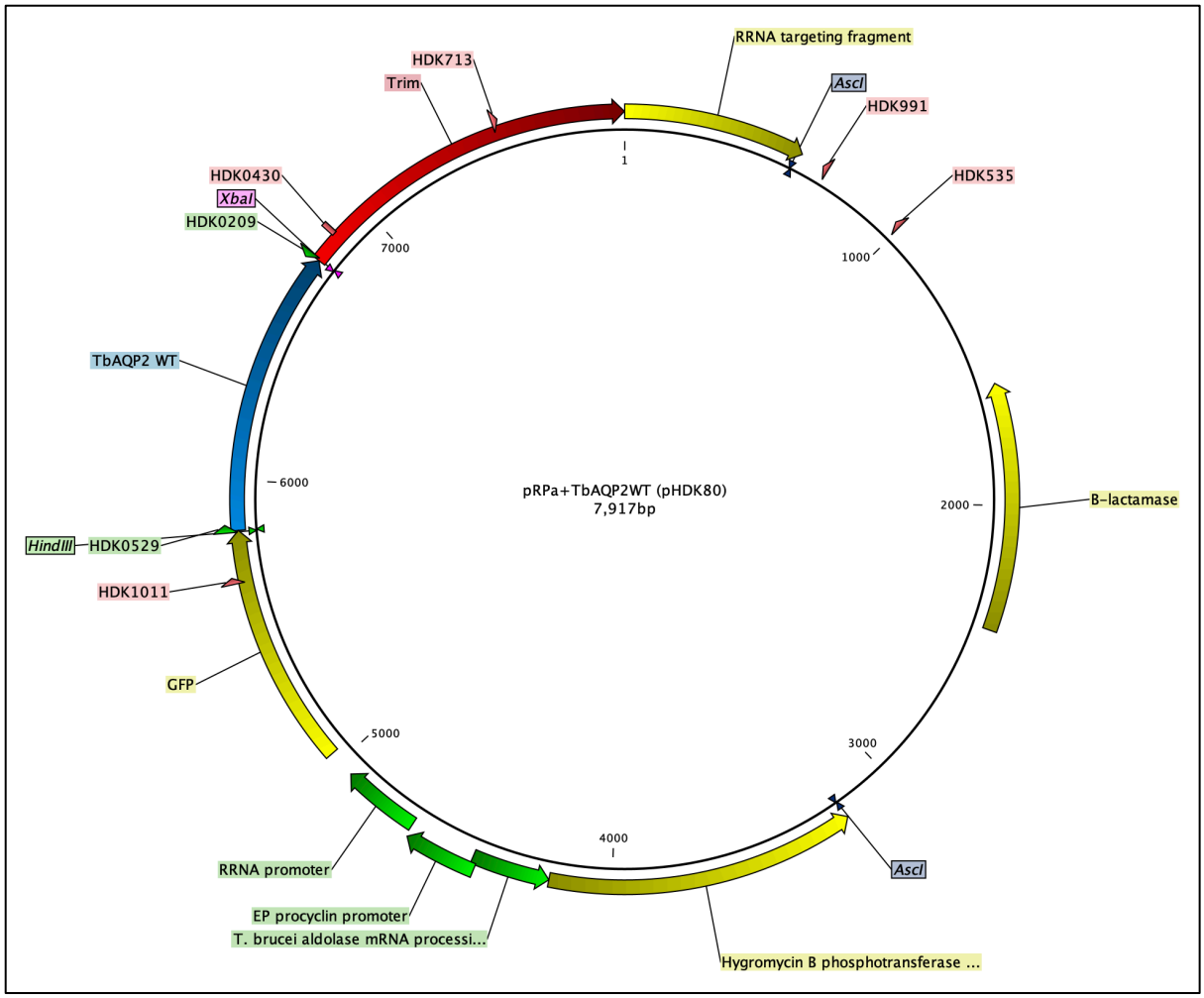

Figure 2.1: Plasmid map of *T. brucei* expression vector pRPa$^{GFP\text{-}TbAQP2\ WT}$ (pHDK80).
The map shows the *Tb*AQP2 WT gene and the vector confers hygromycin resistance to the transfected cells. The rRNA targeting fragment and Hygromycin B phosphotransferase ensures that the constructs are located to the tagged locus in the *T. brucei* genome. This plasmid was used throughout the study as an original template to generate mutation(s) in the TbAQP2WT. The positions of used primers and restriction sites are highlighted. The plasmid maps were generated by the CLC Genomics Workbench program (QIAGEN Bioinformatics).

2.3.4.2. Cloning of PCR products into pGEM-T Easy vector (subcloning vector)

In order to clone the *Leishmania* major aquaglyceroporin 1 wild-type (*Lm*AQP1 WT) into the final destination vectors (either pRPa or pNUS), the gene was initially subcloned into pGEM-T Easy subcloning vectors (Promega). The *Lm*AQP1 WT gene (LmjF.31.0020) was amplified from gDNA using primers with the required restriction sites using High-fidelity proofreading polymerase Phusion (NEB) (Primers in table 2.3). The PCR product was A-tailed using 2 µl 10 mM dATP, 10 µl GoTaq reaction buffer and 0.2 µl GoTaq polymerase (Promega). A-tailing was achieved by incubating

the reaction mix at 72 ºC for 15 min. After incubation, the product was then separated by electrophoresis, using a 1% agarose gel, and visualized with SYBR Safe DNA gel stain (Invitrogen) under a UV light transilluminator (UVP Inc). The expected band size at 959 bp (*Lm*AQP1 WT) was cut out from the agarose gel under ultraviolet (UV) light. The DNA was purified using the NucleoSpin Gel and PCR clean-up Kit (Macherey-Nagel) exactly as recommended by the manufacturer, and ligated into the pGEMT Easy in 10 µl reaction for a ratio of 3:1 insert:vector using the following conditions: 5 µl 2× rapid ligation buffer, 1 µl vector (50 ng), 1 µl T4 DNA Ligase (3 Weiss units/µl), 3 µl insert DNA (50 ng). The mixture was incubated overnight at 4 ºC.

Following ligation, the pGEM-T Easy subcloning vector containing our gene of interest (GOI) was transformed into XL1-Blue competent *E. coli* cells using a heat shock, as follows. The XL1-Blue competent *E. coli* cells were thawed on ice in a 1.5 ml tube (Eppendorf) for ~15 min. 5 µl of the ligation production was added to the tube. The tube was gently flicked 4-5 times to mix. The mixture was placed on ice for 30 min, following by a heat shock for 45 s at 42 ºC. The mixture was then placed on ice for 2 min. 200 µl of room temperature SOC was added into the mixture and was incubated at 37 °C for one h with shaking at 250 rpm. The cells were gently flicked and a volume of 50-100 µl was spread onto a selection plate (LB agar containing 100 µg/ml ampicillin) and incubated at 37 ºC overnight. Next day, colonies from the overnight transformation were screened by PCR using forward primer M13F (5'-CAGGAAACAGCTATGAC-3') and reverse primer M13R (5'-GTAAAACGACGGCCAG-3') to confirm the presence of the target gene. Positive colonies with the correct band size were incubated overnight at 37 ºC in LB containing 100 µg/ml ampicillin. The plasmid extraction kit (Macherey-Nagel) was used to purify the plasmid DNA from the culture according to the manufacturer's instructions, and was sent for Sanger sequencing (Source BioSciences, Glasgow, UK) for sequence confirmation.

Table 2.3: Primers used for cloning of *Lm*AQP1 gene into pGEM-T Easy vector.

Gene	Primer	Direction	Res. Site	Sequence 5' – 3'
*Lm*AQP1	HDK1515	Forward	*Bgl*II	ggccAGATCTATGAACTCTCCTACAAC
*Lm*AQP1	HDK1516	Reverse	*Xho*I	CTCGAGCTAACAGCTGGGCGGAA
*Lm*AQP1	HDK1517	Forward	*Hind*III	ggccAAGCTTATGAACTCTCCTACAAC
*Lm*AQP1	HDK1518	Reverse	*Xba*I	aatcTCTAGACTAACAGCTGGGCGGAA
*Lm*AQP1	HDK1519	Forward	-	ATGAACTCTCCTACAACCATGCC
*Lm*AQP1	HDK1520	Reverse	-	CTAACAGCTGGGCGGAATGAT

Lower case sequence: Random nucleotides, to facilitate directly digestion by restriction enzymes.
Underlining sequence: Restriction site.
Upper case sequence: Gene of interest primer.

2.3.4.3. Generation of pRPa construct (final vector) for *T. b. brucei* expression

The verified, correct DNA sequences of the inserted *Lm*AQP1 gene in the pGEM-T Easy subcloning vector were digested using appropriate restriction enzymes and ligated into the expression vector pRPa (final vector). *Lm*AQP1 was digested out from the plasmid pHDK269 (Appendix 3) (based on the pGEM-T subcloning vector) and was ligated to the backbone of pRPa vector after dropping out the *Tb*AQP2 gene from the plasmid pHDK80 to give pHDK271 (Figure 2.2). The procedure was performed as follows: from bacterial cultures, the vector DNA obtained by miniprep was digested with the required restriction enzymes *Hin*dIII and *Xba*I (NEB, Hitchin, UK) overnight at 37 °C. The reaction was made in a total volume of 100 µl, containing approximately 25 µg of purified DNA, 1× restriction buffer and 2 µl of restriction enzyme and ddH_2O. The digested products were run on a 1% agarose gel and separated by electrophoresis, at 120 V for 45 min. The desired bands were identified by viewing the gel under ultraviolet (UV) light. Bands of the correct size for the DNA fragments for each of the backbone (pRPa) and the gene (*Lm*AQP1) were cut out

from the agarose gel and the DNA was purified using the NuceoSpin gel extraction kit. The ligation reactions were performed exactly as described in section (2.3.4.2) keeping the same ratio (3:1 insert:vector). Ligation productions were then transformed into *E. coli* XL1-Blue cells exactly as explained in section (2.3.4.2). Colonies were screened by PCR using forward primer HDK1011 and HDK430 (Table 2.4) to confirm insertion. Positive clones were cultured in 10 ml LB broth at 37 ºC overnight in the shaking incubator. For confirmation of correct integration in the vector, plasmids were extracted by miniprep (Macherey-Nagel) according to the manufacturer's instructions, and sent for sequencing with primers HDK1519 and HDK1520 (Table 2.4). After sequence confirmation, positive clones of the plasmid were linearised with *Asc*I (NEB, Hitchin, UK) prior to transfection into the *tbaqp1-2-3* null cells. For this, the DNA samples were run on a 1% agarose gel in order to extract the desired band. The samples were cleaned up using the NucleoSpin Gel extraction kit (Macherey-Nagel) according to the manufacturer's instructions, and kept at – 20 ºC until use.

Table 2.4: Primers for confirmation of the pRPa$^{LmAQP1\ WT}$ expression construct used before and after the transfection.

Primer name	Direction	Position	Sequence (5' – 3')
HDK1519	Forward	*Lm*AQP1 WT gene	ATGAACTCTCCTACAACCATGCC
HDK1520	Reverse	*Lm*AQP1 WT gene	CTAACAGCTGGGCGGAATCAT
HDK1011	Forward	located 205 bp upstream of the open reading frame (ORF) of the gene of interest (GOI) in the plasmid backbone	TGCCCGACAACCACTACCTG
HDK430	Reverse	located 100 bp downstream of the open reading frame (ORF) of the gene of interest (GOI) in the plasmid backbone	TAACCAACCTGCAGGCG

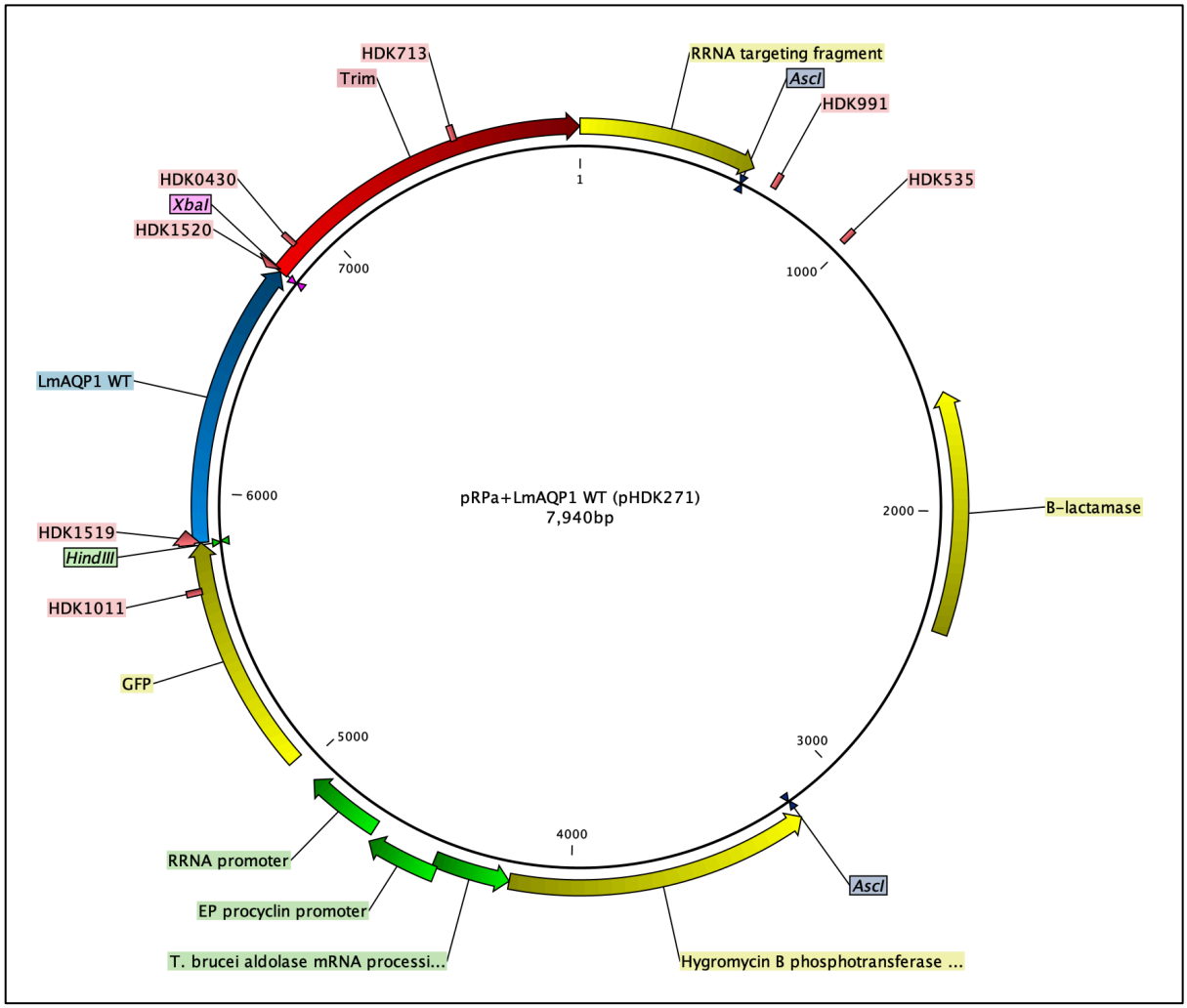

Figure 2.2: The pHDK271 (pRPa+LmAQP1) plasmid map.
The map shows the full *Lm*AQP1 gene, primers, restriction sites and the hygromycin antibiotic cassette.

2.3.4.4. Generation of pNUS-HcN plasmid (final vector) for *L. major* expression

The pNUS-HcN is a non-integrative vector (episomal) and was used to express gene of interest into the *Lm*AQP1 null strain. After verification of the pHDK270 (Appendix 4) (pGEMT containing *Lm*AQP1 WT) by Sanger sequencing, the *Lm*AQP1 gene was digested from the pHDK270 using the *Bgl*II and *Xho*I restriction enzymes (NEB), and cloned into pNUS-HcN using the restriction enzymes *Bgl*II on the 5′ end and *Xho*I on the 3′. The gene was then ligated into the pNUS-HcN backbone to give pHDK272 (Figure 2.3). The procedure of the digestion, ligation and transformation was performed exactly as described in (section 2.3.4.2), except for the digestion with the *Bgl*II and *Xho*I restriction enzymes. Colonies of transformants (containing

plasmids) were confirmed by PCR using HDK1519 and HDK1520 primers (Table 2.5) to confirm insertion. Positive clones were cultured in 10 ml LB broth overnight in the shaking incubator at 37 ºC. The generated plasmids were extracted by miniprep (Macherey-Nagel) according to the manufacturer's instructions, and sent for Sanger sequencing (Source BioScience, Nottingham, UK) with HDK851 and HDK340 primers (Table 2.5) to check the sequence and correct integration in the vector.

Table 2.5: Primers for confirmation of the pNUS$^{LmAQP1\ WT}$ expression construct used before and after the transfection.

Primer name	**Direction**	**Position**	**Sequence (5' – 3')**
HDK1519	Forward	*Lm*AQP1 WT gene	ATGAACTCTCCTACAACCATGCC
HDK1520	Reverse	*Lm*AQP1 WT gene	CTAACAGCTGGGCGGAATCAT
HDK851	Forward	located 152 bp upstream of the open reading frame (ORF) of the gene of interest (GOI) in the plasmid backbone.	GCGCGTGTCCTTTTCGAGCAAACAGC
HDK340	Reverse	located 71 bp downstream of the open reading frame (ORF) of the gene of interest (GOI) in the plasmid backbone.	CGTGGAGCAGCTGAAGGACA

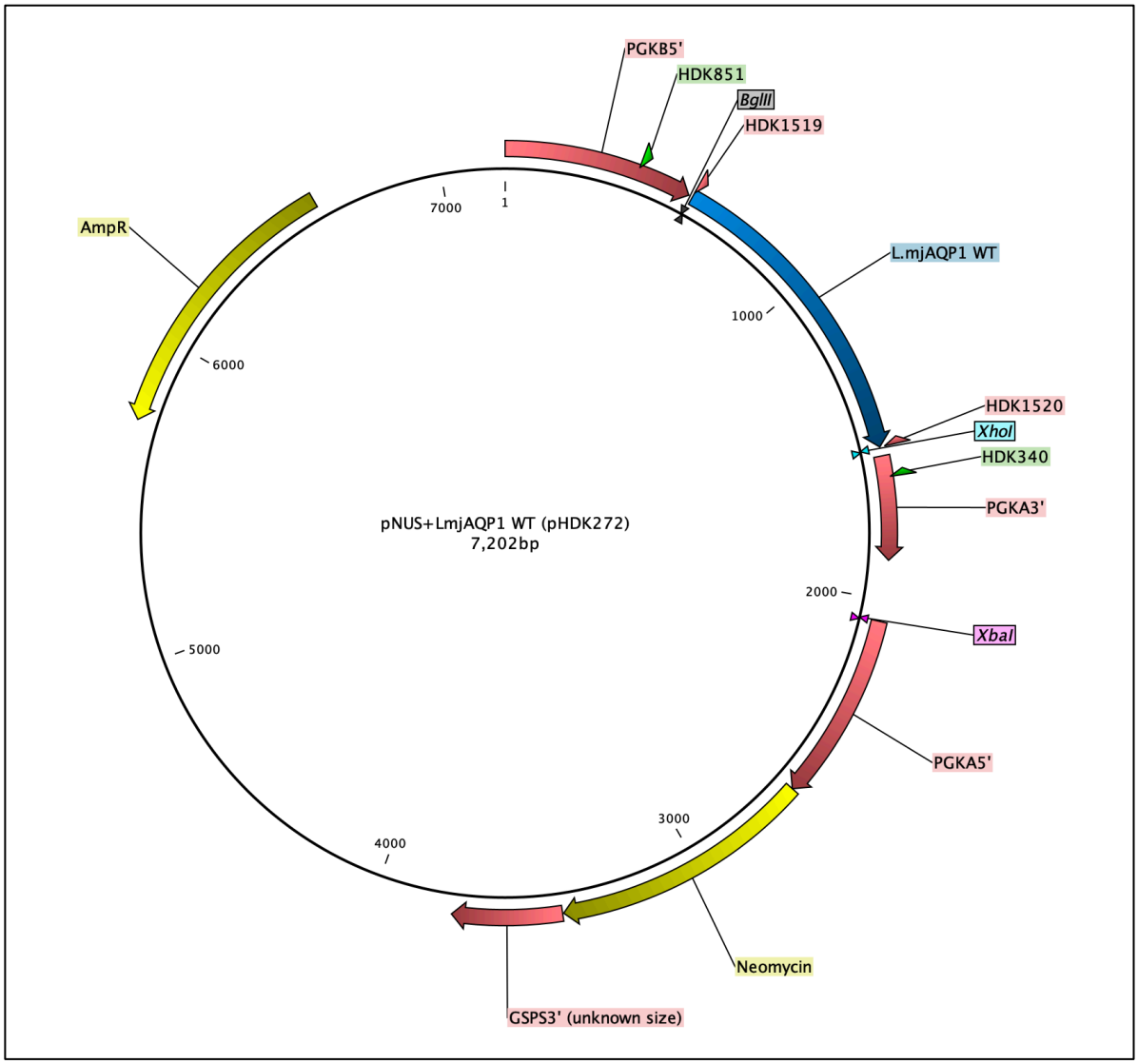

Figure 2.3: The pHDK272 (pNUS+LmAQP1) plasmid map.
The map shows the full *Lm*AQP1 gene, primers, restriction sites and the neomycin antibiotic cassette.

2.4. DNA sequencing

2.4.1. Preparation of sample for sequencing

In order to prepare samples for sequencing, DNA samples were cleaned up using the purification kit (Macherey-Nagel). Volume of the sample 1-2µl was placed onto the pedestal of a Nanodrop spectrophotometer (ThermoFisher Scientific) to measure the purity and the concentration of the DNA. The DNA samples were then prepared exactly as recommended by Source Bioscience as following. For sequencing of plasmid, 5 µl per reaction of both primers at 3.2 pmol/µl and plasmid DNA at 100

ng/µl was used. For PCR product sequence confirmation, 5 µl per reaction was also sent for both primers, at 3.2 pmol/µl, and DNA at 10 ng/µl per 500 bp of the PCR product.

2.4.2. Sequence analysis and alignments

The nucleotide and amino acid sequences for gene of interest (GOI) were imported from TriTrypDB (tritrypdb.org/tritrypdb) or GeneDB (genedb.org) databases. The CLC Genomic workbench software (version 7.0, developed by CLC bio) was routinely used to create alignments and sequence analysis.

2.5. Transfection

2.5.1. In *Trypanosoma brucei*

Prior to transfection, the generated expression construct pRPa (containing our gene of interest and a hygromycin resistance cassette) was digested with *Asc*I (NEB) to linearize the plasmid. Following the digestion, the products were run on 1% agarose gels to confirm the correct length of the desired fragment of the plasmid which was estimated to be around 5.3 kb for the DNA expression cassette. The DNA samples (expression cassette) were extracted from the gel and cleaned up using the NucleoSpin Gel extraction kit (Macherey-Nagel) according to the manufacturer's instructions. The samples were then precipitated with ethanol overnight at 20 ºC, dried and resuspended in 10 µl of sterile water. Bloodstream form of the desired cell line either *aqp2/aqp3* null or *aqp1/aqp2/aqp3* null were cultured and density of 1×10^7 cells/ml were washed in 100 µl Human T-Cell solution and resuspended in 10 µg of the digested plasmid. The mixture was transferred into a cuvette (Amaxa) for transfection. Using an Amaxa Nucleofector (Amaxa AG, Cologne, Germany), the program X-001 was used for electroporation of the cells, which were immediately transferred to a warm medium of HMI-9 and left to recover for 6-18 hours at 37 ºC and 5% CO_2. Appropriate antibiotic (2.5 µg/ml hygromycin) was added before the cells were cloned out using limiting dilutions of (1/10, 1/25 and 1/100) into 96-well plates into 96-well. After around seven days of incubation with the selection

antibiotic, clones (surviving cells) were picked up from the plates, cultured in 5 ml fresh media with the antibiotic (2.5 µg/ml hygromycin). After several passages (3 - 5 passage), the gDNA of clones was extracted using the standard protocol and the Nucleospin tissue kit (Macherey-Nagel). The positive clones were assessed by PCR to confirm correct integration, and to check for the presence of the desired gene. The PCR products cleaned up using the PCR purification kit (Macherey-Nagel). Sanger Sequencing was used to confirm the sequence (SourceBioscience, Glasgow, Scotland, UK).

2.5.2. In *Leishmania major*

Since the plasmid pNUS-HcN was for episomal expression, the generated plasmid DNA (pHDK272) was directly transfected without digestion (As circular plasmid). 20 µg of plasmid DNA was precipitated with ethanol and resuspended in 20 µl of sterile water. Log phase cells of *L. major* AQP1 null promastigotes (5×10^7 cells) were pelleted by centrifugation at 1000 × *g* for 10 min. The pellet was then resuspended in 100 µl Human T-cell buffer, and mixed with the 10 µl precipitated DNA. To electroporate the cells, the program U-033 of the Amaxa Nucleofector II electroporator (Amaxa Biosystems) was used to create the desired strains. Cells were then transferred to pre-warmed HOMEM medium containing 10% FBS and were left to recover overnight in 25 ºC incubator. In the following day, Neomycin G418 (50 µg/ml) was added and the cells were plated out using limited dilutions (1:20, 1:100, 1:200) to generate individual clones. Positive clones produced from this transfection were cells that were resistant to antibiotic Neomycin (G418). The gDNA of the generated clones were extracted using Nucleospin Tissue kit (Macherey-Nagel) according to the manufacturer's instructions. PCR confirmations were performed to confirm correct integration, and to check for the presence of the desired gene.

2.6. Quantitative real-time PCR (qRT-PCR)

2.6.1. Preparation of RNA from *T. brucei*

Following the instructions provided by the manufacturer of the NucleoSpin RNA kit, RNA purifications were prepared from *T. brucei* 2T1 and *CRK12* cell lines. Briefly, 5 x 10^6 cells were centrifuged for about 10 minutes at 1300 × *g*, and the supernatant was discarded. This was followed by lysing the cells by addition of 350 µl Buffer RA1 and 3.5 µl ß-mercaptoethanol reducing agent, before vortexing vigorously. In order to adjust the RNA binding conditions, 350 µl of 70% ethanol was added to the samples and the contents were pipetted up and down to homogenize. This was followed by loading the samples onto the NucleoSpin column for DNA binding, by centrifuging the contents at 11,000 × *g* for about 30 s. To prevent contamination with DNA, it was necessary to intermittently change gloves and collection tube. To desalt the silica membrane, 350 µl of Membrane Desalting Buffer was added into the tube, and centrifuged at 11,000 × *g* for one minute. The remaining DNA in the mix were removed by applying rDNase reaction mixture on the column, followed by incubation at room temperature for about 15 minutes. A washing buffer was used to clean the column before leaving it to dry. Elution of the RNA was done using nuclease-free water, and placing the tubes on ice to prevent RNA degradation. The concentration of RNA was then checked using the NanoDrop spectrophotometer (ThermoFisher Scientific). All samples were collected and stored at -20 ºC for later use.

2.6.2. Complementary DNA synthesis from RNA

Conversion of RNA to complementary DNA (cDNA) was accomplished by the use of SuperScript III Reverse Transcriptase (RT, Invitrogen) as described by Ali and Field (2013). Control samples in which there was no RT added were performed in parallel. There were three phases involved in the production of cDNA. In the first phase, 500 ng of Random primers (Invitrogen), 2 µl of 10 mM dNTPs, 1 µg RNA template and sterile water were mixed to a volume of 29 µl for hot mixing at 65 ºC for 5 minutes. In the second phase, 8 µl of 5× First-Strand Buffer, 1 µl of SuperScript III RT and 2 µl 0.1 M DTT were added to the mixture. Water was added to samples without RT instead of SuperScript III RT. All the samples were then incubated at a temperature

of 25 ºC for 5 min, followed by incubation at 50 ºC for 45 minutes, and then at 70 ºC for 15 minutes. In the third phase, any remaining template of RNA were removed by adding 1 µl (2U) of E. coli RNase H, followed by incubation at a temperature of 37 ºC for 20 minutes. This resulted in pure cDNA that was stored at -20 ºC until use.

2.6.3. Quantitative RT-PCR

Upon generating the required cDNA, quantitative real time PCR (qRT-PCR) was performed using the GoTaq qPCR Master mix (Promega). Using Primer3®, primers were designed (Table 2.6), and efficiency evaluated using the previously described method (Pfaffl, 2001). Endogenous gene *GPI8* (housekeeping gene) with its primers was deployed as control (Table 2.6). The reaction was performed in 25 µl, made up of 12.5 µl of GoTaq master mix, 3.5 µl of water, 2 µl each of 2.5 mM forward and reverse primer, and 5 µl of cDNA where the ratio of dilution of the converted cDNA is 1:10. The samples were then subjected to a very brief vortex and centrifuge before putting them into the machine. The DNA amplification was done in a 7500 Real Time PCR System (Applied Biosystems). The specific reaction conditions were as follows: 50 ºC for 2 min, 95 ºC for 10 min, 45 cycles of 95 ºC for 15 sand 60 ºC for 1 min. A dissociation curve was used to show the amplification of only one product at a time. Samples in which reverse transcriptase was not added or lacked cDNA served as controls. The whole experiment was performed independently on three occasions, from culturing of the cell lines to isolation of RNA.

Table 2.6: Primers used to quantify gene expression by qRT-PCR.

Gene	Primer	Direction	Sequence
CRK12	HDK1779	Forward	5'-AGCGGTCTTGGTCTGTGAAC-3'
CRK12	HDK1780	Reverse	5'-GACATCCAACGGTTTATCTG-3'
GPI8	HDK131	Forward	5'-CGAAGCGCATTTGGATAG-3'
GPI8	HDK132	Reverse	5'-AGCGGTCTTGGTCTGTGAAC-3'

2.7. Drug sensitivity assay

As described by Gould *et al*. (2008), sensitivity assays of both *Trypanosoma* and *Leishmania* species to various drugs using the viability dye resazurin (Alamar Blue) are based on the reduction of resazurin sodium salt (blue, non-fluorescent) to resorufin (pink, fluorescent) by surviving but not by dead cells.

For *T. brucei* strains, in 96-well plates containing doubling dilutions of test compounds were set up in 100 µl HMI-9/FBS medium, each over 2 rows (23 concentrations) The top concentrations were usually 100 µM in culture medium; the last well received 100 µl medium as no- drug control. To each well, 100 µl of 2×10^5 cells/ml were added, and the plates were incubated for 48 h at 37 ºC in 5% CO_2, after which 20 µl of 0.5 mM of resazurin was added and the plates incubated under the same conditions for a further 24 h. Fluorescence intensity was read using a FLUOstar OPTIMA (BMG Labtech, Germany) at wavelengths of 544 nm for excitation and 620 nm for emission.

For *Leishmania* promastigotes strains, cultured in HOMEM/10% FBS, the procedure was identical, except that 100 µl of 2×10^6 cells/ml was added per well, the incubation time before addition of resazurin was 72 h at 25 ºC, and incubation with resazurin was for a further period of 48 hours. Data was plotted to a sigmoid curve with variable slope using Prism 6.0 (GraphPad) and 50% effective concentrations (EC_{50}) were determined for all compounds in 3 – 5 independent experiments.

2.8. Transport Assay

Transport assays - Transport of [^{3}H]-pentamidine was performed exactly as previously described for various permeants (Wallace et al., 2002; Bridges et al., 2007; Teka et al., 2011) in a defined assay buffer (AB; 33 mM HEPES, 98 mM NaCl, 4.6 mM KCl, 0.55 mM $CaCl_2$, 0.07 mM $MgSO_4$, 5.8 mM NaH_2PO_4, 0.3 mM $MgCl_2$, 23 mM $NaHCO_3$, 14 mM glucose, pH 7.3). [^{3}H]-pentamidine was custom-made by GE Healthcare Life Sciences (Cardiff, UK) with a specific activity of 88 Ci/mmol. Incubations of bloodstream form trypanosomes with 30 nM of this label (unless

otherwise indicated) were performed in AB at room temperature for 60 s (unless otherwise indicated) and terminated by addition of 1 ml ice-cold 'stop' solution (1 mM unlabelled pentamidine (Sigma) in AB) and immediate centrifugation through oil (7:1 dibutylphthalate:mineral oil v/v (both from Sigma)) to separate the cells from the aqueous buffer. Transport was assessed in the presence of 1 mM adenosine to block uptake through the P2 aminopurine transporter; adenosine does not affect HAPT1-mediated transport (De Koning, 2001a; Bridges et al., 2007). This mixture was incubated for predetermined times. The reaction was stopped by the addition of 750 µl of an ice-cold 1 mM solution of unlabelled permeant. The tubes were centrifuged at 13,000 ×g for 1 min. The microfuge tube was then placed in liquid nitrogen for flash freezing; the bottom of the frozen tubes, containing the cell pellet, was cut off and collected in a scintillation vial. 250 µl of 2% sodium dodecyl sulphate (SDS) was added to the vial to solubilise the cells. The scientillation vials with cell pellets and SDS were left at room temperature for 30 min. A volume of 3 ml scintillation fluid (Optiphase HiSafe III) was added to each vial, which were then incubated overnight at room temperature. Inhibition assays were performed routinely with 6 - 10 different concentrations of inhibitor over the relevant range, diluting stepwise by one third each time, in order to obtain a well-defined and accurate sigmoid plot and IC_{50} value (inhibitor concentration giving 50% inhibition of pentamidine transport; calculated by non-linear regression using Prism 6.0 (GraphPad), using the equation for a sigmoid curve with variable slope). Highest concentration was usually 1 mM unless this was shown to be insufficient for good inhibition, or when limited by solubility. K_i values were obtained from IC_{50} values using: $K_i = IC_{50}/[1 + (L + K_m)$, in which L is the [^{3}H]-pentamidine concentration and K_m the Michaelis-Menten constant for pentamidine uptake by HAPT1 (Wallace *et al*, 2002). The Gibbs Free energy of interaction ΔG^0 was calculated from $\Delta G^0 = -RT\ln K_i$, in which R is the gas constant and T is the absolute temperature (Wallace *et al*, 2002).

Transport of [^{3}H]-glycerol and [^{3}H]-suramin was performed essentially as for [^{3}H]-pentamidine. For [^{3}H]-glycerol (American Radiolabeled Chemicals, 40.0 Ci/mmol), 10^7 BSF *T. brucei* were incubated with radiolabel at a final concentration of 0.25 µM, for one minute. When the effect of Carbonyl cyanide m-chlorophenyl hydrazone

(CCCP) was studied, CCCP was added 3 minutes prior to the addition of the radiolabel. [^{3}H]-suramin (American Radiolabeled Chemicals, 20.0 Ci/mmol) was also used at 0.25 μM final concentration, using 15 min incubations I the presence and absence of 100 μM unlabelled suramin (used as saturation) control.

2.9. Protein Model

To facilitate visualisation of the TbAQP2 channel and the relative proximity of amino acid residue sites to the selectivity filter (Baker et al., 2013), a 3D homology model of the TbAQP2 protein structure was generated. The FASTA format of the protein sequence was obtained from the NCBI database (https://www.ncbi.nlm.nih.gov/). Best representation of the protein was sought considering the FASTA sequence using the NCBI BLAST tool (https://blast.ncbi.nlm.nih.gov/), with 'chimeric aquaglyceroporin 2/3 [*Trypanosoma brucei gambiense*]' selected as the most similar template to the TbAQP2 protein based on a zero 'e-value', and the highest sequence percentage identity and query coverage. Cross-reference with the SWISS-MODEL software (Waterhouse et al., 2018) ensured that a model had already been generated for this homologous protein structure (UniProtKB AC: U5NJF5). The model was then visualised with PyMOL 2.2 (Schrödinger), with only the original FASTA sequence highlighted in the images produced. Amino acid residue sites were highlighted, along with residue sites that have already been established to constitute the selectivity filter of *Tb*AQP2 (Baker et al., 2013).

Chapter 3 Mutations in TbAQP2 and TbAQP3 affect pentamidine uptake by *Trypanosoma brucei*

3.1. Introduction

Species belonging to the *Trypanosoma brucei*-group can lead to severe infections such as sleeping sickness (humans) and nagana (animals) (Giordani et al., 2016); Büscher et al., 2017). The treatment is determined by the trypanosome subspecies that causes the disease, the host, and the stage of the disease (Giordani et al., 2016; De Koning, 2020). However, various anti-protozoan medications are considered intrinsically cytotoxic, and they are believed to obtain their selectivity through favoured uptake by the pathogen rather than of the host cells (Munday et al., 2015a; De Koning, 2020). In contrast, drug resistance is attributed to the loss of specific drug transporters (Barrett et al., 2011; Baker et a.l, 2013; Munday et al., 2015a; and De Koning, 2020). Drug resistance has been observed in a wide range of trypanocides, such as the fluorinated amino acid analog eflornithine used to treat human cerebral trypanosomiasis (Vincent *et al*, 2010), melaminophenyl arsenicals (melarsoprol for cerebral stage human and cymelarsan for animal trypanosomiasis (Carter & Fairlamb, 1993; Bridges et al., 2007), and diamidines (pentamidine, diminazene) (Carter et al., 1995; De Koning, 2001a; De Koning et al., 2004; and Bridges et a.l, 2007). Consequently, it is imperative to explore transporters when studying the anti-protozoal drug discovery, as well as when investigating drug resistance (Lüscher et al., 2007; Munday et al., 2015a).

Several researchers have conducted various studies to gain more insights into anti-protozoal drug resistance. For instance, Rollo & William (1951) first identified melarsoprol-pentamidine cross-resistance (MPXR) in *Trypanosoma brucei*, and was connected MPXR to decreased uptake instead of shared intracellular target(s) (Frommel & Balber, 1987). The aminopurine transporter TbAT1/P2 was the first transporter associated with the MPXR (Carter & Fairlamb, 1993; Mäser et al., 1999; Munday et al., 2015b). However, two other transporters have been affiliated with melarsoprol-pentamidine cross-resistance to include Low-Affinity Pentamidine Transporter (LAPT1) and High-Affinity Pentamidine Transporter (HAPT1) (De Koning, 2001a; De Koning & Jarvis, 2001; Bridges et al., 2007). HAPT1 is considered the main determinant of MPXR and was identified as Aquaglyceroporin 2 (TbAQP2) through an RNAi library screen (Baker et al., 2012, 2013; Munday et al., 2014). The two motifs

of the asparagine-proline-alanine sequences (NPA), and the aromatic-arginine (ar/R), in the aquaporin water channel family, are the most important structural domains that play a crucial role in water-selective permeation. These two regions have been proposed as filters that block solutes larger than water and charged molecules from moving through. According to crystallographic studies, the two NPA motifs in the narrow central constriction of the pore, contribute to a monomeric pore structure that enables selective, bi-directional, and single-file transport of water in classical AQPs (Sui et al., 2001) and water and glycerol in aquaglyceroporins (Jensen et al., 2001). The aromatic-arginine region, which is narrower than the central NPA constriction and acts as a selectivity filter on the extracellular side of the AQP channel, blocks the entry of molecules larger than water (de Groot & Grubmu; 2005, 2001). Uniquely, TbAQP2 allows substance with high molecular weight due to its highly unusual selectivity filter that is deemed to lack the canonical aromatic/arginine (ar/R) and full NPA/NPA motifs, which make it become a much wider pore (Baker et al., 2012; Munday et al., 2014, 2015a). Introducing TbAQP2 into Leishmania promastigotes significantly increased their sensitivity to pentamidine and melarsen oxide (Munday et al., 2014). Moreover, studies have demonstrated various MPXR laboratory strains of *T. brucei* to have deleted the AQP2 gene and strains with a chimeric AQP2/TbAQP3 gene that is regarded to be different from the AQP2 gene (Munday et al., 2014). This chimeric AQP2/TbAQP3 gene consists of the full, classical ar/R and NPA/NPA selectivity filter motifs, in addition to lacking the capability of transporting either pentamidine or melaminophenyl arsenicals (Munday et al., 2014). Correspondingly, such deletions and chimeric genes have been noted and isolated from individuals with sleeping sickness resistant to melarsoprol treatment (Graf et al., 2013; Pyana Pati et al., 2014). These chimeric genes and deletions also failed to show pentamidine sensitivity when expressed in a *tbaqp2-tbaqp3* null cell line (however, the wild-type TbAQP2 conferred sensitivity) (Munday et al., 2014; Graf et al., 2015). Nevertheless, the mechanism associated with TbAQP2-mediated drug transport in the trypanosomes is still unclear. Therefore, this study aimed to conduct a mutational analysis to determine any role of amino acids along the TbAQP2 pore in assisting in sensitivity and/or uptake of pentamidine. To resolve this, mutation(s) related to *Tb*AQP2 and *Tb*AQP3 genes were

synthesized, expressed, and preserved for characterization focusing on drug sensitivity and uptake capability.

3.2. Results

3.2.1. Positive selection for investigation of the structural determinants of AQP2 for pentamidine transport

Three aquaglyceroporins (TbAQP1-3) exist in the *T. brucei* and are deemed to contribute to the transport of various small solutes, including urea, glycerol, and water (Benga G, 2009; Jeacock et al., 2017). The TbAQP2 and TbAQP3 are 74% amino acids identical and appear as a tandem pair on chromosome 10. However, TbAQP2 facilitates the uptake of pentamidine, which is not observed in TbAQP3 (Baker et al., 2012; Munday et al., 2014) and in a variety of chimeric *AQP2/3* changes that result in pentamidine resistance (Munday et al., 2014; Graf et al., 2015). A phylogenetic analysis of *AQPs* in African trypanosomes was conducted (kindly created by Dr. Mark Carrington, University of Cambridge). Based on the tree considered consistent with the four species' evolutionary history (Hutchinson & Gibson, 2015) (Figure 3.1), *APQ1* was found to be the ancestral *AQP* as it was expressed in all trypanosome species. A duplication was observed in the common ancestor of *T. suis* and *T. brucei*, following divergence from *T. congolense* and a further duplication to form *AQP2* and *AQP3* in the ancestor of *T. brucei* after divergence from *T. suis*. On the other hand, there was a variation in the number of aquaporins, where one aquaporin was noted in *T. vivax* and *T. congolense*, two in *T. suis*, and three in *T. brucei* and its derivatives.

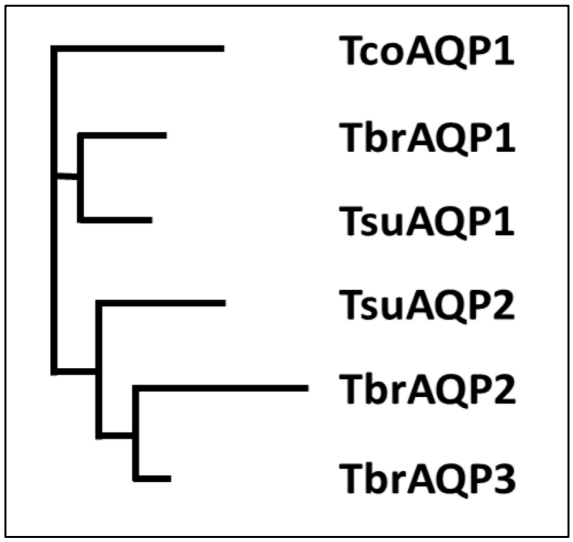

Figure 3.1: Phylogenetic tree of *AQPs* in African trypanosomes; *T. congolense*, *T. b. brucei* and *T. suis*. The tree is a Neighbour-joining tree produced with the lengths of the horizontals proportional to the differences. (Created by Dr. Mark Carrington).

With the exception of *T. brucei* AQP2, all other APQs were found to have the classical NPA/NPA and ar/R AQP selectivity filter elements, indicated by multiple alignments (Figure 3.2). The TbAQP2 and TbAQP3 were observed to be closely related except that TbAQP2 lacks the "aromatic/arginine (a/R)" motif and contains unusual selectivity pore amino acids residues (NSA/NPS/IVLL), unlike TbAQP3 (NPA/NPA/WGYR) (Baker et al., 2013; Figure 3.3). The NPA/NPA is one highly conserved motif of aquaporins and is found in TbAQP3 (not in TbAQP2), where they are deemed to play a significant role in permeant selectivity. The ar/R motif is found in both TbAQP1 and TbAQP3 and is argued to be a part of the larger selectivity filter, mainly WGYR, and distinctively contains $I^{110}V^{249}L^{258}L^{264}$ in TbAQP2 (Baker et al., 2013). In contrast, the AQP3 Tyr-250 accounts for half of the highly conserved aromatic/arginine (ar/R) motif and plays a role in pore restriction as well as proton exclusion (Wu et al., 2009).

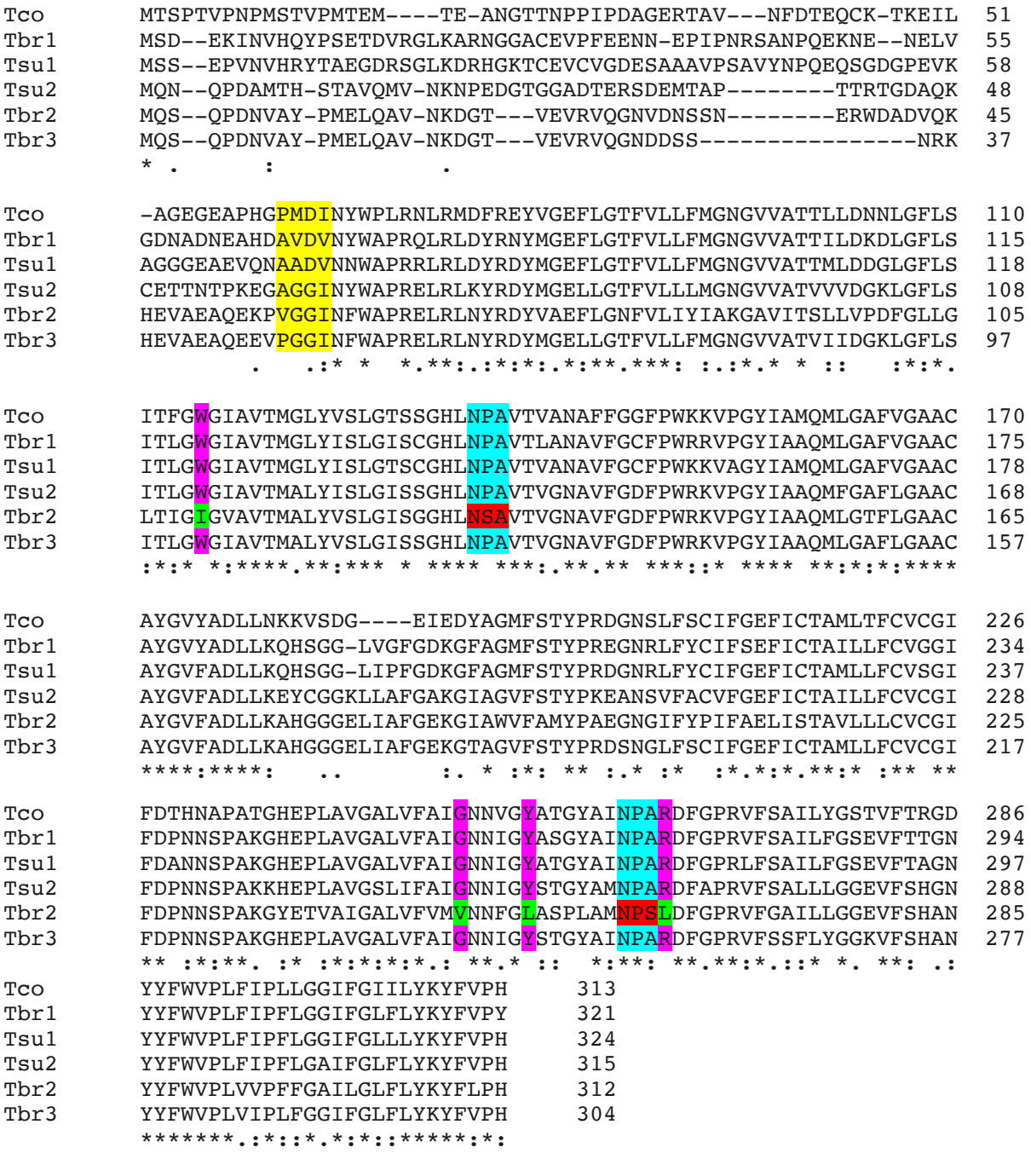

Figure 3.2: Amino acid sequence alignment of aquaporins in African trypanosomes; *T. congolense*, *T. b. brucei* and *T. suis*.

The figure shows the classical AQP selectivity filter elements that present in all of AQPs in African trypanosomes compared to the unique selectivity filter amino acids residues that present in *T. brucei* AQP2. The turquoise highlighting indicates the highly conserved motifs of aquaporins (NPA/NPA), and the red highlighting indicates the unusual motifs (NSA/NPS) present in *T. brucei* AQP2. The pink highlighting indicates the usual residues (WGYR) present in all aquaporins, and the bright green highlighting indicates the uniquely residues (IVLL) in TbAQP2. The yellow highlighting indicates the N-terminus of the sequences used to determine non-synonymous v synonymous ratios (Table 3.1).
*, indicates perfect alignment (fully conserved residue); :, indicates a strong similarity; ., indicates a weak similarity. (Alghamdi et al., 2020).

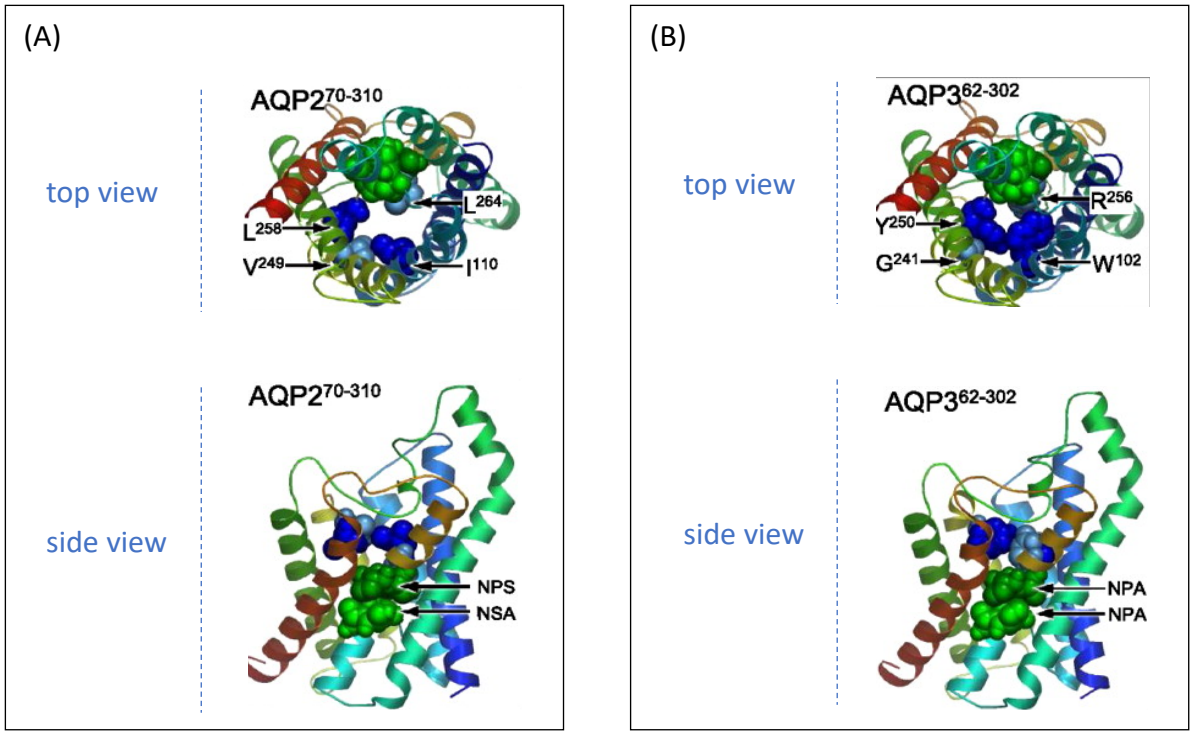

Figure 3.3: Homology models of the TbAQP2 and TbAQP3 protein structures.
The figures show the selectivity filter residues in TbAQP2 (Tb927.10.14170) and TbAQP3 (Tb927.10.14160). (A) top and side views of TbAQP2; the unique selectivity filter IVLL/NSA/NPS motifs are indicated. (B) top and side views of TbAQP3; the classical selectivity filter NPA/NPA/WGYR motifs are indicated. (adapted from Baker et al., 2012).

Investigations were conducted to determine the divergence of *T. brucei AQP2* and *AQP3*, which was achieved by calculating the non-synonymous/synonymous codon ratio (dN/dS) for different *AQPs*, as indicated in Table 3.1. For *T. brucei* versus *T. suis AQP1*, the dN/dS was found to be 0.21, while that of *AQP3* to be 0.30, demonstrating purifying selection. Nonetheless, regarding *T. brucei AQP2* versus *T. brucei AQP3*, the dN/dS was observed to be 2.0, signifying intense selection pressure for divergence on *AQP2* towards an increased size aquaporin's pore.

Table 3.1: The non-synonymous/synonymous codon ratio (dN/dS) calculated for selected comparisons between *T. brucei* and *T. suis* AQPs.

Trypanosoma species	dN/dS
T. brucei AQP1 v *T. suis* AQP1	0.21
T. brucei AQP3 v *T. suis* AQP3	0.30
T. brucei AQP2 v *T. brucei* AQP3	2.00

The ratios were calculated using a region of high confidence alignments from ~amino acid 60 (highlighted in Figure 3.4) to the C-terminus. (calculation made by Dr. Mark Carrington).

3.2.2. Introduction of AQP3 selectivity residues in AQP2 disables pentamidine (and melarsoprol) uptake.

3.2.2.1. Confirmation of the construction and transfection of AQP2 mutants

Selected residues of the classical selectivity filter motifs of the TbAQP3 (ar/R and NPA/NPA) were introduced into the corresponding residues in the selectivity filter of the TbAQP2 pore to test the possible role of these in guiding pentamidine and cymelarsan. The NPA/NPA (TbAQP2$^{S131P/S263A}$), WGYR (TbAQP2$^{I110W/L264R}$) and the AQP3 Tyr-250 (TbAQP2^{L258Y}) mutants were constructed and expressed into *tbaqp2*/*tbaqp3* null cells by Dr. Jane Munday at the De Koning laboratory. To characterise these mutant(s), cells were retrieved from stabilates in liquid nitrogen storage, the presence of the *Tb*AQP2 gene was verified by PCR and confirmed by sequencing for the correct mutation(s). For this, genomic DNA from each cell line was extracted and purified, followed by two PCR reactions that were set up for the confirmation. The first PCR was performed to solely amplify the full *Tb*AQP2 gene using primers HDK529 and HDK209. The second was designed to amplify the gene with a partial fragment of the expression cassette using primers HDK1011 (located 143 bp upstream of the open reading frame of the gene in the plasmid backbone) and HDK430 (located 83 bp downstream of the open reading frame the gene in the plasmid backbone). PCR products were then run on 1% an agarose gel with DNA staining. From the first reaction PCR products were at 950 bp (Figure 3.4 A-B), approximately the size of the *Tb*AQP2 gene (936 bp). Product-sized bands from the second PCR reaction were at ~1250 bp, corresponding to the expected size of the gene with the partial plasmid fragment (1212 bp) (Figure 3.4 C-D). The expected amplification products from the two PCR reactions were indicating successful transfections (See plasmid map (figure 2.1) in section 2.3.4.1; for primers sites).

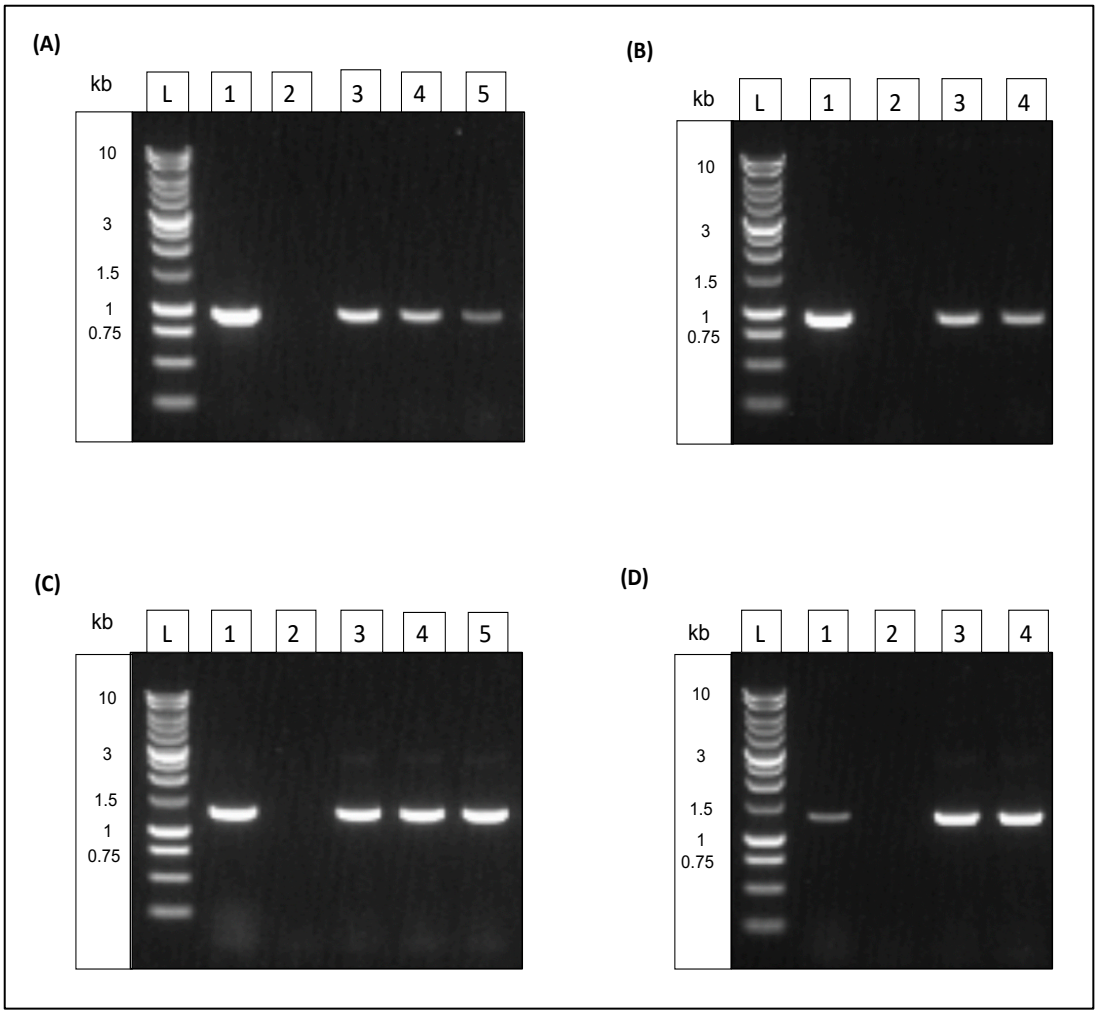

Figure 3.4: Agarose gel electrophoresis of PCR products reveals the presence of the integrated *tbaqp2* (AQP3 selectivity residues) in transfected *tbaqp2/tbaqp3* null cells.
(A) and (B) amplified PCR products at ~939 bp present the full TbAQP2 gene. (A) L: 1kb DNA ladder; 1: TbAQP2 (WT) positive control; 2: TbAQP2 (KO) negative control; 3: TbAQP2 (S131P/S263A); 4: TbAQP2 (L258Y); 5: TbAQP2 (I110W). (B) L: 1kb DNA ladder; 1: TbAQP2 (WT) positive control; 2: TbAQP2 (KO) negative control; 3: TbAQP2 (L264R); 4 (I110W/L264R). Bands in (C) and (D) display fragments at ~1250 bp (TbAQP2 and parts of the expression cassette neighbouring the gene). The order of the samples in (C) are as same as in (A). The order of the samples in (D) are as same as in (B). The positive control (lane 1) in C and D is pRPa$^{GFP\text{-}AQP2\ WT}$ plasmid.

Prior to performing the sensitivity and uptake assays, cell lines were also checked by sequencing. For this, the full *Tb*AQP2 gene was amplified from the genomic DNA of each cell line using a high-fidelity DNA polymerase (New England BioLabs). The products from PCR reactions were purified using a DNA purification kit (Macherey-Nagel) and were then sent for sequencing (SourceBioscience, Glasgow, Scotland, UK) using forward primer (HDK1011) and reverse primer (HDK340). Correct mutation(s) were checked by creating alignments of the amino acid of TbAQP2 WT and the generated TbAQP2 mutant(s) (Appendix 5).

3.2.2.2. Molecular characterization of the introduction of AQP3 residues into the AQP2 selectivity filter.

To assess the effect of introducing the classical selectivity filter motifs of TbAQP3 (ar/R and NPA/NPA) into the TbAQP2 on the pentamidine and cymelarsan susceptibility, the standard protocol of 48 h incubation with the drug, followed by a further 24 h in the presence of the resazurin indicator dye (Alamar blue assay), was performed to determine EC_{50} values. The assay was performed in parallel with the *tbaqp2*/*tbaqp3* null strain (drug-resistant control) and the *tbaqp2*/*tbaqp3* null strain possessing the re-expressed TbAQP2 WT cells (drug-sensitive control). Pentamidine and the melaminophenyl arsenical cymelarsan were the drugs assessed whilst diminazene aceturate and phenylarsine oxide (PAO), which are not TbAQP2 permeants (Graf et al., 2015), were used as positive controls throughout the assessment. The TbAQP2$^{S131P/S263A}$-expressing cells were strongly sensitised to pentamidine ($P<0.0001$ vs *tbaqp2*/*tbaqp3* null) but the EC_{50} was again also significantly different from the TbAQP2WT control ($P<0.05$) (Figure 3.5A). A similar effect was observed for the melaminophenyl arsenical drug cymelarsan (Figure 3.5A), but there was no change in sensitivity to diminazene or PAO. Diminazene is taken up by the TbAT1/P2 transporter (De Koning, 2004) whereas PAO is believed to diffuse directly across the membrane (Fairlamb et al., 1992) (Figure 3.5A). The EC_{50} values of pentamidine and cymelarsan in the mutant L258Y, which has the AQP3 Tyr-250 in the highly conserved aromatic/arginine (ar/R) motif, were also significantly different from both the TbAQP2WT and the *tbaqp2*/*tbaqp3* null controls (Figure 3.5B). Cell lines expressing mutations AQP2^{I110W} and AQP2^{L264R}, either alone or in combination, displayed pentamidine and cymelarsan EC_{50} values that were not significantly different from the *tbaqp2*/*tbaqp3* null controls but highly significantly different from the TbAQP2WT drug-sensitive controls (Figure 3.5 C-E).

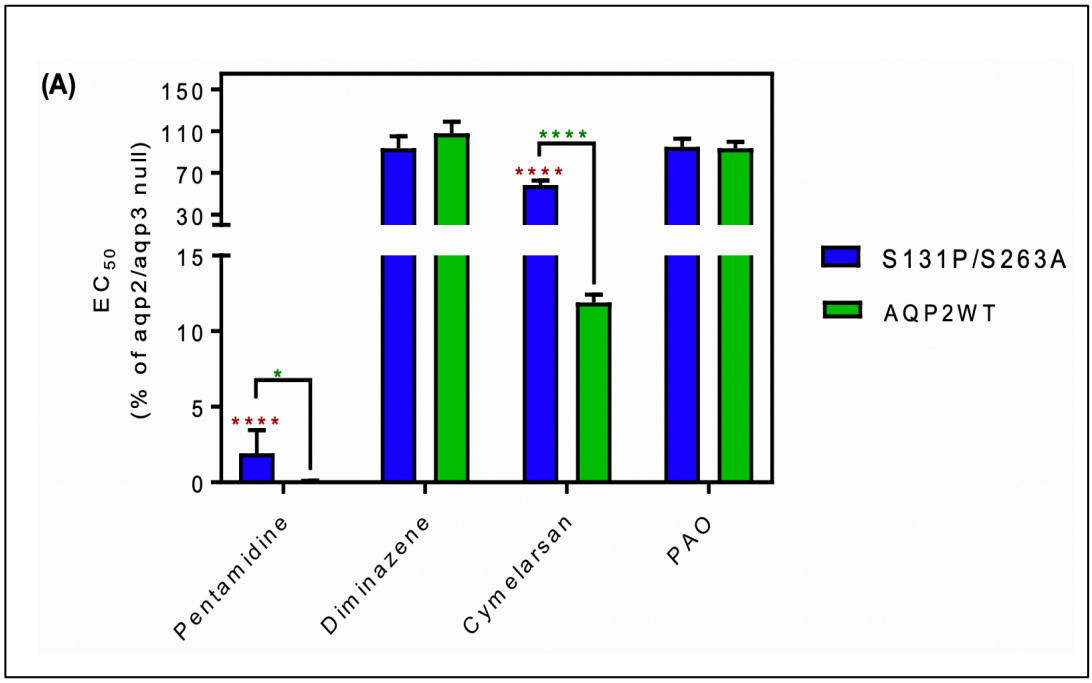
(A)
EC50
(% of aqp2/aqp3 null)
150
110
70
30
15
10
5
0
****
*
****
****
Pentamidine
Diminazene
Cymelarsan
PAO
S131P/S263A
AQP2WT

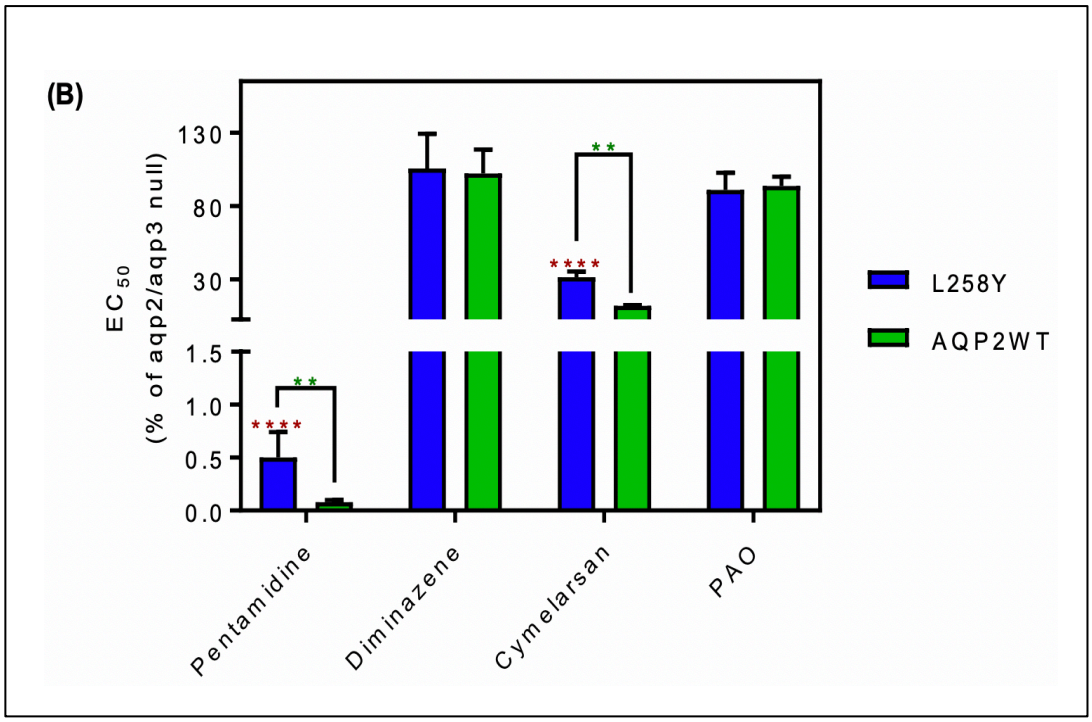
(B)
EC50
(% of aqp2/aqp3 null)
130
80
30
1.5
1.0
0.5
0.0
****
**
****
**
Pentamidine
Diminazene
Cymelarsan
PAO
L258Y
AQP2WT

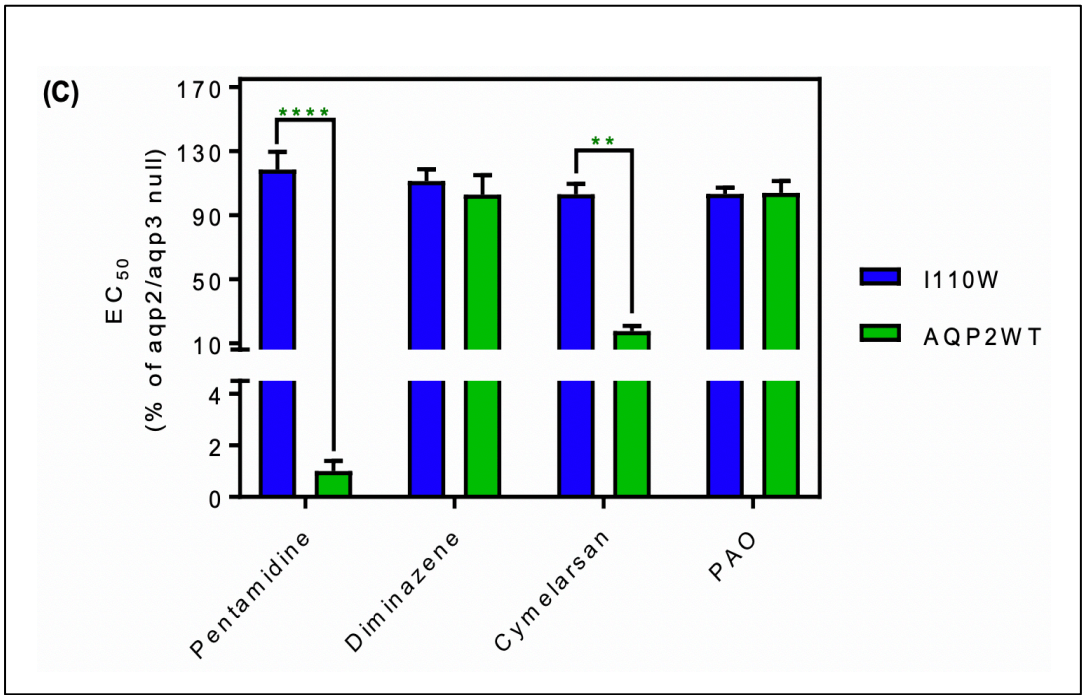
(C)
EC50
(% of aqp2/aqp3 null)
170
130
90
50
10
4
2
0
****
**
Pentamidine
Diminazene
Cymelarsan
PAO
I110W
AQP2WT

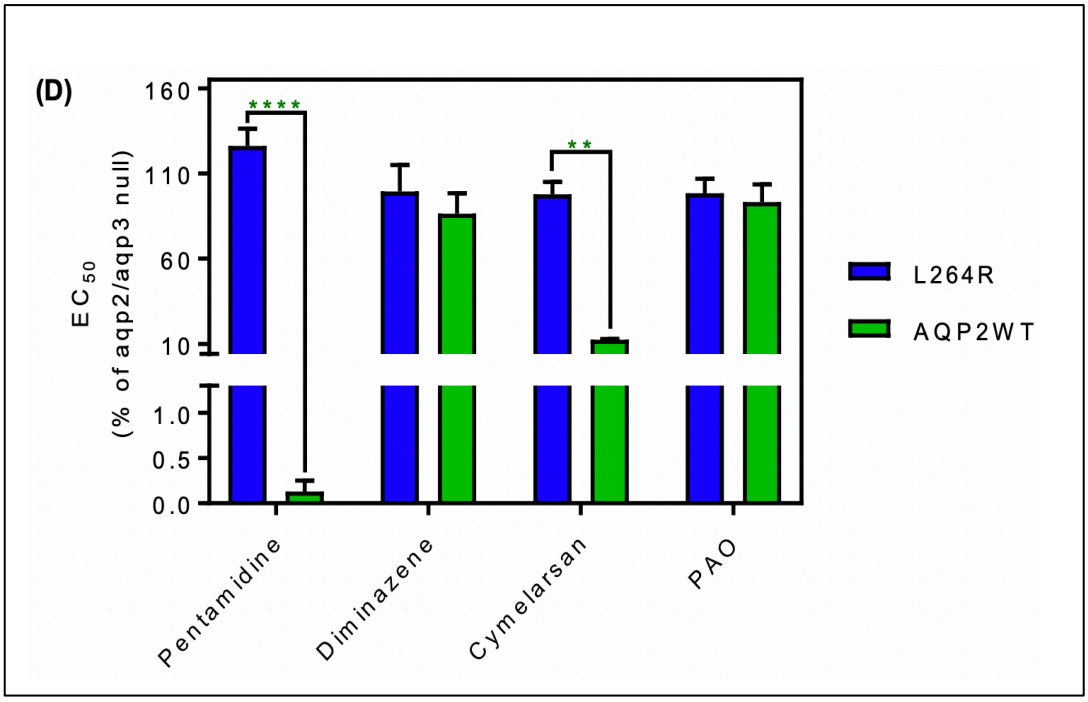
(D)
EC50
(% of aqp2/aqp3 null)
160
110
60
10
1.0
0.5
0.0
****
**
Pentamidine
Diminazene
Cymelarsan
PAO
L264R
AQP2WT

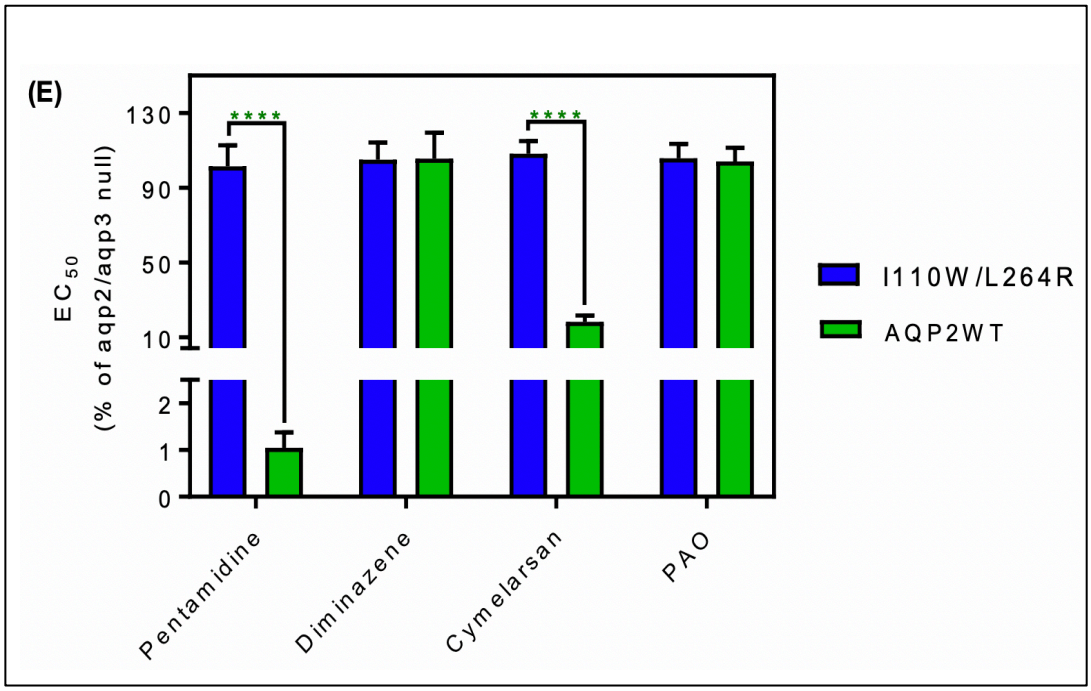

Figure 3.5: Sensitivity assay of TbAQP2 mutants cell lines (the introduction of TbAQP3 residues into the TbAQP2 selectivity filter).
The figures of (A-E) show the EC_{50} values for the indicated test drugs; pentamidine, cymelarsan, and the control drugs diminazene and phenylarsine oxide (PAO), expressed as a percentage of the *tbaqp2/tbaqp3* null (resistant control), against cell lines either expressing the indicated TbAQP2 mutant or TbAQP2WT (sensitive control). Red stars and green stars: comparison with *tbaqp2/aqp3* null or TbAQP2WT-expressing cells, respectively, which were assessed in parallel in each experiment. (A-E) Shows the drug susceptibility of the indicated TbAQP2 mutants. (A) double mutants (S131P/S263A). (B) single mutant (L258Y). (C) single mutant (I110W). (D) single mutant (L264R). (E) double mutants (I110W/L264R). All experiments are the average and SEM of at least 3 independent experiments.
*, P<0.05; **, P<0.01; ***, P<0.001, ****, P<0.0001 by unpaired Student's t-test, two-tailed. (Alghamdi et al., 2020).

Next, transport assays, using radiolabelled [^{3}H]-pentamidine were performed to all derivative and control strains from the Alamar Blue assay over the course of a minute, to determine if the significant loss of pentamidine sensitivity in the cell lines expressing mutants were associated with alterations to pentamidine uptake into the cell. In the TbAQP2$^{S131P/S263A}$ cell line, the calculations recorded a reduction in the rate of uptake of 30 nM [3H]-pentamidine by 4.40 ± 0.71% (n=4) compared to the rate of the control cell line expressing TbAQP2WT (P<0.05, Student's unpaired t-test). Correspondingly, this uptake of [^{3}H]-pentamidine in the TbAQP2$^{S131P/S263A}$ cell line was also observed to be significantly different from the rate calculated in the *tbaqp2/tbaqp3* null cells (P<0.01). Introducing L258Y into the TbAQP2 pore gave the drug transporter the phenotype similar to TbAQP2$^{S131P/S263A}$. This led to a reduction

of the [^{3}H]-pentamidine transport rate to 6.6 ± 1.4% of TbAQP2WT (P<0.01) but stayed considerably above the rate observed in the *tbaqp2/tbaqp3* null cells (P<0.05) (Figure 3.9). However, cell lines with mutations AQP2^{I110W} and AQP2^{L264R}, showed pentamidine transport rates that were not significantly different from those observed in the *tbaqp2/tbaqp3* null controls but highly significantly different from the TbAQP2WT drug-sensitive controls, showing that their ability to uptake pentamidine had been decreased to almost zero (Figure 3.6).

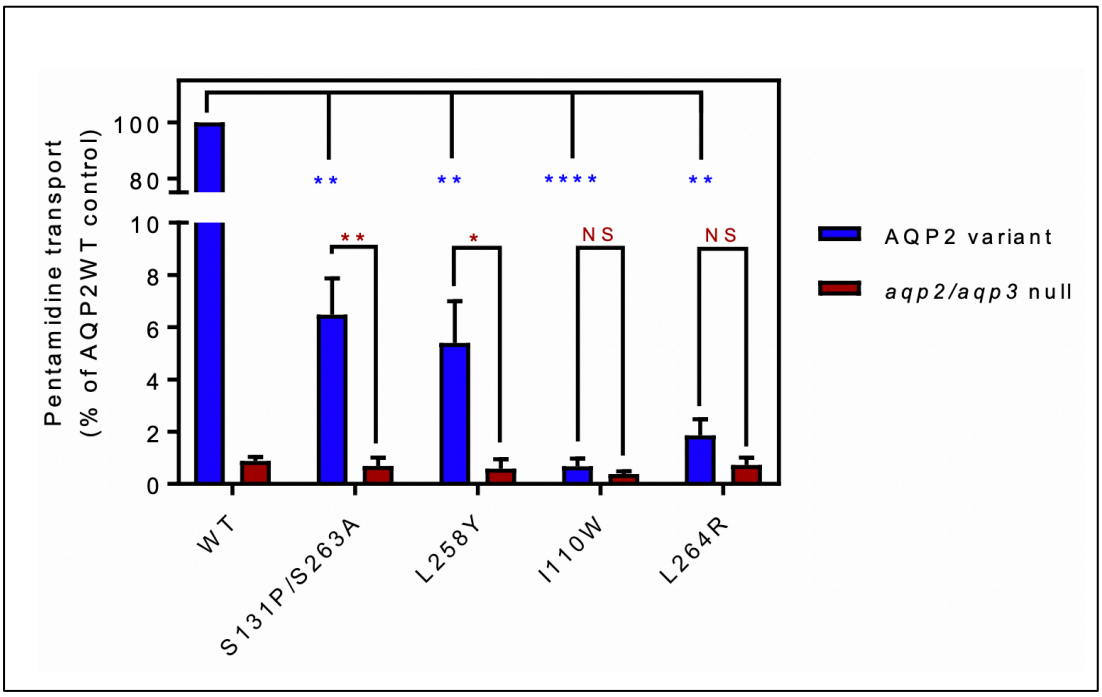

Figure 3.6: Transport of 30 nM [^{3}H]-pentamidineby *tbaqp2/aqp3* null cells expressing TbAQP2-WT or one of the TbAQP2 mutants (TbAQP3 selectivity filter residues) as indicated (blue bars).

The corresponding brown bars are pentamidine transport in the control *tbaqp2/aqp3* null cells assessed in parallel in each experiment. Transport was determined. Bars represent the average and SEM of at least three independent experiments, each performed in triplicate. Blue stars: statistical significance comparison, by two-tailed unpaired Student's tests, between the cells expressing TbAQP2WT and mutants; red stars: statistical comparison between the AQP2-expressing cells and control cells; NS, not significant. *, P<0.05; **, P<0.01; ***, P<0.001, ****, P<0.0001 by unpaired Student's t-test, two-tailed. (Alghamdi et al., 2020).

3.2.3. Introduction of TbAQP2 selectivity filter residues into the AQP3 pore enables pentamidine transport.

3.2.3.1. Confirmation of the construction and transfection of AQP3 mutants

The effects of introducing some of the critical TbAQP2 residues in TbAQP3 were determined to see whether these mutants would give the latter the capability for pentamidine uptake. The mutants TbAQP3$^{W102I/R256L}$ and TbAQP3$^{W102I/R256L/Y250L}$ were constructed and expressed in *tbaqp2/tbaqp3* null cells by Dr. Jane Munday at the De Koning laboratory. To characterise these generated mutants, I therefore followed Munday's work by obtaining the cell lines from stabilate storage and maintaining the cells (3-5 passage) in the standard medium (HMI-9 with 10% FBS) with the addition of the right antibiotic for the transfectants (0.2 µg/ml hygromycin). Next, genomic DNA was extracted from each cell line, and two PCR reactions were then performed for confirmation. Forward primer HDK529 and reverse primer HDK329 (5'-AGGATCTTAGTGTGGCACAAA-3') were used to amplify the presence of the full *Tb*AQP3 gene in the first PCR reaction, whereas the primer HDK1011 (located 143 bp upstream of the open reading frame of the gene in the plasmid backbone) and HDK430 (located 83 bp downstream of the open reading frame the gene in the plasmid backbone) were used to amplify the gene with a partial fragment of the expression cassette in the second PCR reaction. The PCR products were then run on an 1% agarose gel with DNA staining to confirm the correct size of the amplified fragments. PCR products from the first reaction were ~950 bp (Figure 3.7A), i.e. displayed the full size of the TbAQP3 (912 bp). The product-sized bands from the second PCR reaction were at ~1250 bp (Figure 3.7B) corresponding to the expected size of the gene with the partial plasmid fragment (1212 bp). The sizes of the PCR products indicate a successful transfection for each cell line. (See plasmid map in appendix 6).

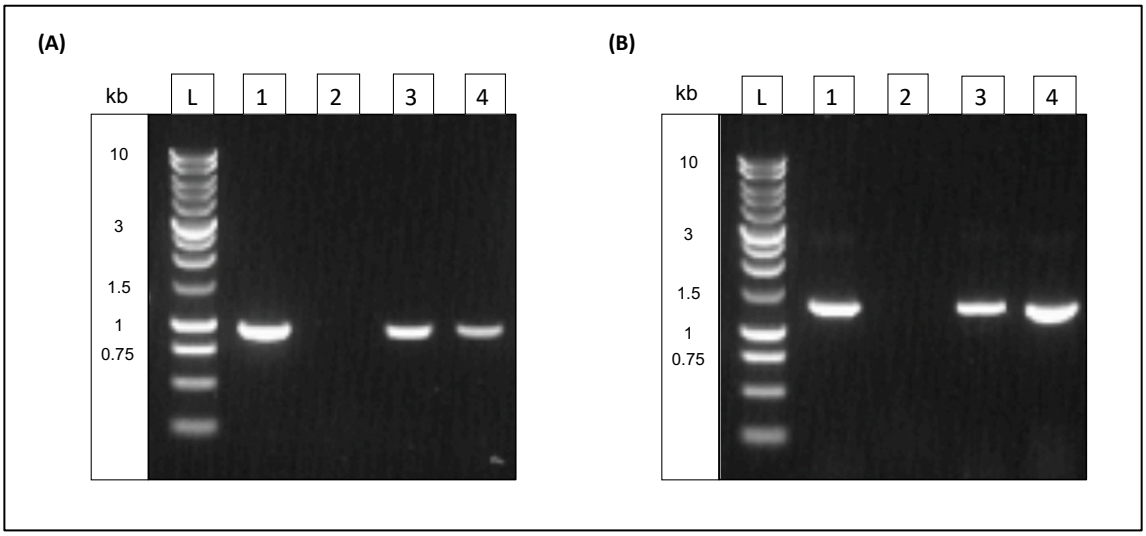

Figure 3.7: **Agarose gel electrophoresis of PCR products reveals the presence of the integrated TbAQP3 mutants (TbAQP2 selectivity filter residues) in transfected *tbaqp2*/*tbaqp3* null cells.** (A) Amplified PCR products at ~950 bp show the full TbAQP3 gene. L: 1kb DNA ladder; 1: TbAQP3 (WT) positive control; 2: TbAQP3 (KO) negative control; 3: TbAQP3 (W102I/R256L); 4: TbAQP3 (W102I/R256L/Y250L). (B) The bands at ~1250 bp displayed fragments containing TbAQP3 gene and part of the expression cassette neighbouring the gene. L: 1kb DNA ladder; 1: (pHDK70) positive control; 2: TbAQP3 (KO) negative control; 3: TbAQP3 (W102I/R256L); 4 TbAQP3 (W102I/R256L/Y250L).

Prior to use the cell lines for drug sensitivity and uptake assays, confirmation for correct mutation was verified by sequencing. The gDNA of the clones that exhibited successful transfection were used to amplify the full *Tb*AQP3 gene using a high-fidelity DNA polymerase (New England BioLabs). The products from PCR reactions were purified using a DNA purification kit (Macherey-Nagel) and were then sent for sequencing (SourceBioscience, Glasgow, Scotland, UK) with forward primer (HDK1011) and reverse primer (HDK430). Correct mutation(s) were checked by creating alignments of the amino acid sequences of TbAQP3 WT and the TbAQP3 mutants (Appendix 7).

3.2.3.2. Molecular characterization of the introduction of TbAQP2 selectivity filter residues into the AQP3 pore

The aim of this study was to test the impacts of the unique selectivity filter elements of the TbAQP2 when introduced into the TbAQP3 selectivity filter on the drug's sensitivity and transport. The Alamar Blue assay was performed to test whether *tbaqp2*/*tbaqp3* null cells transfected with these mutant aquaporins were able to sensitise expressing cells to pentamidine. The strain possessing the re-expressed

TbAQP3 WT cell line (drug-resistant control) was used in parallel with the mutant cell lines. In this study pentamidine was assessed and phenylarsine oxide (PAO) was used as positive control throughout the assays. There was no significant difference between the sensitivity to PAO for the cell lines expressing mutations TbAQP3$^{W102I/R256L}$ and TbAQP3$^{W102I/R256L/Y250L}$ and the TbAQP3 (control cell line) (Figure 3.8). But, when tested with pentamidine, TbAQP3$^{W102I/R256L/Y250L}$ conveyed significant sensitisation into *tbaqp2/tbaqp3* null cells (P<0.0001; Figure 3.8). This indicates that this particular triple mutant (W102I, R256L and Y250L) in the TbAQP3WT can confer increased pentamidine sensitivity.

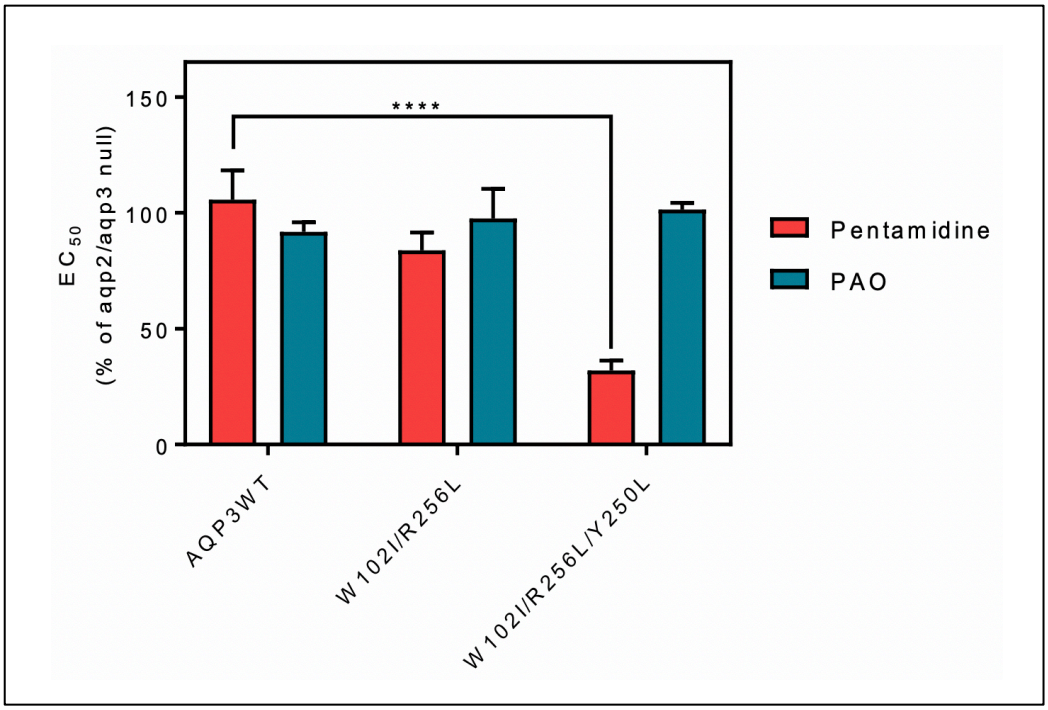

Figure 3.8: Sensitivity assay of *Tb*AQP3 mutants cell lines (the introduction of AQP2 selectivity filter residues).
The figure shows the EC_{50} values of the pentamidine (red bars) and the control drug phenylarsine oxide (blue bars) against *tbaqp2/aqp3* null cells expressing either TbAQP3 or a mutant thereof, expressed as percentage of *tbaqp2/aqp3* null. All experiments are the average and SEM of at least 3 independent experiments. ****, P<0.0001 by unpaired Student's t-test, two-tailed. (Alghamdi et al., 2020).

Next, transport assays of [^{3}H]-Pentamidine were performed to test whether *tbaqp2/tbaqp3* null cells transfected with these mutant aquaporins were able to take up 30 nM [^{3}H]-pentamidine in the presence of 1 mM adenosine (which blocks uptake via TbAT1/P2). Over a time course of 2 minutes, the pentamidine uptake in

the AQP3WT and mutant cell lines was very low compared to the same cells expressing TbAQP2WT (Figure 3.9).

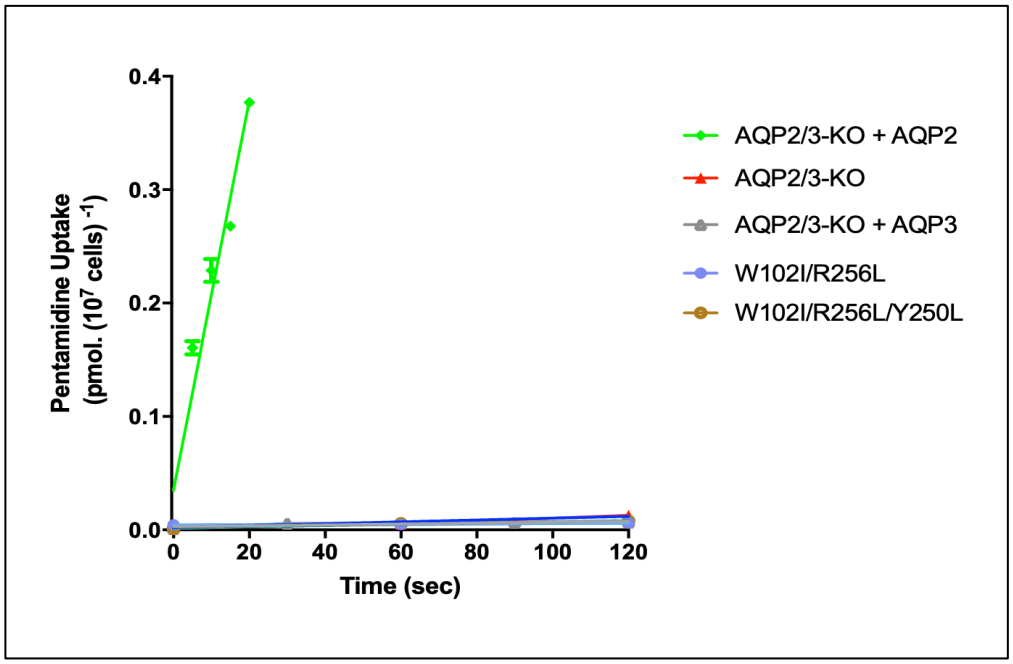

Figure 3.9: The uptake of 30 nM [^{3}H]-Pentamidine over 2 minutes by *tbaqp2/aqp3* null cells expressing TbAQP2WT in comparison with the TbAQP3WT and the TbAQP3 mutant cell lines. Pentamidine uptake in the mutant cell lines, in the presence of 1 mM adenosine, when incubation time points at 0, 5, 10, 15 and 20 seconds for AQP2, and 0, 30, 60 and 120 seconds for the other strains.

The [^{3}H]-pentamidine uptake was reliably and reproducibly determined by measuring its accumulation in every cell line for 30 minutes (Figure 3.10 A,B). The results indicated uptake of TbAQP3$^{W102I/R256L}$ to trend to some extent upwards ($P>0.05$). On the other hand, the mutant AQP3 with all three AQP2 W(G)YR residues (W102I, R256L, and Y250L) had a significantly increased [^{3}H]-pentamidine uptake compared to the *tbaqp2/tbaqp3* null cells ($P<0.01$) or the null cells expressing TbAQP3WT ($P=0.011$). These results showed that introduction of the AQP2 filter residues in AQP3 expressively led to sensitization towards pentamidine in addition to facilitating its uptake by the cell lines.

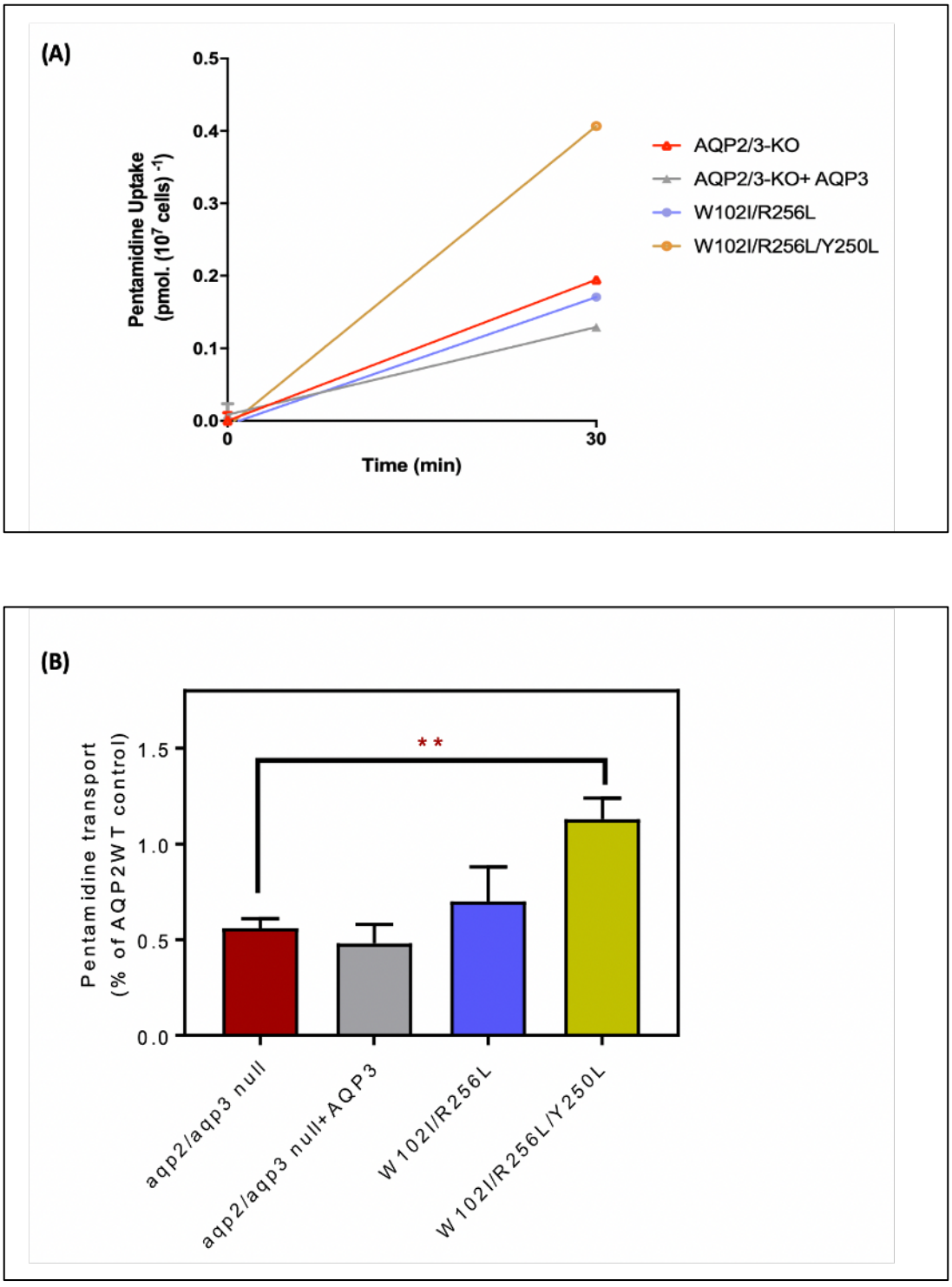

Figure 3.10: Transport of 30 nM [^{3}H]-pentamidine by *tbaqp2/aqp3* null cells expressing TbAQP3 or an TbAQP3 mutant as indicated.
Pentamidine transport performed in 30 min incubation in the control *tbaqp2/aqp3* null cells and assessed with the TbAQP3 mutant cell lines in parallel in each experiment. Transport was determined in the presence of 1 mM adenosine to block the TbAT1/P2 transporter. (A) Representative transport assay shows the accumulation of radiolabelled pentamidine in each cell line when incubation over 30 minutes. (B) Bars represent the average and SEM of at least three independent experiments, each performed in triplicate. Red stars: statistical significance comparison, by two-tailed unpaired Student's tests, between the cells expressing TbAQP2WT and mutants**, $P<0.01$ by unpaired Student's t-test, two-tailed. (Alghamdi et al., 2020).

3.2.4. Mutations of amino acids modelled to potentially bind pentamidine or melarsoprol dramatically reduce pentamidine transport.

3.2.4.1. Confirmation of the construction and transfection of AQP2 mutants

Previous attempts made at the De Koning laboratory focusing on modelling the binding of pentamidine and melarsoprol into TbAQP2 pore led to identifying various residues associated with this activity (Munday et al., 2015a). Among these residues, two residues, Ile190 and Trp192, (Position shown in Figure 3.11) were chosen at the extracellular end of the channel and were predicted to interact with the substrate (s) with main-chain carbonyl oxygen atoms without the side chains affecting this interaction.

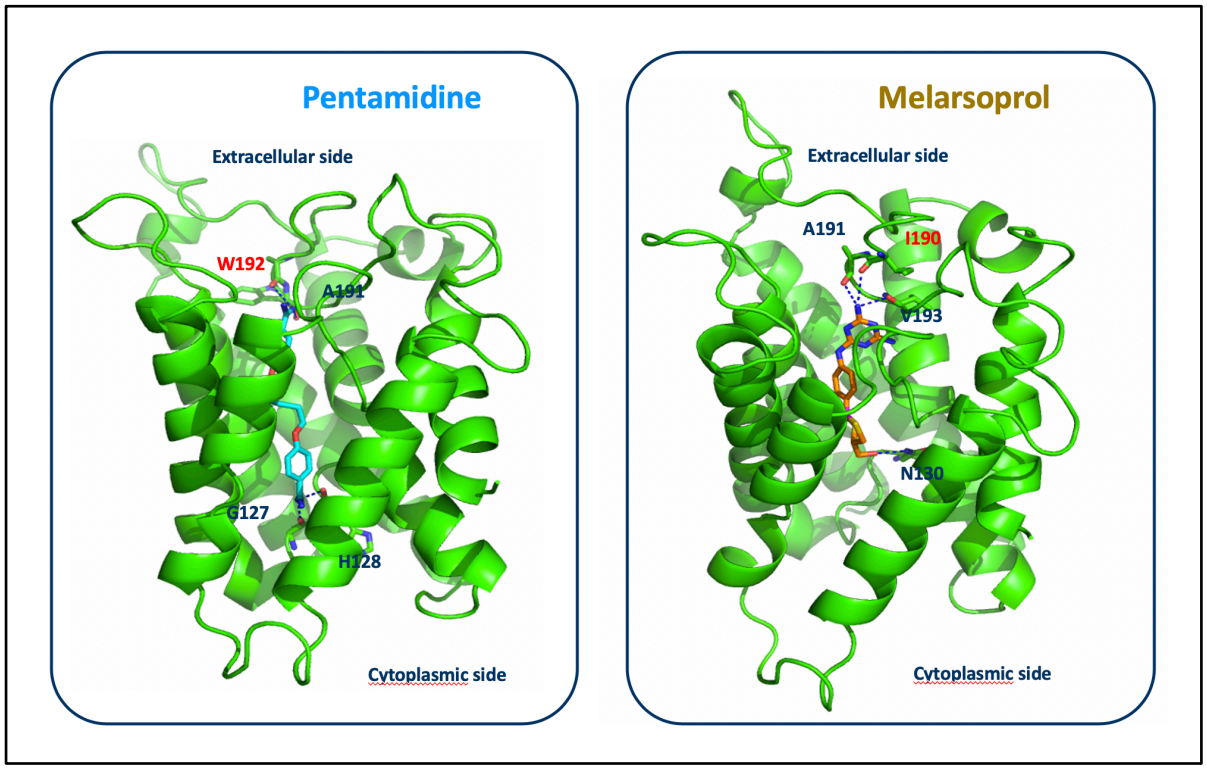

Figure 3.11: Homology models of the predicted binding of pentamidine and melarsoprol in complex with a single TbAQP2 subunit (green).
(A) Binding of pentamidine (cyan carbon atoms). (B) Binding of melarsoprol (orange carbon atoms). Key polar interactions are shown for both (A, B). The Ile190 and Trp192 (red) were the two selected residues which predicted to interact with the substrate(s) with main-chain carbonyl oxygen atoms. Models obtained from (Munday et al., 2015a).

To swap with the corresponding residues of TbAQP3, mutants of TbAQP2^{I190T}, TbAQP2^{W192G} and TbAQP2$^{I190T/W192G}$ were generated. These mutants were created and expressed into *tbaqp2*/*tbaqp3* null cells by Dr. Jane Monday at the De Koning laboratory. This part was followed by characterising generated mutants. Firstly, the cell lines were retrieved form the stabilate storage and were growin in culture medium (HMI-9 + 10% FBS) supplemented with 2.5 µg/ml hygromycin. After passaging the cells (3-5 passages), genomic DNA from each cell line was extracted and two PCR reactions were performed for more confirmation prior to the sensitivity and transport assays. In the 1st PCR, the *Tb*AQP2 gene from each cell line was amplified using the forward and reverse primers (HDK529 & HDK209) to check for the presence of the full *Tb*AQP2 gene. Whilst, the 2nd PCR was used to amplify the gene with a partial fragment of the expression cassette using the primers HDK1011 & HDK430. The PCR products were then run on an agarose gel with DNA staining to confirm the correct size of the amplified fragments. PCR products from the first reaction were ~950 bp (Figure 3.12A), indicating to the expected size of the full *Tb*AQP2 gene (939 bp). Whereas, product-sized bands from the second PCR reaction were ~1,250 bp presented the gene with the partial plasmid fragment (1212 bp) (Figure 3.12B). The correct product-sized bands of the amplified PCR products presenting correct transfections. (See plasmid map (figure 2.1) in section 2.3.4.1; for primers sites)

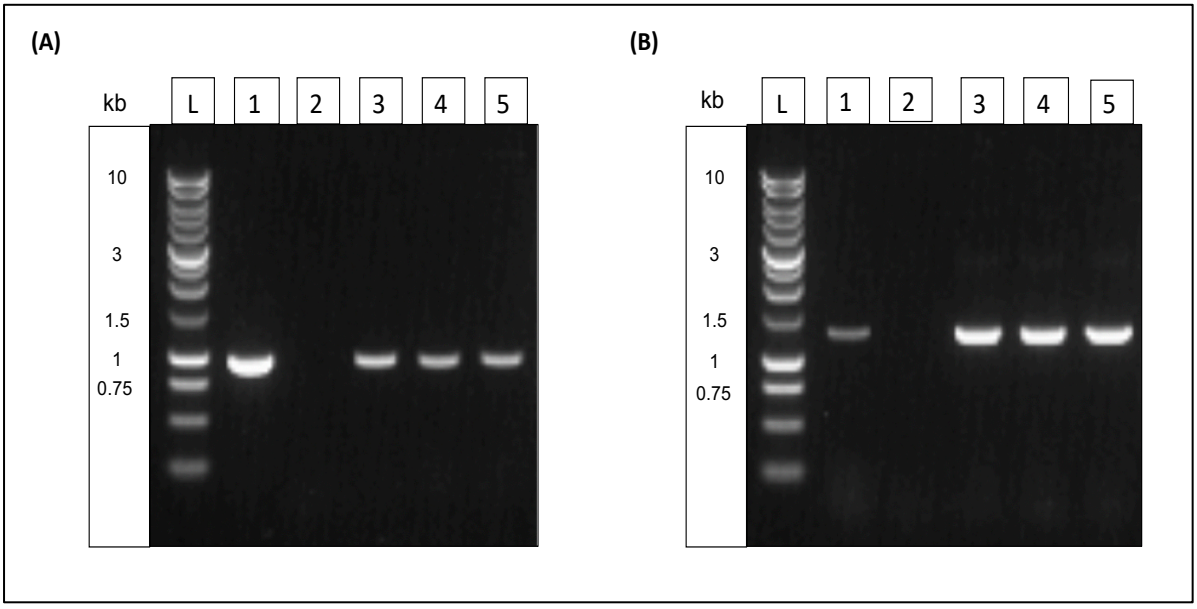

Figure 3.12: PCR screening of the TbAQP2 mutant cell lines (TbAQP2 residues I190 and W192).

PCR products were separated by gel electrophoresis on 1% agarose gel. The expected size of each band was obtained with respect to the standard sizes of the 1kb molecular weight size Ladder (Left columns). (A) amplified PCR products at ~950 bp show the full TbAQP2 gene. (B) Bands at ~1250 bp displayed fragments containing TbAQP2 and part of the expression cassette neighbouring the gene. L: 1kb DNA ladder; 1: TbAQP2 (WT) positive control; 2: TbAQP2 (KO) negative control; 3: TbAQP2 (I190T); 4: TbAQP2 (W192G); 5: TbAQP2 (I190T/ W192G).

The I190T and W192G mutations were verified using Sanger Sequencing (Source BioScience, Nottingham, UK). The *Tb*AQP2 gene was amplified from the genomic DNA of cell lines that displayed successful transfections using a high-fidelity DNA polymerase (New England BioLabs). The products from PCR reactions were purified using a DNA purification kit (Macherey-Nagel) and were then sent for sequencing (SourceBioscience, Glasgow, Scotland, UK) with forward primer (HDK1011) and reverse primer (HDK430). Correct mutation(s) were checked by creating alignments of the amino acid sequences of TbAQP2WT and the TbAQP2 mutants (Appendix 8).

3.2.4.2. Molecular characterizations of mutations of the amino acids modelled to potentially bind pentamidine or melarsoprol.

The Alamar blue assay was performed to determine the EC_{50} values of the mutant cell lines (TbAQP2^{I190T}), (TbAQP2^{W192G}) and (TbAQP$^{I190T/W192G}$) in parallel with the resistant control cell line (*tbaqp2*/*tbaqp3* null), and the strain possessing the re-expressed TbAQP2WT (drug-sensitive control). In this study, pentamidine and cymelarsan drugs were used to investigate the predicted binding model. Phenylarsine oxide (PAO) was used as positive control throughout the study. As previously noted from the information provided above regarding the selectivity of filter mutants, TbAQP2^{I190T} was observed to show high pentamidine sensitivity in the standard resazurin test ($P<0.0001$) but with significantly less sensitization compared to TbAQP2WT ($P<0.001$). Besides, an intermediate sensitivity for pentamidine was also noted for cymelarsan (Figure 3.13A). The substitution of W192G resulted in producing intermediate sensitivity to both pentamidine and cymelarsan (Figure 3.13B). However, the double substitution of TbAQP$^{I190T/W192G}$ led to no significant sensitization to either pentamidine or cymelarsan (Figure 3.13C).

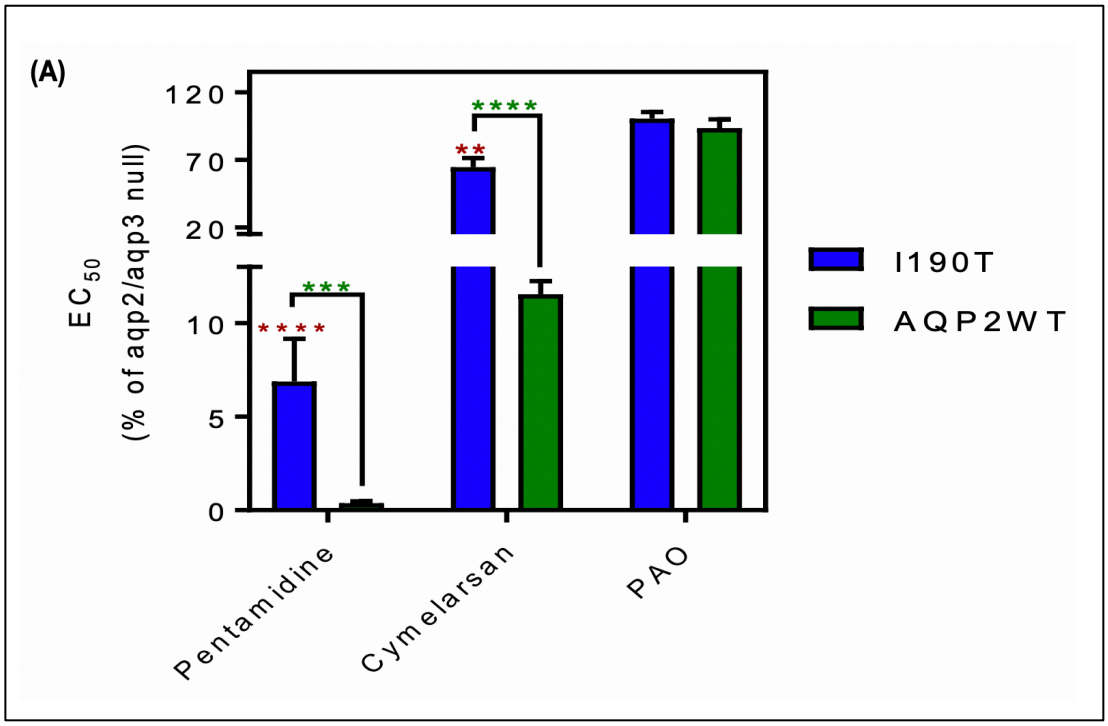
(A)
EC50
(% of aqp2/aqp3 null)
120
70
20
10
5
0
****
***
**
****
Pentamidine
Cymelarsan
PAO
I190T
AQP2WT

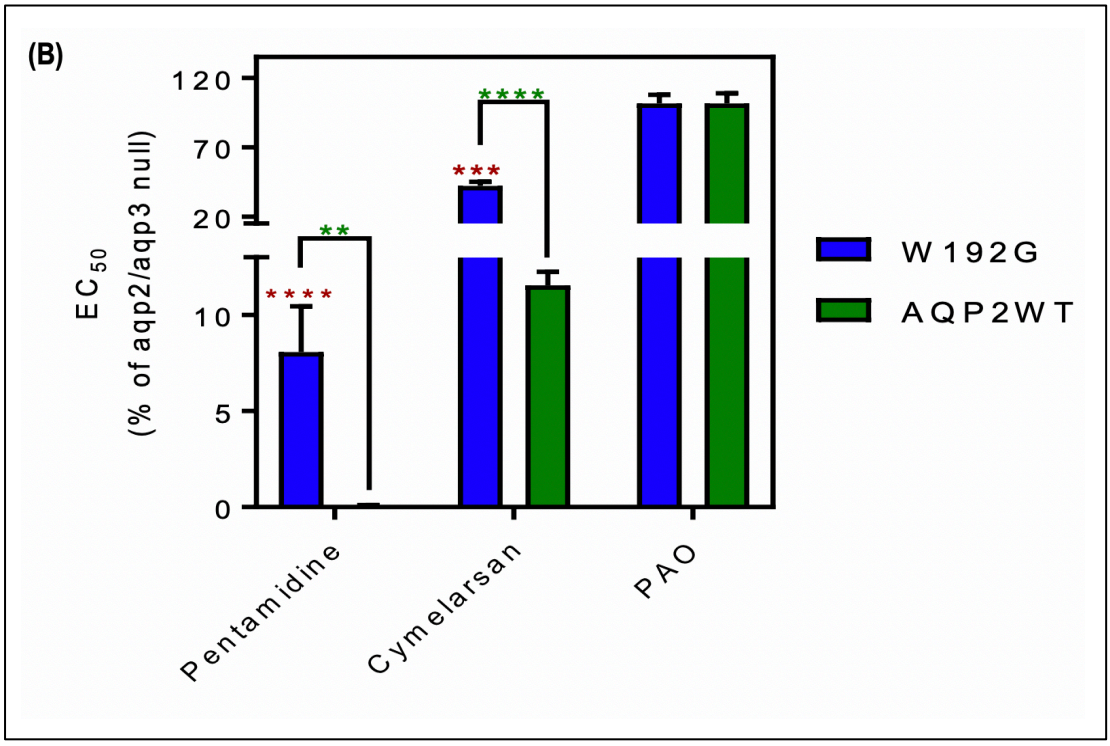
(B)
EC50
(% of aqp2/aqp3 null)
120
70
20
10
5
0
****
**
***
****
Pentamidine
Cymelarsan
PAO
W192G
AQP2WT

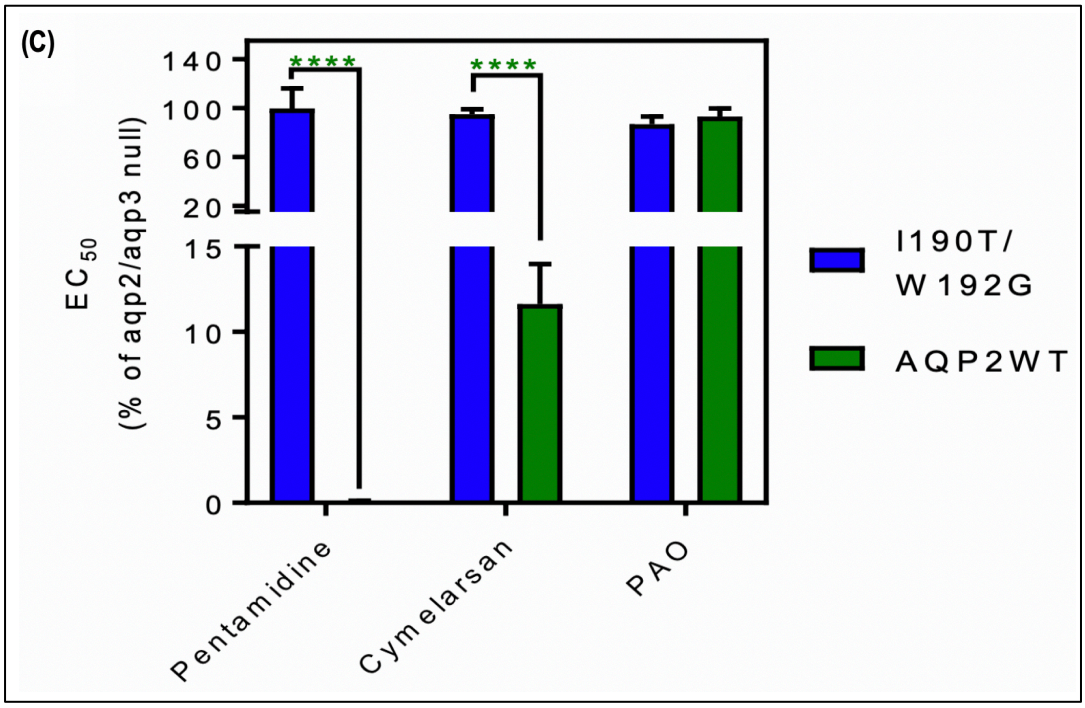

Figure 3.13: Sensitivity assay of TbAQP2 mutant cell lines (TbAQP2 residues I190 and W192). (A) EC_{50} values for the indicated drugs against *tbaqp2/tbaqp3* null cells, and against TbAQP2WT and TbAQP2 mutant cell lines; values were expressed as % of the *tbaqp2/tbaqp3* null (resistant) control. Red stars, comparison with the resistant control; green stars, comparison with the internal sensitive control (TbAQP2WT). The assays for all three strains and all three drugs were done simultaneously on at least 3 different occasions. (B) As A but for $TbAQP2^{W192G}$. (C) As A but for $TbAQP2^{I190T/W192G}$. *, P<0.05; **, P<0.01; ***, P<0.001, ****, P<0.0001 by unpaired Student's t-test. (Alghamdi et al., 2020).

The $TbAQP^{2I190T}$ presented intensely decreased uptake of [^{3}H]-pentamidine at 2.7 ± 0.7% (P<0.0001) of the TbAQP2WT control. However, this uptake rate was still significantly higher compared to the rate observed in the *tbaqp2/tbaqp3* null negative control (P<0.05) (Figure 3.14). In contrast, the double substitution of $TbAQP^{I190T/W192G}$ demonstrated no significant uptake of pentamidine with reference to the *tbaqp2/tbaqp3* null strain (Figure 3.14).

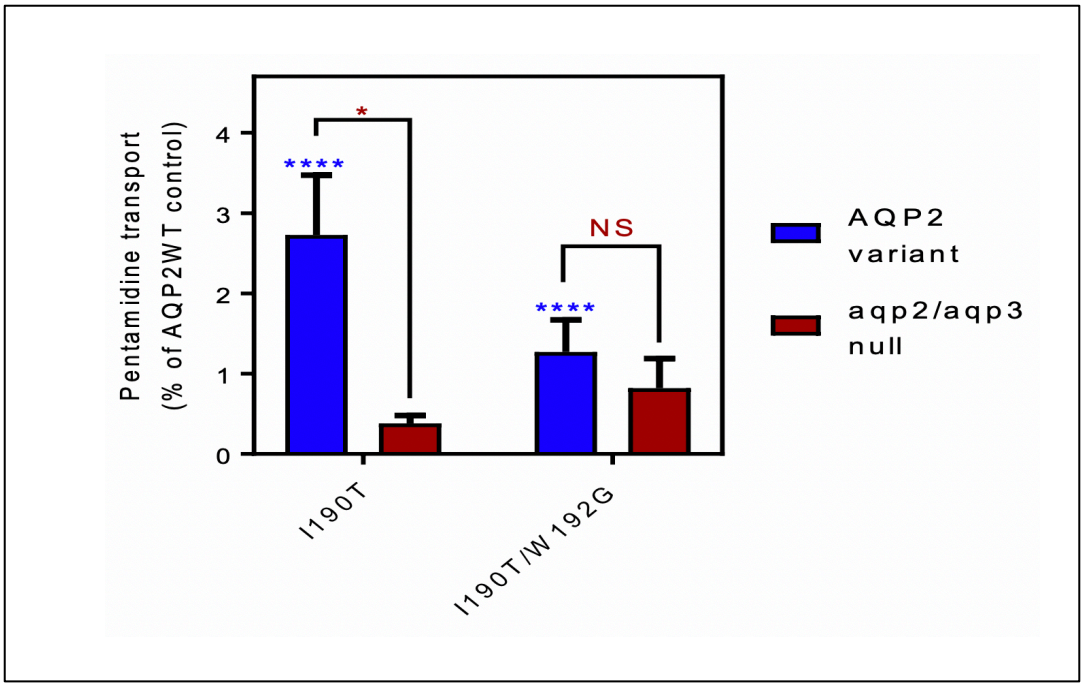

Figure 3.14: Transport of 30 nM [^{3}H]-pentamidine by *tbaqp2/tbaqp3* null cells or TbAQP2 variants (residues I190 and W192) expressed therein.
Transport was expressed as a percentage of the rate of the TbAQP2WT control, performed in parallel. Blue stars are comparison with TbAQP2WT, red stars, comparison with the *tbaqp2/tbaqp3* null control. NS, not significant. The assays for all three strains and all three drugs were done simultaneously on at least 3 different occasions. *, P<0.05; ****, P<0.0001 by unpaired Student's t-test. (Alghamdi et al., 2020).

The I190T mutant was further investigated to see whether this substitution might have altered the K_m of the high affinity pentamidine transport, as might be expected if the substitution disrupted a specific interaction with the substrate. Because of the very low rate of uptake in this mutant a 15 min incubation time was used to obtain a reproducible inhibition curve. (Figure 3.15) shows a biphasic double-sigmoidal inhibition curve for a high affinity component with an average IC_{50} of 30.9 ± 12.2 nM (n=3) and a low affinity component. The latter could be converted to a Michaelis-Menten curve (Figure 3.15A., inset), yielding an average K_m of 59.9 ± 9.1 µM. Figure 3.15B., inset shows the corresponding experiment with the same cells, but expressing TbAQP2WT instead of the mutant and using 20 s incubations. In this case the high affinity component, although showing a very similar IC_{50} in the biphasic plot (41 ± 17 nM; P>0.05), was much more prominent, showing that the rate of TbAQP2-mediated transport, rather than the transporter affinity was altered in the mutant. The low affinity component was statistically identical in the two strains (TbAQP2WT K_m = 82.7 ± 17.5 µM (n=3; P>0.05)).

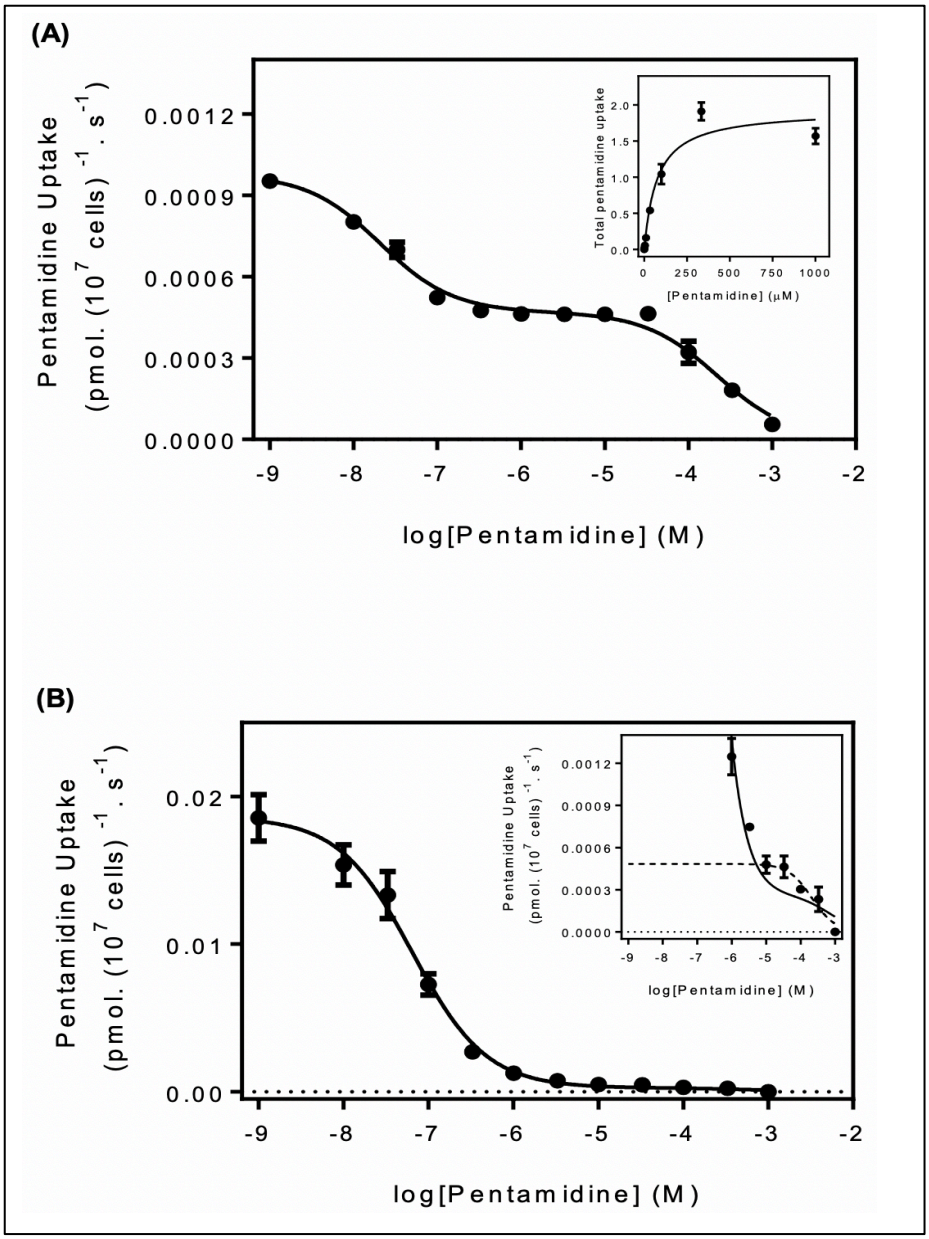

Figure 3.15: The determination of K_m and V_{max} values for the TbAQP2^{I190T} mutant and the *tbaqp2/tbaqp3* null cells expressing TbAQP2WT.

(A) Transport of 30 nM [^{3}H]-pentamidine by TbAQP2^{I190T}, in the presence of unlabelled pentamidine at the indicated concentrations. Incubation time was 15 min, required to ensure sufficient radiolabel for accurate quantification, and uptake was linear and through zero over this period. The inhibition data were plotted to a double sigmoidal curve (Prism 7.0) with the bottom value fixed at 0. The high affinity component displayed IC_{50} of 30.9 ± 12.2 nM (n = 3) and the lower affinity segment could be converted to a Michaelis-Menten plot for determination of K_m and V_{max} (inset), yielding an average Km of 59.9 ± 9.1 μM (n = 3), consistent with the Low Affinity Pentamidine Transporter (LAPT1; Bridges *et al*, 2007). The plot shown is one representative experiment in triplicate of three independent experiments. (B) Like (A) but with *tbaqp2/tbaqp3* null cells expressing TbAQP2WT. Incubation time was 20 s. The inset shows a zoom-in on the low-affinity part of the curve, with the dotted line representing a theoretical sigmoid plot for one inhibitor, with the upper limit fixed at the value obtained for 10 μM pentamidine. Note that the amount of [^{3}H]-pentamidine taken up by the low affinity component is highly similar for the mutant (A) and control (B) cell lines, at approximately 0.0005 pmol(10^7 cells)$^{-1}$s^{-1}.

Both frames show one representative experiment of three repeats, each performed in triplicate. Error bars are SEM, when not shown, fall within the symbol. (Alghamdi et al., 2020).

3.3. Discussion

A vast agreement exists that the expression of TbAQP2 is related to the extraordinary sensitivity of *T. brucei* towards pentamidine, as well as towards melaminophenyl arsenicals, and that mutations and deletions associated with this locus can result in drug resistance (Baker et al., 2012, 2013; Graf et al., 2013, 2015, 2016; Pyana Pati et al., 2014; Munday et al., 2014, 2015a; Unciti-Broceta et al., 2015). However, the mechanisms explaining these phenomena are still unclear, and no current document exists outlining other examples of aquaporins in the transportation of such large molecules. TbAQP2 has evolved through positive selection, as indicated by the high dN/dS ratio, to eliminate all significant constriction points, such as the aromatic amino acids, cationic arginine of the selectivity filter, and the NPA/NPA motif, leading to enlarged pore size. The advantage of this phenomenon in *T. b. brucei* is still not known, but the adaptation is considered to be stable in the brucei group of trypanosomes, where it is found in *T. b. rhodesiense* (Munday et al., 2014; Graf et al., 2016), *T. b. gambiense* (Graf et al., 2013, 2015; Munday et al., 2014; Pyana Pati et al., 2014), *T. equiperdum*, and *T. evansi* (Philippe Büscher and Nick Van Reet, unpublished). Consequently, it is not incongruous to speculate that this enlarged TbAQP2 pore (i) permits the passage of materials that TbAQP1 and TbAQP3 do not transport; (ii) provides a yet unknown advantage to the cell; and (iii) that uptake of pentamidine is a by-product of this evolvement.

In the current study, I demonstrated that modifications in the TbAQP2 WGYR and NPA/NPA motifs provide a passageway for these drugs into the cell, thereby supporting the parasite's very high sensitivity towards the drugs. The introduction of the AQP3 Arg residue in position 264 (TbAQP2^{L264R}) disables the transport of pentamidine, which we concluded was due to the positively charged arginine located in the middle of the pore blocking all cations from passing through the pore (Beitz *et al*, 2006; Wu *et al*, 2009). Certainly, the W(G)YR filter residues seem to be critical determinants for pentamidine uptake by AQPs, and introducing all three TbAQP2 residues into TbAQP3 (AQP3$^{W102I/R256L/Y250L}$) was needed to generate an TbAQP3 with mild sensitization to pentamidine, and which enabled a measurable level of pentamidine uptake. On the other hand, any mutation (I110W, L258Y, or L264R) was

appropriate to all but abolish pentamidine transport by TbAQP2. Likewise, the conserved NPA/NPA motif (predominantly the Asp residues) found in TbAQP3 (but NSA/NPS in TbAQP2) is also affiliated with the blocking of the cations passage (Wree *et al*, 2011). The unique serine residues found in the TbAQP2 motif, halfway down the pore, might have the capacity to make hydrogen bonds with pentamidine because the reestablishment of the NPA/NPA motif created a TbAQP2 variant that demonstrated a 93.5% reduced rate of [^{3}H]-pentamidine uptake.

To conclude, the selectivity filter differences between TbAQP2 and TbAQP3 are largely responsible for their differences in pentamidine sensitivity and transport rates. The unique TbAQP2 replacement of the NPA/NPA motif and all of the WGYR selectivity filter mutations are necessary for the observed pentamidine and melaminophenyl arsenical sensitivity observed in cells expressing wild-type TbAQP2.

Chapter 4 Mutagenesis of leucine residues at the cytoplasmic end of the TbAQP2 pore affects the protein's capacity to transport pentamidine

4.1. Introduction

The drug uptake model suggests that pentamidine traversed through the uniquely permissive aquaglyceroporin (Munday et al., 2015a). However, this model was challenged by a study proposing that pentamidine does not traverse the TbAQP2 but binds to an aspartate residue (Asp265) located near the pore's end on the extracellular side, above the selectivity filter, before it is internalized through endocytosis (Song et al., 2016). Furthermore, the study supported their argument by showing the inability of TbAQP2 to transport organic cations, such as ammonium ions, when expressed in yeast. The study also went further to eliminate size as a factor affecting the transport of organic cation substrates; even for the pentamidine's 44 Da end moiety known as formamidine (HN=CH=NH2), the transporter exhibited no permeability. Therefore, the authors of the study concluded that TbAQP2 does not directly transport pentamidine but acts as a high-affinity receptor for this drug in addition to facilitating its passage in trypanosomes through non-selective endocytosis. This non-selective endocytosis was noted due to D265 residue significance, which is considered to have a strong electrostatic interaction with pentamidine, as indicated by figure 4.1. The flagellar pocket is the only site associated with endocytosis in trypanosomatids (Field & Carrington, 2009). TbAQP2 location in the flagellar pocket (Baker et al., 2012), has led to speculations that pentamidine is transported into the cell through a receptor-mediated endocytosis mechanism. However, no further experimental evidence has been presented or published to support these speculations. It is not typical for such a small-sized channel to control and facilitate the transport of relatively large drug molecules like pentamidine. Hence, more exploration regarding this gene would be imperative to comprehensively understand the mechanism behind this phenomenon and probably at the same time improve the associated treatments.

The question thus remained whether to determine whether TbAQP2 is a fixed transmembrane transporter, with pentamidine acting as a permeant, or a receptor for pentamidine, which is then transported by other mean. Therefore, the hypothesis that the TbAQP2 channel allows the translocation of pentamidine through its pore was tested by investigation of a substitution of small and uncharged amino

acid residues L84, L118 and L218, which reside in the transport channel below the unique *T. brucei* selectivity filter and are not interfering with the D265 residue, for tryptophan and methionine (Figure 4.2). In this study, the purpose of substituting L84, L118, and L218 with tryptophan residues near the pore's cytoplasmic end was to determine if the presence of bulky amino acids in that end would block the transport of pentamidine through the TbAQP2 pore. This study was followed by introducing a medium sized residue (methionine) instead of tryptophan into the same three selected positions of the leucine to allow further discrimination between the models of binding to the extracellular end of the pore (followed by endocytosis) and the requirement for the drug to traverse the full length of the channel.

Site-directed mutagenesis was performed to code an amino acid substitution at the three selected positions of the leucine, expressed the mutant(s) into *tbaqp2*/*tbaqp3* null cells, assessed the sensitivity of the mutant cell lines to cymelarsan and pentamidine, and measured the rate at which the drug is taken up by these mutants.

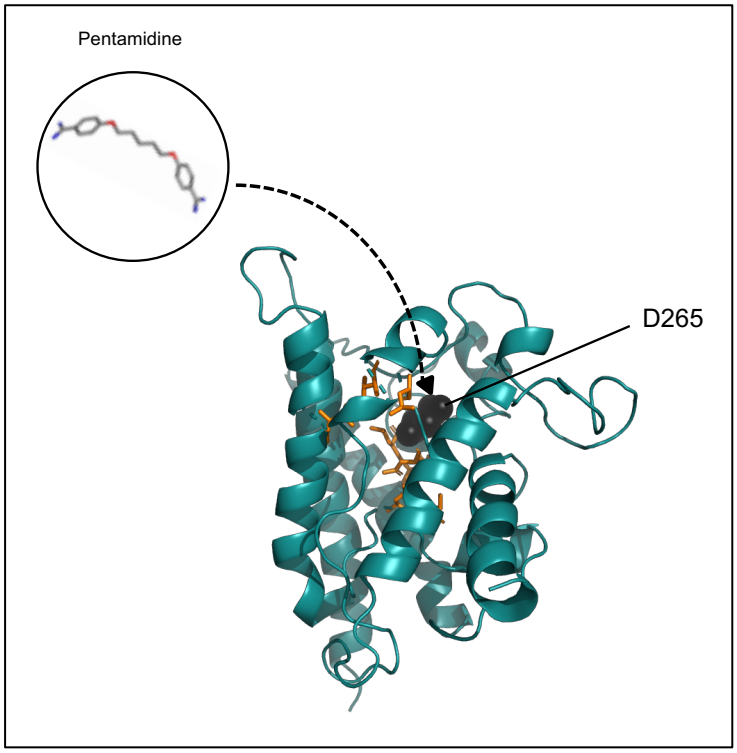

Figure 4.1: Model of the TbAQP2 protein structure.
The figure shows the positions of the D265 residue, central to the theory that *Tb*AQP2 acts as a pentamidine receptor (Song et al., 2016), relative to the selectivity filter (orange). The Song *et al*. model predicts that the pentamidine binds to the Aspartic Acid (D265) with high affinity which likely results from an electrostatic interaction between the pentamidine (positively charged) and the acidic nature of

the residue (negatively charged). This model suggested that the pentamidine internalised via endocytosis of TbAQP2 and the D265 binding is a starting point of receptor-mediated endocytosis. The model was generated using SWISS-MODEL software from the FASTA sequence of TbAQP2 (TriTrypDB Gene ID: Tb927.10.14170) and images created with PyMOL 2.2 (Schrödinger).

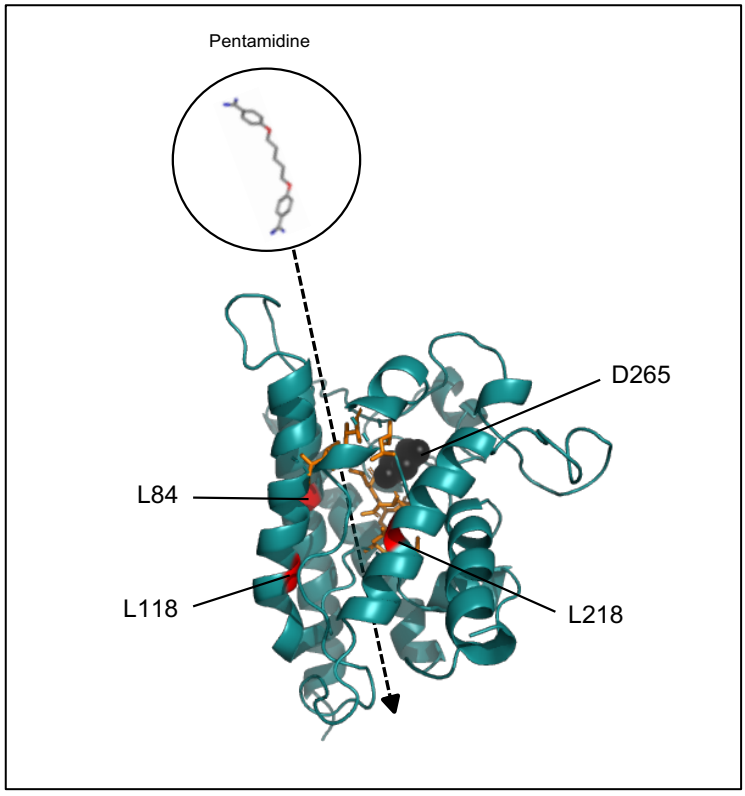

Figure 4.2: Schematic of our predicted model of pentamidine traversal through the TbAQP2 channel.
The model shows the positions of L84, L118 and L218 residues (red) at the cytoplasmic end relative to the selectivity filter (orange), and not interfering with the D265 residue (black). These Leucine residues, lining the pore, were selected for site-specific mutation and were investigated for effects on *T. brucei* sensitivity and pentamidine uptake. The model was generated using SWISS-MODEL software from the FASTA sequence of TbAQP2 (TriTrypDB Gene ID: Tb927.10.14170) and images created with PyMOL 2.2 (Schrödinger).

4.2. Results

4.2.1. Introduction of a large sized amino acid (tryptophan) at the cytoplasmic end of the AQP2 pore displayed reduced sensitivity to pentamidine (and melarsoprol) uptake

4.2.1.1. Successful construction and transfection of AQP2 L-W mutants

The L84W, L118W, and L218W were created by exchanging three leucine residues, each with tryptophan. This was aimed to determine the impact of bulky amino acids at the cytoplasmic end of TbAQP2 on pentamidine transport. Plasmid vectors containing (single or multiple amino acid substitutions) in the TbAQP2 were constructed. The plasmids pHD210 (TbAQP2^{L84W}), pHD208 (TbAQP2^{L118W}), pHD209 (TbAQP2L^{218W}) and pHDK227 (TbAQP2$^{L84W/L118W}$) were all constructed by Q5 Site-Directed Mutagenesis Kit (NEB), following the kit's protocol. The single mutants were introduced by PCR (mixture and programme conditions in section 2.3.3; primers in table 2.1) using the pRPa$^{GFP-AQP2}$ plasmid, which is under the control of a Tet-regulated RRNA promoter (Baker et al., 2012). The combination L84W/L118W mutants were generated based on template pHDK208, producing pHDK227. All the indicated plasmids were verified by Sanger Sequencing to check for the presence of full gene sequence, additional unwanted mutations, and the correct mutation(s), as well as the correct cassette for integration, using the primers HDK1011 and HDK430.

Prior to the transfection, plasmids were linearised with *Asc*I restriction enzyme to allow for correct integration of the expression cassette into the genome of *tbaqp2*/*tbaqp3* null cells (Alsford et al., 2005). Products of the digested plasmid along with undigested plasmid (as control) of each of the generated plasmids were run on 1% agarose gel to confirm the correct fragment of the DNA expression cassette which should be around 5.3 kb long (Figure 4.3). (See plasmid map (figure 2.1) in section 2.3.4.1; for *Asc*I restriction sites).

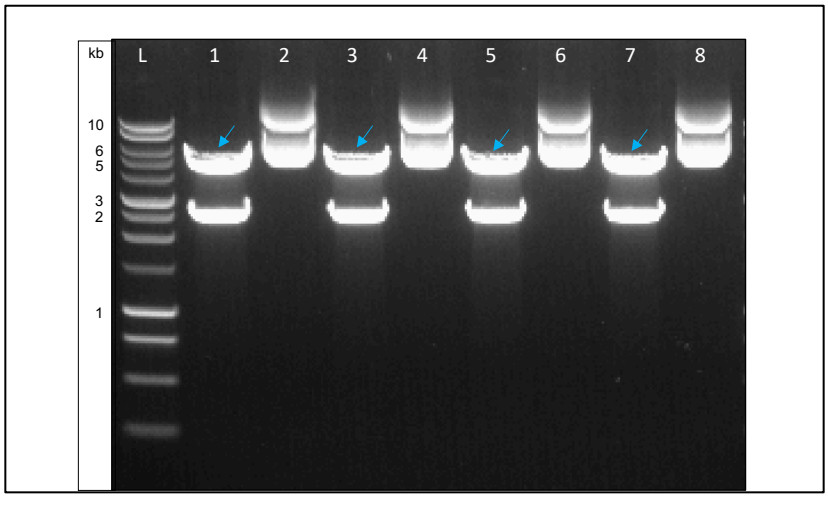

Figure 4.3: Digestion of the produced plasmids (pRPa$^{GFP-AQP2\ L-W\ mutant}$) by *Asc*I enzyme.

The figure shows a successful digestion of the produced plasmids by *Asc*I enzyme prior to the transfection. The bands at ~ 5.3 kb represent the fragments (blue arrows indicate desired bands) of the DNA expression cassette that contain the *Tb*AQP2 (L-W mutant) gene and a selection marker of the plasmid (hygromycin). The bands at ~ 2.6 kb represent the remaining (unwanted) part of the plasmid which containing only B-lactamase. Bands at ~ 7.9 kb represent the undigested plasmid (as control) of each generated plasmid. L: 1kb DNA ladder; 1: pHDK210 (digested plasmid); 2: control (pHDK210 undigested); 3: pHDK208 (digested plasmid); 4: control (pHDK208 undigested); 5: pHDK209 (digested plasmid); 6: control (pHDK209 undigested); 7: pHDK227 (digested plasmid); 8: control (pHDK227 undigested).

Following the linearization, DNA cassettes (bands of approximately 5.3 kb) were extracted from the gel and cleaned up using the NucleoSpin Gel extraction kit (Macherey-Nagel) according to the manufacturer's instructions, and were transfected into *tbaqp2/aqp3* cells (Baker et al., 2012). Transfected cells were then selected and cloned out with the presence of hygromycin, and genomic DNA was extracted from the new cell lines using the NucleoSpin Tissue kit (Macherey-Nagel) following the manufacturer's instructions. Clones were screened by PCR amplifications using Go Taq DNA polymerase (Promega) for the presence of the *Tb*AQP2 gene and for the correct integration of the plasmid into the genome (Figure 4.4). Three PCR reactions were set up to confirm this: the first PCR was used to amplify the *Tb*AQP2 gene using primers HDK529 and HDK209. The second PCR was performed to amplify the gene with surrounding parts of the expression cassette using primers HDK1011 and HDK430. The third PCR was to assess whether the expression cassette was correctly linearised, thus integrated into the *T. brucei* genome using primers HDK713 and HDK991. PCR products were separated on a 1.5% agarose gel and visualised with SYBR™ Safe DNA gel stain. Figure 4.4A shows PCR products from the first reaction of ~950 bp, the expected size of the full-length *Tb*AQP2 gene (939 bp). Product-sized bands from the second PCR reaction were ~1250 bp corresponding to the expected size of gene with the partial plasmid fragment (1212 pb) (Figure 4.4B). The amplified PCR products of the clones from the third PCR reaction showed no bands to that of the undigested plasmid control (~1100 bp), suggesting correct linearization by *Asc*I restriction enzyme, thus correct integration into the genome (Figure 4.4C) (See plasmid map (figure 2.1) in section 2.3.4.1; for primers sites).

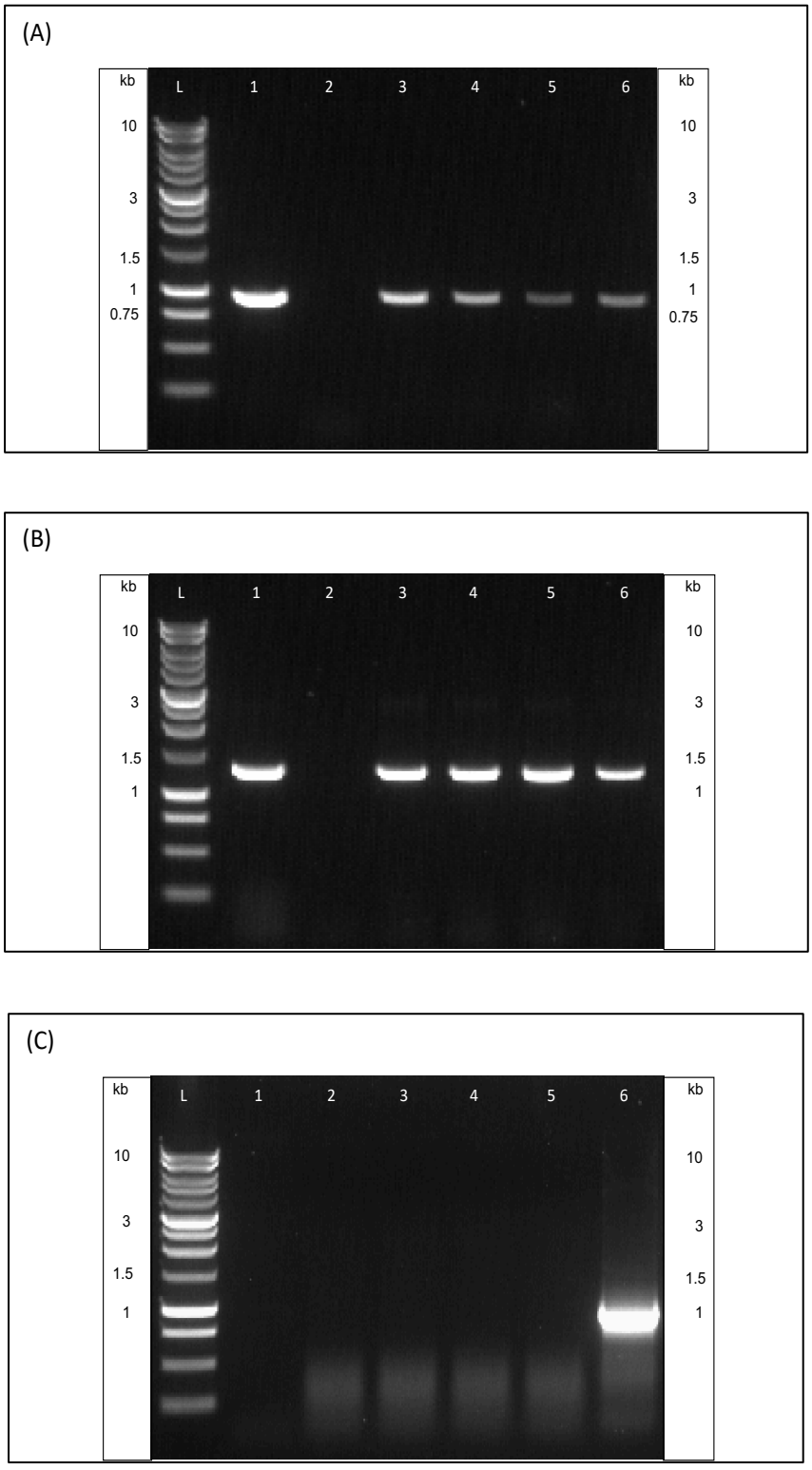

Figure 4.4: Agarose gel electrophoresis of PCR products reveals the presence of the integrated TbAQP2 mutants (L-W) transfected in *aqp2/aqp3* null cells.

Amplified PCR products shown of (A) the full *Tb*AQP2 gene at ~950 bp, (B) shows fragment at ~1250 bp containing *Tb*AQP2 and parts of the expression cassette neighbouring the gene, (c) represent a fragment containing an *Asc*I restriction site (~1100 bp). (A-B) L: 1kb Ladder; 1: pRPa$^{GFP\text{-}AQP2}$ (positive control); 2: TbAQP2 (KO) negative control; 3: TbAQP2 (L84W); 4: TbAQP2 (L118W); 5: TbAQP2 (L218W); 6: TbAQP2 (L218W/L118W). (C) L: 1Kb Ladder; 1: no DNA (negative control); 2: TbAQP2 (L84W); 3: TbAQP2 (L118W); 4: TbAQP2 (L218W); 5: TbAQP2 (L218W/L118W); 6: pRPa$^{GFP\text{-}AQP2}$ (undigested).

Following the PCR confirmations, the *Tb*AQP2 gene was then amplified from the genomic DNA of each strain using Phusion High-Fidelity DNA Polymerase (NEB). The PCR products were purified using the NucleoSpin PCR kit (Macherey-Nagel), and were sent for sequencing using the forward (HDK1011) and reverse primer (HDK430), to confirm that the generated cell lines have the correct introduction of the tryptophan residues into the three selected positions of leucine in the AQP2 (L84, L118, L218) (Appendix 9).

4.2.1.2. Molecular investigation of the AQP2 L-W mutants

After introducing all the mutants successfully into *tbaqp2*/*tbaqp3* null cells, the L-W mutants were tested for drug susceptibility and transport assays. The L-W mutants were initially evaluated through the standard Alamar Blue assay just as described (Wallace et al., 2002; Bridges et al., 2007) to determine their impact on the drug's sensitivity at the cytoplasmic end of TbAQP2. On the other hand, the resistant cells (*tbaqp2*/*tbaqp3* null) and the sensitive cells (*tbaqp2*/*tbaqp3* null re-expressed TbAQP2WT) were employed as controls of the experiment. This study used four drugs throughout the assay: pentamidine, cymelarsan, diminazene aceturate, and phenylarsine oxide (PAO). AQP2/HAPT1 transports both pentamidine and cymelarsan, and in this study were used for the drug susceptibility (Bridges et al., 2007; Baker et al., 2012). In contrast, diminazene aceturate and phenylarsine oxide were used as positive controls because they are not AQP2's substrates (Munday et al., 2014). The expression of each of the L-W mutants in *tbaqp2*/*tbaqp3* null cells resulted in cells reducing their sensitivity to pentamidine compared to similar cells expressing TbAQP2WT, as shown by Figure 4.5A. Additionally, all the L-W mutants were observed to be more resistant to cymelarsan compared to resistance observed in the expressed TbAQP2WT cell line control, but not that different from the *tbaqp2*/*tbaqp3* null control, as indicated by Figure 4.5B. On the other hand, none of the L-W mutants demonstrated any sensitivity to diminazene or PAO (Figure 4.5C-D). Nonetheless, the L218W mutant showed slight sensitivity towards diminazene, which was considered to be less (~2-fold, $P<0.05$) compared to that of pentamidine (20-fold $P<0.0001$) (Figure 4.5C).

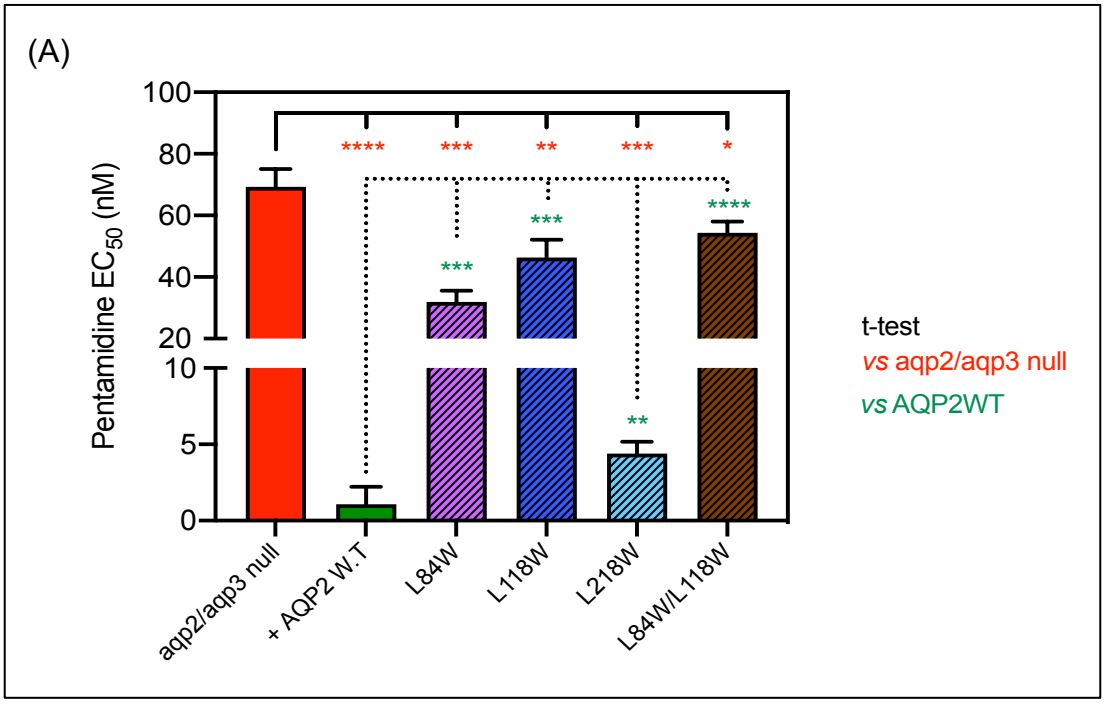
(A)
Pentamidine EC50 (nM)
100
80
60
40
20
10
5
0
****
***
**
***
*
***
***
**
****
aqp2/aqp3 null
+ AQP2 W.T
L84W
L118W
L218W
L84W/L118W
t-test
vs aqp2/aqp3 null
vs AQP2WT

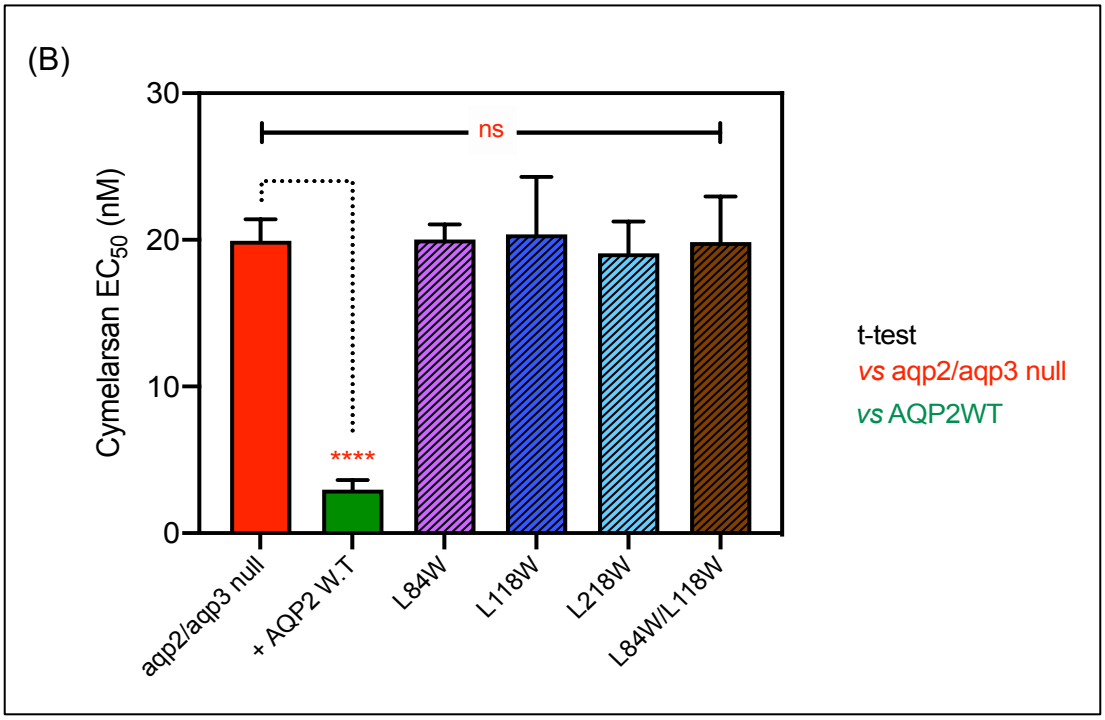
(B)
Cymelarsan EC50 (nM)
30
20
10
0
ns
****
aqp2/aqp3 null
+ AQP2 W.T
L84W
L118W
L218W
L84W/L118W
t-test
vs aqp2/aqp3 null
vs AQP2WT

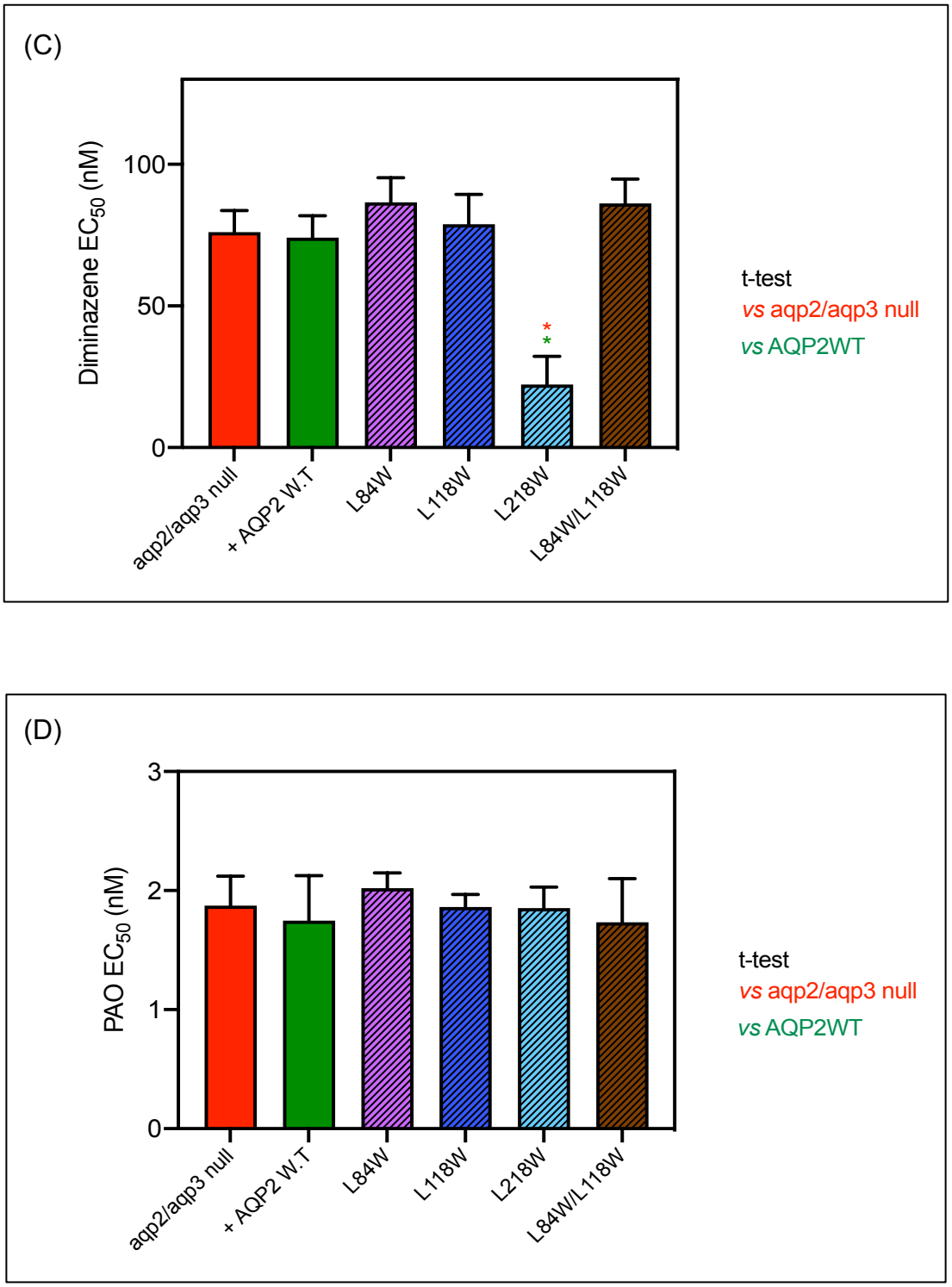

Figure 4.5: Sensitivity assay of TbAQP2 mutants (L-W) cell lines.
(A-D) EC_{50} values of the tested drugs; pentamidine, cymelarsan, diminazene and phenylarsine oxide (PAO), against *tbaqp2/tbaqp3* null (resistant control) and cell lines either expressing the TbAQP2 L-W mutants or TbAQP2WT (sensitive control). Red stars and green stars: comparison with *tbaqp2/aqp3* null or TbAQP2WT-expressing cells, respectively, which were assessed in parallel in each experiment showing the drug susceptibility of the indicated cell lines to; (A): pentamidine; (B): cymelarsan; (C): diminazene; (D): phenylarsine oxide (PAO). All experiments are the average and SEM of three independent experiments. *, P<0.05; **, P<0.01; ***, P<0.001, ****, P<0.0001 by unpaired Student's t-test, two-tailed.

The [^{3}H]-pentamidine transport assays were carried out to confirm the drug susceptibility phenotypes towards pentamidine with respect to control cell lines *tbaqp2/tbaqp3* null, the re-expressed TbAQP2WT, as well as the L-W mutants. Also, these transport assays were conducted in the presence of 1 mM adenosine, which is considered to block the TbAT1/P2 transporter (De Koning and Jarvis, 1999). The data obtained were plotted to equations for linear regression using Prism 7.04 (GraphPad software). The two control cell lines were used to present the highest and the lowest slope rates for pentamidine uptake over up to 60 s as shown in (Figure 4.6A). The rate of transport of [^{3}H]-pentamidine was measured in all mutants and showed strong reductions upon introduction of the tryptophan residues (Figure 4.6B). The L84W, L118W and L84W/L118W mutants showed a strongly diminished rate of pentamidine transport compared to the TbAQP2WT and the uptake rates of these cell lines were almost equal to the control resistant *tbaqp2/tbaqp3* null cell line (Figure 4.6B). The L218W mutant showed a very low uptake rate of the radiolabelled substrate but still above the level of the knockout cell line (Figure 4.6A-B).

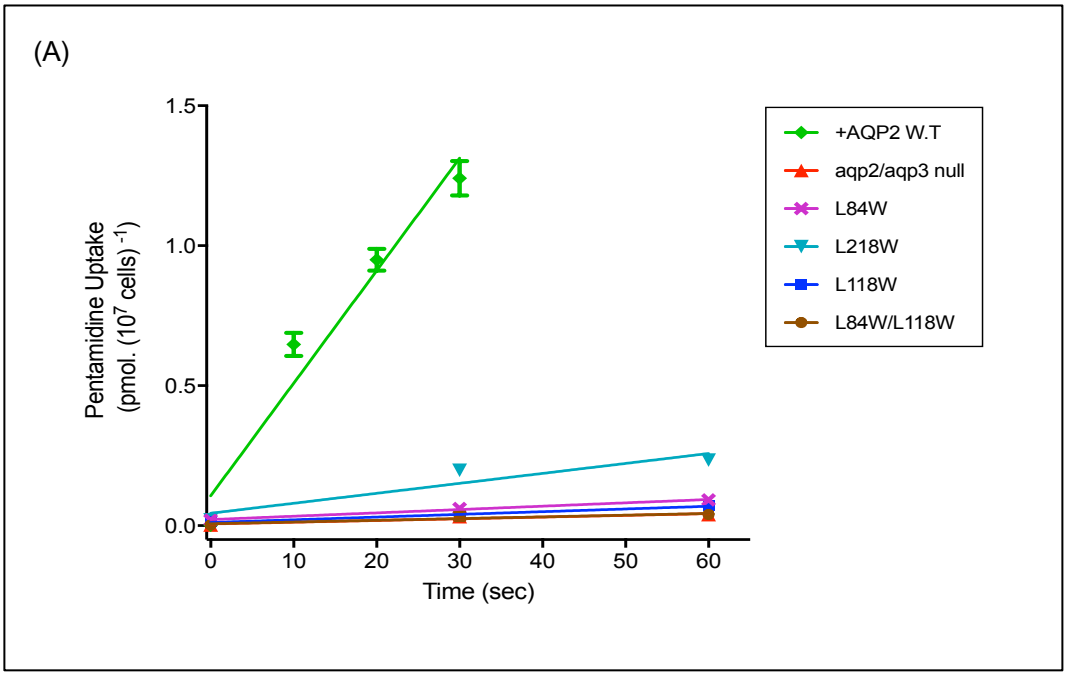

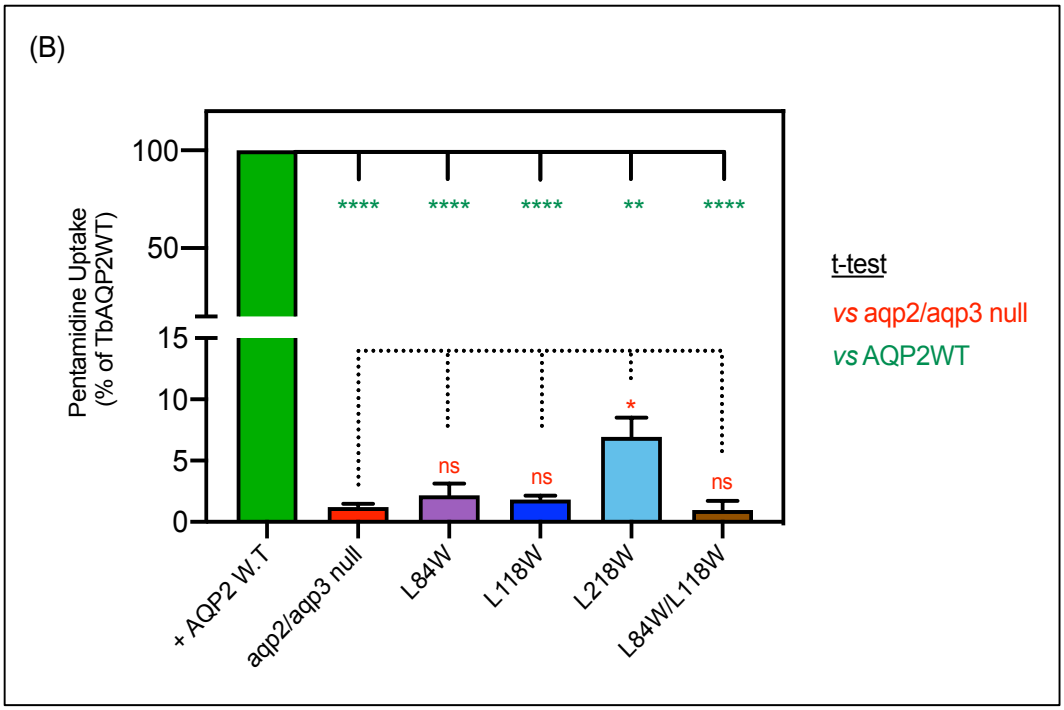

Figure 4.6: Transport of 25 nM [^{3}H]-pentamidine by *aqp2/aqp3* null, the expressing TbAQP2WT and the L-W mutant cell lines.
Transport was determined in the presence of 1 mM adenosine to block the TbAT1/P2 transporter. (A) Pentamidine uptake over a time course of 60s. Uptake rate of re-expressed wild-type TbAQP2 strain plotted only to 30s due to depleted [^{3}H]-pentamidine. Slope calculated based on linear regression using Prism 7.04 (GraphPad). (B) Bars represent the average and SEM Pentamidine uptake rates in mutant strains, relative to wild-type levels (set to 100%). Averages and SEM of three independent replicates. Significance determined by two-tailed unpaired Student's tests in comparison to TbAQP2WT (green star) and *tbaqp2/aqp3* null (red star) respectively: *, P<0.05; **, P<0.01; ***, P<0.001, ****, P<0.0001; ns, non-significant.

4.2.2. Introduction of a medium sized amino acid (methionine) at the cytoplasmic end of the AQP2 pore restores sensitivity to pentamidine (and melarsoprol) uptake

4.2.2.1. Successful construction and transfection of AQP2 L-M mutants

Based on the previous results of introducing bulky residues (tryptophan) to the cytoplasmic end of the AQP2 pore, I thought that it would be interesting to introduce a medium sized amino acid such a methionine, which is relatively similar in size to leucine, into the same selected positions (L84, L118 and L218). The combination of the effects of the Trp and Met mutations potentially allow to distinguish between an endocytosis model and a channel model for pentamidine. Therefore, genetic mutations were created in *Tb*AQP2 using the Q5 Site-Directed Mutagenesis Kit,

following the kit's protocol. The TbAQP2 L-M mutants were generated by PCR (mixture and programme conditions in section 2.3.3; primers in table 2.1) using three plasmid vectors: pHDK210, pHDK208 and pHDK209 as template plasmids to give pHDK234 (TbAQP^{L84M}), pHDK235 (TbAQP^{L118M}) and pHDK236 (TbAQP^{L218M}), respectively. All the plasmids were originally based on the vector pRPa$^{AQP2\text{-}WT}$ which is under the control of a Tet-regulated RRNA promoter (Baker et al., 2012). The indicated plasmids were then verified by Sanger sequencing for the existence of the expected mutation using the primers HDK1011 and HDK430. Before transfecting the expression cassettes into the genome of *tbaqp2*/*tbaqp3* null cells, plasmids were digested overnight with the *Asc*I restriction enzyme (NEB) for linearization, to ensure correct integration in a prepared locus in the ribosomal rRNA spacer region of the (Alsford et al., 2005). The digested products along with undigested plasmids (control) were run on 1% agarose gel. (Figure 4.7) shows band- sized at around 5.3 kb indicating to correct digestions. (See plasmid map (figure 2.1) in section 2.3.4.1 for *Asc*I restriction sites).

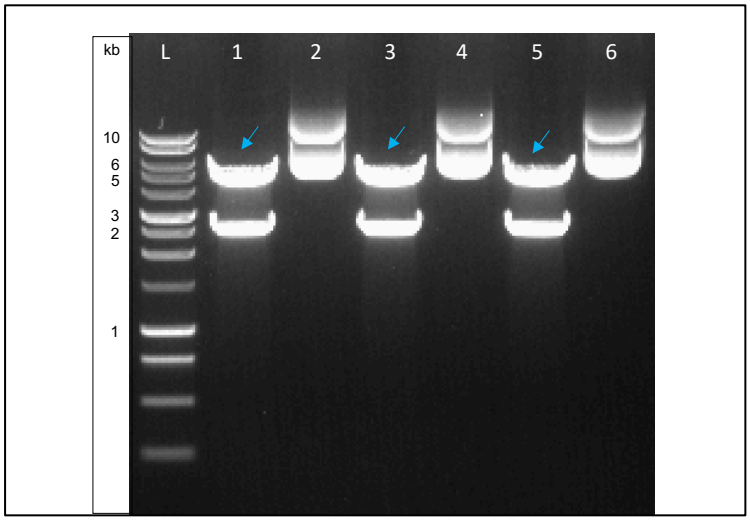

Figure 4.7: Digestion of the produced plasmids (pRPa$^{AQP2\ L\text{-}M\ mutants}$) by *Asc*I enzyme.
The figure shows a successful digestion of the produced plasmids by *Asc*I enzyme prior to the transfection. The bands at ~ 5.3 kb represent the fragments (blue arrows indicate desired bands) of the DNA expression cassette that contain the *Tb*AQP2 (L-M mutant) gene and a selection marker of the plasmid (hygromycin). The bands at ~ 2.6 kb represent the remaining unwanted part of the plasmid which contain only B-lactamase. Bands at ~ 7.9 kb represent the undigested plasmid (as control) of each plasmid. L: 1kb DNA ladder; 1: pHDK234 (digested plasmid); 2: control (pHDK234 undigested); 3: pHDK235 (digested plasmid); 4: control (pHDK235 undigested); 5: pHDK236 (digested plasmid); 6: control (pHDK236 undigested).

After the linearisation, DNA was extracted and transfected into *tbaqp2/aqp3* null cells. Clones were grown up in the presence of hygromycin, gDNA from each cell lines were extracted using the NucleoSpin Tissue kit (Macherey-Nagel) following the manufacturer's instructions, and PCR confirmation were carried out. Three PCR amplifications were performed using GoTaq polymerase (Promega), for the existing of the *Tb*AQP2 gene and for the correct integration of the expression cassette into the genome (Figure 4.8A-C). 1st PCR was used to amplify the full *Tb*AQP2 gene using forward primer (HDK529) and reverse primer (HDK209). Whereas, the forward primer (HDK1011) and the reverse primer (HDK430) both from the vector were used in the 2nd PCR to amplify parts of the expression cassette containing the *Tb*AQP2 gene. The 3rd PCR was to confirm the correct integration of the expression cassette into the genome of the *T. brucei* using (HDK713) and (HDK991) primers. PCR products were then run on an 1% agarose gel with DNA staining to validate the correct size of the DNA amplified. From the first reaction, PCR products were ~950 bp (Figure 4.8A) displayed the full size of the *Tb*AQP2 (939 bp). Whilst, product-sized bands from the second PCR reaction were at ~1250 bp (Figure 4.8B) indicating to the expected size of the gene with the partial plasmid fragments (1212 bp). (Figure 4.8C) presents PCR products from the 3rd PCR reaction showing no bands to that of the undigested plasmid control (~1110bp), suggestion a correct linearization and integration to the genome. The expected bands sizes of the PCR products that were obtained from the amplifications of the three PCR indicate to successful transfections (See plasmid map (figure 2.1) in section 2.3.4.1; for primers sites).

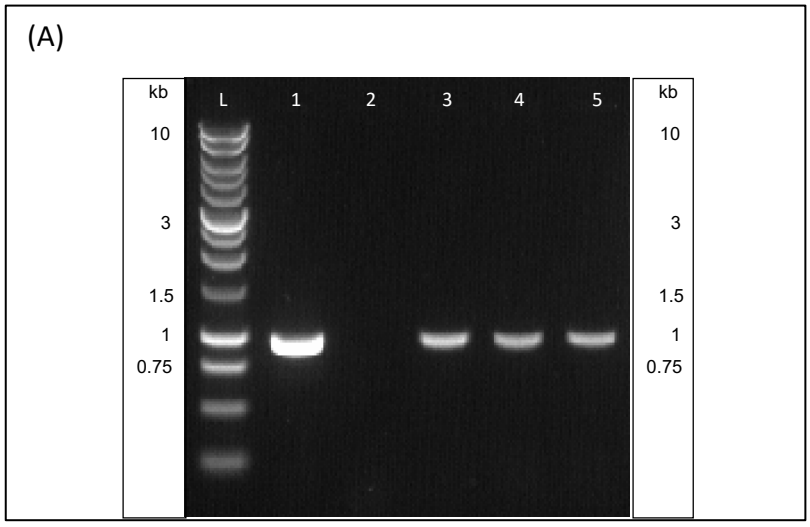

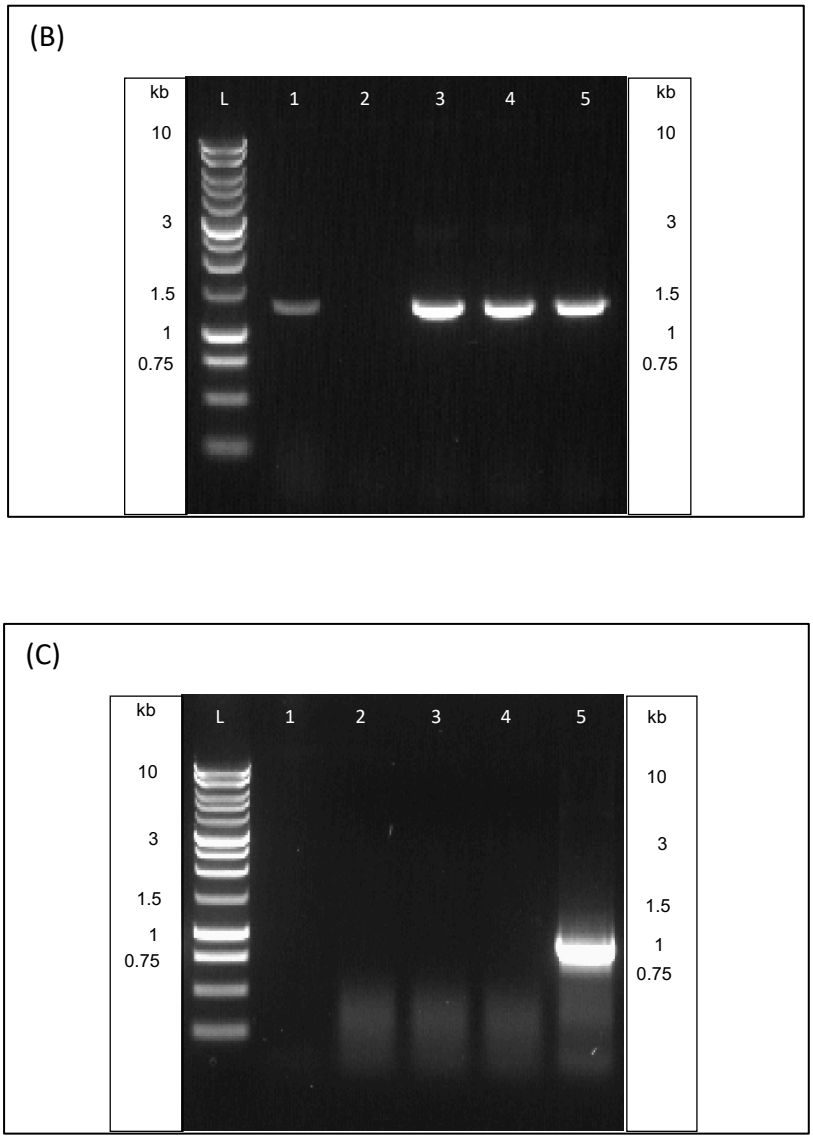

Figure 4.8: PCR evidence of plasmid integration of the TbAQP2 (L-M) mutants into the *tbaqp2/tbaqp3* null cells.
(A) is a gel using forward primer (HDK529) and revers primer (HDK209), shown the full TbAQP2 gene at ~950 bp. While (B) is gel using forward primer (HDK1011) and revers primer (HDK430) presents bands around 1250bp, indicated to fragments of the expression cassette containing the AQP2 gene. (C) is gel using forward primer (HDK713) and revers primer (HDK991), shown no bands to that of the undigested plasmid control at ~1100bp indicated to correct linearization and integration. (A-B) L: 1Kb Ladder; 1: pRPa^{AQP2WT} (positive control); 2: TbAQP2 (KO) negative control; 3: TbAQP2 (L84M); 4: TbAQP2 (L118M); 5: TbAQP2 (L218M). (C) 1: no DNA (negative control); 2: TbAQP2 (L84M); 3: TbAQP2 (L118M); 4: TbAQP2 (L218M); 5: pRPa^{AQP2WT} (undigested).

Before testing the generated cell lines for drugs sensitivity and transport assays, the correct substitutions of leucine to methionine were confirmed by sequencing. The *Tb*AQP2 gene was amplified from the genomic DNA of each cell lines using Phusion High-Fidelity DNA Polymerase (NEB); using the forward (HDK1011) and reverse primer (HDK430). The amplified products from the PCR reaction were purified using

a DNA purification kit (Macherey-Nagel) and were then sent for sequencing (SourceBioscience, UK) using the mentioned primers. The DNA sequencing represent that the mutant cell lines contain *Tb*AQP2 gene and carry the correct mutations (L-M) at right positions (Appendix 10).

4.2.2.2. Molecular investigation of the AQP2 L-M mutants

To confirm the importance of the three selected positions of the leucine residues, substitution mutations to a medium-sized amino acide, L84M, L118M and L218M were created and expressed in the null-background strain *tbaqp2/tbaqp3* (Baker et al., 2012) using the tetracycline-inducible pRPa vector (Alsford et al., 2005). Sensitivity of the L-M mutants to pentamidine and the melaminophenyl arsenical cymelarsan was assessed using the Alamar Blue assay. Additionally, the mutant strains were assessed against diminazene and the control drug PAO, which is not a TbAQP2 permeant (Graf et al., 2015). EC_{50} values obtained with the mutants were compared with values obtained with the *tbaqp2/tbaqp3* null strain (drug-resistant control) and the strain possessing the re-expressed wild-type TbAQP2 (drug-sensitive control). Substituting the same leucine residues with methionine rather than tryptophan, variants L84M and L218M show no difference compared to TbAQP2WT in terms of pentamidine sensitivity with a significant difference with regards to tryptophan variants (Figure 4.9A). However, replacing Met at position 118 led to developing the same effects as observed with the Trp variant (Figure 4.9A). The L84M and L218M mutants also sensitised to cymelarsan ($P<0.01$) (Figure 4.9B). By the same comparison, there was no significant difference between the sensitivity of all the mutants to diminazene (Figure 4.9C) and PAO (Figure 4.9D), with exception of the L218M mutant that was, surprisingly, somewhat sensitised to diminazene (~2-fold, $P<0.05$). Thus, an amino acid substitution to the cytoplasmic end of L84, L118 and L218 residues is sufficient for determining sensitivity of *T. brucei* cells to *Tb*AQP2-transported pentamidine.

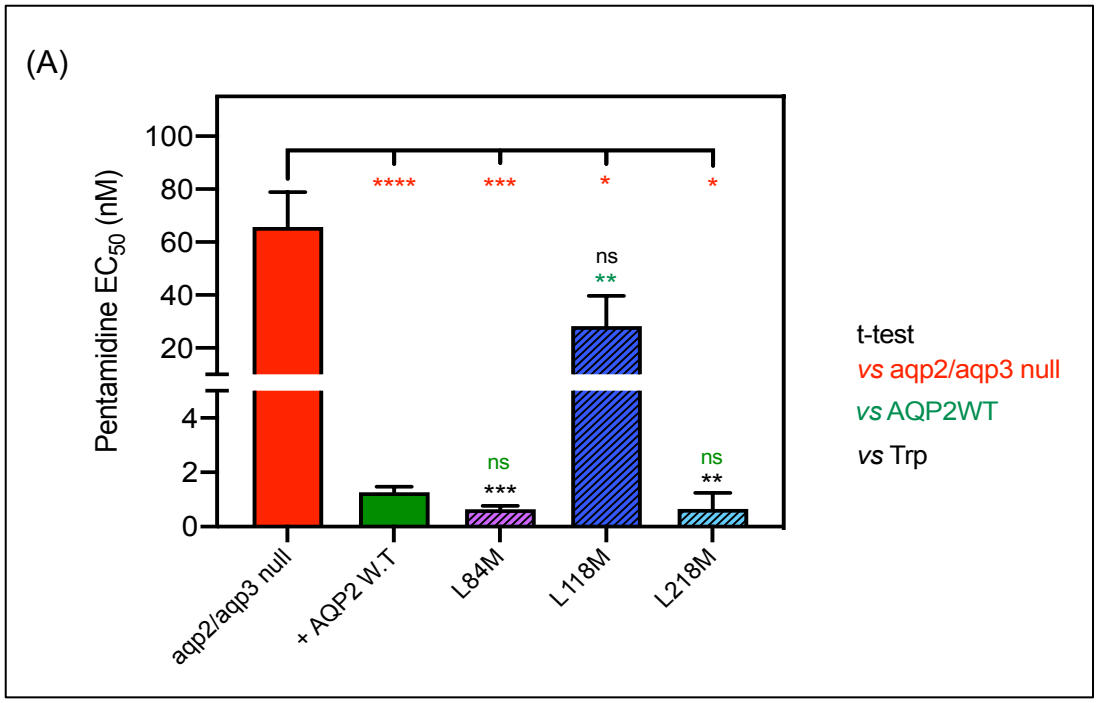
(A)
Pentamidine EC50 (nM)
100
80
60
40
20
4
2
0
****
***
*
*
ns
**
ns
***
ns
**
aqp2/aqp3 null
+ AQP2 W.T
L84M
L118M
L218M
t-test
vs aqp2/aqp3 null
vs AQP2WT
vs Trp

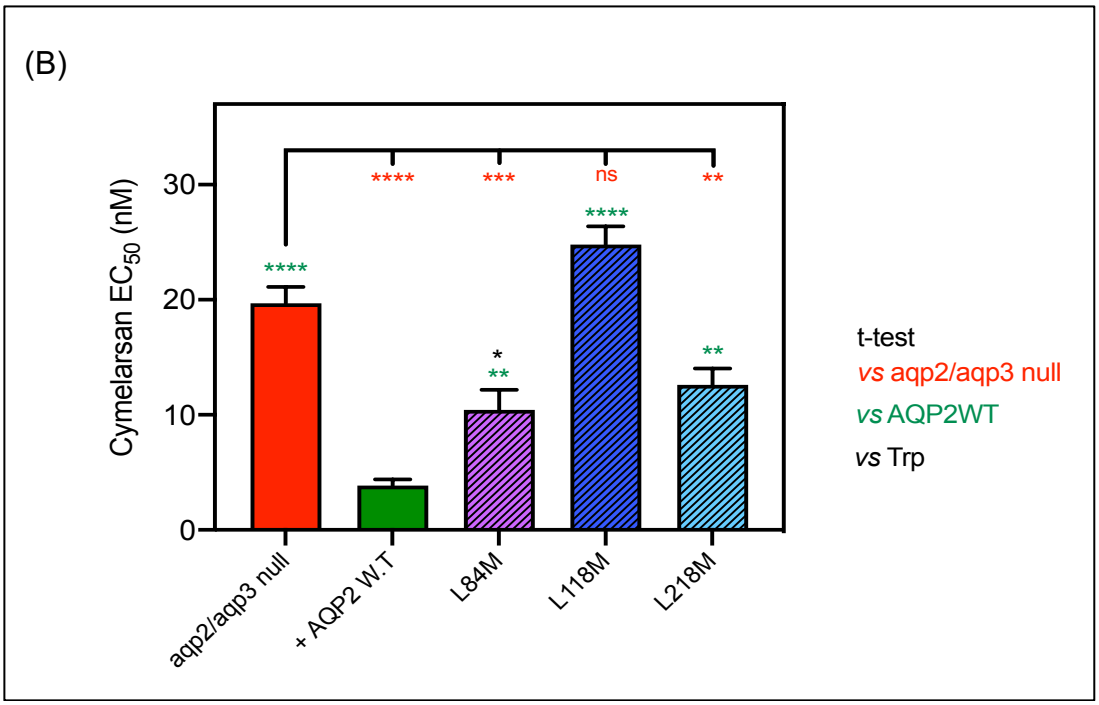
(B)
Cymelarsan EC50 (nM)
30
20
10
0
****
***
ns
**
****
*
**
****
**
aqp2/aqp3 null
+ AQP2 W.T
L84M
L118M
L218M
t-test
vs aqp2/aqp3 null
vs AQP2WT
vs Trp

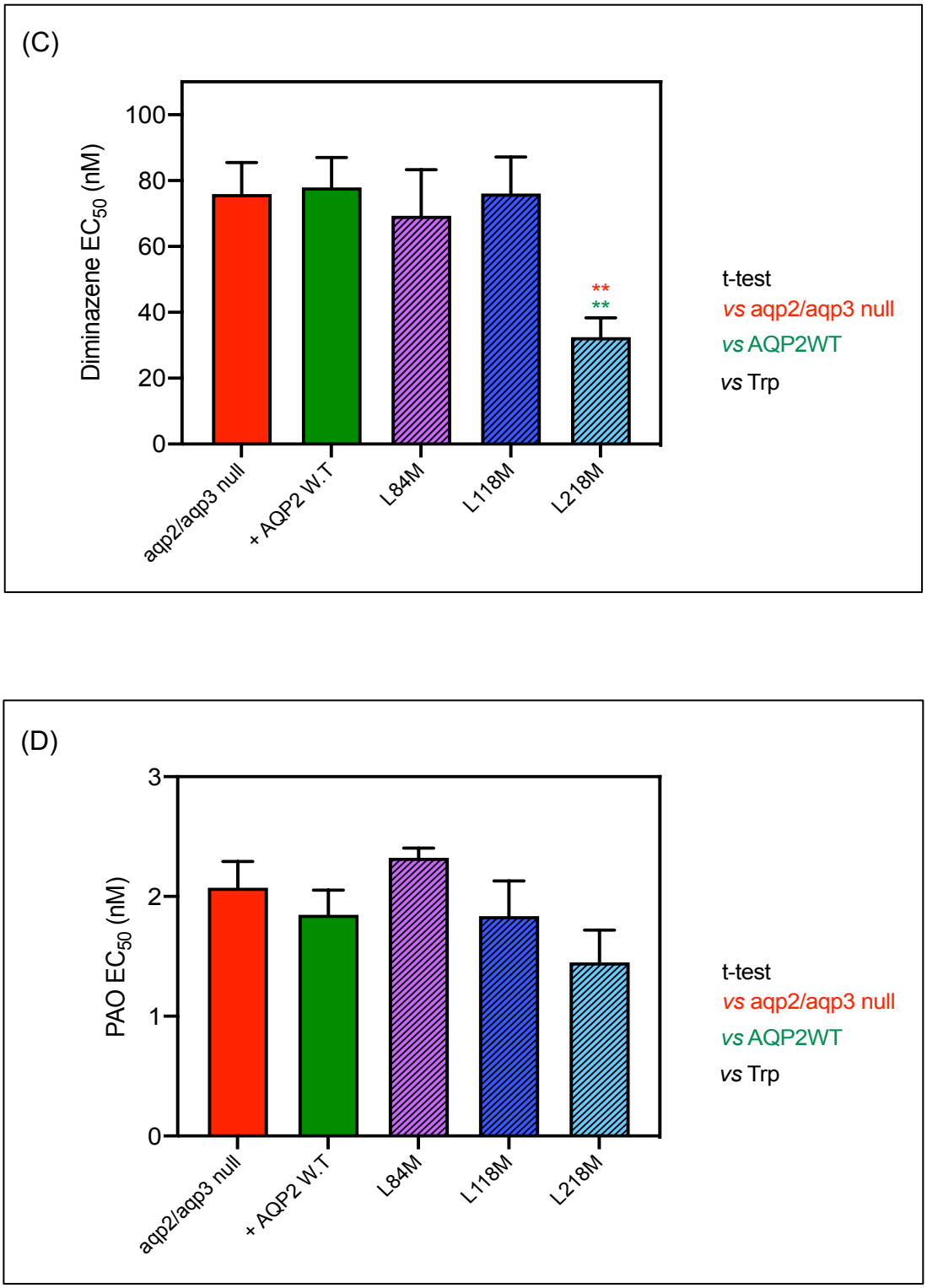

Figure 4.9: Sensitivity assay of TbAQP2 mutants (L-M) cell lines.
The controls and the L-M mutant cell lines and *tbaqp2/tbaqp3* null (resistant control) and cell line expressing the TbAQP2WT (sensitive control) were assessed against a serial dilution of (a) pentamidine (b) cymelarsan (c) the control drug diminazene and (d) the control drug phenylarsine oxide (PAO). Bars represent the average and SEM of three independent replicates. Significance was determined by two-tailed unpaired Student's tests in comparison to *tbaqp2-tbaqp3* null cell line (red star), TbAQP2WT (green star) and tryptophan variants (black star), respectively: *, P<0.05; **, P<0.01; ***, P<0.001, ****, P<0.0001; ns, non-significant.

In order to determine whether the significant changes of pentamidine sensitivity in the mutants expressing L-M were associated with alterations to pentamidine uptake into the cell, direct uptake assays of [^{3}H]-pentamidine were performed to all derivative and control strains over the course of a minute. The transport assessment was conducted in triplicate and on three independent occasions in the presence of 1 mM adenosine (for blocking the TbAT1/P2 transporter, De Koning and Jarvis, 1999). Observations indicated all expressed L-M mutants exhibited higher pentamidine uptake rates compared to the rate observed in the *tbaqp2/tbaqp3* null strain in 60 s (Figure 4.10A). The introduction of methionine residues into the L84, L118 and L218 sites in the TbAQP2 showed that in two out of the three cases (L84M and (L218M), the pentamidine uptake was largely restored, whereas L118M showed a very low uptake rate of the [3H]-pentamidine but still above the level of the knockout cell line (Figure 4.10A). The rate of [^{3}H]-pentamidine uptake for the L84M and L218M mutants was significantly increased compared to the previous results of the (L-W) mutants, and were nearly normal to the rate of the TbAQP2WT, with an approximate rate of 50% for L84M and 68% for L218M, respectively (Figure 4.10B).

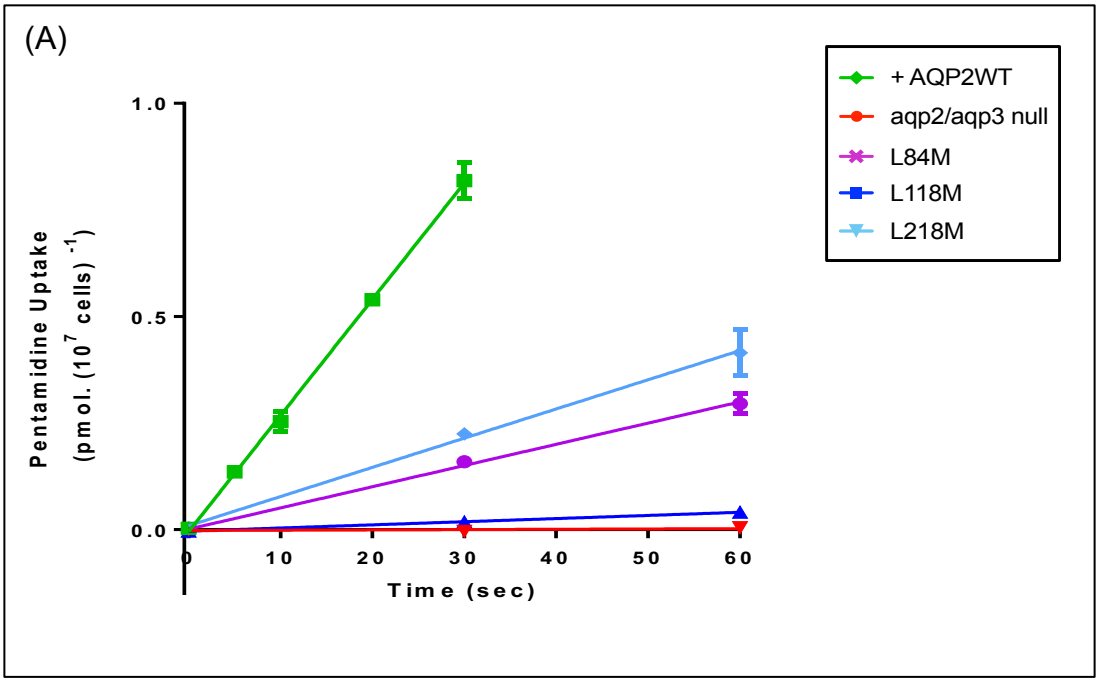

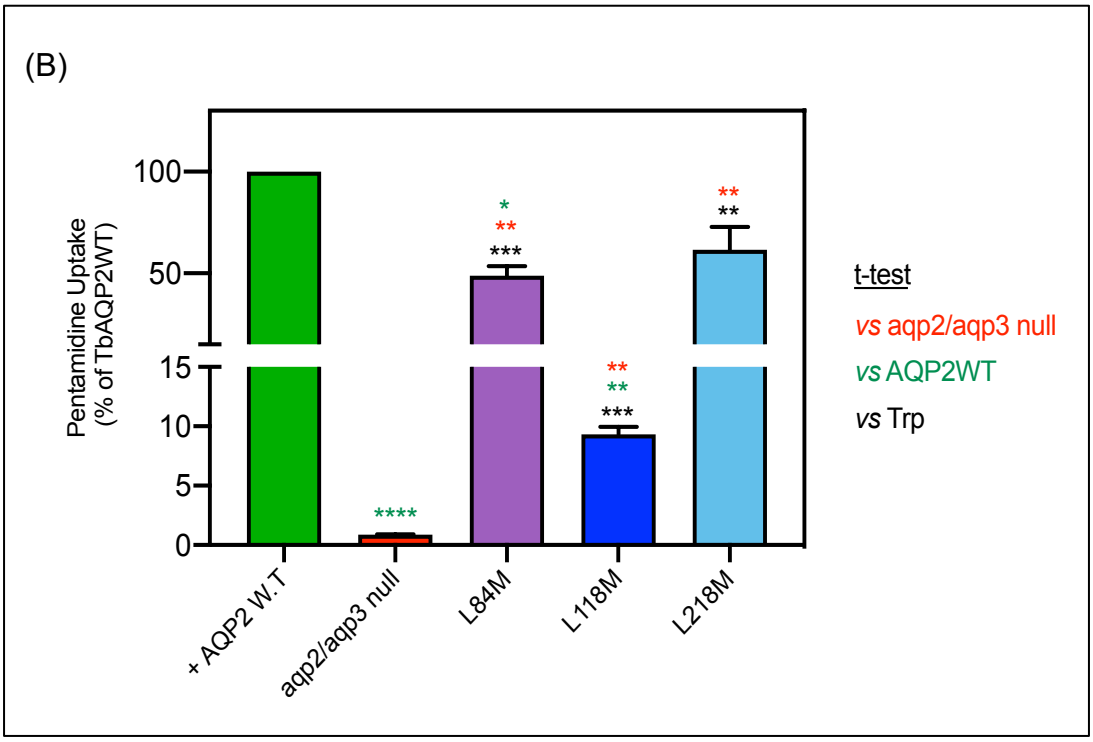

Figure 4.10: **Transport of 25 nM [^{3}H]-pentamidine by *tbaqp2/aqp3* null cells, expressing TbAQP2 WT and the L-M mutant cell lines as indicated.**
Transport was determined in the presence of 1 mM adenosine to block the TbAT1/P2 transporter. (A) Pentamidine uptake over a time course of 60s. Uptake rate of re-expressed wild-type TbAQP2 strain plotted only to 30s due to depleted [^{3}H]-pentamidine. Slopes were calculated by linear regression using Prism 7.04 (GraphPad). (B) Bars represent the average and SEM Pentamidine uptake rates in mutant strains, relative to wild-type levels (set to 100%); averages and SEM of three independent replicates. Significance was determined by two-tailed unpaired Student's tests in comparison to TbAQP2WT (green star), *tbaqp2/aqp3* null (red star) and tryptophan variants (black star), respectively: *, P<0.05; **, P<0.01; ***, P<0.001, ****, P<0.0001; ns, non-significant.

4.2.3. The TbAQP2 (L-W) and (L-M) variants are still functional aquaglyceroporins

In aerobic conditions, the bloodstream-form trypanosomes (BSF) can survive by utilizing glycerol as a carbon source (Bakker *et al*, 1997). However, the accumulation of higher glycerol levels can result in harmful conditions to the parasites, need to be disposed from the cells through aquaglyceroporins (Jeacock *et al*, 2017). In contrast, *T. brucei* is considered to have a mitochondrial protein called the trypanosome alternative oxidase (TAO), which is believed to facilitate the respiration of the BSF parasites (Clarkson et al., 1989). It has proposed that the trypanosome parasites tend to produce large quantities of glycerol to survive anaerobically when the (TAO) is inhibited (Balogun et al., 2013). Salicylhydroxamic

Acid (SHAM) is a known TAO inhibitor that can simulate the case of growing trypanosomes under anaerobic conditions (Opperdoes et al.,1976). A very recent study noted that trypanosomes could not efficiently dispose glycerol in the absence of aquaglyceroporins, leading to higher SHAM susceptibility (Jeacock et al., 2017). The same study continued to propose that TbAQP2 has a more significant contribution to glycerol utilization and efflux compared to TbAQP1 and TbAQP3.

From the above experiments, the results clearly showed that introducing large amino acids at the cytosolic end can block the pentamidine transport. The data also show the Leu-Met substitution mutants to be more sensitive towards pentamidine but not cymelarsan. In order to check whether these variants were still functional aquaglyceroporins, the observation of Jeacock et al. (2017) was used, that when *T. brucei* cells lack all three APQs, they become sensitized to (SHAM) Trypanosome Alternative Oxidase inhibitor (TAO) due to cellular glycerol accumulation. Here in this study, the TbAQP2 (L-W) and (L-M) mutants were assessed for their ability to transport glycerol as aquaglyceroporins. This was achieved by expressing the mutants into the *T. brucei* AQP null background (*tbaqp*1-3 null) and test them for SHAM sensitivity and glycerol uptake.

4.2.3.1. Successful transfection of TbAQP2 variants into *tbaqp1/tbaqp2/tbaqp3* null cells

In order to verify whether the L-W and L-M AQP2 mutants are still functional, the AQP2 variants were expressed in the *tbaqp1-2-3* null cell line (Jeacock et al., 2017) (made available by David Horn, University of Dundee, UK). *E. coli* containing each of the plasmid constructs of the AQP2 (L-W) and (L-M) mutants, including the pRPa$^{GFP\text{-}TbAQP2WT}$ vector, were cultured overnight in LB broth and plasmids were isolated by miniprep kits (Macherey-Nagel) according to the manufacturer's instructions. Prior to the transfection, the vectors were digested using *Asc*I restriction enzyme (NEB) to linearise the expression cassette for correct integration into the *T. bruce*i genome (Alsford et al., 2005). After the linearisation, the digested products, along with undigested plasmids (control), were loaded onto a 1% agarose gel. Figure 4.11 shows bands of the digested plasmids sized at 5.3 kb and 2.6 kb,

indicating the correct digestions of the DNA expression cassette. (See plasmid map (figure 2.1) in section 2.3.4.1 for *Asc*I restriction sites).

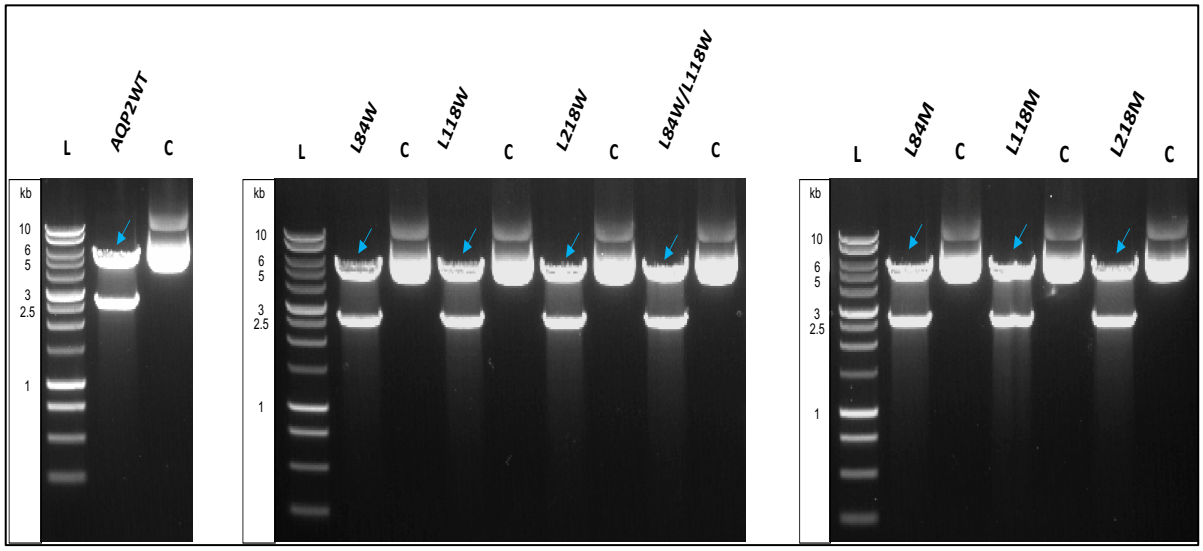

Figure 4.11: Confirmation of correct linearisation of the plasmids of (pRPa$^{AQP2L-W}$) and (pRPa$^{AQP2L-M}$) prior to the transfection.
The plasmids were digested with *Asc*I restriction enzyme, resulting in two distinct bands refenced to 1 kb DNA ladder (L). Band at ~ 5.3 kb represent fragment of the DNA expression cassette that contain the gene of interest and the hygromycin resistance marker (blue arrows indicate desired band). The band at ~ 2.6 kb represent the remaining unwanted fragment of each plasmid that containing only B-lactamase. (C) as a control (undigested plasmid of each L-W and L-M mutant) band at ~ 7.9 kb.

For each of the digested plasmids, the DNA expression cassette (band at 5.3 kb) was extracted from the gel using the NucleoSpin Gel extraction kit (Macherey-Nagel) and was transfected into *tbaqp1*/*tbaqp2*/*tbaqp3* null cells. The produced clones were grown up in the presence of hygromycin (2.5 µg /ml; selection for the expression cassette), followed by gDNA extraction from each cell line (after 5 passages with the selection marker) using the NucleoSpin Tissue kit (Macherey-Nagel). In order to use for the sensitivity and uptake assays, the positive clones were verified by PCR. Two PCR amplifications were set up using GoTaq polymerase (Promega), one to verify the existence of the *Tb*AQP2 gene and one for the correct integration of the expression cassette into the genome. The 1st PCR was used to amplify the full *Tb*AQP2 gene using forward primer HDK529 and reverse primer HDK209, whereas, for the 2nd PCR reaction forward primer HDK713 (located 989 bp upstream of the AscI site in the plasmid backbone) and the reverse primer HDK535 (located 338 bp downstream of the AscI site in the plasmid backbone) were used. PCR products were

then run on a 1% agarose gel with DNA staining to validate the correct size of the DNA amplified. From the 1st PCR reaction, PCR products were at ~950 bp (Figure 4.12A), i.e. approximately the full size of the *Tb*AQP2 gene (939 pb). Figure 4.12B represents PCR products from the 2nd PCR reaction showing no bands other than that of the undigested plasmid control (1384 bp), suggestion a correct linearization and integration into the genome. The PCR products of the two PCR reactions indicate a successful transfection of the *Tb*AQP2 WT gene and its variants into the genome of the *aqp1*/*aqp2*/*aqp3* null cells (See plasmid map (figure 2.1) in section 2.3.4.1; for primers sites).

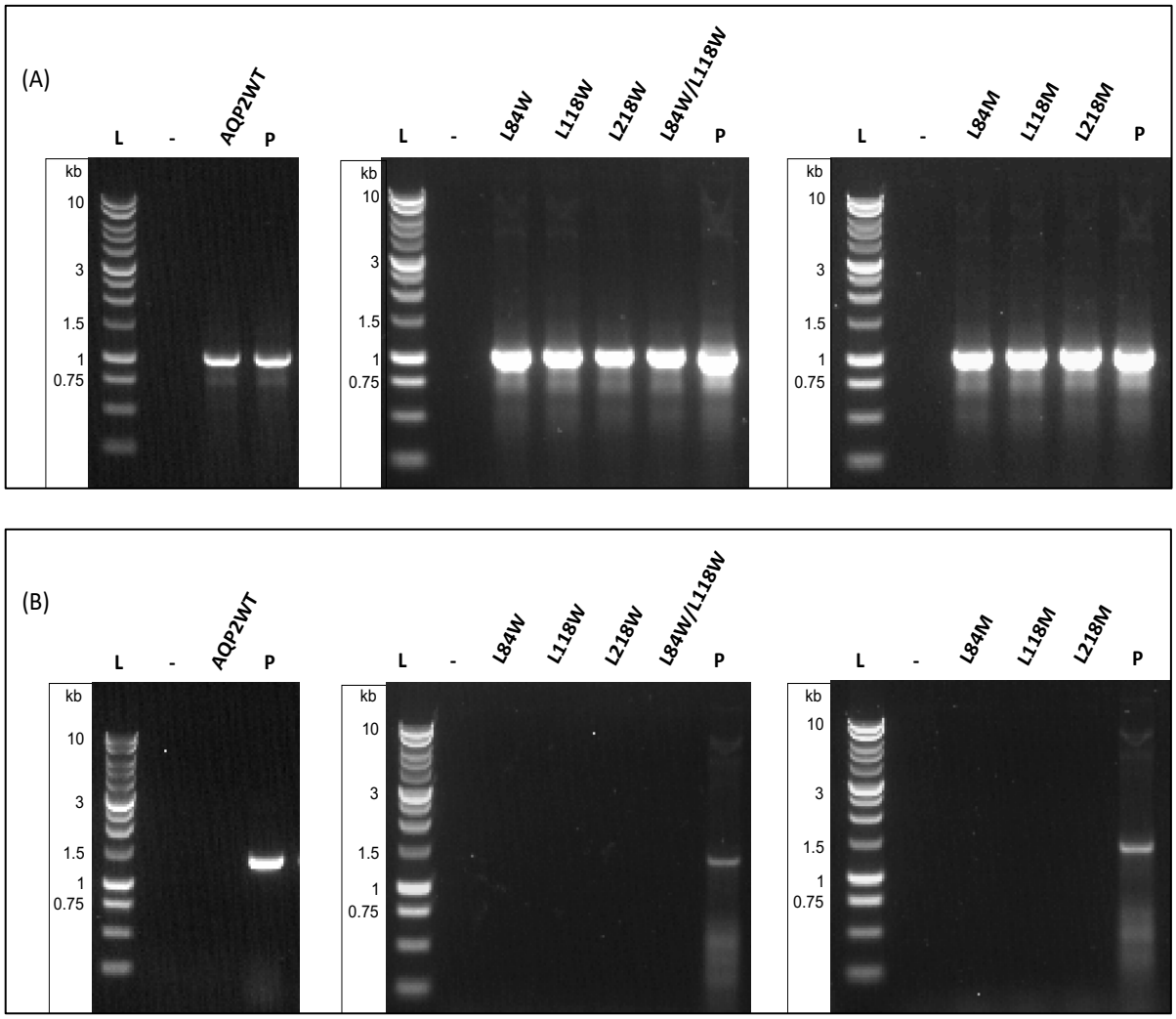

Figure 4.12: Gel images show the result of the PCR confirmation for the presence and the correct integration of the linearized expression constructs of the TbAQP2WT, the TbAQP2 L-W and L-M mutants into the *tbaqp1/aqp2/aqp3* null cells.
(A) PCR products of ~1 kb indicates the presence of the full TbAQP2 gene using primers HDK529 and HDK209. (B) No bands indicate to the complete linearisation of the circular plasmids that were confirmed by PCR using the primers HDK713 and HDK535. Bands at ~1400 bp represent the positive, circular control. L: 1 kb DNA ladder; -: no DNA (negative controls); P: plasmid of pRPa$^{AQP2\text{-}WT}$ (positive control).

4.2.3.2. Expressing the TbAQP2 variants into *aqp1-3 null* cells correlates with reversal of sensitisation to SHAM

The assessment of both AQP2WT and the variants sensitivities towards the TAO inhibitor SHAM was conducted as a proxy for glycerol transport after the expression in *tbaqp1-2-3* null cells (Jeacock et al., 2017). For this, the Alamar blue assays were used to determine the EC_{50} of the L-W and L-M mutants to verify whether these cells are resistant to SHAM. The assay was performed in parallel with the sensitive (*tbaqp1-2-3* null) and the resistant (expressing TbAQP2WT) strains, which were used as controls (Jeacock et al., 2017). The sensitivity of these cells to pentamidine (control drug) was also determined throughout the assessment for more validation. For pentamidine, we found that all the mutants expressed in the triple *tbaqp1*/*tbaqp2*/*tbaqp3* null cells behave almost in a same manner to that when they were previously expressed in the *tbaqp*2/*tbaqp*3 null cells (Figure 4.5A, 4,9A), showing similar EC_{50} profiles (Figure 4.13). This observation is consistent with TbAQP1 having no role in pentamidine uptake or activity.

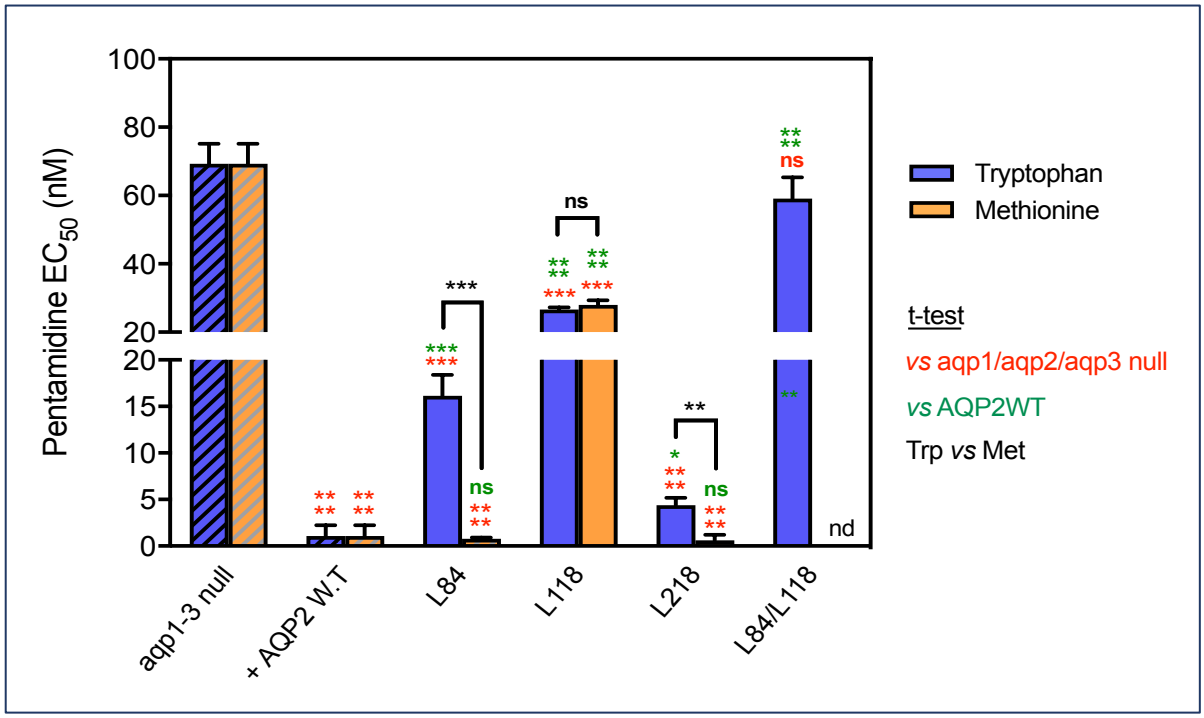

Figure 4.13: Sensitivity assay of pentamidine by TbAQP2 variants with a leucine-to-tryptophan or leucine-to-methionine substitution near the cytoplasmic end of the pore.
Pentamidine (control drug) EC_{50} values (nM) for mutant and WT TbAQP2 expressed in *tbaqp1/tbaqp2/tbaqp3* cells (aqp1-3 null), performed in parallel with the determination of EC_{50} values for SHAM, shown in (Figure 6.4). The mutant AQPs contain either a Trp (blue bars) or Met (orange

bars) substitution at the indicated positions. The resistant control (aqp1-3 null) and sensitive control (AQP2WT) for the separate datasets (Trp or Met) are indicated as hatched bars in the same colours. All bars represent the average and SEM of at least three independent replicates. *, P<0.05; **, P<0.01; ***, P<0.001, ****, P<0.0001 by unpaired Student's t-test; ns, not significant; nd, not determined.

On the other hand, cells expressing the variants all displayed highly significant reversal of the sensitisation to SHAM seen in the *tbaqp1/tbaqp2/tbaqp3* null cells, although some showed an intermediate phenotype indicating a somewhat reduced ability to mediate glycerol efflux (Figure 4.14). This is not surprising considering the introduction of tryptophan at the narrow cytoplasmic end. At position 118 the substitutions with Trp and Met produced, surprisingly, a very similar, intermediate effect, which may indicate a particularly important role for this residue. All the Trp and Met mutants at positions 84, 118, and 218 were noted to have the capacity to transport glycerol as indicated by SHAM EC_{50} values that appear to be much higher than those observed in the *tbaqp1-2-3* null cells (Figure 4.14). These mutants demonstrated an intermediate SHAM EC_{50}, which was considerably different from that observed in TbAQP2WT, showing some reduction in those mutants' glycerol efflux capacity.

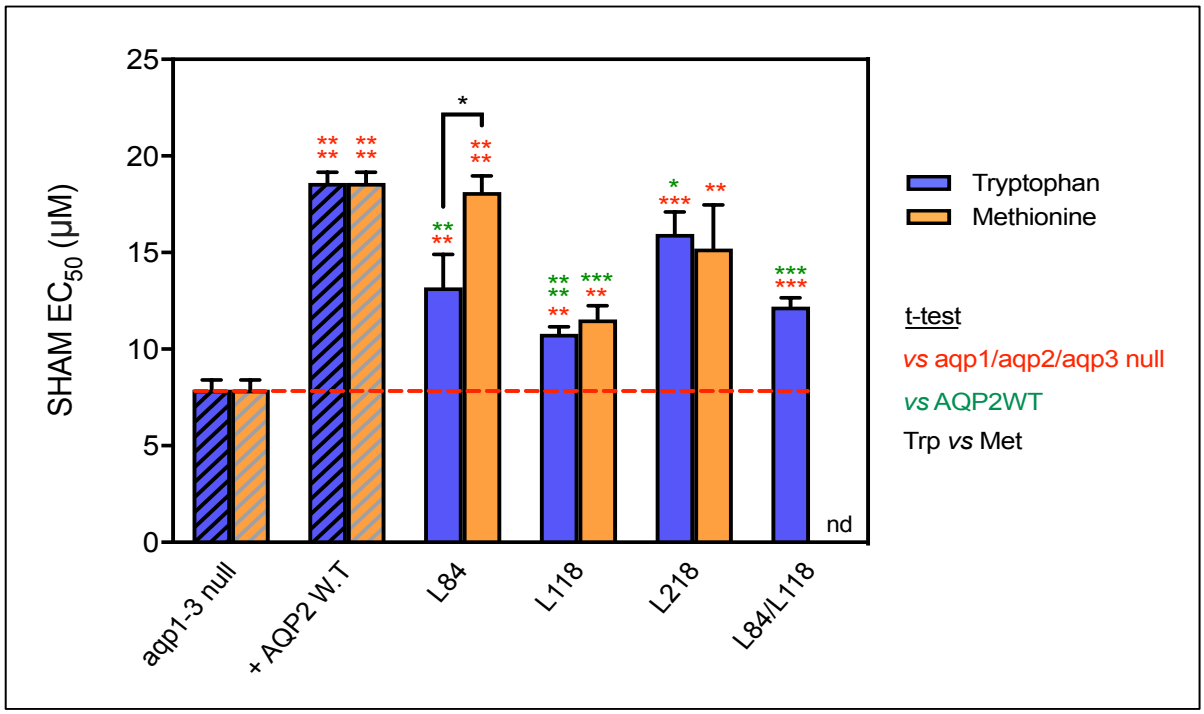

Figure 4.14: Sensitivity assay of SHAM by TbAQP2 variants with a leucine-to-tryptophan or leucine-to-methionine substitution near the cytoplasmic end of the AQP2 pore.
The figure shows SHAM EC_{50} values (µM) for mutant and WT TbAQP2 expressed in *tbaqp1/tbaqp2/tbaqp3* cells (aqp1-3 null). The mutants are either a Trp (blue bars) or Met (orange bars)

substitution at the indicated positions. The resistant control (aqp1-3 null) and sensitive control (AQP2WT) for the separate datasets (Trp or Met) are indicated as hatched bars in the same colours. All mutants effectively reversed the increased SHAM-sensitivity of the *aqp1-2-3* null cell line. All bars represent the average and SEM of at least three independent replicates. *, P<0.05; **, P<0.01; ***, P<0.001, ****, P<0.0001 by unpaired Student's t-test; ns, not significant; nd, not determined.

4.2.3.3. Expressing the TbAQP2 variants into *aqp1-3 null* cells displayed ability to mediate glycerol transport

We then sought to determine if the mutant cells (both L-W and L-M) displayed measurable glycerol uptake capacity and the glycerol-efflux capability as observed from the above experiments. As a result, the assessment was conducted on the rate of radiolabelled glycerol uptake in *aqp1/aqp2/aqp3* null cells expressing AQP2 variants. Then, this rate was presented as a percentage of the transport rate of [^{3}H]-glycerol recorded in the TbAQP2WT control cells. The aqp1-2-3 cells were noted to have a low glycerol uptake rate (Figure 4.15), which was considered consistent with reduced glycerol diffusion across the plasma membrane. Based on this measure, glycerol's transport occurred in all Trp and Met mutants at 84, 118, and 218. However, this glycerol transport did not happen in the double mutants of L84W/L118W due to bulky residues (tryptophan) at the pore's lower point. Certainly, our results demonstrate the uptake of [^{3}H]-glycerol reflected what was observed in SHAM (Figure 4.14).

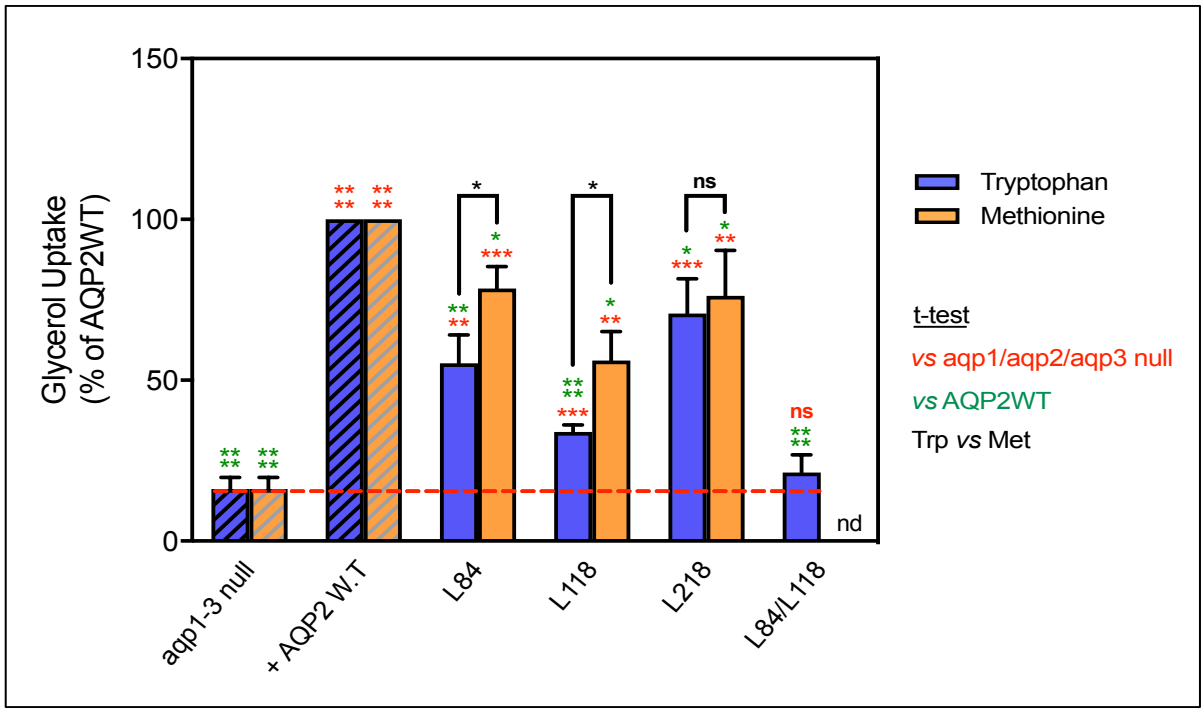

Figure 4.15: [^{3}H]-glycerol uptake by T*b*AQP2 variants with a leucine-to-tryptophan or leucine-to-methionine substitution near the cytoplasmic end of the pore.
The figure shows uptake of 0.25 µM [^{3}H]-glycerol by *aqp1/aqp2/aqp3* null cells expressing TbAQP2WT or an TbAQP2 variants as indicated, expressed as percentage (100%) of the transport rate in the TbAQP2 control cells. The resistant control (aqp1-3 null) and sensitive control (AQP2WT) for the separate datasets (Trp or Met) are indicated as hatched bars in the same colours. All bars represent the average and SEM of at least three independent replicates. *, P<0.05; **, P<0.01; ***, P<0.001, ****, P<0.0001 by unpaired Student's t-test; ns, not significant; nd, not determined.

4.3. Discussion

TbAQP2 plays an essential role in pentamidine uptake in *T. brucei*. However, the mechanism by which it mediates and facilitates this uptake is still unclear. No adequate information has been provided to understand better whether TbAQP2 has direct transporter activity (Munday et al., 2014; Baker et al., 2013; Graf et al., 2013) or acts as a receptor with a high affinity for pentamidine (Song et al., 2016). Here, several genetic mutations (single or multiple amino acid substitutions) were constructed in the TbAQP2 pore to assess their effects on the ability of the gene for drug sensitivity and drug transport. This study replaced leucine residues with tryptophan and methionine at positions L84, L118, L218 near the cytoplasmic end of TbAQP2, potentially allowing to distinguish between an endocytosis model and a channel model for pentamidine.

Introducing tryptophan in the selected three sites (L84, L116, and L218) at the cytoplasmic end of the Tb*AQP2* resulted in a loss of pentamidine sensitivity in L84 and L118 mutants compared to the wild-type cells. On the other hand, the L218 mutant demonstrated a sensitivity similar to that of the wild-types. The double mutant of L84W/L118W displayed an even greater loss of pentamidine susceptibility. In addition, the transport rates of [^{3}H]-pentamidine were measured in all mutants and showed strong reductions upon introduction of the tryptophan residues. Thus, it can be concluded that the introduction of the bulky amino acids in the three selected positions at a low point in the aquaporin duct could block the passage of pentamidine through the TbAQP2 channel.

In contrast, introduction of the methionine residues into the same three positions showed that in two out of three cases, L84M and L218M were significantly sensitive

to pentamidine, as well as these two mutants were restored near-normal rates of pentamidine uptake of the AQP2 wild type. All L-W mutants were affiliated with reduced pentamidine and cymelarsan sensitivity with a >90% decrease in [^{3}H]-pentamidine uptake. This effect was dependent on size because the pentamidine transport rate associated with L84M and L218M was statistically similar to that observed in TbAQP2 cells. Besides, L118M demonstrated a higher transport rate compared to L118W ($P<0.0001$).

From the homology protein model, the outcomes of the specific mutations of L84, L118 and L218 residues appear far below down the selectivity filter, indicating that pentamidine must traverse through the constriction points of the channel. The AQP2 (L-W) and (L-M) mutants were also investigated for their ability to transport glycerol as aquaglyceroporins. The introduction of large amino acid residues at AQP2 cytoplasmic end resulted in reducing the entry of pentamidine but maintained the glycerol flux. This implies that even though the TbAQP2 mutants lost their ability to transport pentamidine, they were still functional aquaglyceroporins because their expression in *tbaqp1-2-3* null cells increased glycerol uptake and decreased sensitivity towards the TAO inhibitor SHAM.

Together with the data from all mutants presented previously in chapter 3, these observations stand up for the conclusion that TbAQP2 is a conduit for pentamidine and the principal determinant of pentamidine and melarsoprol resistance (Munday et al., 2014).

Chapter 5 Partially blocking endocytosis does not alter the rate of pentamidine transport and pentamidine does not trigger AQP2 endocytosis in bloodstream form *T. brucei*

5.1. Introduction

There are few licensed drugs for the treatment of Human African Trypanosomiasis (HAT): pentamidine, suramin, melarsoprol, eflornithine and nifurtimox (Migchelsen et al., 2011). The choice of the drug to treat sleeping sickness in humans is mainly based on the stage of the disease and the causative organism (Burri et al., 2010). The WHO recommends pentamidine for the treatment of the initial stage of sleeping sickness caused by *T. b. gambiense*. Pentamidine has the ability to access trypanosomes via different routes (Figure 5.1). The aminopurine transporter P2, also known as *Trypanosoma brucei* AT1 (*Tb*AT1), facilitates partial transport as evidenced by reduction in knockout studies involving pentamidine sensitivity with encoding gene (*TbAT1*) (Matovu et al., 2003), as well as partial inhibition of pentamidine transport by adenine, a known substrate of *Tb*AT1 (Carter and Fairlamb, 1993). The bulk of pentamidine transport is facilitated by two other channels discovered in 2001: a High Affinity Pentamidine Transporter (HAPT1) and a Low Affinity Pentamidine Transporter (LAPT1). This has been further supported by competitive inhibition work using radiolabelled [^{3}H]-pentamidine with increasing concentrations of unlabelled pentamidine substrate, causing significant biphasic uptake inhibition in *tbat1*-null mutants (de Koning, 2001; Matovu et al., 2003). It has been documented that knock-down of the HA1–3 plasma membrane proton pumps of *T. brucei* (which are vital for preserving the potential of plasma membrane), confers the resistance against pentamidine (Alsford et al., 2012; Baker et al., 2013). The HA1-3 pumps are thought to provide the proton motive force necessary for HAPT1 activity and pentamidine uptake (De Koning, 2001). The former channel, HAPT1, has since been identified as *Trypanosoma brucei* aquaglyceroporin 2 (*Tb*AQP2), located at the flagellar pocket of *T. brucei* cells (Munday et al., 2014).

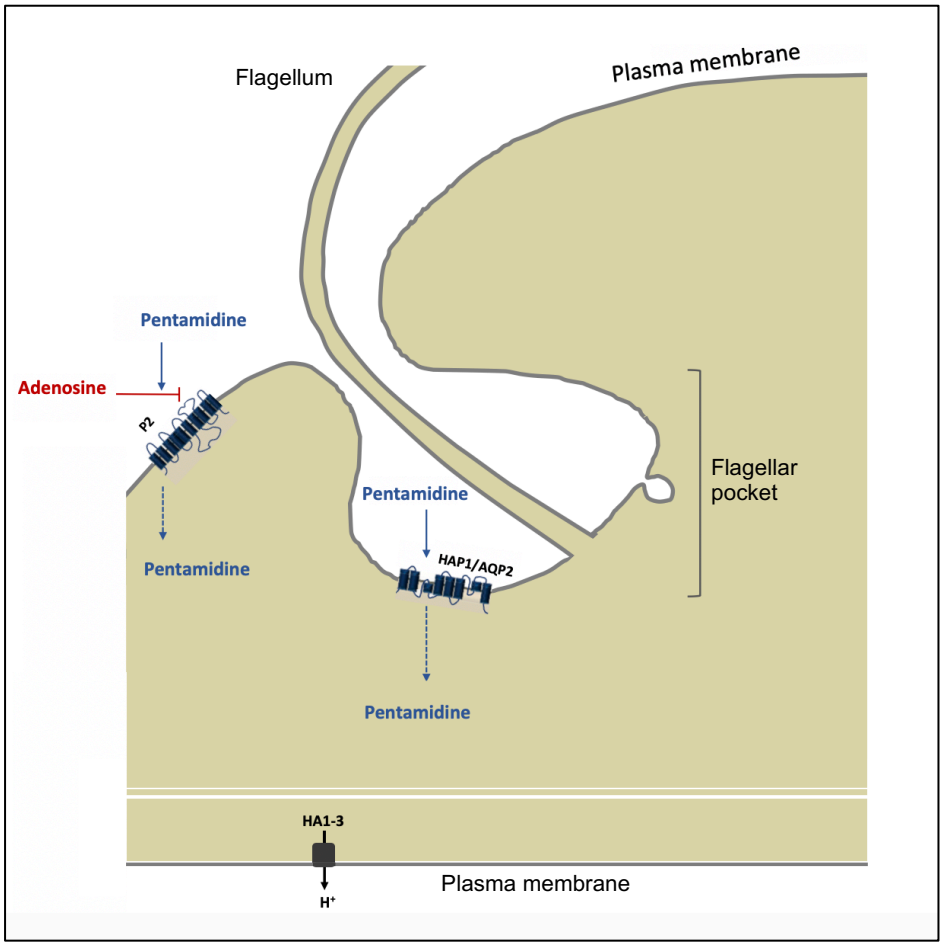

Figure 5.1: Overview of the transporters implicated in uptake of pentamidine in *Trypanosoma brucei.*
Model shows known and putative mechanisms of the *T. brucei* AQP2 and P2 transporters thought to facilitate the uptake of pentamidine. Adenosine competitively inhibits pentamidine uptake by P2. The presence of the *Tb*AQP2 gene appears to correlate with HAPT1 activity. The P-type H^+ ATPases (HA1–3) generates a proton motive force that could drive pentamidine uptake. (adapted from Molla-Herman et al., 2010; Baker et al., 2012).

Suramin is one of the few drugs available for treating sleeping sickness in humans, exclusively to treat *T. b. rhodesiense* infections that occur at early stages (De Koning, 2001). The drug is relatively large in size and possesses a six-fold negative charge, which hinders passive cell transport into the parasite cells (De Koning, 2020). Suramin was proposed to be taken up by *T. brucei* via receptor-mediated endocytosis (Stewart et al., 2005; Damper et al., 1967). Many pieces of evidence show that the drug enters the parasite cell by endocytosis mechanism facilitated by its receptor, the Invariant Surface Glycoprotein (ISG75) (Alsford et al., 2012; Pal et al., 2002). These findings were supported by later studies that revealed the current model of suramin uptake (Figure 5.2), which involves several stages of the

endocytosis process starting from the binding of the drug to the ISG75, until the release of the drug in the cytoplasm via a Major Facilitator Superfamily Transporter (MFST) (Zoltner et al., 2016; Alsford, 2013).

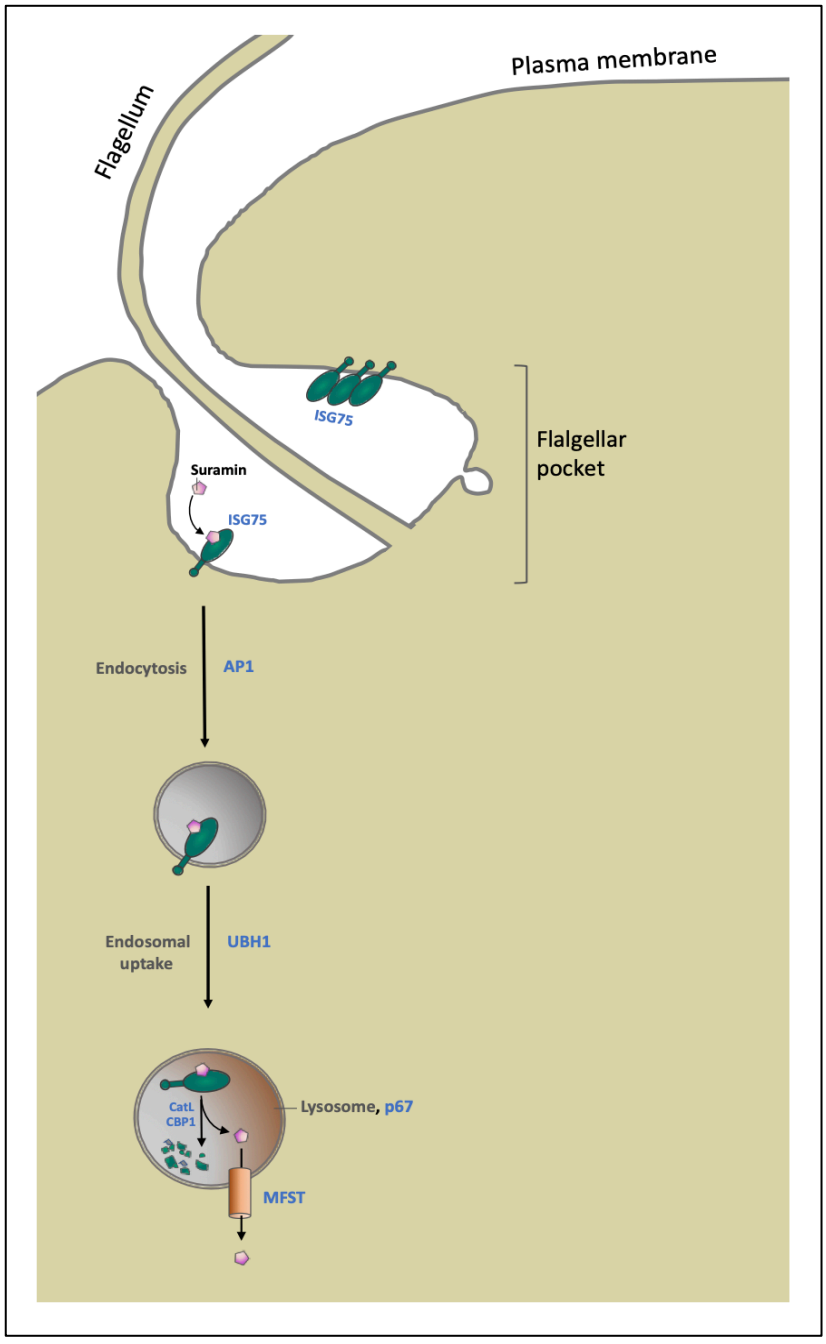

Figure 5.2: A simplified schematic model of the trypanosome endosomal system.
The figure shows the way in which the suramin drug enters the *T. brucei* cell via endocytosis mechanism. ISG75 has been proposed as the major surface receptor for suramin uptake but other cell-surface proteins may make some contribution as well, since suramin is a prolific binder. The drug enters the cell by binding to ISG75 followed by uptake into the endosome by endocytosis (relies on four protein subunits that form adaptor protein complex 1, AP1) and transfers to the lysosome where it is broken down by proteolysis (involving the proteins UbH1, CatL, CBP1 and p67). The free drug is then released into the cytoplasm with the aid of transport protein MFST. (adapted from Alan et al., 2012).

In trypanosomes, endocytosis occurs rapidly, and is even more rapid in the flagellar pocket zone than in the mammalian cells (Allen et al., 2003). The knockdown of CRK12 kinase, an essential protein kinase (Mackey et al., 2011), is reported to cause a highly reproducible endocytosis defect in *T. brucei* (BSF) that affects approximately twenty percent of cells 12 hours after induction of RNAi and is eventually lethal (Monnerat et al., 2013). Therefore, to examine the conceivable existence of a connection between pentamidine transport and endocytosis, the CRK12 RNAi cell line was utilized. Parallel uptake experiments were performed involving [3H]-pentamidine and [3H]-suramin, with suramin as a positive control because it is known to bind to the ISG75 surface protein and enter bloodstream forms of *T. brucei* through endocytosis (Zoltner et al., 2016, 2020). This approach was chosen because no stable *T. brucei* cell lines with endocytosis defects are possible, as this rapidly leads to gross distortions of the cell (swelling of the flagellar pocket) and cell death (Monnerat et al., 2013; Allen et al., 2003; Field et al., 2009; García et al., 2004). However, induced knockdown of CRK12 is a relatively mild method to progressively reduce the endocytosis rate, and unambiguously distinguishes between endocytosis and secondary-active transporters.

5.2. Results

5.2.1. Growth analysis of CRK12 RNAi cells

To determine the earliest time points at which endocytosis becomes disrupted, and without causing excessive cellular pathology or affecting cell viability when carrying out transport assays, growth analysis of the CRK12 RNAi cell line (Monnerat et al., 2013), was performed in the presence and in the absence of tetracycline. Therefore, the initial step was to test the effect of the tetracycline based on varying concentrations of the antibiotic (tet 0.1 µg/ml, 0.5 µg/ml and 1 µg/ml) on the cell growth, in parallel with corresponding control (-tet). For the purpose of this test, the bloodstream parasites were seeded at 1×10^5 cells ml^{-1} both in the presence and in the absence of tetracycline, followed by incubation at 37 °C with 5% carbon dioxide. After every 24 hours, a cell count was done using a haemocytometer, for three consecutive days. The experiments were conducted independently on three

separate occasions. It was observed that there was continued normal growth of CRK12 RNAi cell line when there was no addition of tetracycline to the media over the 72 hours (Figure 5.3). On the other hand, the rate of growth of the induced cells was lower in the first 24 hours in the presence of tetracycline in comparison to growth rate in the control (-tet). After day 1, there was a steep decline in cell density caused by cell death. Mackey et al., (2011) notes that this observation is because CRK12 is an important protein kinase in bloodstream form *T. brucei*. The growth curve indicates that the varying concentrations of tetracycline have a very similar effect on the cell growth.

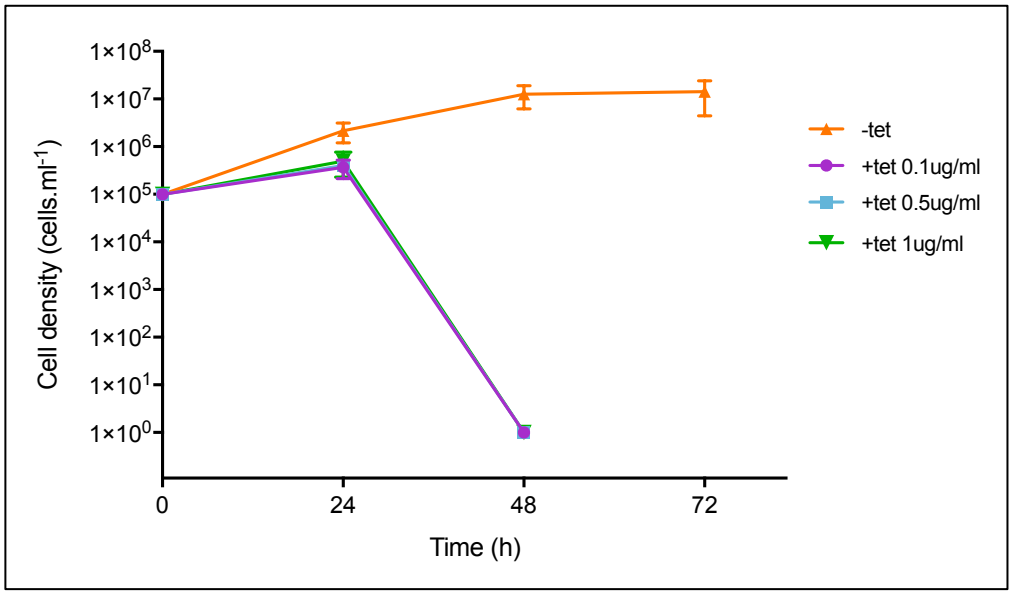

Figure 5.3: CRK12 RNAi cell growth curve in full HMI-9 medium by incubated at 37 ºC with 5% carbon dioxide, with and without tetracycline (tet).
From this graph, there is no considerable difference in the CRK12 RNAi growth phenotype when induced with three different concentrations of 0.1 µg/ml tet, 0.5 µg/ml tet or 1 µg/ml tet. In the absence of tetracycline (-tet), CRK12 RNAi acted as a control. The results presented in the graph are based on the data obtained from three similar but independent experiments. (Alghamdi et al., 2020).

Bloodstream *Trypanosoma* cells normally divide after about every 6 h under standard culture conditions, and reach a cell density of 1.5 - 2 × 10^6 cells/ml at late log phase after every 48 h, when seeded at 1 x 10^5 cells/ml (Vassella et al., 1997). Based on this, and on the growth analysis shown in figure 5.3, an additional growth analysis was performed on the CRK12 cells to determine the peak growth rate so that viable cells are harvested prior to apparent growth arrest. Hence, the cells were induced using the highest tetracycline concentration from the previous experiments over 24

hours to ensure as much inhibition from endocytosis as possible without affecting cell viability. The experiments were independently conducted on three different occasions. Cell induction with tetracycline 1 µg/ml was performed, followed by cell counts after every 4 h. For controls, un-induced CRK12 RNAi cells were used throughout the assay. From figure 5.4, it is evident that the induction of CRK12 blood stream form RNAi cell line using tetracycline arrested cell growth in the first 12 hours, causing cell death after longer RNAi induction. These experimental findings were consistent with previous data published under the investigation of the function of CRK12 (Monnerat et al., 2013). Culture samples collected at this time point reveal an increased abundance of swelling cells, which is a characteristic of endocytosis defects in *T. brucei*. However, it was difficult to quantify this characteristic since only a minority of cells was affected and to varying degrees, as intended at the 12 h time point selected for that very reason. Our subsequent experiments of drug uptake were optimized on the basis of these growth assay.

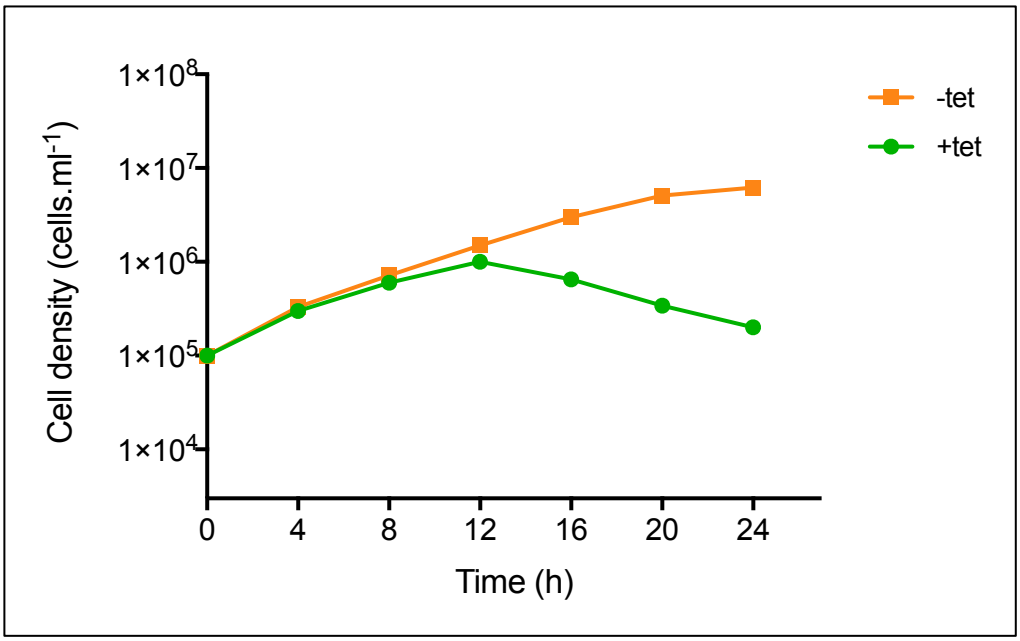

Figure 5.4: CRK12 RNAi cell growth curve in full HMI-9 medium at 37 ºC with 5% carbon dioxide, with or without 1 µg/m tetracycline (tet).
The graph shows the growth curve of the CRK12 RNAi cells within a period of 24 hours, when induced with 1 µg/ml tetracycline. In the absence of tetracycline (-tet), CRK12 RNAi acted as a control. The cells were counted using a haemocytometer and the mean of duplicate determinations has been shown. (Alghamdi et al., 2020)

5.2.2. Quantitative RT-PCR on the CRK12 RNAi cell line

Based on the growth analysis assay in figure 5.4, it was evident that in the presence of tetracycline, the cells experienced a steady growth until after 12 hours when a decline in growth was observed. Therefore, the mRNA expression of CRK12 was determined 12 h after induction with 1 µg/ml tetracycline. For the quantification of RNA, 5 x 10^6 cells were harvested from CRK12 RNAi cells induced with tetracycline and un-induced 2T1 parental cells which acted as the control. RNA was extracted from the cells by use of the NucleoSpin RNA extraction kit. After the extraction of RNA, the RNA was converted to cDNA by use of SuperScript III Reverse Transcriptase (Invitrogen). The RT-PCR process was performed using qRT-PCR primers specific for *CRK12* gene, and using cDNA to measure the levels of mRNA normalized to *GPI8* expression which is usually used as a standard reference gene in *T. brucei* cell (Kang *et al*, 2002). The 2T1 cell line contains the two endogenous alleles of the *CRK12* gene and is therefore set to 100%. The levels of *CRK12* mRNA were reduced by 42% ($P<0.001$) compared to un-induced controls as shown by qRT-PCR (Figure 5.5). Our analysis of the *CRK12* transcript is closely consistent with the observations made by Monnerat et al, (2013) that mRNA transcript reduces by nearly 67% 18 hours after induction with tetracycline.

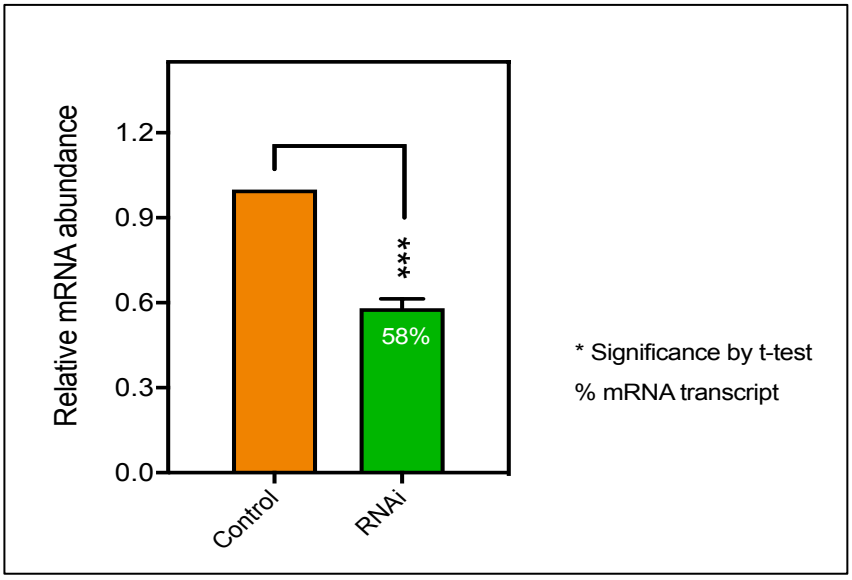

Figure 5.5: Relative gene expression for the CRK12 RNAi cell line using qRT-PCR.
Gene expression is normalised to housekeeping gene GPI8 (n=3) and the 2T1 parental cells (control) set at 100. Induction with 1 µg/ml tetracycline for 12 h. The error bar shows ± standard deviation. **, p=0.0027 by Student's unpaired, two-tailed t-test.

5.2.3. Knockdown of CRK12 slows down endocytosis and suramin uptake but not pentamidine transport in *T. brucei*

A study previously done on CRK12 kinase by Monnerat et al. (2013) showed that about 20% of population of the CRK12 RNAi cells in *T. brucei* tend to have enlargement of the flagellar pockets 12 hours after inducing the cells with tetracycline. Allen et al. (2003) also showed that there is a link between the enlarged *T. brucei* parasite flagellar pocket and defects in endocytosis. Therefore, this system was used to inhibit endocytosis in order to demonstrate that this does not impact pentamidine uptake. [^{3}H]-suramin and [^{3}H]-pentamidine were performed in two parallel experiments. [^{3}H]-suramin was used as a positive control since, upon binding to the protein ISG755, it can reach *T. brucei* bloodstream forms via endocytosis (Zoltner et al, 2016, 2020). Transport of 0.025 μM [3H]-pentamidine, after 12 h of CRK12 RNAi induction, was the same as that observed in the control (non-induced) and was linear for at least 30 s at 0.00658 ± 0.00061 pmol (107 cells)-1 s-1 and 0.00650 ± 0.00067 pmol (107 cells)-1 s-1, respectively. After 12 h of CRK12 RNAi induction, transport of 0.025 μM [^{3}H]-pentamidine in the presence of 1 mM adenosine (to block the P2 transporter) was the same as that observed in the control (non-induced) and was linear for at least 30 s at 0.00658 ± 0.00061 pmol (107 cells)-1 s-1 and 0.00650 ± 0.00067 pmol (107 cells)-1 s-1, respectively. (Figure 5.6 A). The addition of 200 μM unlabelled pentamidine inhibited the uptake of [^{3}H]- pentamidine for all the cells and was not significantly greater than 0 (P > 0.05). This indicates that [^{3}H]-pentamidine uptake is transporter-mediated and is completely saturated at 200 μM pentamidine. There was no significant reduction in the rate of uptake of pentamidine (n=5) by the RNAi cells in comparison to the control cells (Figure 5.6 B), indicating that partial inhibition on endocytosis does not impact on pentamidine uptake.

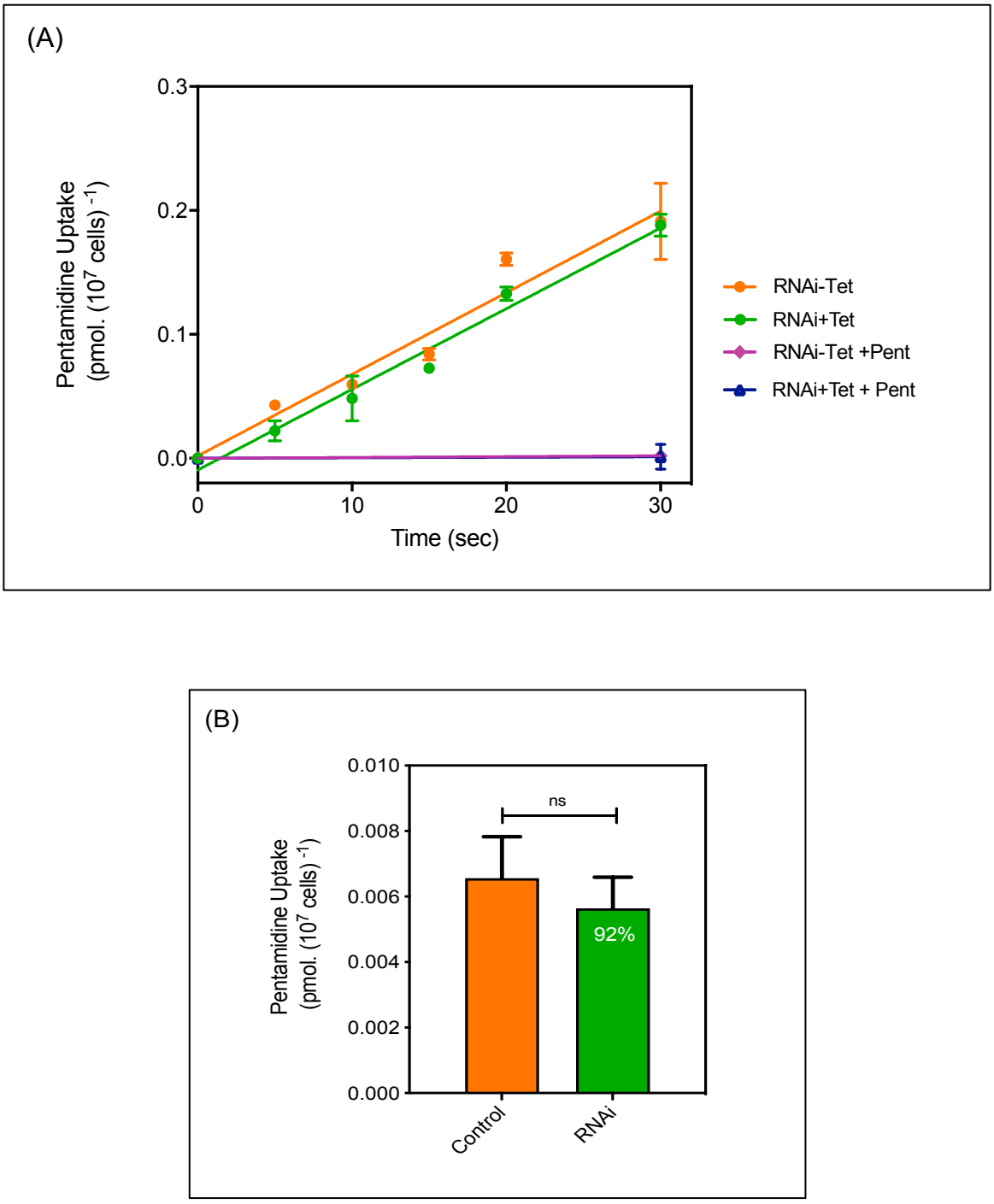

Figure 5.6: Transport of 0.025 µM [^{3}H]-Pentamidine measured in control (non-induced) and CRK12 RNAi cell after exactly 12 h of tetracycline induction.
Transport was measured over a course of 30 seconds in the presence of 1 mM adenosine to block P2/TbAT1 transporter. [A] Representative pentamidine uptake experiment, the slope was determined using linear regression with Prism 7.04 (GraphPad). [B] The bars represent the mean and SEM rates of pentamidine uptake in CRK12 RNAi, relative to the control. The means and SEM of five independent experiments were determined in triplicate. Using unpaired Student's t-test, NS is not significant.

The uptake of 0.25 µM [^{3}H]-suramin was evaluated in a way similar to the [^{3}H]-pentamidine experiment above, only that suramin was determined in over 15

minutes. [^{3}H]-suramin is a drug accumulated by endocytosis via the flagellar pockets in *T. brucei* (Zoltner et al., 2016), thus, it was used as a positive control. After 12 hours of CRK12 RNAi induction, it was shown that the rate of labelled suramin was lower (0.001656 ± 0.00067 pmol (10^7 cells)$^{-1}$ s^{-1}) than in the control cells (0.00237 ± 0.00061 pmol (107 cells)$^{-1}$ s^{-1}) (Figure 5.7A). 100 µM unlabeled suramin was used as a saturation control but did not fully out-compete the radiolabel, indicating that suramin binds with quite low affinity to its receptor, ISG75. Hence, the uptake of 0.25 µM [^{3}H]-suramin by the two cells was significantly greater than zero, but not significantly different from each other. Considering the mean of five repeats, the [^{3}H]-suramin uptake was inhibited by 32% in comparison to the control cells (P=0.019, n=5) (Figure 5.7B). Although this approach is limited to partially inhibited endocytosis in BSF *T. brucei*, the results obtained from these experiments show that inhibition on endocytosis has no impact on the uptake of pentamidine, but does reduce suramin uptake, consistent with current models.

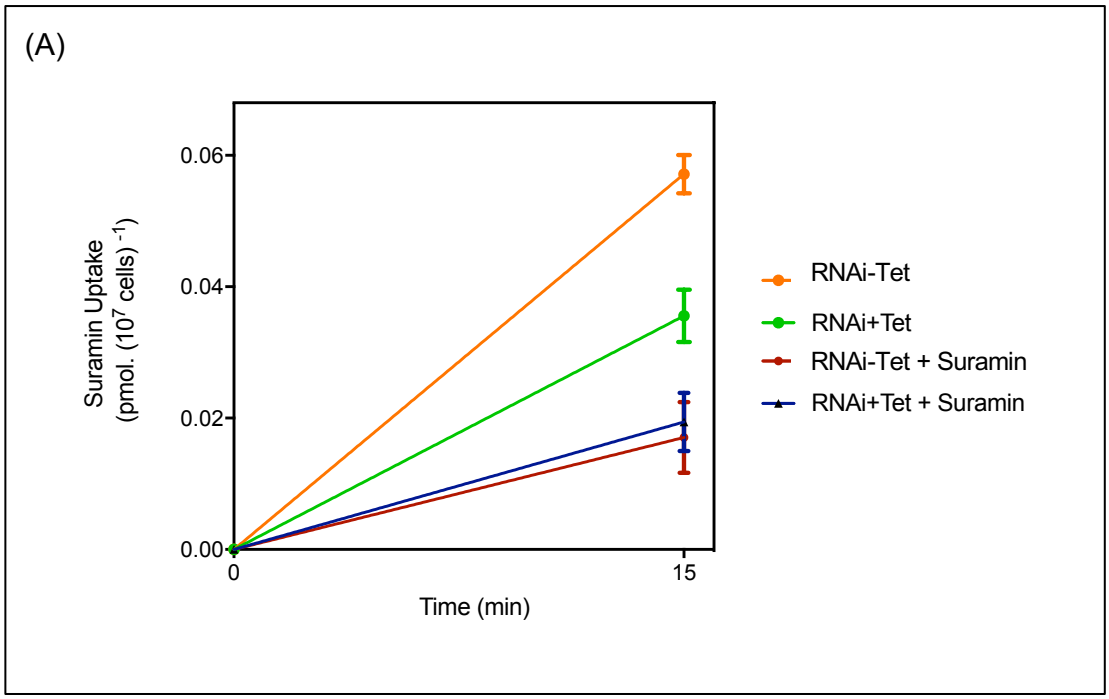

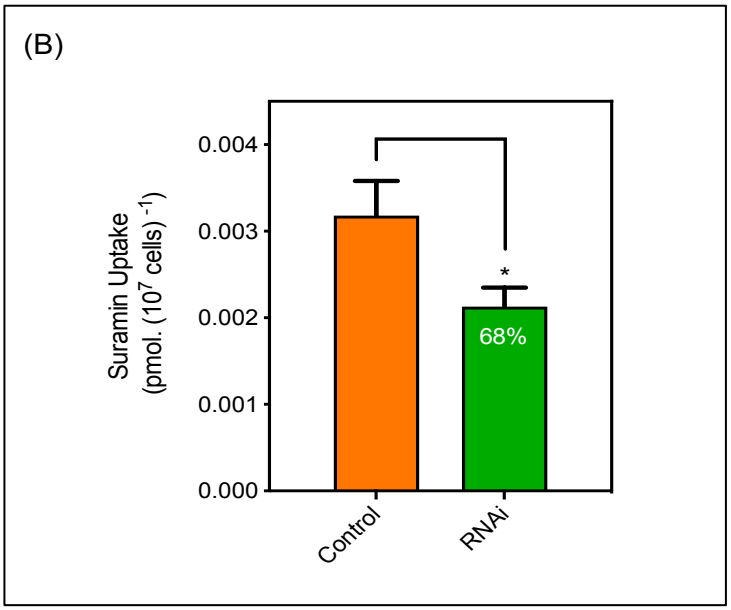

Figure 5.7: **Measurement of 0.25 µM [^{3}H]-suramin over a time period of 15 minutes in the control and in CRK12 RNAi cells after exactly 12 h of tetracycline induction.**
(A) representative experiment of suramin uptake, the slope is determined by linear regression in Prism 7.04 (GraphPad). (B) Bars represent the mean and SEM rates of suramin uptake in CRK12 RNAi in relation to the control. Means and SEM of five independent experiments were performed in quadruplicate. Using Student's unpaired, two-tailed t-test, p =0.0027.

5.2.4. The protonmotive force drives uptake of AQP2-mediated pentamidine uptake in bloodstream forms of *T. brucei*

Studies by Alsford et al. (2012) and Baker et al. (2013) have reported that knock-down of the HA1–3 proton pumps in *T. brucei* confers the resistance to pentamidine. The HA1–3 proton pumps are important in maintaining a stable plasma membrane potential. An interesting fact is that this locus conferred resistance to only pentamidine (dicationic), and not to melaminophenyl arsenicals (neutral), unlike the case with the knockdown of the TbAQP3/TbAQP2 locus, which gave resistance to both drugs (Alsford et al., 2012). Previous studies by De Koning (2001a) have reported that the uptake of pentamidine in *T. brucei* procyclics, mediated by HAPT has a strong correlation with the proton-motive force (PMF) in procyclic *T. brucei*. Many *T. brucei* transporters are associated with proton symporter-mediated nutrient uptake (De Koning & Jarvis, 1997a, b, 1998; De Koning et al., 1998). However, it is uncertain if this dependence means that pentamidine uptake is mediated by a proton symporter or is simply a result of the energetics of cationic pentamidine uptake being guided by the strong negative membrane potential (V_m). There is no impact of HA1-3

on sensitivity to neutral melaminophenyl arsenicals, a claim that strongly goes against a proton symport mechanism for HAPT1/AQP2, but if the substrate crosses the channel, there would be a partial dependence on HAPT1/AQP2-mediated dicationic pentamidine uptake on V_m or PMF, as opposes to a single Asp residue, according to the endocytosis model, binding on the extracellular side of the protein (Song *et al*, 2016). Alghamdi et al. (2020) show that in *T. brucei* the same ionophores that dose-dependently inhibit the uptake of hypoxanthine in procyclic (De Koning and Jarvis, 1997a) and in BSF (De Koning and Jarvis, 1997b) also inhibit the transport of [^{3}H]-pentamidine in BSF and HAPT1-mediated pentamidine in procyclic cells. This is a confirmation that, as expected by the reliance on the HA1–3 proton pumps, a membrane potential must be present for rapid uptake of pentamidine.

Zoltner et al. (2016) observe that [^{3}H]-suramin, an endocytosed substrate, was also inhibited by 20 μM carbonyl cyanide m-chlorophenyl hydrazone (CCCP), by about 32.6% (P=0.029; 3 minutes pre-incubation, and suramin accumulation of more than 10 minutes) (Figure 5.8). Although this means that the ionophore does not absolutely discriminate between trans-channel transport and endocytosis for di-cationic pentamidine, the inhibition of transport did not occur for neutral melaminophenyl arsenicals. That is, these neutral TbAQP2 substrates do not depend on the proton gradient as noted by Alsford et al. (2012), an indication that they are not endocytosed like suramin, nor driven thermodynamically by the negative membrane potential.

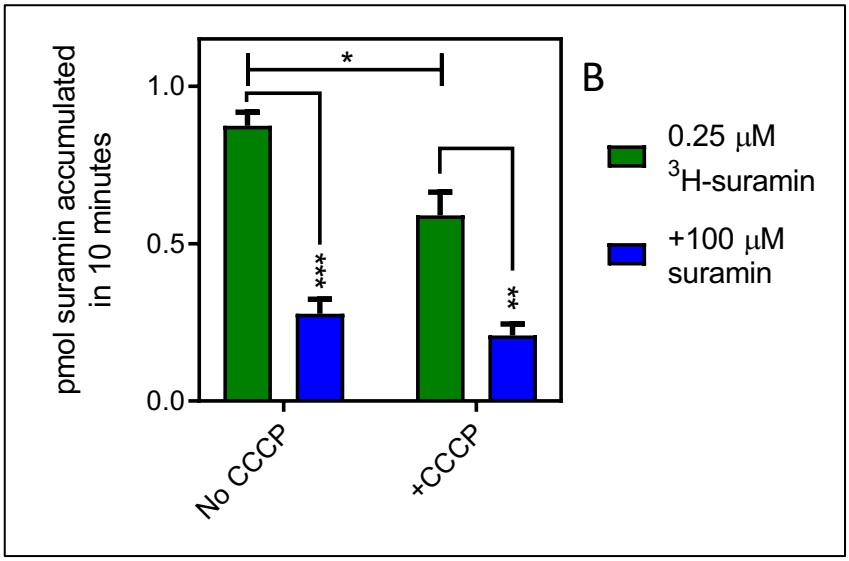

Figure 5.8: The 0.25 μM [^{3}H]-suramin uptake by *T. b. brucei* s427WT cells in just over 10 minutes.

Cells were incubated in the presence or in the absence of 20 µM CCCP (additional 3 minutes of pre-incubation) and in parallel. The 100 µM unlabelled suramin (shown by the blue bars) was included to demonstrate saturation of the suramin-receptor interaction. The bars represent the mean and SEM of the three experiments which are independent of each other, all performed in quadruplicate. Following the Student's unpaired t-test: *P<0.05; **P<0.01; ***P<0.001. (Alghamdi, et al., 2020)

There is a good correlation between TbAQP2-mediated pentamidine transport and the proton-motive force (Figure 5.9), but CCCP has a stronger effect than expected from previously observations for the uptake of [^{3}H]-hypoxanthine in *T. brucei* bloodstream forms as noted by De Koning and Jarvis (1997b).

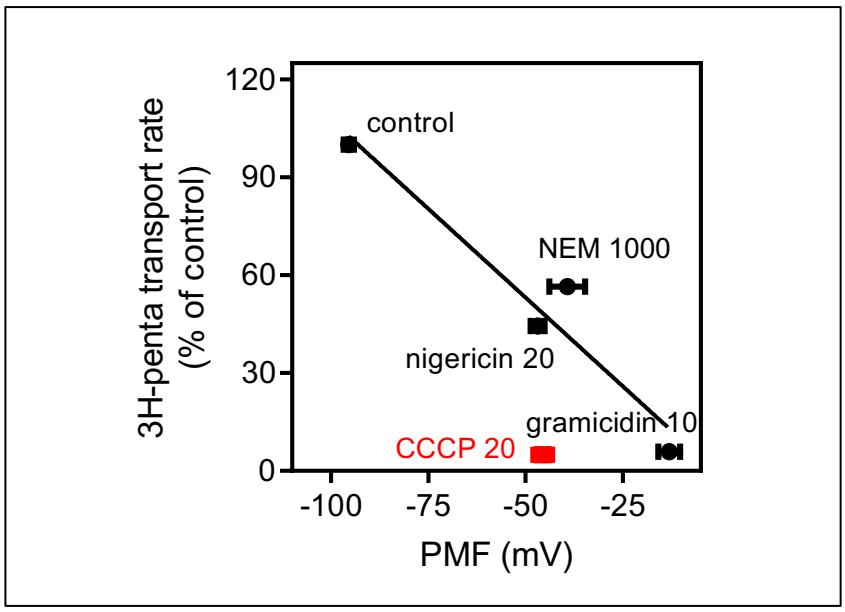

Figure 5.9: High affinity pentamidine uptake in *T. b. brucei* is sensitive to ionophores.
The labels indicate the concentrations in µM. A plot showing the correlation between the rate of pentamidine transport and protonmotive force (PMF). The black points show several ionophores that strongly inhibited pentamidine uptake, including N-ethylmaleimide (NEM), nigericin and gramicidin. The red point shows the CCCP outlier and has not been used in the regression analysis. The data points represent the average of four or more independent repeats conducted in quadruplicate. The PMF values were taken from De Koning and Jarvis (1997b).

Thus, an investigation of any direct effect of CCCP on TbAQP2 was conducted and found that the uptake of [^{3}H]-glycerol (neutral) in *tbaqp1-2-3* null cells expressing TbAQP2-WT was inhibited by CCCP, with an IC_{50} value of 20.7 ± 2.6 µM (n=3) (Figure 5.10). The uptake of [^{3}H]-pentamidine was also inhibited in the same cells, with the same IC_{50} value (Figure 5.11). Additionally, the results also show that pentamidine (which acts as a control) inhibits the uptake of [^{3}H]-glycerol, with a mean EC_{50} value of 27.5 nM (n=2), same as the EC_{50} value of pentamidine inhibiting [^{3}H]-pentamidine

uptake. This shows that CCCP inhibits TbAQP2 directly, independent of the effects on the membrane potential.

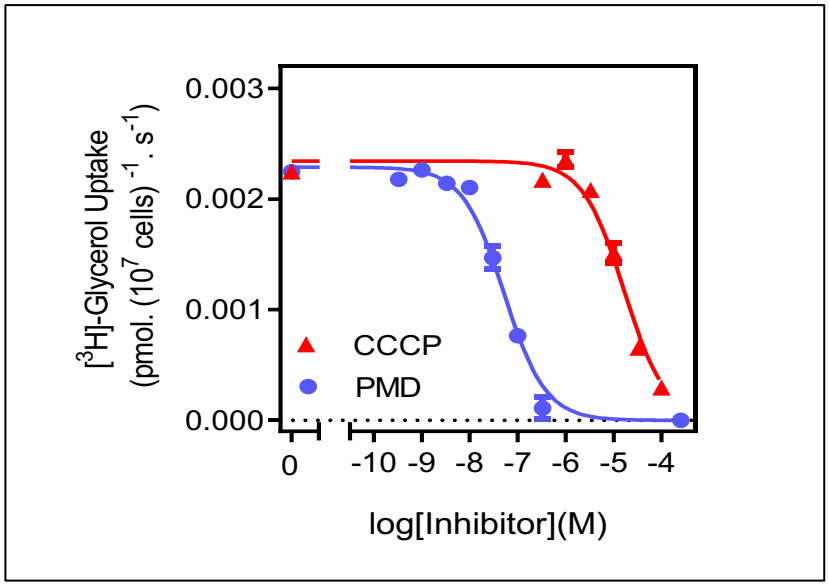

Figure 5.10: The 0.25 µM [^{3}H]-glycerol uptake by *aqp1/aqp2/aqp3* null cells expressing TbAQP2WT.

Dose response of pentamidine (PMD) and CCCP based on an incubation time of 1 minute. The graph shown was performed in triplicate and representative of three independent repeats. (Alghamdi et al., 2020)

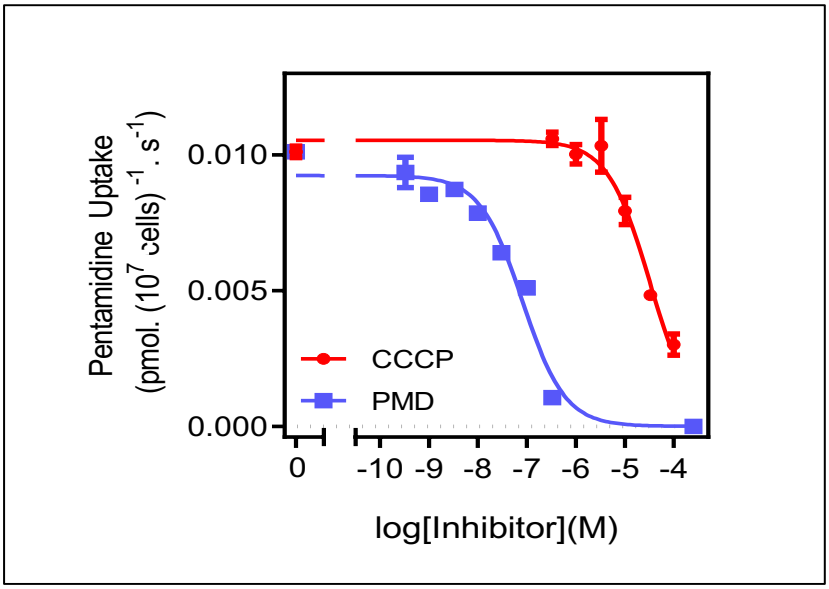

Figure 5.11: Uptake of 0.025 µM [^{3}H]-pentamidine by *aqp1/aqp2/aqp3* null cells expressing TbAQP2WT.

The graph represents dose response with CCCP and pentamidine (PMD), using an incubation time of 30 second. The graph shown was performed in triplicate and representative of three independent. (Alghamdi et al., 2020)

5.3. Discussion

To investigate the independence from endocytosis, the tetracycline-inducible CRK12 RNAi cell line that was employed to provide an endocytosis defect that is highly reproducible and progressive in *T. brucei* (Monnerat et al., 2013). The aim of this study was to distinguish between uptake by transporters and via endocytosis, since the current evidence (Morgan et al., 2002; Allen et al., 2003) suggest that all endocytosis in *T. brucei* exclusively occurring in the flagellar pocket is dependent on clathrin and independent of AP-2. The implication of this is that the endocytotic mechanisms of TbAQP2 and suramin receptor ISG75, which are both directed to the lysosome after ubiquitylation (Quintana et al., 2020; Zoltner et al., 2015), are likely to be similar enough for a direct comparison. After 12 h of CRK12 RNAi induction, pentamidine transport was not significantly reduced although uptake of [3H]-suramin, which is accumulated by endocytosis through the *T. brucei* flagellar pocket (Zoltner et al., 2016), was reduced by 33% (P=0.0027), an indication that the experiment was successfully timed to the early stage of endocytosis slow-down.

Similar to previous studies on protonmotive force-influenced transport processes in *T. brucei* (De Koning and Jarvis, 1997a, b, 1998; De Koning et al., 1998), ionophore CCCP strongly inhibited pentamidine uptake. This is most likely due to the internal negative membrane potential of -125 mV, which attracts the dicationic pentamidine (De Koning and Jarvis, 1997b). This result is in line with the prediction of molecular dynamics modelling (Alghamdi et al., 2020) and the role of HA1-3 proton pumps in pentamidine transport, as stated in previous studies, but not in the resistance of melarsoprol (Alsford et al., 2012; Baker et al., 2013). Even though CCCP inhibits pentamidine directly through competitive TbAQP2 inhibition, this only begins to have a major impact above ~5 µM (IC_{50} of 20.7 µM), while its effects after combined competitive inhibition and reduced protonmotive force (preincubation) shows pentamidine transport inhibition of about 63% at 1 µM and about 90% at 5 µM. This shows the important role of CCCP after PMF reduction. This is in agreement with the conclusion made on the molecular dynamics analysis (Alghamdi et al., 2020) that inward pentamidine flux depends on the inside-negative membrane potential.

For HAPT-mediated pentamidine uptake, the experimental V_{max} in *T. brucei* BSF can be expressed as 9.5×10^5 molecules/cell/h, whereas that in procyclics is 8.5×10^6 molecules/cell/h (De Koning, 2001). Given that the stoichiometric ratio of AQP2: pentamidine is 1:1, the endocytosis model would require as many units of TbAQP2 as possible to be internalised and recycled, which seems impossible particularly in procyclic cells, since the half-life time for TbAQP2 turnover in BSF is almost 4 hours (Quintana et al., 2020). In addition, the rate of endocytosis in procyclic cells is lower, making it difficult to internalise the aquaporins spread over the surface of the cell as mentioned above. Based on the rates of uptake and turnover observed, about 4×10^6 TbAQP2 units would be required per BSF cell in the flagellar pocket. All these observations are not consistent with the argument that uptake of pentamidine by trypanosomes mainly depends on endocytosis. Even though AQP2-bound pentamidine is likely to be internalised as part of the protein's natural turnover, this is unlikely to have a significant contribution to the overall rate of the drug's uptake.

Altogether, it can be concluded that the remarkably large pore of TbAQP2 is the primary entry of drugs melarsoprol and pentamidine into *T. brucei* spp. for treatment of sleeping sickness. This renders the parasite extra-sensitive to the drugs in comparison to *Leishmania* mexicana (Munday et al., 2014).

Chapter 6 Insights into the role of *Leishmania major AQP1* gene in drug transport

6.1. Introduction

Treatment of leishmaniasis is complicated because the disease is caused by different species of *Leishmania* parasite, which lead to varied clinical manifestations. Although there exist more than 25 compounds exhibiting anti-leishmanial effects, only a handful are actually used in treatment of the human disease (Fidalgo & Gille, 2011). In the past six decades, the organic pentavalent antimonial compounds meglumine antimoniate (Glucantime), and stibogluconate (Pentostam) have been the most preferred first line treatment options against all forms of leishmaniasis, while pentamidine, amphotericin B, and Alkyl-lysophospholipids (ALP) such as edelfosine and miltefosine have been employed as options for the second line of treatments. However, with the emergence of acquired resistance, the clinical efficacy of these drugs in the treatment of leishmaniasis is being challenged (Ashutosh et al., 2007). For example, Sundar and Chakravarty (2012) report that more than 60% of Indian VL patients have shown no response against antimonial treatment. Pentavalent antimonials [Sb (V)] are pro-drugs which get reduced to the active form, trivalent antimony [Sb (III)] (Ephros et al., 1999). This process occurs in the parasite, but it is still not well understood, including the mechanism through which antimonials enter into macrophages and phagolysosomes (Shaked et al., 2001). Yet, according to Gourbal, et al. (2004), *Leishmania major* aquaglyceroporin 1 (LmAQP1) is the first Sb (III) facilitator in *Leishmania*. In 2014, Mukhopadhyay stated that AQP1 plays an essential role of accumulating metalloids, methylglyoxal, glyceraldehyde, glycerol, water, alongside other solutes in *Leishmania* amastigotes and promastigotes.

It is thought that the *Leishmania major* genome encodes for five aquaporins: LmAQP1, LmAQPα, LmAQPβ, LmAQPγ, and LmAQPδ. Out of these five, it is only LmAQP1 that exhibits adventitious permeability to antimonite. Mukhopadhyay (2014) affirms that the roles of the other four aquaporins are not yet known. A growing amount of evidence suggests that changes to, or loss of LmAQP1, plays a vital role in *L. major* antimony resistance. Marquis, et al. (2005) reported that if one of the two AQP1 alleles present in *Leishmania major* is interrupted, a 10-fold decrease in sensitivity to Sb (III) is recorded compared to wild-type (WT) cells. Conversely, if LmAQP1 is overexpressed, then cells exhibit 100-fold higher sensitivity

to Sb (III) compared to WT cells. In addition, overexpression of LmAQP1 can possibly reverse the phenotype in isolates exhibiting drug resistance (Figarella et al., 2007). In a more recent study, generated *Lm*AQP1-knockout *L. major* strains have been shown to exhibit 30-fold increases in resistance to Sb (III) compared to WT parent strains (Plourde et al., 2015). As well as the evidence focused on *L. major*, it appears that the strong association between AQP1 and Sb (III) mode of action is conserved in other *Leishmania* species. An example of this was highlighted in a study by Imamura et al. (2016) where *L. donovani* clinical isolates from areas of sub-continental India associated with high antimonial treatment failure were found to have acquired an insertion in the *Leishmania donovani* AQP1 gene, spread by means of genetic recombination.

In this chapter, the *Leishmania major* AQP1 WT gene (*Lm*AQP1 WT) was constructed into two expression vectors and then transfected in parasite cells for characterisation. The study aimed to carry out a systematic examination on the role LmAQP1 plays in drug sensitivity and response. This was achieved by cloning and expressing the encoding gene in two different trypanosomatidae systems: (i) *L. major* AQP1 null and the *T. brucei* AQP1-3 null cell lines in order to evaluate the effect of LmAQP1 on sensitivity to antimony and arsenic drugs.

6.2. Results

6.2.1. Successful cloning and expression of *Leishmania major* AQP1 in *Trypanosoma* cells

6.2.1.1. Construction of plasmids and transfection

Section 2.3.4.2, describes how pHDK269 plasmid was constructed by sub-cloning the *Lm*AQP1 gene into the pGEM-T Easy subcloning vector (Appendix 3), which was to verify the DNA sequence prior to cloning the gene into the pRPa vector (Alsford and Horn, 2008). After verifying that the DNA sequence of *Lm*AQP1 was correct, restriction enzymes *Hin*dIII and *Xba*I were used to digest the gene out from pHDK269 plasmid, followed by ligating into the pRPa vector, which is the final destination, given pHDK271 plasmid (plasmid map in figure 2.2, section 2.3.4.3). Sanger

sequencing was used to verify the presence of the *Lm*AQP1 gene on the pHDK721 plasmid generated using HDK1519 and HDK430 primers. Further digestions were performed to validate the correct cloning (Figure 6.1). The presence of the *Lm*AQP1 gene was tested using restriction enzymes *Hin*dIII and *Xba*I, whereas *Asc*I was used to verify whether the *Lm*AQP1 gene and the pRPa plasmid are integrated correctly together. In Figure 6.1, the bands at ~950 bp indicate the presence of the full *Lm*AQP1 gene (959 bp) when the generated plasmid was digested using the restriction enzymes *Hin*dIII and *Xba*I. The band at ~5.3 kb indicates the proper linearization of the plasmid when digested with *Asc*I enzyme. (See plasmid map (figure 2.2) in section 2.3.4.3; for restriction sites).

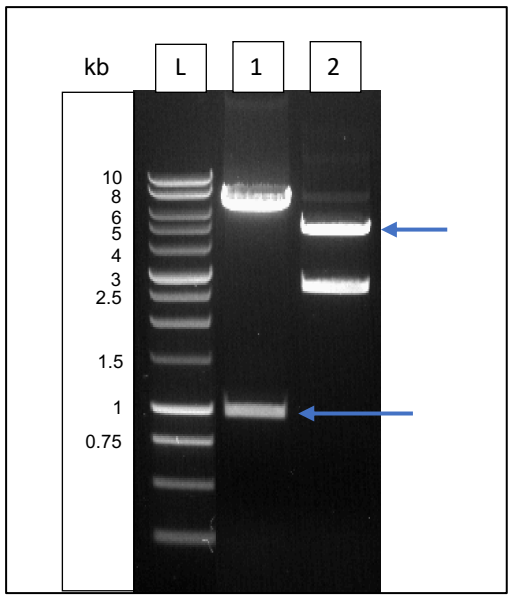

Figure 6.1: The generated pHDK271 plasmid was digested by restriction enzymes, prior to transfection to ensure correct cloning of *Lm*AQP1 gene into pHDK271.
L: 1 kb DNA ladder; 1: arrow indicates expected band at ~950 bp for full *Lm*AQP1 gene, whereas the band at ~7 kb represents the expected remaining backbone of the plasmid, when digested using restriction enzymes *Hin*dIII and *Xba*I; 2: arrow indicates expected band at ~5.3 kb for the DNA expression cassette (containing the *Lm*AQP1 gene and hygromycin antibiotic marker), whereas the band at ~2.6 kb represents the expected remaining part of the plasmid, when digested with *Asc*I restriction enzyme.

Prior to transfection, *Asc*I restriction enzyme was used to linearize pHDK271 so that the expression cassette is properly integrated into the *T. brucei* genome (Alsford et al., 2005). Both the digested products and undigested plasmids (which act as control)

were run on 1% agarose gel to verify that the linearization was correct, and was expected to be at ~5.3 kilobases (kb) long (Figure 6.2).

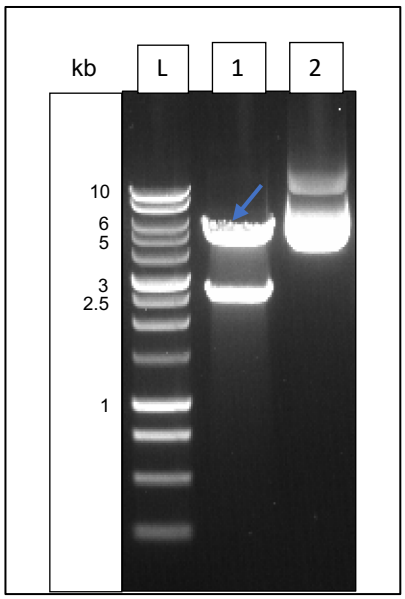

Figure 6.2: The generated plasmid (pHDK271) is digested by the *Asc*I enzyme before transfection for proper integration of the expression cassette into the genome of *tbaqp1/tbaqp2/tbaqp3* null cells.
L: 1 kb DNA ladder; 1: arrow indicates expected band at ~5.3 kb for the DNA expression cassette (containing the *Lm*AQP1 gene and hygromycin antibiotic marker), whereas the band at ~2.6 kb represents the remaining part of the plasmid, when digested with *Asc*I restriction enzyme; 2: control plasmid pHDK271 (undigested).

After the linearization process, extraction of the DNA cassettes from the gel were performed, followed by cleaning the extracted DNA using the NucleoSpin Gel extraction kit (Macherey-Nagel) as per the manufacturer's instructions. As described in section 2.7.1, the cleaned DNA cassettes were then transfected into the *tbaqp1/tbaqp2/tbaqp3* null cell line (Jeacock et al., 2017) (kind gift from David Horn, University of Dundee, UK) which was derived from the 2T1 strain of *T. b. brucei* (Alsford & Horn, 2008). This was followed by selection and cloning of the transfected cells in the presence of 2.5 µg/ml hygromycin. The new cell line was then tested using PCR to determine the success of transfection. Here, genomic DNA obtained from the clones was screened, using Go Taq DNA polymerase (Promega) PCR amplifications, for proper integration of the plasmid into the genome of *T. brucei* and to establish the presence of the *Lm*AQP1 gene. Correct transfection was confirmed by setting up two PCR reactions. The first PCR reaction was used to

amplify the full *Lm*AQP1 gene based on the HDK1519 and HDK1520 primers. In the second PCR reaction, the *Lm*AQP1 gene was amplified with surrounding part of the expression cassette using HDK1011 and HDK430 primers. Separation of the PCR products was done on a 1.5% agarose gel, and visualization was done using SYBR™ Safe DNA gel stain. The PCR products obtained from the first reaction are shown in Figure 3.3A, band at ~950 bp indicates the expected size of the full *Lm*AQP1 gene (959 bp). The second PCR reaction gave product-sized bands at ~1250 bp, which corresponds to the expected size of the full *Lm*AQP1 gene with a partially fragmented plasmid (1240 bp) (Figure 6.3B). Successful transfection of the clones with *Lm*AQP1 was confirmed by the amplified PCR products (See plasmid map (figure 2.2) in section 2.3.4.3; for primers sites).

After confirming the PCR, Phusion High-Fidelity DNA Polymerase (NEB) was used to amplify the *Lm*AQP1 gene from genomic DNA of each clone. The NucleoSpin PCR kit (Macherey-Nagel) was then used to purify the PCR products, and confirmed using the forward and reverse primer for HDK1519 and HDK1520 respectively by Sanger sequencing.

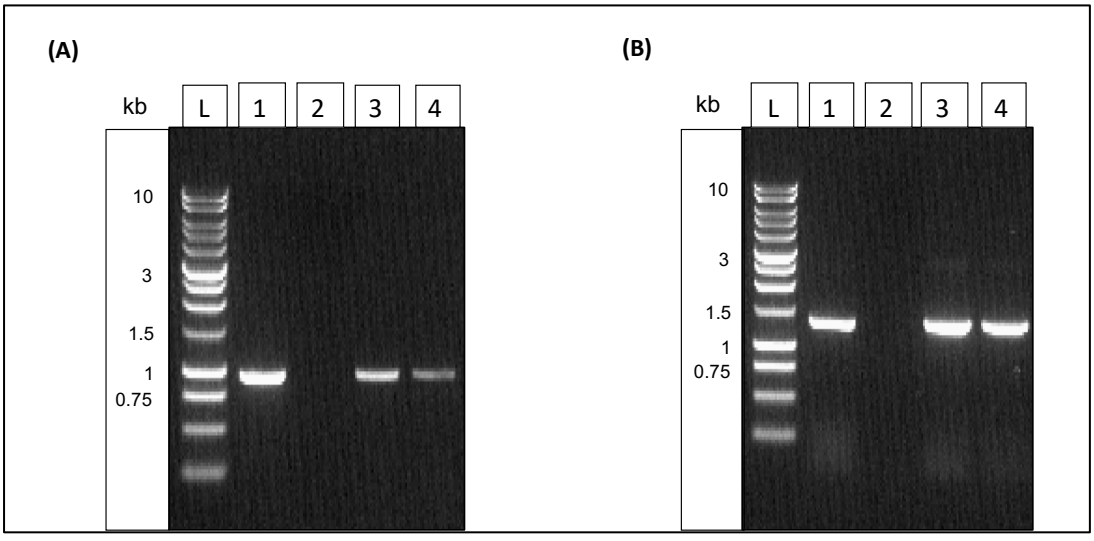

Figure 6.3: PCR products electrophoresis using Agarose gel showing the LmAQP1 expression cassette integrated in *tbaqp1/aqp2/aqp3* null cells.
PCR product amplification of: (A) the full *Lm*AQP1 gene at ~950 bp, (B) fragment at ~1250 bp represents *Lm*AQP1 and parts of the expression cassette surrounding the gene. The size of each band was approximated with respect to the standard size of the 1Kb molecular weight Ladder. (A-B) L: 1Kb Ladder; 1: $pRPa^{LmAQP1}$ (positive control); 2: *Tb*AQP1-3 KO (negative control); 3: *Lm*AQP1 (clone 1); 4: *Lm*AQP1 (clone 2).

6.2.1.2. The impact of LmAQP1 on *T.b aqp1-3* null strain growth

Once it was confirmed that the clones were expressing the desired gene, the effect of introducing the *Lm*AQP1 into the *tbaqp1/tbaqp2/tbaqp3* null cells were examined. Growth of clones 1 and 2 were then determined and compared to the *tbaqp1/tbaqp2/tbaqp3* null cells and 2T1 strains. The *tbaqp1-3* null cell line shown in Figure 6.4 indicates a reduced rate of growth compared to 2T1, with a substantially reduced maximum cell density. In terms of maximum observed cell density, both clones expressing the *Lm*AQP1 gene fall between the 2T1 and *tbaqp1/tbaqp2/tbaqp3* null cell lines. These two clones remained at max cell density on day 4, which was already achieved on day 3 before they reduced on day 5.

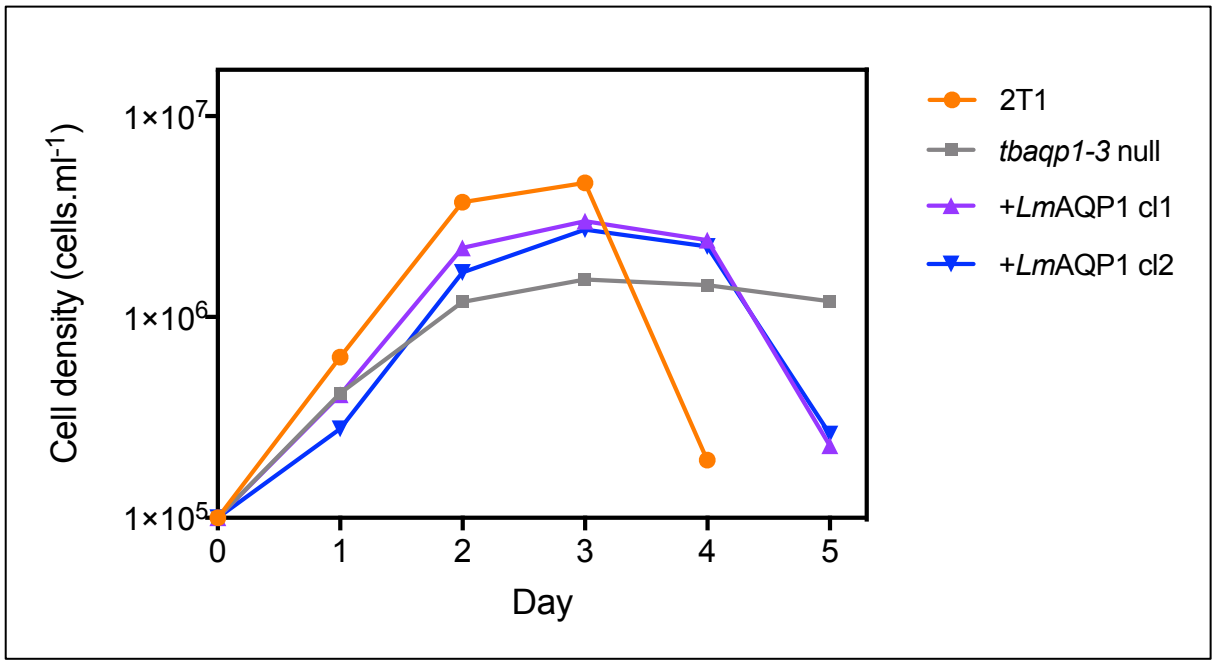

Figure 6.4: *T. brucei* cell lines growth curves in HMI-9 medium, incubation with 5% CO_2 at 37 °C. Clones 1 and 2 of of *tbaqp1-3* null cells that expressing the LmAQP1 (+LmAQP1) were compared to 2T1 and *tbaqp1-3* null strains. On the first day, a culture of 1×10^5 cells/mL were set up for each cell line, with selective marker added to both clones (2.5 µg/ml hygromycin). Using a haemocytometer, live cells were counted every day for 5 days.

6.2.1.3. Expression of LmAQP1 in *Trypanosoma brucei aqp1-3* null strain enables antimonial transport

After expressing the LmAQP1 in *tbaqp1/tbaqp2/tbaqp3* null cells, the sensitivity of the cells to arsenical and antimonial drugs were determined. Here, the Alamar blue assay was used to calculate EC_{50} of the clones to confirm whether the generated cells show sensitivity to the following compounds; Arsenic Oxide, Potassium Antimony Tartrate and Sodium Arsenite. The assay was performed alongside the *aqp1-2-3* null and 2T1 strains, which both acted as controls. Phenylarsine oxide (PAO) and pentamidine were used as drug controls throughout the assessment. From Figure 3.5a and Figure 3.5e, it is clear that the value of EC_{50} of *tbaqp1/tbaqp2/tbaqp3* null cells is significantly higher (276 ± 15.9 nM) and (71.7 ± 8.6 nM) than that of 2T1 cells (40 ± 7.7 nM) and (4 ± 1.6 nM) for Potassium Antimony Tartrate and Pentamidine, respectively, an indication that the presence of aquaporins 1-3 influences the sensitivity of *T. b. brucei* to these drugs. On the other hand, the sensitivity of *T. brucei* to Arsenic Oxide, Sodium Arsenite and Phenylarsine Oxide is not significantly affected by these aquaporins (Figure 6.5B-D). For Potassium Antimony Tartrate (PAT), the two clones expressing the LmAQP1 show an almost 10-fold lower value of EC_{50} ($P<0.001$) compared to the *tbaqp1/tbaqp2/tbaqp3* strain (Figure 6.5A). The EC_{50} is closely comparable to that of 2T1 cells, showing that that the LmAQP1 restores sensitivity to PAT. None of the tested cell lines were sensitised to Arsenic Oxide, Sodium Arsenite and PAO, all arsenic compounds, and all had nearly the same average values of EC_{50}, i.e. no significant differences were observed (Figure 6.5B-D). Conversely, the clones expressing the LmAQP1 fails to restore sensitivity to pentamidine given that the EC_{50} values (cl1= 61.2 ± 7.5, cl2= 55 ± 7.8) are significantly higher than the values of 2T1 cells (EC_{50}= 4.0±1.6), and are very similar to EC_{50} values of the *tbaqp1/tbaqp2/tbaqp3* null strain (EC_{50}= 71.7 ± 8.6; $P>0.05$) (Figure 6.5E). Following this outcome, it is suggested that expression of the LmAQP1 gene in *T. brucei* parasites only enables the cells to facilitate the transport of PAT.

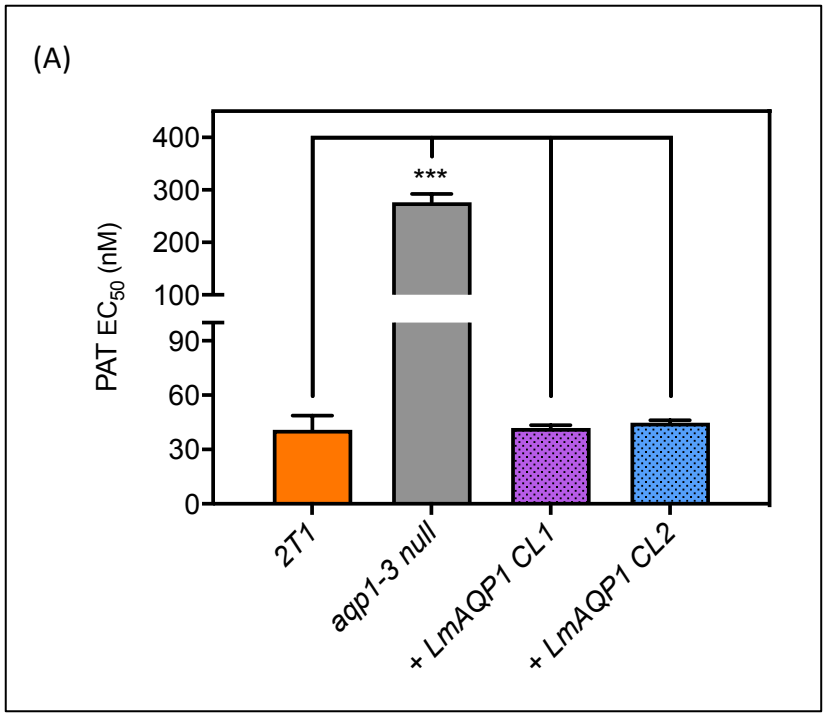
(A)
PAT EC50 (nM)
400
300
200
100
90
60
30
0
***
2T1
aqp1-3 null
+ LmAQP1 CL1
+ LmAQP1 CL2

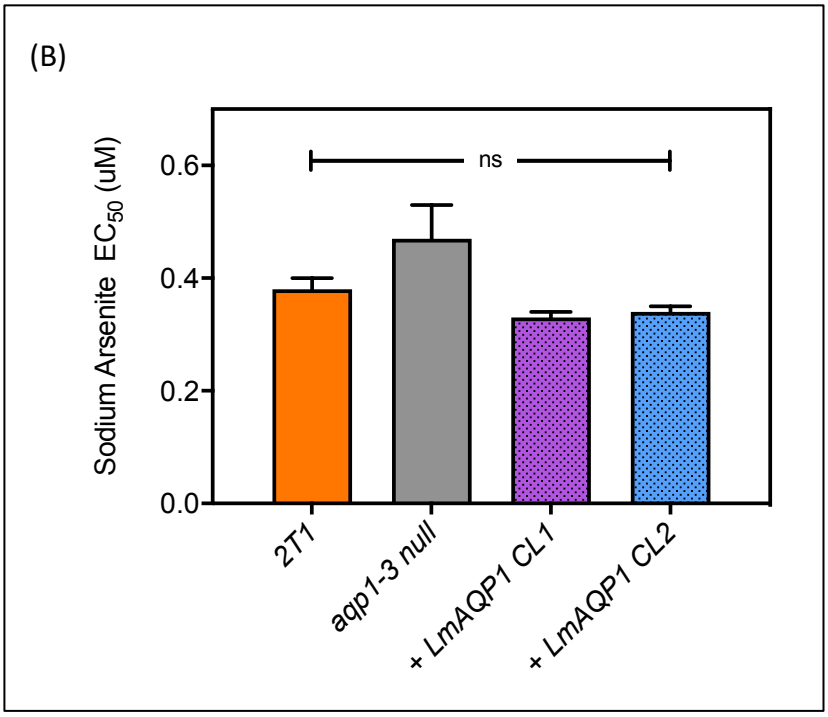
(B)
Sodium Arsenite EC50 (uM)
0.6
0.4
0.2
0.0
ns
2T1
aqp1-3 null
+ LmAQP1 CL1
+ LmAQP1 CL2

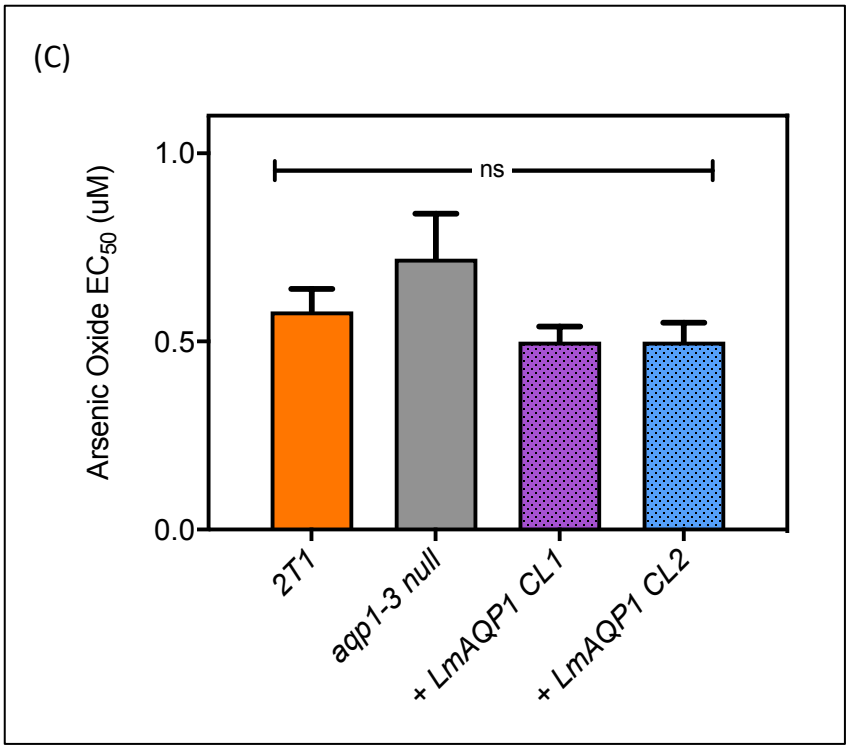
(C)
Arsenic Oxide EC50 (uM)
1.0
0.5
0.0
ns
2T1
aqp1-3 null
+ LmAQP1 CL1
+ LmAQP1 CL2

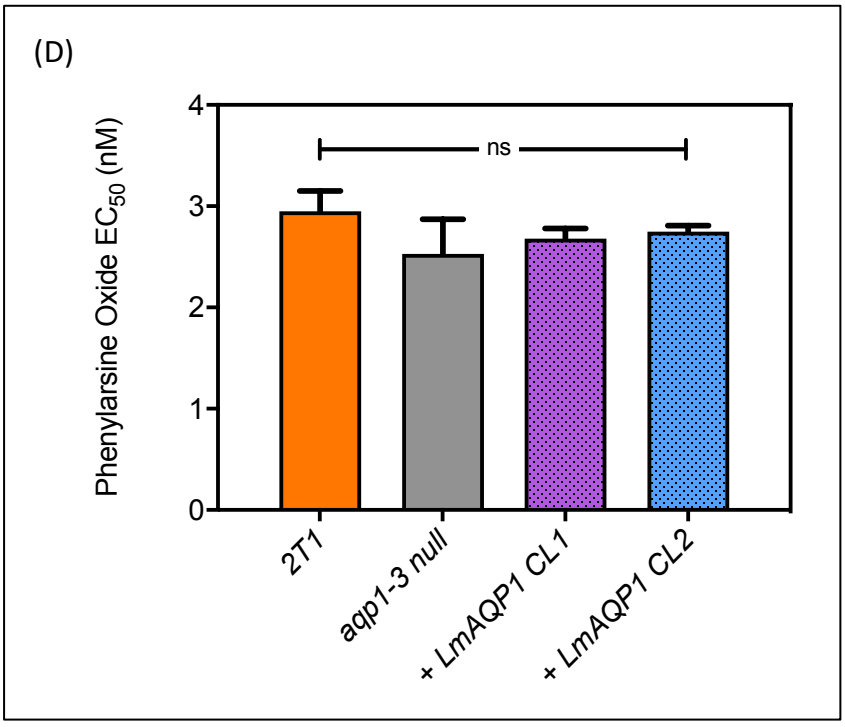
(D)
Phenylarsine Oxide EC50 (nM)
4
3
2
1
0
ns
2T1
aqp1-3 null
+ LmAQP1 CL1
+ LmAQP1 CL2

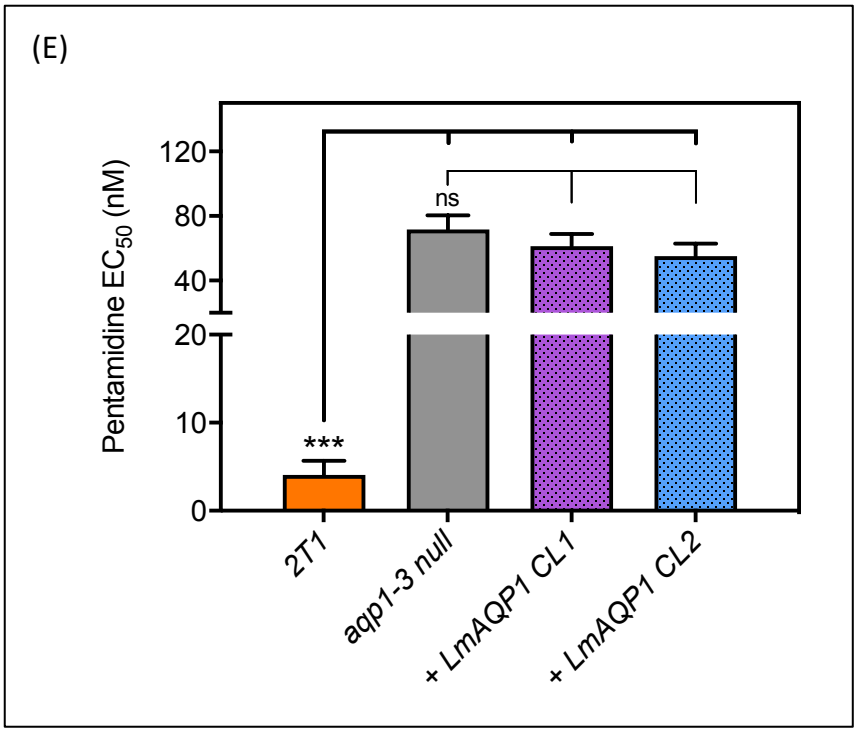

Figure 6.5: Drug sensitivity of clones 1 and 2 that expressing LmAQP1 compared to *tbaqp1-3* null and 2T1 strains.
The cells were incubated at 37 °C for 48 hours, with 5% CO_2 and serial dilutions of: (A) Potassium Antimony Tartrate, (B) Sodium Arsenite, (C) Arsenic Oxide, (D) Phenylarsine Oxide (PAO) and (E) Pentamidine, followed by incubation with Alamar Blue dye for another 24 hours. All experiments are the average and SEM of three independent experiments. Significance was determined by two-tailed unpaired Student's tests. ***, P<0.001, ns, non-significant.

6.2.2. Successful cloning and expression of *Leishmania major* AQP1 in *Leishmania* cells

6.2.2.1. Construction of plasmids and transfection

The same techniques that were described in section 6.2.1.1 were applied in cloning *Lm*AQP1 gene into the expression vector for *Leishmania* cells. Initially, the *Lm*AQP1 gene was sub-cloned into the pGEMT Easy subcloning vector to produce pHDK270 (Appendix 4), before cloning the gene into the pNUS-HcN plasmid, i.e. pNUS vector, which is an appropriate vector of expression in *Leishmania* (Tetaud et al., 2002). The produced plasmid pHDK270 was confirmed by Sanger sequencing. Next, both the *Lm*AQP1 gene and the plasmid were digested with restriction enzymes and ligated into the backbone of the expression vector pNUS-HcN, giving the new plasmid pHDK272. The generated plasmid (pHDK272) was digested using three restriction

enzymes as a method of validating the proper cloning (Figure 6.6). Testing for the presence of the full *Lm*AQP1 gene was accomplished by *Bgl*II and *Xba*I, whereas *Bgl*II and *Xho*I were used to check for correct integration of the gene into the PNUS-HcN plasmid. In Figure 6.6, the bands can be observed at 950 bp and 1500 bp, showing that *Lm*AQP1 gene is present and correctly integrated into the pNUS-HcN plasmid (See plasmid map in figure 2.3 for restriction sites). The primers HDK1519 and HDK340 were used in Sanger sequencing to verify the plasmid pHDK272 prior to transfection into *L. major* AQP1 null strain. Following the confirmation of the sequence, pHDK272 was transfected, exactly as described in section 2.5.2, into *Lm*AQP1 null cells (Marie et al., 2015) (obtained from Marc Ouellette lab). The generated clones were then grown in the presence of geneticin (G418), a neomycin analogue, at 50 μg/ml – an antibiotic for the neomycin resistance marker in the plasmid. After selecting surviving clones, gDNA was extracted for confirmation of the correct transfections by PCR. The presence of the *Lm*AQP1 gene in the mutant null cells was confirmed by performing two PCR reactions. The results of PCR 1 are shown in Figure 6.7A; the expected bands appear at ~950 bp and they represent the full gene (942 bp) based on the forward primer (HDK1519) and reverse primer (HDK1520). PCR 2 was applied for gene amplification with the plasmid partially fragmented and using HDK851 and HDK340 primers (Figure 6.7B). The bands appeared as expected at 1228 bp of the fragment (See plasmid map (figure 2.3) in section 2.3.4.4 for primers sites). Based on the results of the two PCR amplifications, the transfection of the *Lm*AQP1 gene into the mutant null cells is a success. After the PCR confirmations, the *Lm*AQP1 gene was then amplified from the genomic DNA of each strain using Phusion High-Fidelity DNA Polymerase (NEB). The PCR products were purified using NucleoSpin PCR kit (Macherey-Nagel), and were confirmed by Sanger sequencing using the forward primer (HDK1519) and reverse primer (HDK1520).

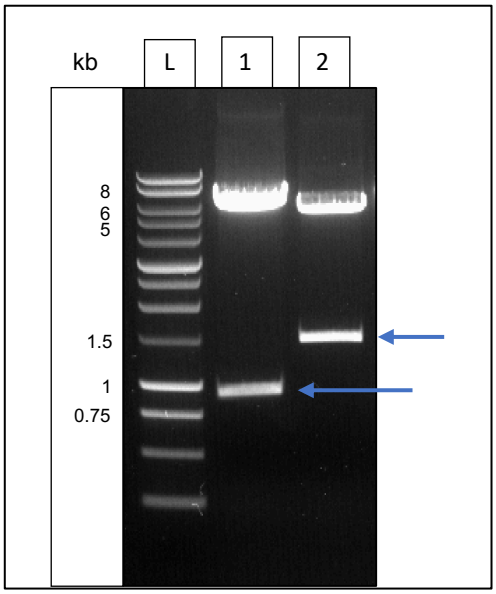

Figure 6.6: The generated pHDK272 plasmid was digested by restriction enzymes, prior to transfection to ensure correct cloning of *Lm*AQP1 gene into pHDK272.
L: 1 kb DNA ladder; 1: arrow indicates expected band at ~950 bp for full *Lm*AQP1 gene, whereas the band at ~6.2 kb represents the remaining backbone of the plasmid, when digested using restriction enzymes *Bgl*II and *Xho*I; 2: arrow indicates expected band at ~1.5 kb for the full *Lm*AQP1 gene and parts of the expression cassette surrounding the gene, whereas the band at ~5.7 kb represents the remaining part of the plasmid, when digested with *Bgl*II and *Xba*I restriction enzyme.

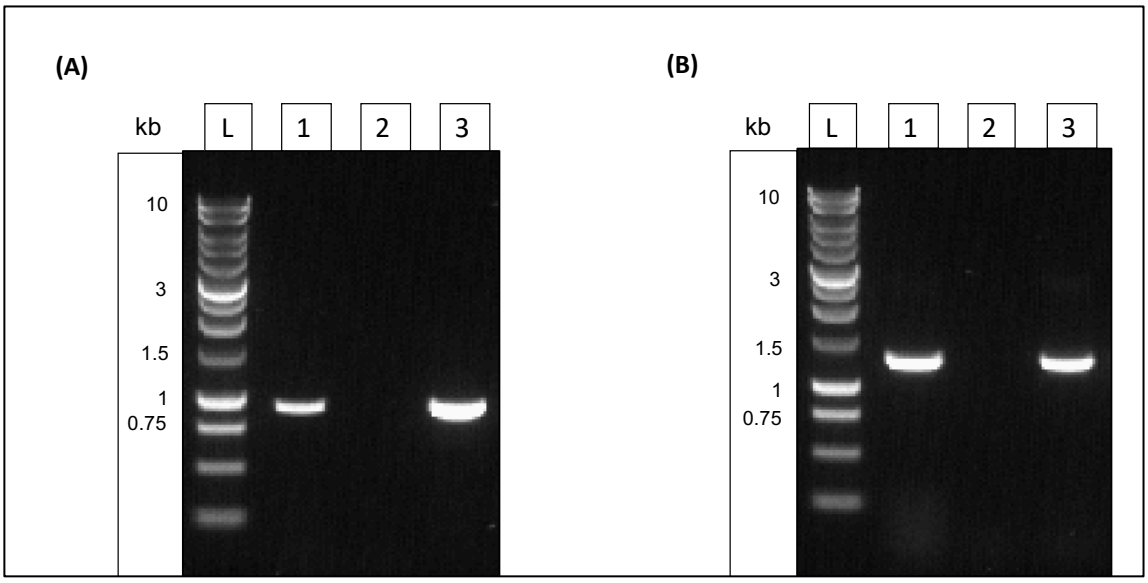

Figure 6.7: PCR products electrophoresis using Agarose gel showing the LmAQP1 expression cassette integrated in *Lm*AQP1 null cells.
PCR product amplification of: (A) the full *Lm*AQP1 gene at ~950 bp, (B) fragment at ~1250 bp represents *Lm*AQP1 and parts of the expression cassette surrounding the gene. The size of each band was approximated with respect to the standard size of the 1Kb molecular weight Ladder. (A and B) L: 1Kb Ladder; 1: *Lm*AQP1 (clone 1); 2: gDNA *Lm*AQP1 KO (negative control); 3: *Lm*AQP1 (clone 2).

6.2.2.2. The impact of LmAQP1 on *Leishmania major aqp1* null strain growth

It was observed that the time between passages was longer for *Lm*AQP1 null cells than for the *L. major* WT cells. Hence, cell counting was performed to establish whether reintroduction of *Lm*AQP1 into the null mutant cells would reinstate cell growth as the WT strain. Cultures of the clones (+ *Lm*AQP1) were established growth was compared with that of the *L. major* AQP1 null and *L. major* WT strains. These cell lines were cultured in HOMEM medium at a starting density of 1×10^5 cells/ml. Hygromycin B antibiotic was added to culture 100 ug/mL for the AQP1 null cells and G418 antibiotic (50 μg/ml) for the clones, necessary for cell selection based on hygromycin B and neomycin resistance markers present in the respective integrated cassettes (Plourde et al., 2015; Tetaud et al., 2002). Cell counts were performed in triplicate after every 24 h for 6 days. According to Figure 6.8, the rate of growth of the add-back clones is slightly higher than the rate of growth in the null mutant cell line, but it is however slower than in the WT cells.

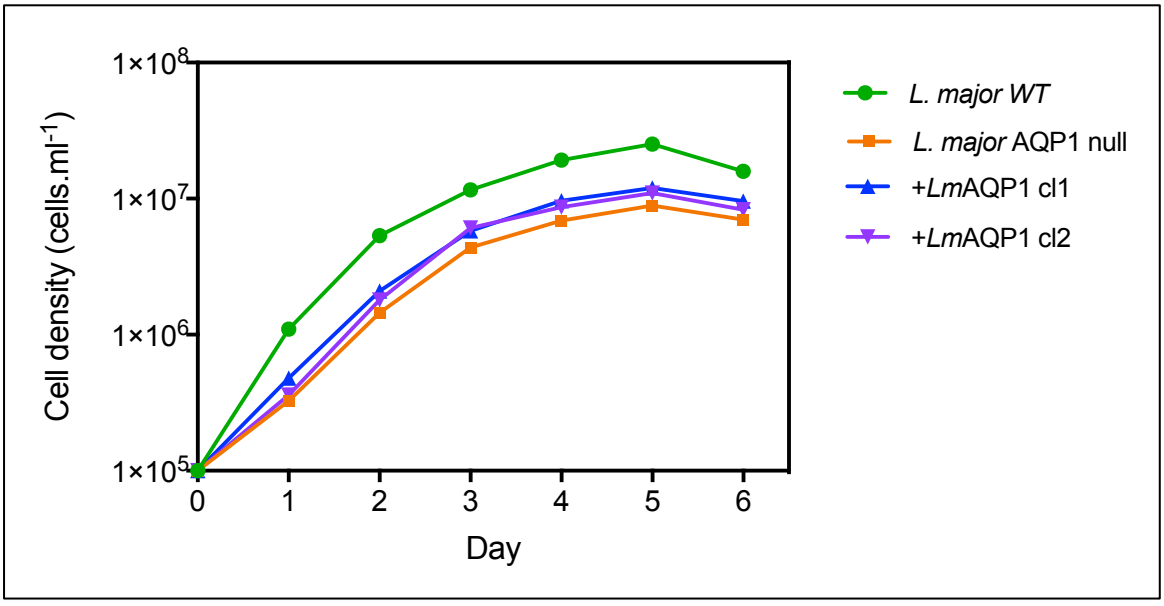

Figure 6.8: **The growth curve for *L. major* cell lines in HMI-9 medium, incubation at 25 °C.**
The rate of growth of the clones (+ *Lm*AQP1) was compared to that of *L. major* AQP1 null and *L. major* WT strains. For every cell line, a culture of 1×10^5 cells/mL was initially prepared. Each day, cells were counted using counting haemocytometer, for 6 days.

6.2.2.3. Reintroduction of *Lm*AQP1 gene in *Leishmania major aqp1* null strain restores antimonial and arsenical sensitivity

The next step was to test our clones (+ *Lm*AQP1) to find out if they can restore the sensitivity of antimonial and arsenical drugs when the *Lm*AQP1 is re-introduced into the null mutant cells. In this case, the Alamar blue assay was used to determine the EC_{50} for Arsenic Oxide, Potassium Antimony Tartrate (PAT) and Sodium Arsenite in the add-back strain. This assay was carried simultaneously with the *Lm*AQP1 null and *L. major* WT strains, which both acted as controls. Pentamidine was used as a control drug. As shown in figure 6.9A-C, the EC_{50} values of the *aqp1*-null strain are significantly higher (220 ± 2.7, 52.8 ± 0.6, and 75.4 ± 0.6) for PAT, Sodium Arsenite and Arsenic Oxide than those of the WT control or the AQP1 add-back clones. This suggests that AQP1 is a crucial factor on sensitivity to these heavy metals. Interestingly, the average values of EC_{50} of the two add-back clones was even much lower than those of the WT cell line, i.e., 0.18 ± 0.01, 0.6 ± 0.18 and 1.13 ± 0.3 instead of 8.4 ± 0.2, 3.7 ± 0.20, and 5.2 ± 0.17 for PAT, Sodium Arsenite and Arsenic Oxide, respectively. In addition, it was surprising that the add-back strain appears to have lower sensitivity to pentamidine, which is significantly different in comparison to WT *L. major* strain (P<0.0001) (Figure 6.9D).

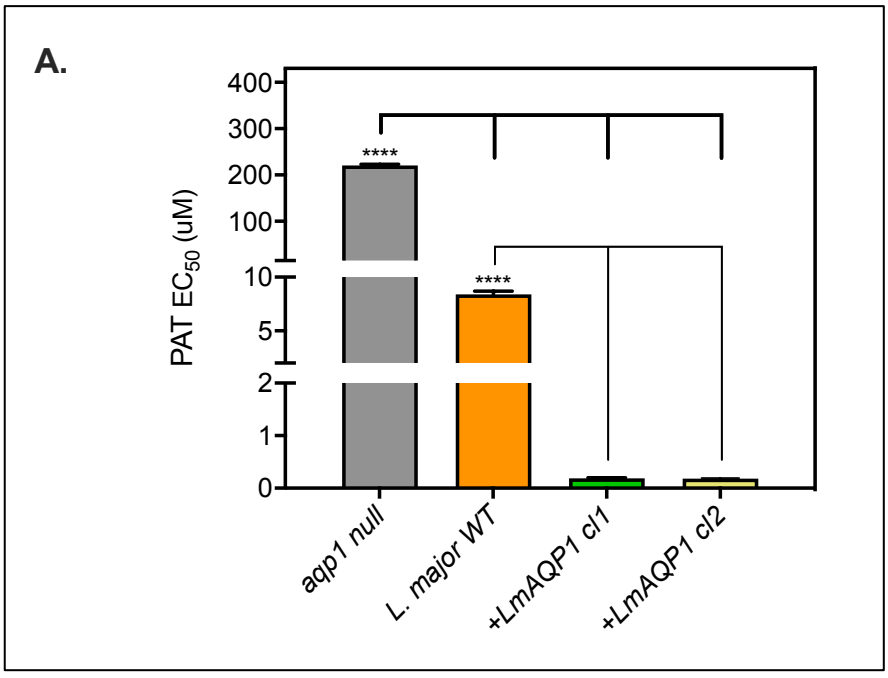

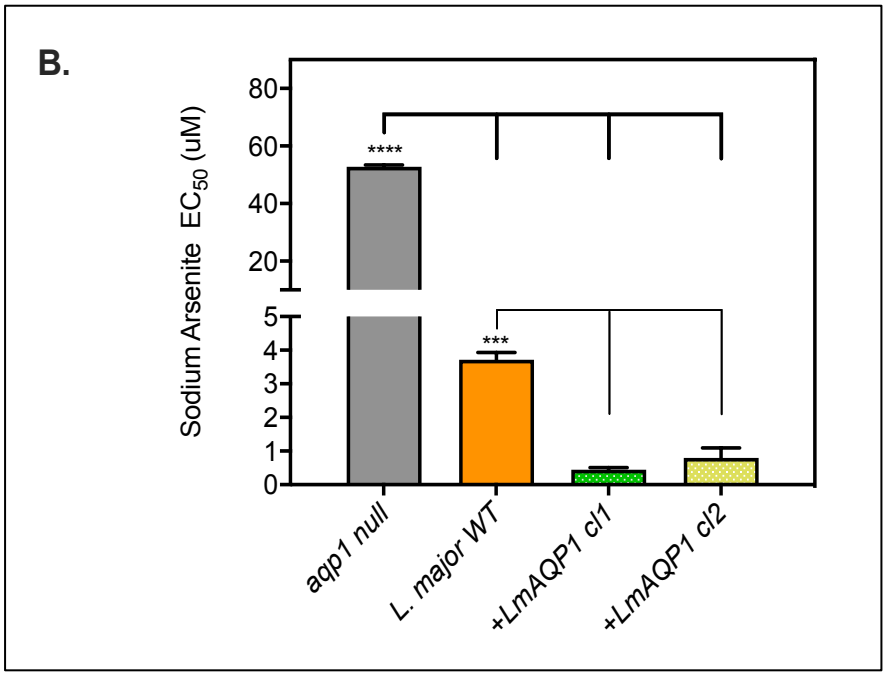
B.
Sodium Arsenite EC50 (uM)
80
60
40
20
5
4
3
2
1
0
****
***
aqp1 null
L. major WT
+LmAQP1 cl1
+LmAQP1 cl2

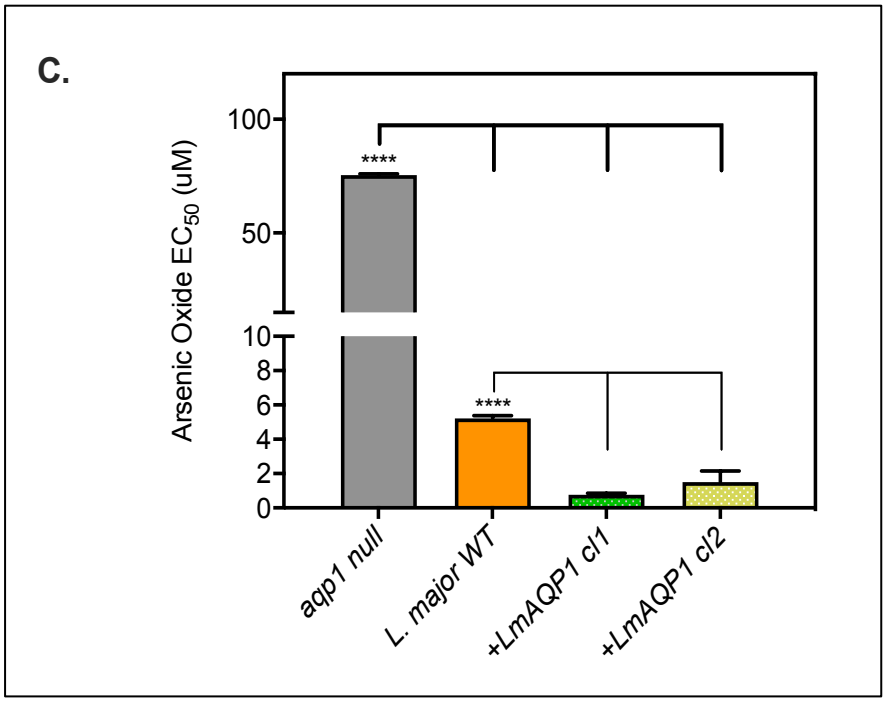
C.
Arsenic Oxide EC50 (uM)
100
50
10
8
6
4
2
0
****
****
aqp1 null
L. major WT
+LmAQP1 cl1
+LmAQP1 cl2

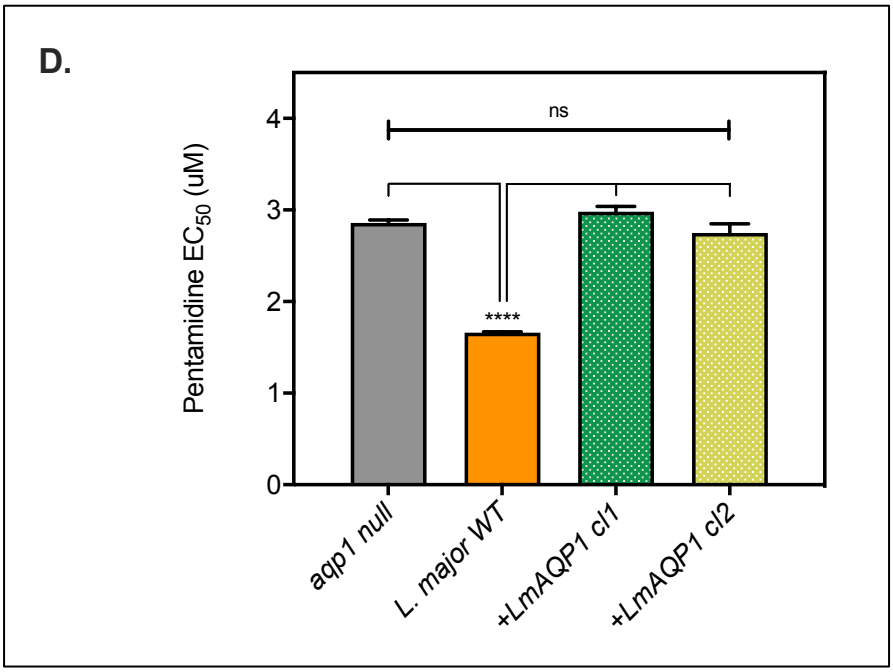

Figure 6.9: Sensitivity of *L. major* cell lines, evaluated by use of the Alamar blue assay. The cells were incubated at 25°C for 72 hours, with serial dilutions of: (A) Potassium Antimony Tartrate, (B) Sodium Arsenite, (C) Arsenic Oxide, and (D) Pentamidine. This was followed by incubation with Alamar Blue dye for another 48 hours. The experimental results are the average and SEM of three experiments performed independently. The significance was determined by use of two-tailed unpaired Student's tests. ***, P<0.001, ****, P<0.001, ns, non-significant.

6.3. Discussion

The aim of this study was to create new cell lines for further work by successfully cloning the *Lm*AQP1 gene and transfecting this into *Leishmania* and *Trypanosoma* strains. PCR confirmed that the two expression vectors generated had the desired *Lm*AQP1, before transfecting the vectors into *Trypanosoma and Leishmania* cell lines. Again, using PCR, it was confirmed that the transfection process was successful when *Lm*AQP1 gene was correctly inserted into the genome of the parasites. The next step was to perform growth curve assays to establish if the removal or insertion of the *Lm*AQP1 gene in *Trypanosoma* cell lines hindered or improved the rate of growth, given the important role *Lm*AQP1 exhibits in *Leishmania* cellular physiology and drug response (Mandal et al., 2014; Plourde et al., 2015).

It was observed that the *AQP1* knockout (KO) in *Leishmania major* cells grew at a rate slower than the WT strain. Given that the *AQP1*-coded aquaporin protein helps to facilitate water transport in the cells (Figarella et al., 2007), it was suspected

that the absence of *AQP1* in the KO cell line resulted in poor regulation of cell homeostasis and a subsequent slower growth rate as observed in a previous study (Plourde et al., 2015). Surprisingly, the WT phenotype was not restored in the transfected cell lines as expected. Rather than having a growth rate similar to the WT, the growth rates in the transfected clones were more or less the same with the *AQP1* KO cell line with a very slight increase. One explanation for this result may be a much faster water recovery rate experienced by transfected cell lines compared to the WT or AQP1 null-lines, as described in Plourde et al. (2015). A faster water recovery rate may disrupt the osmoregulation abilities of cells previously compensating without a non-essential AQP1 transporter, and the sudden change in osmoregulation caused by fast water recovery may be subsequently hindering cell growth.

The observation of the trypanosome cells revealed a much slower growth rate in the *tbaqp1*/*tbaqp2*/*tbaqp3* null cells in comparison to 2T1 cells, most likely the result of reduced drug uptake and defects in transport, accumulation and metabolism of glycerol important for many cell activities including self-replication (Jeacock et al., 2017). Additionally, it was observed that transfected cell lines with *Lm*AQP1 reintroduced showed a marginally increased cell growth rate, particularly after day 2. Given that this cell line did not contain three different aquaporin genes, it is speculated that the introduction and expression of the *Lm*AQP1 gene overcame a glycerol defect in these cells, and this subsequently led to higher growth rates. However, it is clear that LmAQP1 does not compensate for three lost *T. brucei* aquaporins, which would be required to create the cumulative restorative effect on glycerol uptake and metabolism in trypanosomes. In turn, this may be necessary for reaching the growth rate observed with 2T1 cells.

In the subsequent steps, drug sensitivity Alamar blue assays were performed for the cell lines in attempt to establish the role played by AQP1 in the transportation of heavy metals antimony and arsenic. *Leishmania* infections are treated using antimonial drugs, which are transported via *Leishmania* AQP1 (Kell et al., 2014). As a matter of fact, AQP1 is the key route of entry of antimony in *Leishmania* parasites (Mandal et al., 2010). Additionally, previous research suggests that arsenic contamination in Indian subcontinent water has given rise to high treatment failures

with antimonial treatment, supported both with work in mouse models *in vitro* and *in vivo*, and from patients that contracted VL local to these areas (Perry et al., 2013; Perry et al., 2015). Hence, it was expected that the potassium antimony tartrate (PAT) drug assay would give interesting results. The experiments on the trypanosome parasites yielded some significant results. The *tbaqp1*/*tbaqp2*/*tbaqp3* null cell line showed significant resistance to the PAT drug assay. It was observed that transfecting the *Lm*AQP1 gene reversed the resistance, an observation that has been made in previous studies (Gourbal et al., 2004). As for arsenic oxide and sodium arsenate in the *Lm*AQP1 null strain, it was observed that removal of the *Lm*AQP1 gene confers resistance to these compounds, which is reverted when the gene is reinstated, conferring a higher level of sensitivity in transfected cell lines compared to WT cells. These observations support previous conclusions that AQP1 plays an important role in the transportation of arsenic compounds, as well as antimonial compounds, in *Leishmania* (Gourbal et al., 2004; Plourde et al., 2015). These observations would also support reasoning that prolonged exposure to arsenic compounds through contaminated water, may have led to the long-term selection of antimonial resistant parasites as established by Perry et al. (2013, 2015). Therefore, changes to, or loss of, *Leishmania* AQP1 transporter functionality, from such selection have plausibly led to widespread antimonial drug resistance and high treatment failure rates observed in subcontinental India.

Though AQPs, including AQP1, are known transport mediators of arsenite (As (III)) and Sb (III) (Uzcátegui et al., 2013), observations made on the effect of AQP1 of sensitivity to arsenic and antimonial compounds for *Leishmania* were not replicated in *T. brucei*. Instead, it was found that neither removal of *AQP1-3* in *T. brucei* 2T1 cells, nor transfection of *Lm*AQP1 to *tbaqp1*/*tbaqp2*/*tbaqp3* null cell line during *T. brucei* arsenic oxide and sodium arsenate assays made a significant difference to *T. brucei* sensitivity. Indeed, it is likely that *T. brucei* uptake of arsenic and antimonial compounds is dependent on other transport channels than just the AQPs, as has already been demonstrated with the uptake of the trivalent organoarsenical melarsoprol (Matovu et al., 2003). Therefore, the addition of *Lm*AQP1 makes little change to levels of cell sensitivity as *T. brucei* cells remain sensitive despite the loss of AQPs.

Testing of Phenylarsine oxide (PAO) was only done with the *Trypanosoma* parasites. From the results obtained, AQP1 failed to show any impact on transportation of PAO. This was expected because PO diffuses freely across membranes (Fairlamb et al., 1992) and was therefore an excellent control. Lastly, pentamidine (PMD), a drug that has been used in the treatment of *Trypanosoma* and *Leishmania* infections, was tested. The exact mechanism of PMD uptake in *Leishmania* is not well understood, but its actions include the disruption of the mitochondrial inner membrane potential of the parasite (Basselin et al., 1996; Coelho et al, 2007). In this observation, the loss and reinstatement of AQP1 in *T. brucei* did not substantially alter its sensitivity to PMD. Removal of *AQP1-3* from *T. brucei* 2T1 cells resulted in a significant loss in PMD sensitivity compared to 2T1 cells, whilst transfection of *Lm*AQP1 to *tbaqp1/tbaqp2/tbaqp3* null cells made little impact in reversing the sensitivity profile of these cells. This was expected, as previous research has established AQP2, rather than AQP1, as the major determinant for PMD uptake in African trypanosomes (Baker et al., 2012). On the other hand, it was observed that *Leishmania* aqp1-null lines exhibited a significant loss in PMD sensitivity compared to WT cells. It appeared that re-introduction of LmAQP1 by transfection to *aqp1*-null cell lines made no impact towards restoring cells to the WT sensitivity phenotype. This observation may also be attributed to the significant increase in cell volume recovery rate observed when LmAQP1 is reintroduced to aqp-1 null cell lines (Plourde et al., 2015). This could have a possible disruptive effect on *T. brucei* cell osmoregulation activities, and in turn, disrupt pentamidine uptake in transfected cell lines leading to the resistance profiles observed.

Chapter 7 General discussion

Kinetoplastid parasites, particularly *Leishmania* and *Trypanosoma* species cause a range of diseases in humans, most of which are neglected in the world. Although the WHO and other non-governmental organisations have put significant efforts in fighting these insect-transmitted diseases, they remain a major challenge in public health, especially for the populations directly affected. The development of vaccines, which has proven to be a successful approach to management of many infectious diseases, has not been successful in the case of trypanosomatid diseases. This is because the parasites that cause these diseases possess immune-suppression and evasion mechanisms that are very efficient, such as intracellular locations for *T. cruzi* and for *Leishmania* spp. in the human host (Cardoso et al., 2016; McConville & Naderer, 2011), and antigenic variation by African trypanosomes (Gehrig & Efferth, 2008; Horn, 2014). Given the lack of vaccines, and the practical impossibility of vector control over enormous rural areas, the only viable alternative to control these diseases is chemotherapy. However, the drugs used in treating the diseases are far from ideal because they are ineffective at certain stages of the disease or to some parasite strains, or the routes of administering the drug are not convenient, have unacceptable toxicity, have induced resistance, and/or are not cost-effective (Kalel et al., 2017; Ranjbarian et al, 2017; Barrett & Croft, 2012; Field et al, 2017). With the rapid development of resistance, treatment efforts have diminished efficacy, and there is little or no financial incentive for the development of newer drugs to replace those against which resistance has developed (Fairlamb et al., 2016; Giordani et al., 2016). The major mechanisms of resistance involve: reducing the level of free drug at the target site, reducing the drug-binding affinity, reducing drug uptake, target overexpression, or failure to activate a prodrug (De Koning, 2017; Fairlamb et al., 2016).

The key to the survival of kinetoplastid parasites such as *Trypanosoma brucei* and *Leishmania major* is the ability to overcome different environmental challenges in insect and mammalian hosts. Thus, the interface between the environment and the kinetoplastid cell, the plasma membrane, plays an important role in managing the survival in these different niches. Together with uptake of essential nutrients and outflow of metabolites, plasma membrane transporters sometimes also facilitate

the entry of drug compounds of high clinical importance (Tetaud et al., 1997; Landfear, 2008; Munday et .al, 2015a).

Aquaporins (AQPs) are integral membrane proteins, known to play an important role in allowing the movement of water into- and out of the cell in a rapid and regulated manner (Borgnia et al., 1999). Aquaglyceroporins are type of aquaporins, also known to conduct and some very small uncharged solutes such as glycerol, CO_2, ammonia, and urea across the membrane (Gourbal et al., 2004, Verkman, 2014). Unlike most known aquaglyceroporins, TbAQP2 is responsible for the increased sensitivity of *T. brucei* to melarsoprol (398 Da) and pentamidine (340 Da) (Baker et al., 2012). Although TbAQP2 is described as the first aquaporin with the potential to transport drug-like molecules, the mechanism that underpins these phenomena remained unclear. However, a structural analysis described in Munday et al (2015) hypothesised that the key difference that allowed TbAQP2 to take up large drug-like molecules was the size of several of the selectivity filter residues, and the absence of the cation-repulsing arginine that sticks out into the pore. To investigate this hypothesis a mutational analysis, swapping TbAQP2 and TbAQP3 selectivity filter residues, and altering the pore width at the cytoplasmic end was performed.

With the evolution of TbAQP2 by positive selection due to the high ratio of dN/dS, eliminating all points of constriction including the NPA/NPA motif, the cationic arginine of the ar/R selectivity filter, and the aromatic amino acids, the pore size has been enlarged to an unprecedent degree (Baker et al., 2012; Munday et al., 2015). It is worth noting that this enlargement apparently stemmed from a copy of the existing AQP in the ancestor (now called TbAQP3), which itself was left unchanged and with a completely conventional selectivity and cation filter, while in the copy all those residues were systematically replaced towards a larger pore while keeping an otherwise strong homology. This could be interpreted as the species deriving a benefit from both genes - conventional AQP3 and enlarged-pore AQP2. This is consistent with the observation that the AQP2-AQP3 allele seems to be very stable. Hypothesising that it first evolved in *Trypanosoma brucei* (as far as evidence allows) the arrangement remained unchanged in the subsequent sub-speciation events to *T. b. gambiense*, *T. b. rhodesiense*, *T. evansi* and *T. equiperdum*. What remains completely unclear is what advantage the trypanosome derives from this

situation. Apart from the conventional AQP substrates such as small trioses and glycerol (Uzcategui et al., 2004; 2013) no metabolite substrate could be identified for TbAQP2 (Alghamdi et al., 2020), having tested everything from amino acids to polyamines, nucleosides and vitamins. It may well be that the gained function TbAQP2 is not related to uptake at all, but to the efflux of an unwanted metabolite. Untargeted metabolomics sampling the cells and medium of WT and tbaqp2-3 null cells did not identify any candidate substrates, however (Munday and De Koning, unpublished), but it is possible that the TbAQP2 function is not operational in vitro in rich culture medium, only in vivo; moreover, it may give an advantage in the tsetse fly stage or short-stumpy stage rather than the short-slender bloodstream form that is the only one present in culture with these strains. Nonetheless, chances are that the advantage is in the mammalian host rather than in the insect as TbAQP2 is retained unchanged in *T. evansi* and *T. equiperdum*, which do not require passage and development in the tsetse fly. To address these issues, strains of WT and tbaqp2-null *T. b. brucei* have been transfected with different fluorescent markers (collaboration with Mark Carrington, University of Cambridge) and will be co-infected in mice, to see whether either gains an advantage in vivo. Should that not be the case, the experiment will be repeated with tsetse fly infections.

It is thus reasonable to speculate that the widened pore of TbAQP2 allows for the passage of substances other than those transported by TbAQP1 and TbAQP3. The work on the W(G)YR filter residues shows that these residues indeed appear to be important determinants for the transport of pentamidine by AQPs, and introducing all three TbAQP2 residues into TbAQP3 was required to create an AQP3 that can at least facilitate mild sensitisation to pentamidine, and a detectable level of pentamidine uptake. On the other hand, any mutations in the unusual selectivity filter of the three amino acids residues I(V)LL of TbAQP2 was sufficient to all but eradicate the transport of pentamidine. Likewise, the conserved NPA/NPA motif in TbAQP3, which contains two serine residues N<u>S</u>A/NP<u>S</u> in TbAQP2, is also linked to the blockage of cations passage (Wree et al., 2011). The TbAQP2 motif has unique serine residues halfway down the pore, which could be able to make hydrogen bonds with pentamidine. Reinstating the NPA/NPA motif resulted in a TbAQP2 variant with a significant reduction in [^{3}H]-pentamidine transport rate.

Yet, it could be argued that the selectivity filter of TbAQP2 allows access to a pentamidine binding site halfway in the pore and is still not clear evidence of the drug traversing the pore into the cytoplasm. In order to further investigate this, I engineered constrictions at the cytoplasmic end of the pore, well below the selectivity filter, by making a site-specific mutation to each of the cytoplasmic-end amino acids L84, L118 and L218 that reside in the transport channel below the unique *T. brucei* selectivity filter (Baker et al., 2012). The introduction of bulky tryptophan on the cytoplasmic end of the TbAQP2 pore showed a disabling of pentamidine transport. In contrast, the result of a swap back to a medium size amino acid (methionine) into the same three positions showed a significant increase in uptake rates of pentamidine. Altogether, with the presented results of glycerol efflux and uptake being maintained in the mutant strains, verifying that these mutant AQPs weather they still functional aquaglyceroporins, it is likely that this effect depended on the amino acid size at the cytoplasmic end of the TbAQP2 pore. Interestingly, the position of L118 showed an almost similar phenotype (significant pentamidine resistance) for substitution with either tryptophan or methionine, showing that the original leucine may be in a quite critical position for pentamidine passage. This should be further investigated with further mutagenesis and modelling. Altogether, it can be concluded that the remarkably large pore of TbAQP2 is the primary entry of drugs melarsoprol and pentamidine into *T. brucei* spp. for treatment of sleeping sickness.

The project also aimed to distinguish between pentamidine uptake by transporters and via endocytosis. Indeed, it is not sufficient to prove that pentamidine can traverse the TbAQP2 pore, as it is not unthinkable that the total cellular entry of pentamidine via TbAQP2 is the sum of the two processes, in which case the division into the separate contributions becomes of interest. Current evidence (Morgan et al., 2002; Allen et al., 2003) suggest that all endocytosis in *T. brucei* exclusively occurs in the flagellar pocket, is clathrin-dependent and AP-2 independent. This means that the endocytotic mechanisms of TbAQP2 and suramin receptor ISG75, which are both directed to the lysosome after ubiquitylation (Quintana et al., 2020; Zoltner et al., 2015), are likely to be similar enough for a direct comparison. The tetracycline-inducible CRK12 RNAi cell line was employed to provide an endocytosis

defect. Although this approach is necessarily limited to partially inhibited endocytosis in BSF *T. brucei*, because full inhibition of endocytosis is lethal in bloodstream trypanosomes (Monnerat et al., 2013). The data obtained from this work showed that, inhibition on endocytosis has little or no impact on the uptake of pentamidine, but does reduce suramin uptake, consistent with current models that propose suramin uptake via edocytosis mechanism (Zoltner et al., 2016; Alsford, 2013).

The proton ionophore carbonyl cyanide m-chlorophenyl hydrazone (CCCP) has an obvious effect for the uptake of [3H]-hypoxanthine in *T. brucei* bloodstream forms (De Koning and Jarvis 1997b). Through a combination of competitive inhibition and reducing the protonmotive force, an investigation of whether the CCCP has a direct effect on TbAQP2-mediated pentamidine transport was conducted. The results showed an important role of CCCP after protonmotive force (PMF) reduction. This is in agreement with the conclusion made on the molecular dynamics analysis (Alghamdi et al., 2020) that inward pentamidine flux depends on the inside-negative membrane potential. It is also reported that the rate of endocytosis of TbAQP2 would not be able to account for the amount of pentamidine internalised (Quintana et al., 2020). With the conducted investigation of the structure-activity relationship (SAR) of the interactions between pentamidine and TbAQP2 and the molecular dynamics (Alghamdi et al., 2020), which shows minimal energy to be associated with a near-elongated pentamidine centrally in the TbAQP2 pore, the current study offers detailed, multifarious evidence of the uptake of organic drugs with molecular weights of 340 and 398 by an aquaporin.

Moreover, reconciling the literature on transport/resistance of pentamidine with uptake through endocytosis poses a challenge. For example, bloodstream trypanosomes exhibit a higher rate of endocytosis than the procyclic lifecycle forms (Langreth & Balber, 1975; Zoltner et al., 2016), but the rate of uptake of HAPT-mediated [^{3}H]-pentamidine in procyclics is nearly 10 times higher than that in bloodstream forms (De Koning, 2001a; Teka et al., 2011). This is despite the fact that the level of TbAQP2 expression is similar in both cases (Siegel et al., 2010; Jensen et al., 2014). In addition, TbAQP2 is spread out over the surface of procyclic cells (Baker et al., 2012), whereas endocytosis occurs exclusively in the flagellar

pocket (Field & Carrington, 2009), which is about three times smaller in procyclics compared to the bloodstream forms (Demmel et al., 2014), since the pellicular microtubule networks under the plasma membrane precludes endocytosis (Zoltner et al., 2016). This implies that the uptake of pentamidine mediated by TbAQP2 should not be possible in procyclic *T. brucei*, if it all depends on endocytosis. Likewise, the TbAQP2 expression in *Leishmania mexicana* promastigotes showed a [^{3}H]-pentamidine uptake rate of more than ten times higher than the rate observed in *T. brucei* BSF (Munday et al., 2014), despite the fact that these cells have a much lower rate of endocytosis (Langreth & Balber, 1975). There was no difference between the K_m and the inhibitor profile of the pentamidine transport mediated by TbAQP2 in these promastigotes (Munday *et al*, 2014) and that of HAPT in bloodstream or procyclic form *T. brucei* (De Koning, 2001a). The endocytosis model would require the same number of units of TbAQP2 to be internalised and recycled, which seems impossible particularly in procyclic cells, since the half-life time for TbAQP2 turnover in BSF is almost 4 hours (Quintana *et al*, 2020). In addition, the rate of endocytosis in procyclic cells is lower, making it difficult to internalise the aquaporins spread over the surface of the cell. All these observations are not consistent with the argument that uptake of pentamidine by trypanosomes mainly depends on endocytosis. Even though AQP2-bound pentamidine is likely to be internalised as part of the protein's natural turnover, this is unlikely to have a significant contribution to the overall rate of the drug's uptake. It should be noted that the paper by Song *et al* (2016) that proposed the endocytosis model did not actually measure any endocytosis or uptake of pentamidine, lacking a pentamidine radiolabel, but hypothesised it on the basis that other, smaller cations could not apparently pass through the channel. In a very recent paper the authors of that study stated that the method they use for measuring AQP permeation would not have been sensitive enough to detect pentamidine at the observed transport rate, which is of course much slower than that of water or glycerol (Petersen & Beitz, 2020). Thus, there is a strong suggestion, incorporating all these strands of data, that pentamidine is not taken up by endocytosis, nor does induce endocytosis of TbAQP2.

The last part of my project was to get insight in the role of *Leishmania major* AQP1 in drug transport. It has been reported that the Sb(III) traverses the pore of AQP1

and that loss of functionality of this aquaporin contributes to antimonial resistance. While pentavalent antimonials are still the first-line drugs against *Leishmania* spp., their effectiveness is hindered by high levels of toxicity and drug resistance (Ashutosh et al., 2007). *Leishmania* AQP1 was found to be one of markers that is commonly linked to antimonial resistance (Marquis et al., 2005; Decuypere et al., 2005; Mandal et al., 2010; Maharjan et al., 2008; Kazemi-Rad et al., 2013). Therefore, a further exploration of LmAQP1 functions, including their regulatory mechanisms, will eventually reveal their real potential for novel chemotherapeutic approaches and/or transmission intervention(s). Herein, a systematic examination of the LmAQP1 in sensitivity and response to antimony and arsenic drugs was conducted. The results of expressing LmAQP1 into *tbaqp1*/*tbaqp2*/*tbaqp3* null cells suggested that it is likely that *T. brucei* uptake of arsenic and antimonial compounds is dependent on other transport channels than just the AQPs. This conclusion has been demonstrated with the uptake of the trivalent organoarsenical melarsoprol (Matovu et al., 2003). On the other hand, the outcomes of the reintroduction of LmAQP1 into LmAQP1 null cells support previous conclusions that AQP1 plays an important role in the transportation of arsenic compounds, as well as antimonial compounds, in *Leishmania* (Gourbal et al., 2004; Plourde et al., 2015). Therefore, changes to, or loss of, *Leishmania* AQP1 transporter functionality, could lead to widespread antimonial drug resistance and high treatment failure rates.

Due to time constraints, however, I was unable to make microscopy observations for the transfected cells (LmAQP1 null + LmAQP1). Thus, I recommend staining the cells with fluorescent probes such as Lyso Tracker and Mito Tracker, since the shape of the cells appear much rounder, which could be due to an enhanced water influx rate experienced by those cells, as previously described in Plourde et al. (2015). Fluorescence experiments would determine the organelle localizations and sizes in those cells. Importantly, with the knowledge about the characteristics that enable the transport of large, supple, molecules via TbAQP2, similar investigations should be also done on the LmAQP1 to gain insight into the structural determinants that enable it to transport Sb(III) and arsenic.

In conclusion, the results of the TbAQP2 work provide strong evidence of pentamidine being able to permeate TbAQP2 directly, through the central pore. This

should now allow the evaluation of aquaporins in other species for similar adaptations. In addition, the cloning of the LmajAQP1 gene provides an essential molecular tool for studying the role of transporters in drug uptake and their potential involvement in the development of drug resistance. This might allow the identification and cloning of additional aquaporin members from additional species and give important new insights into the role of these important proteins in many organisms. Taken together, the outcomes of this thesis anticipate that better knowledge of the role of these AQPs will aid optimisation of future drugs and/or their delivery, as well as the development of diagnostic tools for drug resistance.

Appendices

Appendix 1: General buffers and solutions

Luria Bertani (LB) broth (pH 7)
LB powder (Sigma-Aldrich) 12.5 g
Distilled water 500 ml

LB Agar
Luria Agar (Sigma-Aldrich) 17.5 g
Distilled water 500 ml

Appendix 2: Protocol for gradient PCR

PCR Mix: 52 µl GoTaq green buffer
13 µl 10 mM dNTPs
13 µl Forward primer (taken from a 10 µM stock solution)
13 µl Reverse primer (taken from a 10 µM stock solution)
2.6 µl gDNA (10 ng/µl conc)
2.6 µl GoTaq G2 polymerase
163.8 µl dH_2O

Put 20 µl of this mix into 12 tubes, and run the following PCR program:

Put hot lid on

Temperature step: 95°C - 3 min

Start cycle x35

Temperature step: 95°C - 30s

Gradient step: 50°C to 70°C – 1.30s

Temperature step: 72°C - 3 min

End cycle

Temperature step: 72°C - 10 min

Store: 10°C

Appendix 3

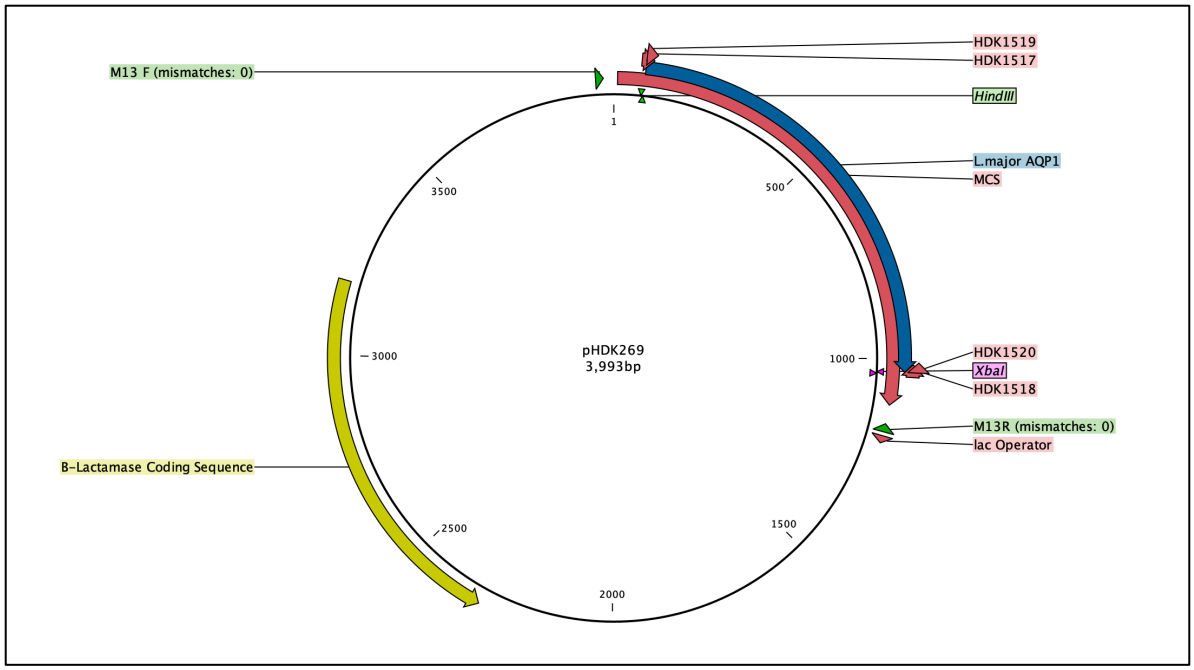

The pHDK269 plasmid map showing the full *Lm*AQP1gene sub-cloned into the pGEMT Easy sub-cloning vector prior to cloning the gene into the final destination (pRPa vector).

Appendix 4

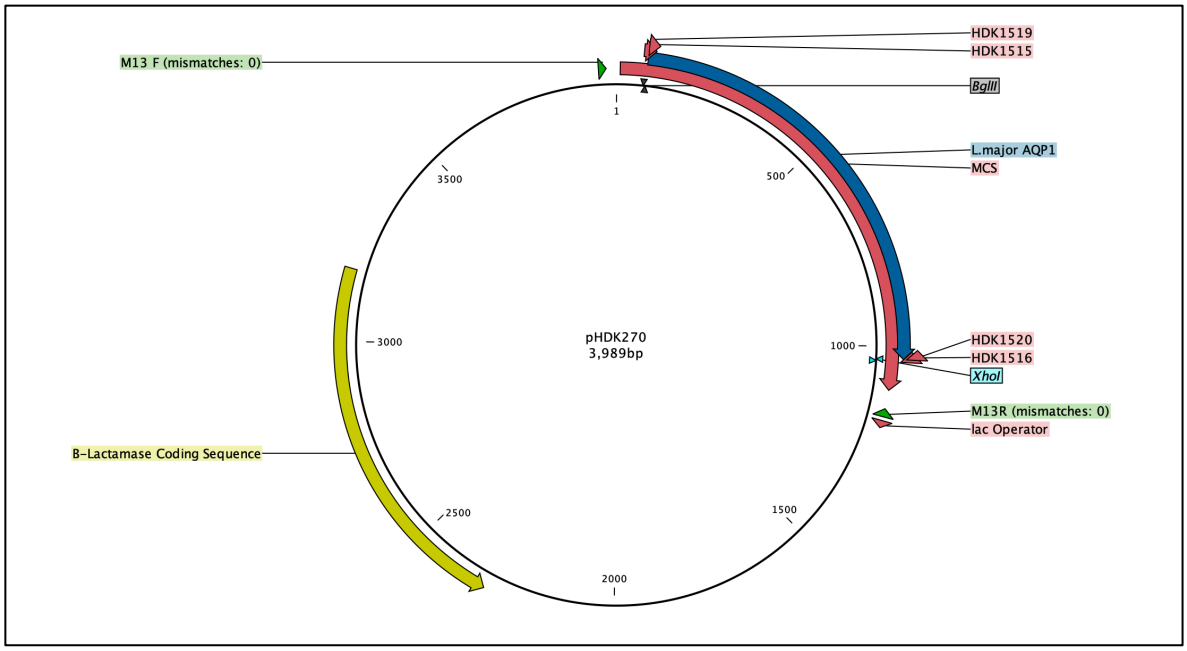

The pHDK270 plasmid map showing the full *Lm*AQP1 gene sub-cloned into the pGEMT Easy sub-cloning vector, prior to cloning the gene into the pNUS-NcH vector (final destination) to verify the sequence of DNA.

Appendix 5: Amino acid sequence alignments of TbAQP2 WT and the TbAQP2 mutants (AQP3 selectivity filter residues).

(A)

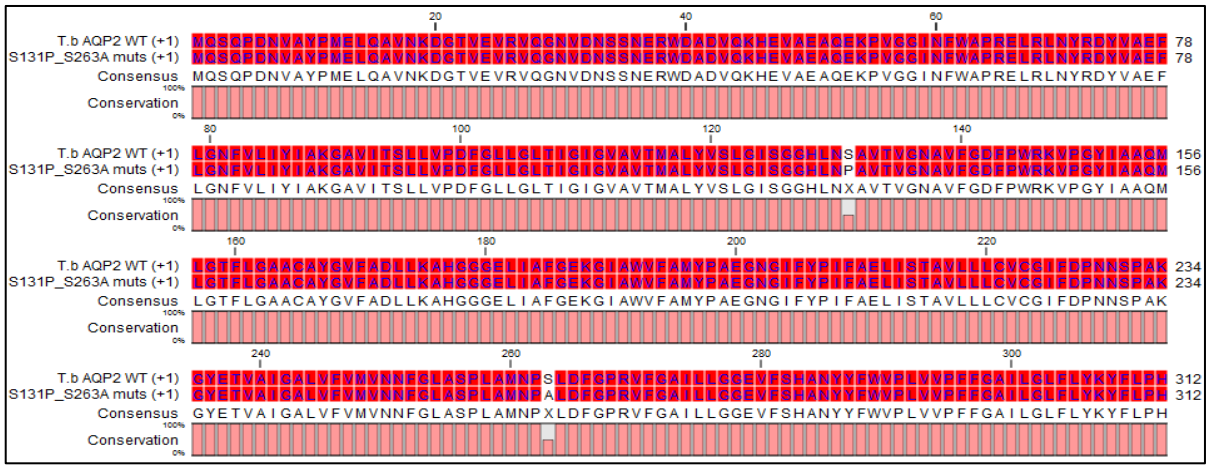

(B)

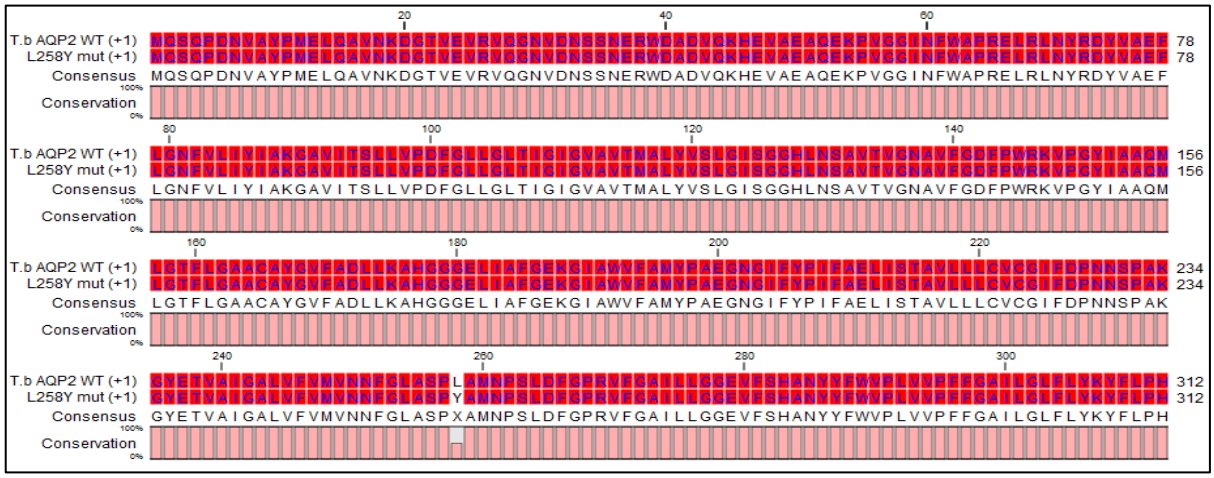

(C)

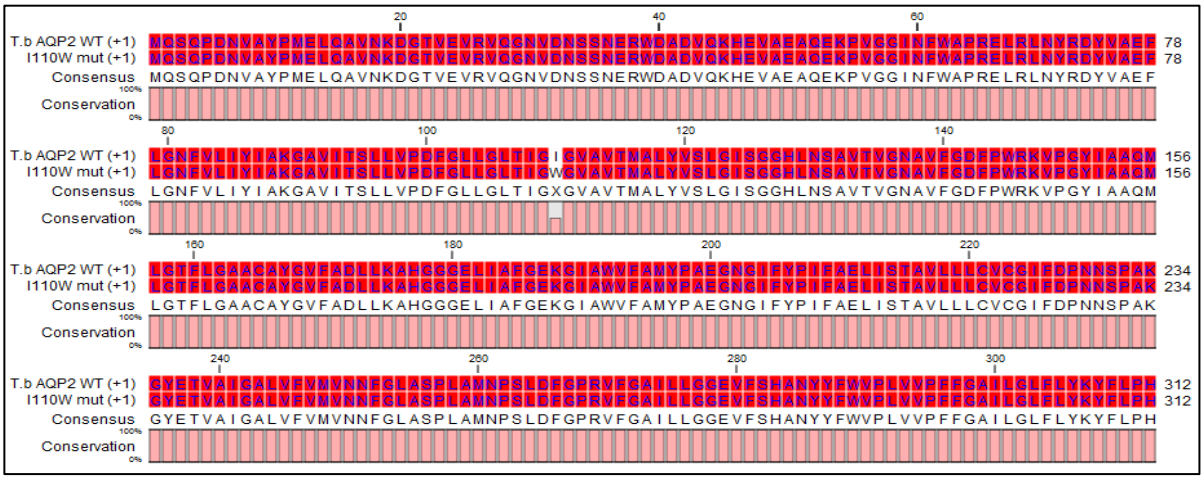

(D)

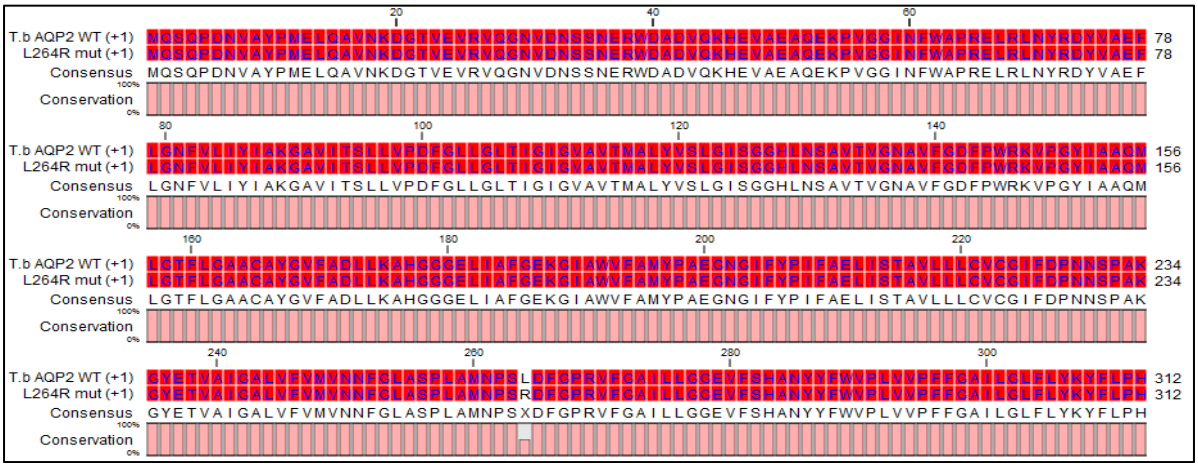

(E)

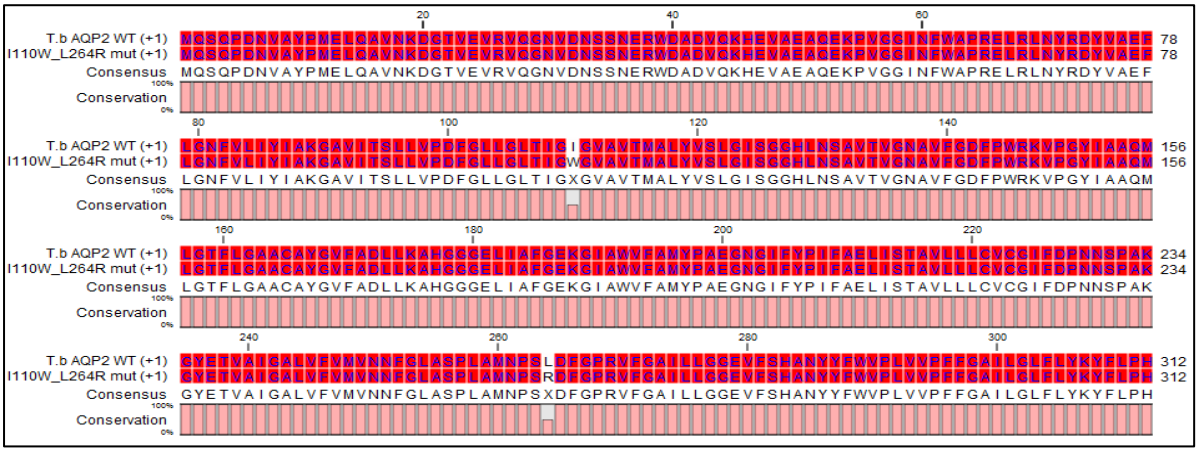

The figures show correct mutation(s) at the right position in the mutant cell lines. (A) Double mutations (S131P/S263A). (B) Single mutation (L258Y). (C) Single mutation (I110W). (D) Single mutation (L264R). (E) Double mutations (I110W/L264Y). Alignments were created using the CLC Genomic workbench software (version 7.0, developed by CLC bio).

Appendix 6: Plasmid map of pRPa$^{+GFP\text{-}TbAQP3WT}$ (pHDK070).

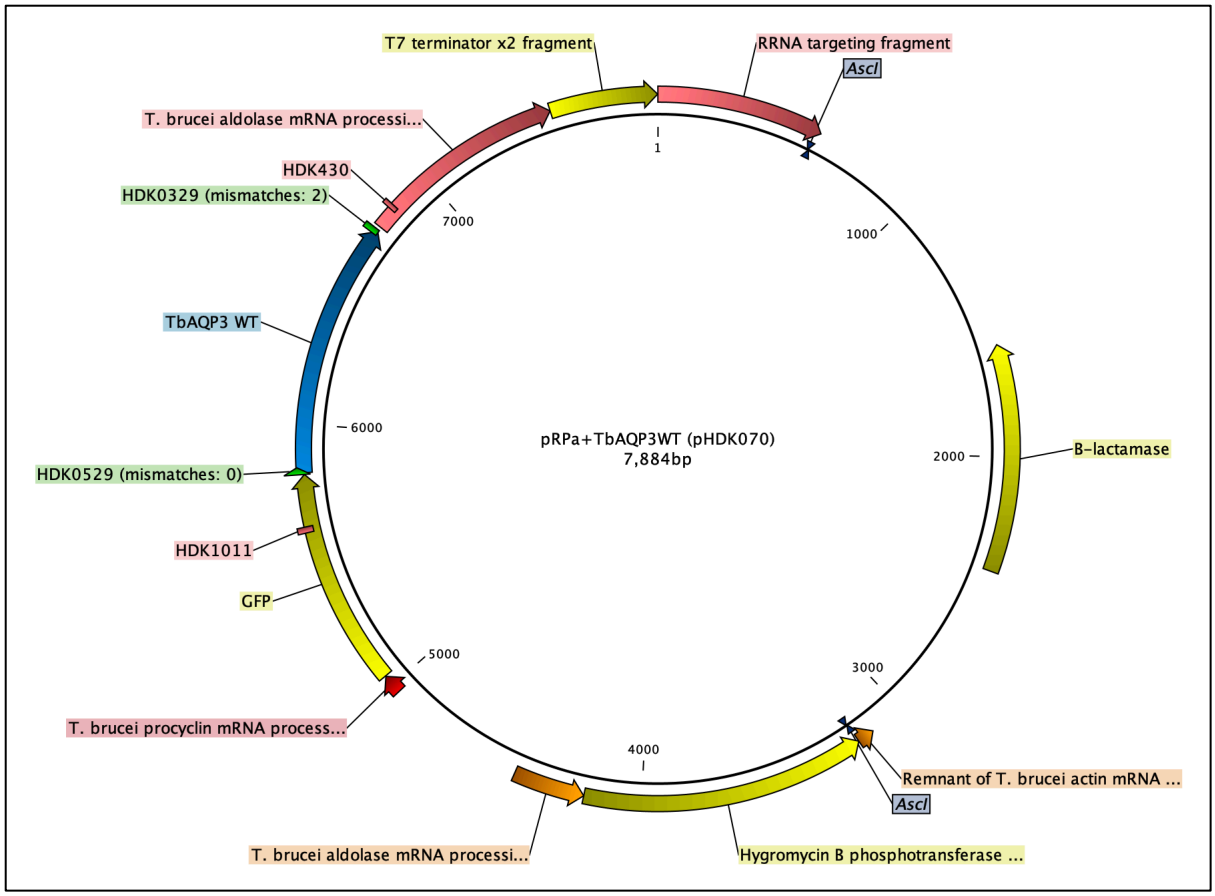

The plasmid map shows the TbAQP3WT and the vector confers hygromycin resistance to the transfected cells. The rRNA targeting fragment and Hygromycin B phosphotransferase ensures that the constructs are located to the tagged locus of 2T1 cells. This plasmid was used as a template to generate mutation in the AQP3 throughout the project. The positions of the primers that were used for the amplification of the AQP3 gene (HDK0529, HDK0329), and for the gene with the partial plasmid fragment (HDK1011, HDK430) are highlighted. The plasmid maps were generated by the CLC Genomics Workbench program (QIAGEN Bioinformatics).

Appendix 7: Amino acid sequence alignments of TbAQP3WT and the TbAQP3 mutants (the introduction of AQP2 selectivity filter residues).

(A)

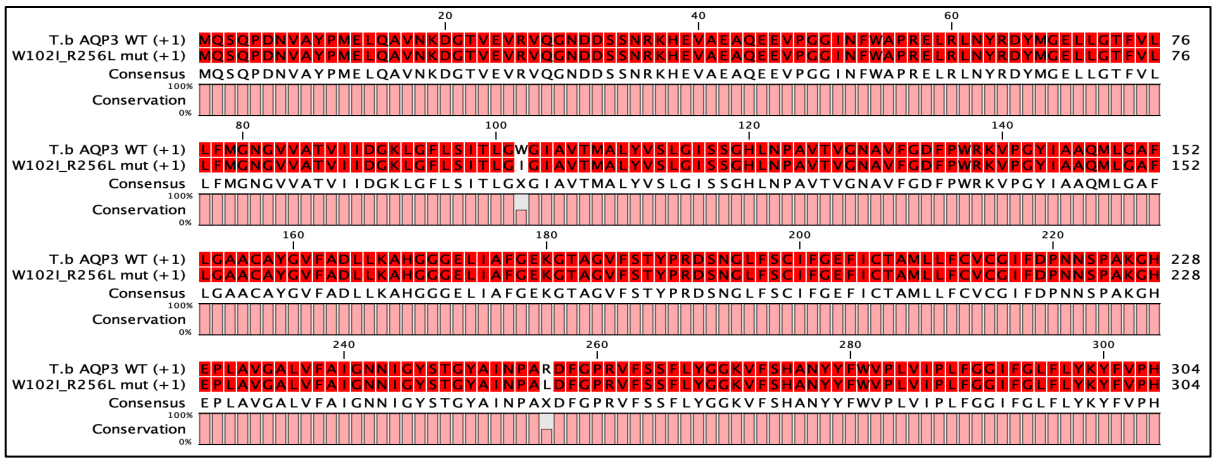

(B)

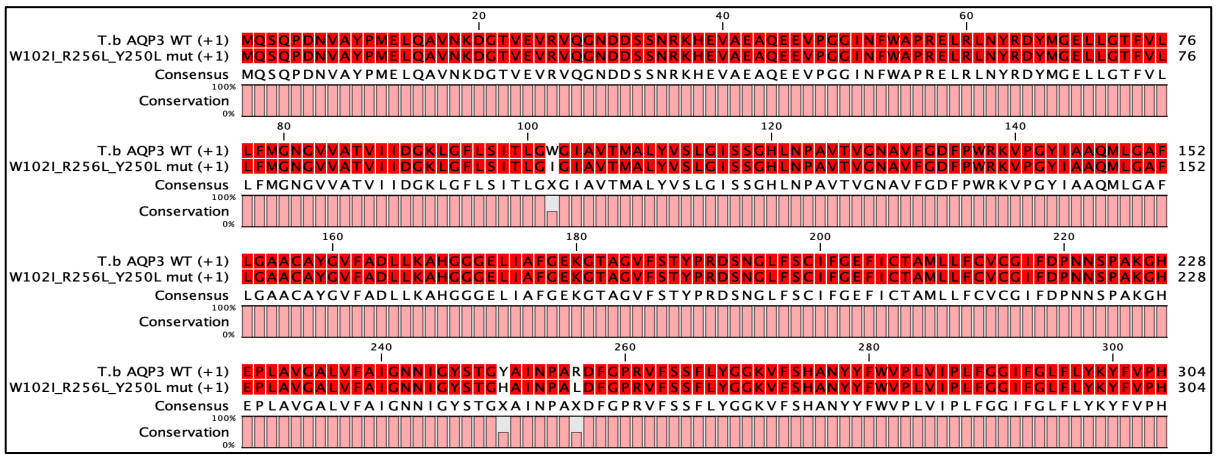

The figures show correct mutation at the right position in transfected *tbaqp2*/*tbaqp3* null cells. (A) Sequence of the double mutation W102I/R256L. (B) Triplicate mutation W102I/R256L/Y250L. Alignments were created using the CLC Genomic workbench software (version 7.0, developed by CLC bio).

Appendix 8: Amino acid sequence alignments of TbAQP2WT and the TbAQP2 mutants (TbAQP2 residues I190 and W192).

(A)

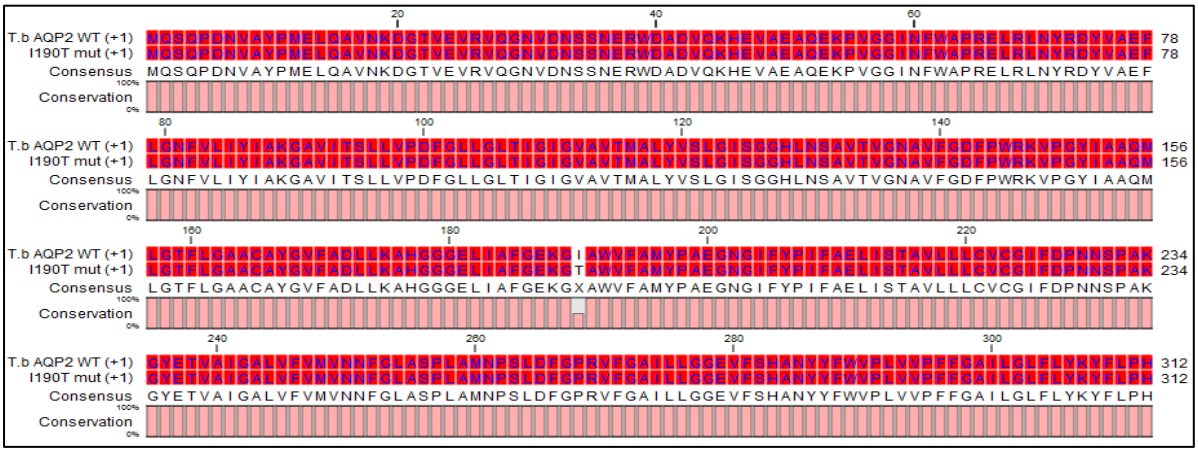

(B)

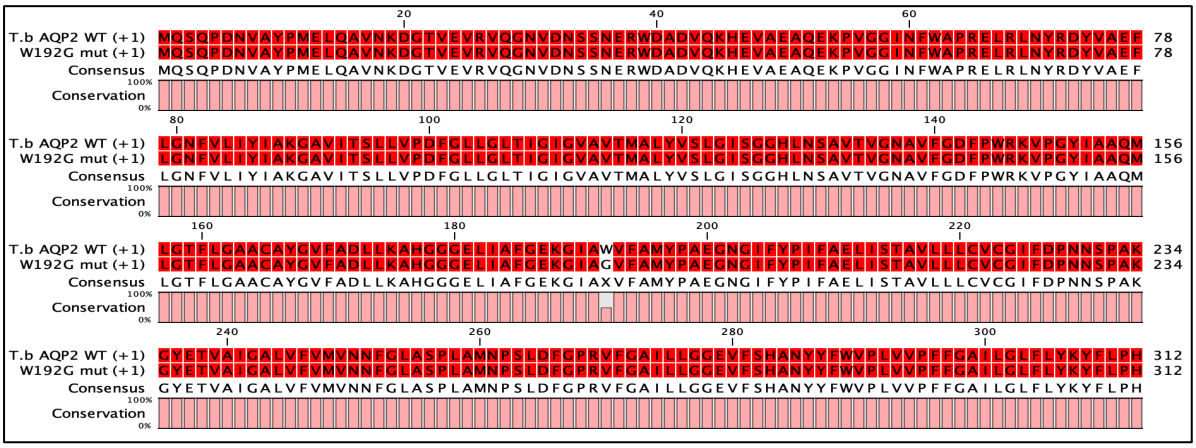

(C)

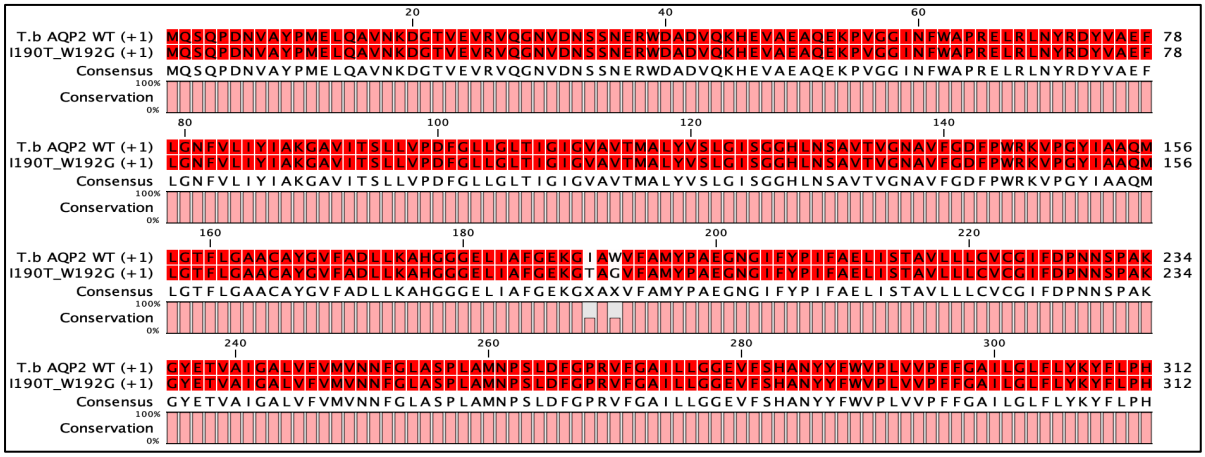

The figures show correct mutation at the right positions. (A) Single mutation I190T. (B) Single mutation W192G. (C) Double mutation I190T/W192G. The generated cell lines were checked by Sanger Sequencing (Source BioScience, Nottingham, UK) for the presence of TbAQP2 and the correct mutation(s). Alignments were created using the CLC Genomic workbench software (version 7.0, developed by CLC bio).

Appendix 9: Amino acid sequence alignments of TbAQP2WT and the TbAQP2 mutants (L-W).

(A)

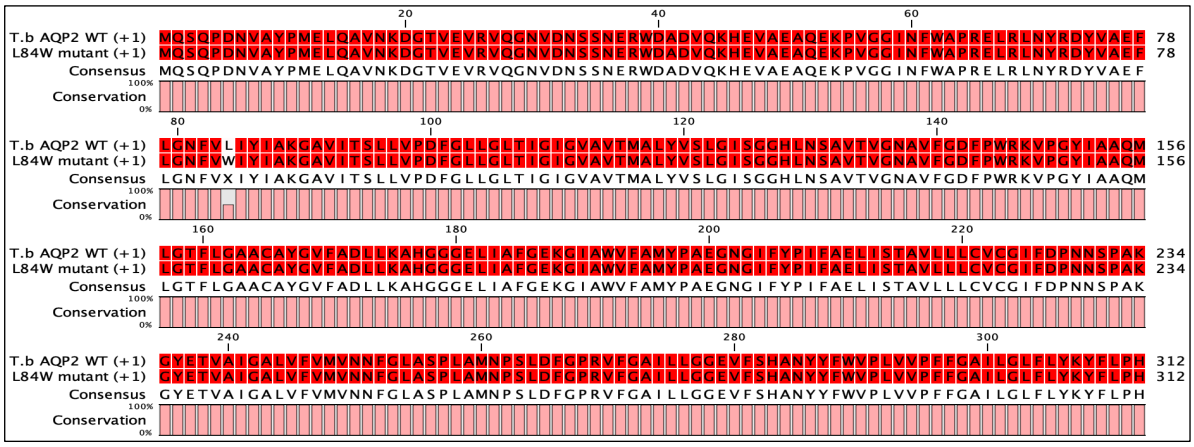

(B)

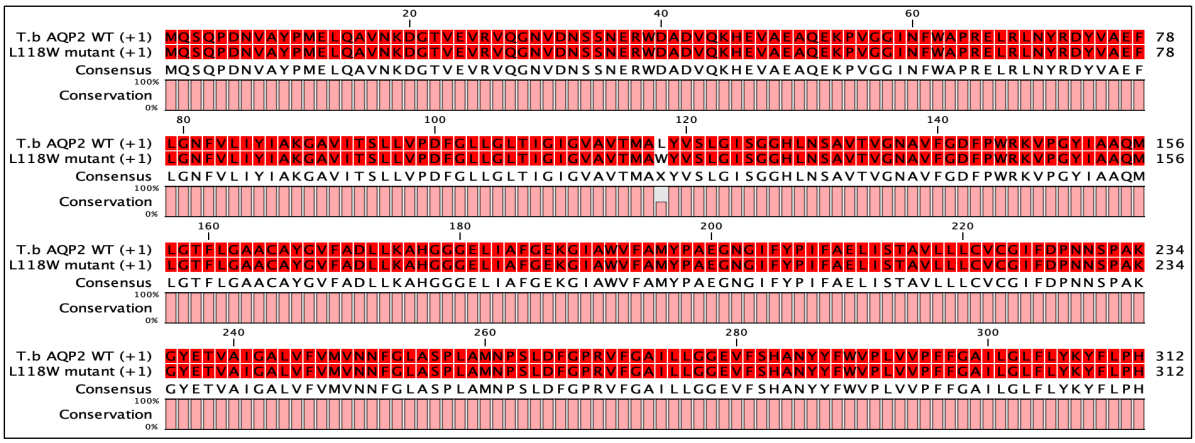

(C)

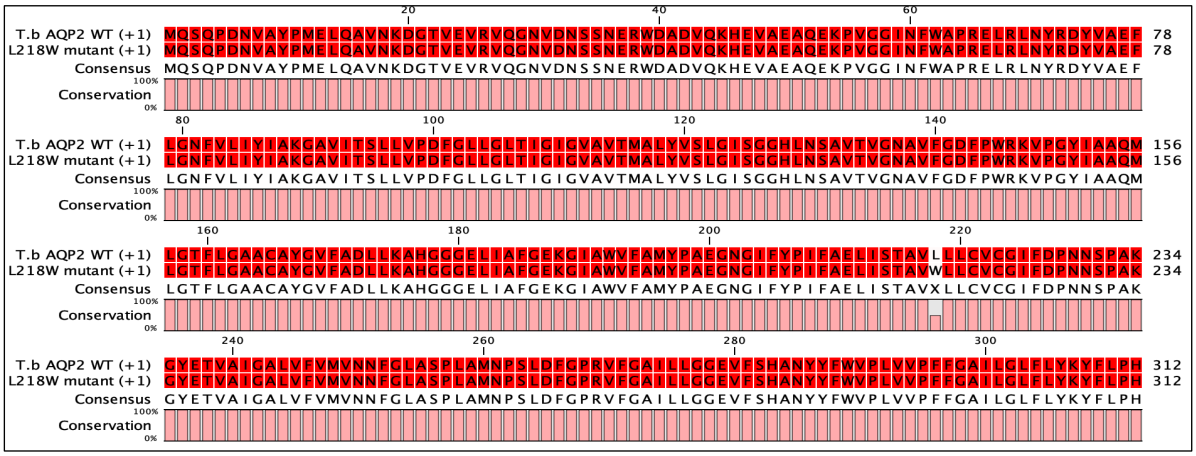

(D)

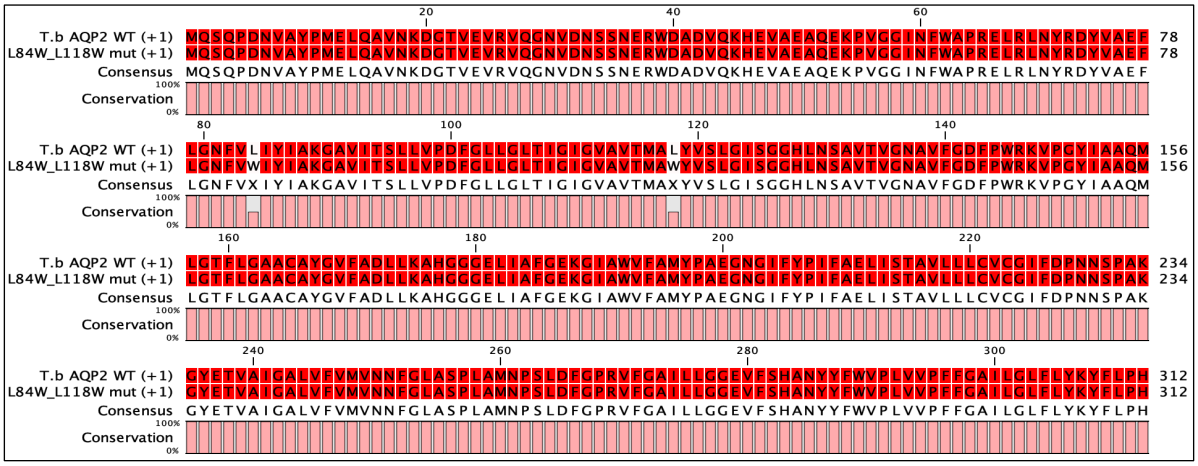

The figures show correct introduction of tryptophan into the positions of the three selected leucine. (A) single mutation (L84W). (B) single mutation (L118W). (C) single mutation (L218W). (D) double mutation (L84W/L118W). Alignments were created using the CLC Genomic workbench software (version 7.0, developed by CLC bio).

Appendix 10: Amino acid sequence alignments of T.b AQP2 W.T and the T.b AQP2 (L-M) mutants.

(A)

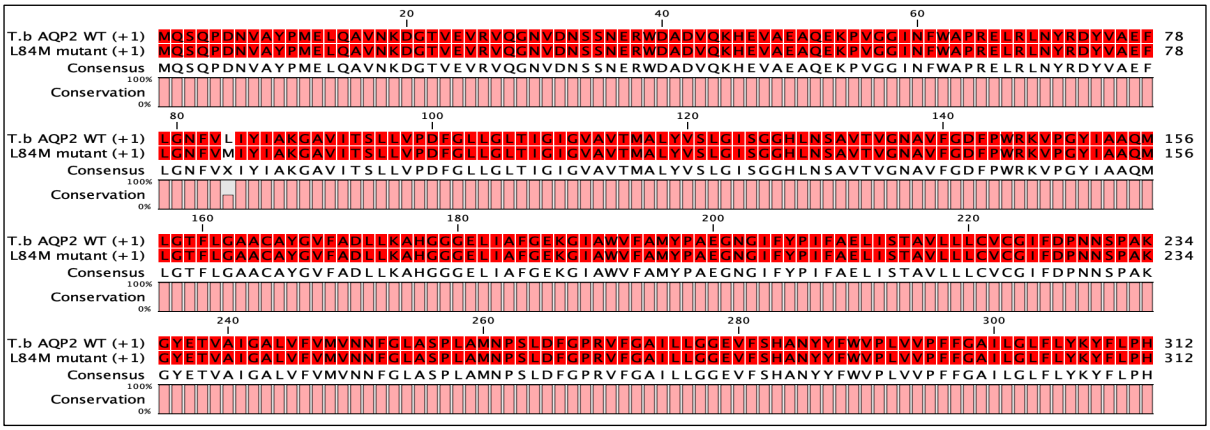

(B)

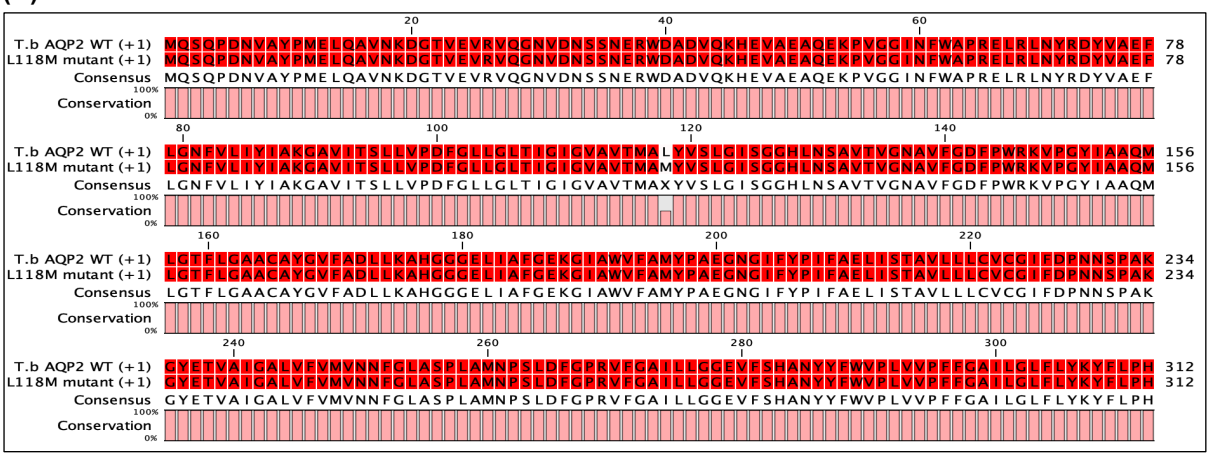

(C)

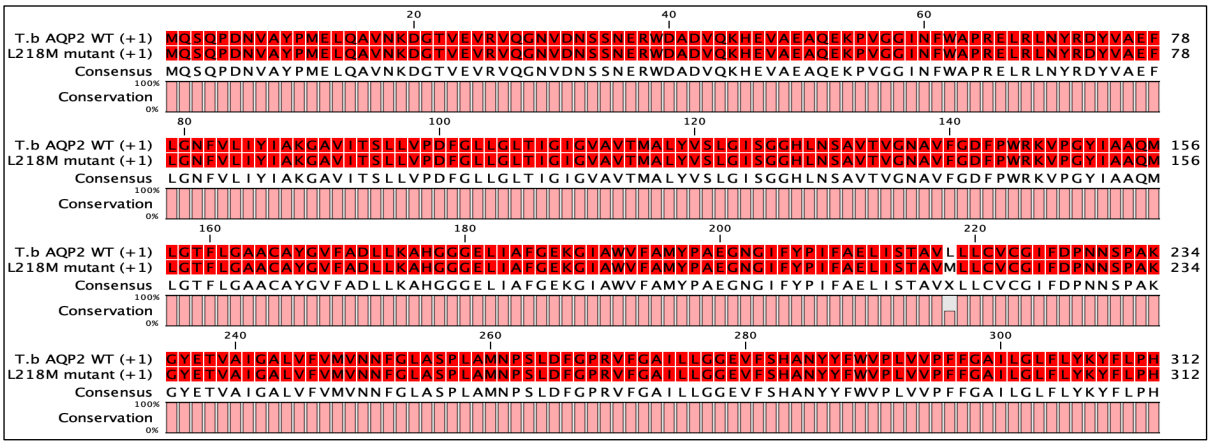

The figures show correct substitution of leucine to methionine at the three selected positions. (A) single mutation (L84M). (B) single mutation (L118M). (C) single mutation (L218M). Alignments were created using the CLC Genomic workbench software (version 7.0, developed by CLC bio).

References

Abuzaid, A. A., Abdoon, A. M., Aldahan, M. A., Alzahrani, A. G., Alhakeem, R. F., Asiri, A. M., Alzahrani, M. H. & Memish, Z. A. (2017). Cutaneous leishmaniasis in Saudi Arabia: a comprehensive overview. *Vector Borne Zoonotic Dis*, *17*(10), 673-684.

Adler-Moore, J. & Proffitt, R. T. (2003). Effect of tissue penetration on AmBisome efficacy. *Curr Opin Investig Drugs*, *4*(2), 179-185.

Aguirre, J. P. B. & Hamid, A. M. R. (2015). Amphotericin B deoxycholate versus liposomal amphotericin B: effects on kidney function. *Cochrane Database Syst Rev*, *23*(11), CD010481.

Al-Salabi, M. I., Wallace, L. J. & De Koning, H. P. (2003) A *Leishmania major* nucleobase transporter responsible for allopurinol uptake is a functional homolog of the *Trypanosoma brucei* H2 transporter. *Mol Pharmacol*, 63(4), 814-20.

Al-Salem, W. S., Pigott, D. M., Subramaniam, K., Haines, L. R., Kelly-Hope, L., Molyneux, D. H., Hay, S. I. & Acosta-Serrano, A. (2016). Cutaneous leishmaniasis and conflict in Syria. *Emerg Infect Dis*, *22*(5), 931-933.

Alghamdi, A. H., Munday, J. C., Campagnaro, G. D., Gurvic, D., Svensson, F., Okpara, C. E., Kumar, A., Quintana, J., Martin Abril, M. E., Milić, P., Watson, L., Paape, D., Settimo, L., Dimitriou, A., Wielinska, J., Smart, G., Anderson, L. F., Woodley, C. M., Kelly, S., Ibrahim, H. M. S., Hulpia, F., Al-Salabi, M. I., Eze, A. A., Sprenger, T., Teka, I. A., Gudin, S., Weyand, S., Field, M., Dardonville, C., Tidwell, R. R., Carrington, P. O., Boykin, D. W., Zachariae, U. & De Koning, H. P. (2020). Positively selected modifications in the pore of TbAQP2 allow pentamidine to enter *Trypanosoma brucei*. *eLife*, *9,* e56416.

Allen, C. L., Goulding, D. & Field, M. C. (2003). Clathrin-mediated endocytosis is essential in *Trypanosoma brucei*. *EMBO J, 22*, 4991-5002.

Alsford S., Eckert, S., Baker, N., Glover, L., Sanchez-Flores, A., Leung, K. F., Turner, D. J., Field, M. C., Berriman, M. & Horn, D. (2012). High-throughput decoding of antitrypanosomal drug efficacy and resistance. *Nature*, *482,* 232–236.

Alsford, S., Horn, D. (2008). Single-locus targeting constructs for reliable regulated RNAi and transgene expression in Trypanosoma brucei. *Mol Biochem Parasitol*, *161*, 76–79.

Alsford, S., Kawahara, T., Glover, L., Horn, D. (2005). Tagging a *T. brucei* RRNA locus improves stable transfection efficiency and circumvents inducible expression position effects. *Mol Biochem Parasitol*, *144,* 142–148.

Alsford, S., Kelly, J. M., Baker, N., and Horn, D. (2013). Genetic dissection of drug resistance in trypanosomes. *Parasitology*, *140*, 1478-1491.

Alsford, S., Turner, D. J., Obado, S. O., Sanchez-Flores, A., Glover, L., Berriman, M., Hertz-Fowler, C. & Horn, D. (2011). High-throughput phenotyping using parallel sequencing of RNA interference targets in the African trypanosome. *Genome Res*, *21*(6), 915-24.

Alvar, J., Croft, S. & Olliaro, P. (2006). Chemotherapy in the treatment and control of leishmaniasis. *Adv Parasitol*, *61*, 223-274.

Alvar, J., Vélez, I. D., Bern, C., Herrero, M., Desjeux, P., Cano, J., Jannin, J., den Boer, M. & WHO Leishmaniasis Control Team. (2012). Leishmaniasis worldwide and global estimates of its incidence. *PLoS One*, *7*(5), e35671.

Alves, F., Bilbe, G., Blesson, S., Goyal, V., Monnerat, S., Mowbray, C., Ouattara, G. M., Pécoul, B., Rijal, S., Rode, J., Solomos, A., Strub-Wourgaft, N., Wasunna, M., Wells, S., Zijlstra, E. E., Arana, B., Alvar, J. (2018). Recent Development of Visceral Leishmaniasis Treatments: Successes, Pitfalls, and Perspectives. *Clin Microb Rev*, *31*(4), e00048-e18.

Ambit, A., Woods, K. L., Cull, B., Coombs, G. H., & Mottram, J. C. (2011). Morphological events during the cell cycle of *Leishmania major*. *Eukaryot Cell*, *10*(11), 1429-1438.

Andrade-Narváez, F. J., Vargas-González, A., Canto-Lara, S. B. & Damián-Centeno, A. G. (2001). Clinical picture of cutaneous leishmaniases due to *Leishmania (Leishmania) mexicana* in the Yucatan peninsula, Mexico. *Mem Inst Oswaldo Cruz*, *96*(2), 163-167.

Ashutosh, Sundar, S. & Goyal, N. (2007). Molecular mechanisms of antimony resistance in Leishmania. *J Med Microbiol*, *56*, 143–153.

Asilian, A. & Davami, M. (2006). Comparison between the efficacy of photodynamic therapy and topical paromomycin in the treatment of Old World cutaneous leishmaniasis: a placebo-controlled, randomized clinical trial. *Clin Exp Dermatol*, *31*(5), 634-637.

Atayde, V. D., Aslan, H., Townsend, S., Hassani, K., Kamhawi, S. & Olivier, M. (2015). Exosome Secretion by the Parasitic Protozoan Leishmania within the Sand Fly Midgut. *Cell Reports,* 13, 957-967.

Babokhov, P., Sanyaolu, A. O., Oyibo, W. A., Fagbenro-Beyioku, A. F. & Iriemenam, N. C. (2013). A current analysis of chemotherapy strategies for the treatment of human African trypanosomiasis. *Pathog Glob Health*, *107*(5), 242-252.

Bacchi, C. J. (2009). Chemotherapy of human African trypanosomiasis. *Interdiscip Perspect Infec Dis*, 2009, 195040.

Bahrami, F., Harandi, AM. & Rafati, S. (2018). Biomarkers of cutaneous leishmaniasis. *Front Cell Infect Microbiol*. 8, 222.

Baker, N, De Koning, H. P., Mäser, P., Horn, D. (2013). Drug resistance in African trypanosomiasis: the melarsoprol and pentamidine story. *Trends Parasitol, 29*, 110–118.

Baker, N., Glover, L., Munday, J.C., Aguinaga Andrés, D., Barrett, M.P., De Koning, H.P., Horn, D. (2012). Aquaglyceroporin 2 controls susceptibility to melarsoprol and pentamidine in African trypanosomes. *Proc Natl Acad Sci USA, 109*, 10996–11001.

Bakker BM, Michels P.A., Opperdoes, F. R., Westerhoff, H. V. (1997). Glycolysis in bloodstream form trypanosoma brucei can be understood in terms of the kinetics of the glycolytic enzymes. *J Biol Chem, 272*, 3207-3215

Balogun, E. O., Inaoka, D. K., Shiba, T., Kido, Y., Nara, T., Aoki, T., Honma, T., Tanaka, A., Inoue, M., Matsuoka, S., Michels, P. A., Harada, S. & Kita, K. (2013). Biochemical characterization of highly active *Trypanosoma brucei gambiense* glycerol kinase, a promising drug target. *J Biochem*, *154*, 77e84.

Bamorovat, M., Sharifi, I., Afltatoonian, M. R., Sharifi, H., Karamoozian, A., Sharifi, F., Khosravi, A. & Hassanzadeh, S. (2018). Risk factors for anthroponotic cutaneous leishmaniasis in unresponsive and responsive patients in a major focus, southeast of Iran. *PLoS One*, *13*(2), e0192236.

Bari, A. U. (2006). Epidemiology of cutaneous leishmaniasis. *J Pak Med Assoc, 16*(3), 156-162.

Barrett, M. P. & Croft, S. L. (2012). Management of trypanosomiasis and leishmaniasis. *Br Med Bull*, *104*, 175-96.

Barrett, M. P., Boykin, D. W., Brun, R. & Tidwell, R. R. (2007) Human African trypanosomiasis: pharmacological re-engagement with a neglected disease. *Br J Pharmacol*, *152*(8), 1155-1571.

Barrett, M. P., Burchmore, R. J. S., Stich, A., Lazzari, J. O., Frasch, A. C., Cazzulo, J. J. & Krishna, S. (2003). The trypanosomiases. *Lancet*, *362*(9394), 1469-1480.

Barrett, M. P., Vincent, I. M., Burchmore, R. J., Kazibwe, A. J., Matovu, E. (2011). Drug resistance in human African trypanosomiasis. *Future Microbiol, 6*, 1037-47

Bassarak, B., Uzcátegui, N. L., Schönfeld, C., Duszenko, M. (2011). Functional characterization of three aquaglyceroporins from Trypanosoma brucei in osmoregulation and glycerol transport. *Cell Physiol Biochem, 27,* 411–420.

Basselin, M., Badet-Denisot, M. A. & Robert-Gero, M. (1998). Modification of kinetoplast DNA minicircle composition in pentamidine-resistant *Leishmania*. *Acta Trop*, *70*(1), 43-61.

Basselin, M., Denise, H., Coombs, G. H. & Barrett, M. P. (2002). Resistance to pentamidine in Leishmania Mexicana involves exclusion of the drug from the mitochondrion. *Antimicrob Agents Chemother*, *46*(12), 3731-3738.

Basselin, M., Lawrence, F., Robert-Gero, M. (1996). Pentamidine uptake in *Leishmania donovani* and *Leishmania amazonensis* promastigotes and axenic amastigotes. *Biochem J*, *315,* 631–634.

Bates, P. A. (2008). *Leishmania* sand fly interaction: progress and challenges. *Curr Opin Microbiol*, *11*, 340-344.

Beitz, E. (2005). Aquaporins from pathogenic protozoan parasites: Structure, function and potential for chemotherapy. *Biol Cell, 97*, 373–383

Beitz, E., Wu, B., Holm, L. M., Schultz, J. E., Zeuthen, T. (2006). Point mutations in the aromatic/arginine region in aquaporin 1 allow passage of urea, glycerol, ammonia and protons. *Proc Natl Acad Sci USA, 103*, 269–274

Bellofatto, V., Fairlamb, A. H., Henderson, G. B. & Cross, G. A. (1987). Biochemical changes associated with alpha-difluoromethylornithine uptake and resistance in *Trypanosoma brucei*. *Mol Biochem Parasitol*, *25*(3), 227-238.

Benga, G. (2009). Water channel proteins (later called aquaporins) and relatives: past, present, and future. *IUBMB Life*, *61*(2), 112–33

Bentivoglio, M., Grassi-Zucconi, G., Olsson, T., and Kristensson, K. (1994). Trypanosoma brucei and the nervous system. *Trends Neurosci*. 17:325-329.
Bhattacharjee, H., Rosen, B. P. & Mukhopadhyay, R. (2009). Aquaglyceroporins and metalloid transport: implications in human diseases. *Handb Exp Pharmacol, 190*, 309–325.

Birhanu, H., Fikru, R., Said, M., Kidane, W., Gebrehiwot, T., Hagos, A., Alemu, T., Dawit, T., Berkvens, D., Goddeeris, B. M. & Buscher, P. (2015). Epidemiology of *Trypanosoma evansi* and *Trypanosoma vivax* in domestic animals from selected districts of Tigray and Afar regions, Northern Ethiopia. *Parasit Vectors*, *8*, 212.

Biyani, N., Mandal, S., Seth, C., Saint, M., Natarajan, K., Ghosh, I. & Madhubala, R. (2011). Characterization of Leishmania Donovani Aquaporins Shows Presence of Subcellular Aquaporins Similar to Tonoplast Intrinsic Proteins of Plants. *PLoS One*, *6*, e24820.

Blackwell, J. M., Fakiola, M., Ibrahim, M. E., Jamieson, S. E., Jeronimo, S. B., Miller, E. N., Mishra, A., Mohamed, H. S., Peacock, C. S., Raju, M., Sundar, S & Wilson, M. E. (2009). Genetics and visceral leishmaniasis: of mice and man. *Parasite Immunol*, *31*(5), 254-266.

Blum, J. A., Burri, C., Hatz, C., Kazumba, L., Mangoni, P. & Zellweger, M. J. (2007). Sleeping hearts: the role of the heart in sleeping sickness (human African trypanosomiasis). *Trop Med Int Health*, *12*(12), 1422-1432.

Bonnet, J., Boudot, C., Courtioux, B., (2015). Overview of the diagnostic methods used in the field for human African trypanosomiasis: what could change in the next years? *BioMed research international*.

Borgnia, M., Nielsen, S., Engel, A. & Agre, P. (1999). Cellular and molecular biology of the aquaporin water channels. *Annu Rev Biochem*, *68*, 425–458.

Braga, S. S. (2019). Multi-target drugs active against leishmaniasis: a paradigm of drug repurposing. *Eur J Med Chem*, *183*, 111660.

Bray, P. G., Barrett, M. P., Ward, S. A. & De Koning, H. P. (2003). Pentamidine uptake and resistance in pathogenic protozoa: past, present and future. *Trends Parasitol*, *19*(5), 232-239.

Bridges, D., Gould, M. K., Nerima, B., Mäser, P., Burchmore, R. J. S. & De Koning, H. P. (2007). Loss of the High Affinity Pentamidine Transporter is responsible for high levels of cross-resistance between arsenical and diamidine drugs in African trypanosomes. *Mol Pharmacol*, *71*, 1098–1108

Brochu, C., Wang, J., Messier, N., Wang, X., Saravia, N. G. & Ouellette, M. (2003). Antimony Uptake Systems in the Protozoan Parasite Leishmania and Accumulation Differences in Antimony-Resistant Parasites. *Antimicrob Agents Chemother, 47*, 3073−3079.

Brun, R., Blum, J., Chappuis, F. & Burri, C. (2010). Human African trypanosomiasis. *Lancet*, *375*(9709), 148–159.

Burri, C. (2010). Chemotherapy against human African trypanosomiasis: is there a road to success? *Parasitology*, *137*(14), 1987-94.

Burri, C. & Brun, R. (2003). Eflornithine for the treatment of human African trypanosomiasis. *Parasitol Res*, *90*, S49-S52.

Büscher, P, Cecchi, G, Jamonneau, V. & Priotto, G. (2017). Human African trypanosomiasis. *Lancet 390*, 2397–2409.

Cairns, J. E. (1968). Cutaneous leishmaniasis (oriental sore) a case with corneal involvement. *Brit J Opthal*, 52, 481.

Capewell P, CrerTravaillé C, Marchesi F, Johnston P, Clucas C, Benson RA, Gor man T-A, Calvo-Alvarez E, Crouzols A, Jouvion G, et al. (2016). The skin is a significant but overlooked anatomical reservoir for vector-borne African trypanosomes. *eLife Sciences* 5: e17716.

Cardoso, M. S., Reis-Cunha, J. L. & Bartholomeu, D. C. (2016). Evasion of the immune response by Trypanosoma cruzi during acute infection. *Frontiers immunol, 6*, 659.

Carter N. S. & Fairlamb A. H. (1993). Arsenical-resistant trypanosomes lack an unusual adenosine transporter. *Nature, 361,* 173–176.

Carter, N. S. & Fairlamb, A. H. (1993). Arsenical-resistant trypanosomes lack an unusual adenosine transporter. *Nature, 361*, 173–176.

Carter, N. S., Berger, B. J. & Fairlamb, A. H. (1995). Uptake of diamidine drugs by the P2 nucleoside transporter in melarsen-sensitive and -resistant Trypanosoma brucei brucei. *J Biol Chem, 270*, 28153-28157.

Chakravarty, J. & Sundar, S. (2010). Drug resistance in leishmaniasis. *J Glob Infect Dis*, *2*(2), 167-176.

Channon, J. Y., Roberts, M. B., & Blackwell, J. M. (1984). A study of the differential respiratory burst activity elicited by promastigotes and amastigotes of *Leishmania donovani* in murine resident peritoneal macrophages. *Immunology*, *53*, 345-355.

Chawla, B., Jhingran, A., Panigrahi, A., Stuart, K. D. & Madhubala, R. *PLoS One*. *6*(10), e26660.

Checchi, F., Piola, P., Ayikoru, H., Thomas, F., Legros, D. & Priotto, G. (2007). Nifurtimox plus efl ornithine for late-stage sleeping sickness in Uganda: a case series. *PLoS Negl Trop Dis, 1*, e64.

Chen, X. M., O'Hara, S. P., Huang, B. Q., Splinter, P. L., Nelson, J. B. & LaRusso, N. F. (2005). Localized glucose and water influx facilitates Cryptosporidium parvum cellular invasion by means of modulation of host-cell membrane protrusion. *Proc Natl Acad Sci USA*, *102,* 6338-6343.

Chrusciak-Talhari, A., Dietze, R., Chrusciak Talhari, C., Da Silva, R. M., Gadelha Yamashita, E. P., De Oliveira Penna, G., Lima Machado, P. R. & Talhari, S. (2011). Randomized controlled clinical trial to access efficacy and safety of miltefosine in the treatment of cutaneous leishmaniasis caused by *Leishmania (Viannia) guyanensis* in Manaus, Brazil. *Am J Trop Med Hyg*, *84*(2), 255-260.

Clarkson, A. B., Bienensb, E. J., Pollakisz, G. & Gradyll, W. (1989). Respiration of Bloodstream Forms of the Parasite Trypanosoma Brucei Brucei Is Dependent on a Plant-like Alternative Oxidase. *J Biol Chem, 264*(30), 17770–76.

Coelho, A. C., Beverley, S. M. & Cotrim, P. C. (2003). Functional genetic identification of PRP1, an ABC transporter superamily member conferring pentamidine resistance in *Leishmania major*. *Mol Biochem Parasitol*, *130*(2), 83-90.

Coelho, A. C., Gentil, L. G., Da Silveira, J. F. & Cotrim, P. C. (2008). Characterization of *Leishmania (Leishmania) amazonensis* promastigotes resistant to pentamidine. *Exp Parasitol*, *120*(1), 98-102.

Coelho, A. C., Messier, N., Ouellette, M. & Cotrim, P. C. (2007). Role of the ABC transporter PRP1 (ABCC7) in pentamidine resistance in *Leishmania* amastigotes. *Antimicrob Agents Chemother*, *51*(8), 3030-3032.

Croft, S. L., Sundar, S. & Fairlamb, A. H. (2006). Drug resistance in leishmaniasis. *Clin Microbiol Rev*, *19*(1), 111-126.

Cunha, M. A., Leao, A. C. Q., De Cassia Soler, R. & Lindoso, J. A. L. (2015). Efficacy and safety of liposomal amphotericin B for the treatment of mucosal leishmaniasis from the new world: a retrospective study. *Am J Trop Med Hyg*, *93*(6), 1214-1218.

Cunningham, M. L., Zvelebil, M. J. J. M. & Fairlamb, A. H. (1994). Mechanism of inhibition of trypanothione reductase and glutathione reductase by trivalent organic arsenicals. *Eur J Biochem*, *221*(1), 285-295.

Damper, D. & Patton, C. L. (1976). Pentamidine transport in *Trypanosoma brucei* - kinetics and specificity. *Biochem Pharmacol*, *25*, 271-276.

de Groot BL, Grubmüller H. (2001). Water permeation across biological membranes: Mechanism and dynamics of aquaporin-1 and GlpF. *Science,* 294:2353–2357.

De Koning H. P. & Jarvis, S. M. (1997b). Purine nucleobase transport in bloodstream forms of *Trypanosoma brucei brucei* is mediated by two novel transporters. *Mol Biochem Parasitol, 89,* 245–258.

De Koning, H. P. (2001a). Uptake of pentamidine in *Trypanosoma brucei brucei* is mediated by three distinct transporters. Implications for cross-resistance with arsenicals. *Mol Pharmacol, 59,* 586–592

De Koning, H. P. (2020). The drugs of sleeping sickness: their mechanisms of action and resistance, and a brief history. *Trop Med Infect Dis, 5,* 14

De Koning, H. P. (2020). The Drugs of Sleeping Sickness: their mechanisms of action and resistance, and a brief history. *Trop Med Infect Dis*, *5*(1), 14.

De Koning, H. P. & Jarvis S. M. (1999). Adenosine transporters in bloodstream forms of *Trypanosoma brucei brucei*: Substrate recognition motifs and affinity for trypanocidal drugs. *Mol Pharmacol, 56*, 1162–1170.

De Koning, H. P. & Jarvis, S. M. (1997a). Hypoxanthine uptake through a purine-selective nucleobase transporter in *Trypanosoma brucei brucei* procyclics is driven by protonmotive force. *Eur J Biochem, 247*, 1102–1110.

De Koning, H. P. & Jarvis, S. M. (1998). A highly selective, high affinity transporter for uracil in *Trypanosoma brucei brucei*; evidence for proton-dependent transport. *Biochem Cell Biol, 76,* 853–858.

De Koning, H. P. & Jarvis, S. M. (2001). Uptake of pentamidine in *Trypanosoma brucei brucei* is mediated by the P2 adenosine transporter and at least one novel, unrelated transporter. *Acta Trop, 80,* 245-250.

De Koning, H. P., Stewart, M., Anderson, L., Burchmore, R., Wallace, L. J. M. & Barrett, M. P. (2004). The trypanocide diminazene aceturate is accumulated predominantly through the TbAT1 purine transporter; additional insights in diamidine resistance in African trypanosomes. *Antimicrob Agents Chemother, 48*, 1515–1519.

De Menezes, J. P., Saraiva, E.M., & Da Rocha-Azevedo, B. (2016). The site of the bite: *Leishmania* interaction with macrophages, neutrophils and the extracellular matrix in the dermis. *Parasit Vectors*, *9*, 264.

Decuypere, S., Rijal, S., Yardley, V., De Doncker, S., Laurent, T., Khanal, B., Chappuis, F. & Dujardin, J. C. (2005). Gene expression analysis of the mechanism of natural Sb(V) resistance in Leishmania donovani isolates from Nepal. *Antimicrob Agents Chemother, 49*, 4616–4621.

Deeks, E. (2019). Fexinidazole: first global approval. *Drugs* 79: 215–220

Delespaux, V. & De Koning, H. P. (2007). Drugs and drug resistance in African trypanosomiasis. *Drug Resist Updat*, *10*, 30-50.

Demmel, L., Schmidt, K., Lucast, L., Havlicek, K., Zankel, A., Koestler, T., Reithofer, V., de Camilli, P. & Warren, G. (2014). The endocytic activity of the flagellar pocket in *Trypanosoma brucei* is regulated by an adjacent phosphatidylinositol phosphate kinase. *J Cell Sci, 127,* 2351–2364.

Dey, R., Joshi, A. B., Oliveira, F., Pereira, L., Guimaraes-Costa, A. B., Serafim, T. D., De Castro, W., Coutinho-abreu, I. V., Bhattacharya, P., Townsend, S., Aslan, H., Perkins, A., Karmakar, S., Ismail, N., Karetnick, M., Meneses, C., Duncan, R., Nakhasi, H. L., Valenzuela, J. G. & Kamhawi, s. (2018). Gut Microbes Egested during Bites of Infected Sand Flies Augment Severity of Leishmaniasis via Inflammasome-Derived IL-1beta. *Cell Host Microbe, 23*, 134-143 e6.

Dolezel, D., Jirku, M., Maslov, D. A. & Lukes, J. (2000). Phylogeny of the bodonid flagellates (Kinetoplastida) based on small-subunit rRNA gene sequences. *Int J Syst Evol Microbiol*, 50 Pt 5, 1943-51.

Dorlo, T. P.C., Huitema, A. D. R., Beijnen, J. H. & De Vries, P. J. (2012). Optimal dosing of miltefosine in children and adults with visceral leishmaniasis. *Antimicrob Agents Chemother*, *56*(7), 3864-3872.

Dostalova, A & Volf, P. (2012). Leishmania development in sand flies: parasite-vector interactions overview. *Parasites & Vectors,* 5.

Eichenberger, A., Buechi, A. E., Neumayr, A., Hatz, C., Rauch, A., Huguenot, M., Diamantis-Karamitopoulou E. & Staehelin, C. (2017). A severe case of visceral leishmaniasis and liposomal amphotericin B treatment failure in an immunosuppressed patient 15 years after exposure. *BMC Infect Dis, 17*, 81.

Ellenberger, T. E. & Beverley, S. M. (1986). Multiple drug resistance and conservative amplification of the H region in *Leishmania major*. *J Biol Chem*, *264*, 15094-15103.

Elmahallawy, E. K. & Agil, A. (2015). Treatment of leishmaniasis: a review and assessment of recent research. *Curr Pharm Des, 21*(17), 2259-2275.

Ephros, M., Bitnun, A., Shaked, P., Waldman, E. & Zilberstein, D. (1999). Stage-specific activity of pentavalent antimony against Leishmania donovani axenic amastigotes. *Antimicrob Agents Chemother*, *43*: 278–282.

Fairlamb A. H., Carter, N. S., Cunningham, M. & Smith, K. (1992). Characterisation of melarsen- resistant *Trypanosoma brucei brucei* with respect to cross-resistance to other drugs and trypanothione metabolism. *Mol Biochem Parasitol, 53*, 213–222

Fairlamb, A. H. & Horn, D. (2018). Melarsoprol resistance in African trypanosomes. *Trends Parasitol*, *34*(6), 481-492.

Fairlamb, A. H., Carter, N. S., Cunningham, M. & Smith, K. (1992). Characterisation of melarsen- resistant *Trypanosoma brucei brucei* with respect to cross-resistance to other drugs and trypanothione metabolism. *Mol Biochem Parasitol, 53*, 213–222.

Fairlamb, A. H., Gow, N. A., Matthews, K. R. & Waters, A. P. (2016). Drug resistance in eukaryotic microorganisms. *Nature microbiology, 1*, 16092.

Fidalgo, L. M. & Gille, L. (2011). Mitochondria and trypanosomatids: targets and drugs. *Pharm Res*, *28*(11), 2758-70.

Field, M. C. & Carrington, M. (2009). The trypanosome flagellar pocket. *Nat Rev Microbiol 7,* 775–786.

Field, M. C., Horn, D., Fairlamb, A. H., Ferguson, M. A. J., Gray, D. W., Read, K. D., De Rycker, M., Torrie, L. S., Wyatt, P. G., Wyllie, S. & Gilbert, I. H. (2017). Anti-trypanosomatid drug discovery: an ongoing challenge and a continuing need. *Nat Rev Micro*, *15*(4), 217-231.

Figarella, K., Uzcategui, N.L., Zhou, Y., LeFurgey, A., Ouellette, M., Bhattacharjee, H. & Mukhopadhyay, R. (2007) Biochemical characterization of *Leishmania major* aquaglyceroporin LmAQP1: Possible role in volume regulation and osmotaxis. *Mol Microbiol*, *65,* 1006–1017.

Franco, J. R., Simarro, P. P., Diarra, A. & Jannin, J. G. (2014a). Epidemiology of human African trypanosomiasis. *Clin Epidemiol*, *6*, 257-275.

Franco, J. R., Simarro, P. P., Diarra, A., Ruiz-Postigo, J. A. & Jannin, J. G. (2014b). The journey towards elimination of gambiense human African trypanosomiasis: not far, nor easy. *Parasitology*, *141*(6), 748-760.

Franco, JR., Cecchi, G., Priotto, G., Paone, M., Diarra, A., Grout L., *et al*. (2020). Monitoring the elimination of human African trypanosomiasis at continental and country level: Update to 2018. *PLoS Negl Trop Dis*. 14(5), e0008261.

Freźard, F.; Monte-Neto, R. & Reis, P. G. (2014). Antimony Transport Mechanisms in Resistant Leishmania Parasites. *Biophys Rev, 6*, 119−132.

Frommel, T. O. & Balber, A. E. (1987). Flow cytofluorimetric analysis of drug accumulation by multidrug-resistant *Trypanosoma brucei brucei* and *T. b. rhodesiense*. *Mol Biochem Parasitol, 26*, 183–191

Gagnaire, M. H., Galambrun, C., & Stéphan, J. L. (2000). Hemophagocytic syndrome: a misleading complication of visceral leishmaniasis in children – a series of 12 cases. *Paediatrics*, *106*(4), e58.

García-Salcedo J.A., Pérez-Morga D., Gijón P., Dilbeck V., Pays E., Nolan D.P. (2004) A differential role for actin during the life cycle of *Trypanosoma brucei*. *EMBO Journal*. 23:780–789.

Gehrig, S. & Efferth, T. (2008). Development of drug resistance in Trypanosoma brucei rhodesiense and Trypanosoma brucei gambiense. Treatment of human African trypanosomiasis with natural products (Review). *Int J Mol Med, 22*, 411-419.

Georgiadou, S. P., Makaritsis, K. P. & Dalekos, G. N. (2015). Leishmaniasis revisited: current aspects on epidemiology, diagnosis and treatment. *J Transl Int Med*, *3*(2), 43-50.

Ghaddar, K., Merhi, A., Saliba, E., Krammer, E. M., Prévost, M. & André, B. (2014). Substrate-induced ubiquitylation and endocytosis of yeast amino acid permeases. *Mol Cell Biol, 34*, 4447–4463.

Giordani, F., Morrison, L. J., Rowan, T. G., De Koning, H. P. & Barrett, M. P. (2016). The animal trypanosomiases and their chemotherapy: a review. *Parasitology, 143*, 1862–1889

Gluenz, E., Ginger, M. L. & McKean, P. G. (2010). Flagellum assembly and function during the *Leishmania* life cycle. *Curr Opin Microbiol*, *13*(4), 473-479.

Gomes, R. & Oliveira, F. (2012). The immune response to sand fly salivary proteins and its influence on Leishmania immunity. *Frontiers in Immunology,* 3.

Gould, M. K., Vu, X. L., Seebeck, T. & De Koning, H. P. (2008) Propidium iodide-based methods for monitoring drug action in the kinetoplastidae: Comparison with the Alamar Blue assay. *Anal Biochem*, 382(2), 87-93.

Gourbal, B., Sonuc, N., Bhattacharjee, H., Legare, D., Sundar, S., Ouellette, M., Rosen, B.P. & Mukhopadhyay, R. (2004) Drug uptake and modulation of drug resistance in Leishmania by an aquaglyceroporin. *J Biol Chem*, *279*, 31010–31017.

Gournas, C., Amillis, S., Vlanti A. & Diallinas, G. (2010). Transport-dependent endocytosis and turnover of a uric acid-xanthine permease. *Mol Microbiol, 75*, 246–260.

Gournas, C., Saliba, E., Krammer, E. M., Barthelemy, C., Prévost, M. & André, B. (2017). Transition of yeast Can1 transporter to the inward-facing state unveils an α-arrestin target sequence promoting its ubiquitylation and endocytosis. *Mol Biol Cell, 28*, 2819–2832.

Graf, F. E., Baker, N., Munday, J. C., De Koning, H. P., Horn, D. & Mäser, P. (2015). Chimerization at the AQP2-AQP3 locus is the genetic basis of melarsoprol-pentamidine cross-resistance in clinical *Trypanosoma brucei gambiense* isolates. *Int J Parasitol Drugs Drug Resist, 5*, 65–68.

Graf, F. E., Ludin, P., Arquint, C., Schmidt, R. S., Schaub, N., Kunz-Renggli, C., Munday, J. C., Krezdorn, J., Baker, N., Horn, D., Balmer, O., Caccone, A., De Koning H. P. & Mäser, P. (2016). Comparative genomics of drug resistance of the sleeping sickness parasite Trypanosoma brucei rhodesiense. *Cell Mol Life Sci, 73*, 3387–3400.

Graf, F. E., Ludin, P., Wenzler, T., Kaiser, M., Pyana, P., Büscher, P., De Koning, H. P., Horn, D. & Mäser, P. (2013). Aquaporin 2 mutations in Trypanosoma b. gambiense field isolates correlate with decreased susceptibility to pentamidine and melarsoprol. *PLoS Negl Trop Dis 7*, e2475.

Guerin, P. J., Olliaro, P., Nosten, F., Druilhe, P., Laxminarayan, R., Binka, F., Kilama, W. L., Ford, N., & White, N. J. (2002). *Lancet Infect Dis, 2*, 564 –573.

Haldar, A. K., Sen, P. & Roy, S. (2011). Use of antimony in the treatment of leishmaniasis: current status and future directions. *Mol Biol Int*, *2011*, 571242.

Handler, M. Z., Patel, P. A., Kapila, R., Al-Qubati, Y. & Schwarts, R. A. (2015). Cutaneous and mucocutaneous leishmaniasis: clinical perspectives. *J Am Acad Dermatol*, *73*(6), 897-908.

Handman, E. (1999). Cell biology of *Leishmania*. *Adv Parasitol*, *44*, 1-39.

Handman, E., & Bullen, D. V. R. (2002). Interaction of *Leishmania* with the host macrophage. *Trends Parasitol*. 18(8), 332-334.

Holt, H. R., Selby, R., Mumba, C., Napier G. B. & Guitian, J. (2016). Assessment of animal African trypanosomiasis (AAT) vulnerability in cattle-owning communities of sub-Saharan Africa. *Parasit Vectors*, *9*, 53.

Horn, D. (2014). Antigenic variation in African trypanosomes. *Molecular and Biochemical Parasitology*, *195*, 123-129.

Hutchinson, O. C., Picozzi, K., Jones, N. G., Mott, H., Sharma, R., Welburn, S. C. & Carrington, M. (2007). Variant surface glycoprotein gene repertoires in *Trypanosoma brucei* have diverged to become strain-specific. *BMC Genomics*, *8*, 234-243.

Hutchinson, R. & Gibson, W. (2015). Rediscovery of *Trypanosoma (Pycnomonas) suis*, a tsetse- transmitted trypanosome closely related to *T. brucei*. *Infect Genet Evol 36*, 381–388.

Ibrahim, A. A., El-Housseiny, G. S., Aboshanab, K. M., Yassien, M. A. & Hassouna, N. A. (2019). Paromomycin production from *Streptomyces rimosus* NRRL 2455: statistical optimization and new synergistic antibiotic combinations against multidrug resistant pathogens. *BMC Microbiol*, *19*, 18.

Imamura, H., Downing, T., Van den Broeck, F., Sanders, M. J., Rijal, S., Sundar, S., Mannaert, A., Vanaerschot, M., Berg, M., De Muylder, G., Dumetz, F., Cuypers, B., Maes, I., Domagalska, M., Decuypere, S., Rai, K., Uranw, S., Bhattarai, N. R., Khanal, B., Prajapati, V. K., Sharma, S., Stark, O., Schönian, G., De Koning, H. P., Settimo, L., Vanhollebeke, B., Roy, S., Ostyn, B., Boelaert, M., Maes, L., Berriman, M., Dujardin, J. C. & Cotton, J. A. (2016). Evolutionary genomics of epidemic visceral leishmaniasis in the Indian subcontinent. *eLife, 5*, e12613.

Jeacock, L., Baker, N., Wiedemar, N., Mäser, P. & Horn, D. (2017). Aquaglyceroporin-null trypanosomes display glycerol transport defects and respiratory-inhibitor sensitivity. *PLoS Pathog, 13*, e1006307.

Jensen, B. C., Ramasamy, G., Vasconcelos, E. J., Ingolia, N. T., Myler, P. J. & Parsons, M. (2014). Extensive stage-regulation of translation revealed by ribosome profiling of Trypanosoma brucei. *BMC Genomics, 15*, 911.

Jhingran, A., Chawla, B., Saxena, S., Barrett, M. P. & Madhubala, R. (2009) Paromomycin: uptake and resistance in *Leishmania donovani*. *Mol Biochem Parasitol*, 164(2), 111-7.

Kalel, V. C., Emmanouilidis, L., Dawidowski, M., Schliebs, W., Sattler, M., Popowicz, G. M. & Erdmann, R. (2017). Inhibitors of glycosomal protein import provide new leads against trypanosomiasis. *Microbial Cell*, *4*(7), 229-232.

Kang, X., Szallies, A., Rawer, M., Echner, H. & Duszenko, M. (2002). GPI anchor transamidase of Trypanosoma brucei: *in vitro* assay of the recombinant protein and VSG anchor exchange. *J Cell Sci, 115*, 2529-2539.

Kaye, P. & Scott, P. (2011). Leishmaniasis: complexity at the host-pathogen interface. *Nat Rev Microbiol, 11*(8), 604-615.

Kazemi-Rad, E., Mohebali, M., Khadem-Erfan, M. B., Saffari, M., Raoofian, R., Hajjaran, H., Hadighi, R., Khamesipour, A., Rezaie, S., Abedkhojasteh, H., Heidari, M. (2013). Identification of antimony resistance markers in *Leishmania tropica* field isolates through a cDNA-AFLP approach. *Exp parasitol*, *135*, 344–349.

Keener, J. M. & Babst, M. (2013). Quality control and substrate-dependent downregulation of the nutrient transporter Fur4. *Traffic, 14,* 412–427.

Kell, D. & Oliver, S. (2014). How Drugs Get into Cells: Tested and Testable Predictions to Help Discriminate between Transporter-Mediated Uptake and Lipoidal Bilayer Diffusion. *Frontiers in Pharmacology*, *5,* 231.

Kennedy, P. G. E. (2013). Clinical features, diagnosis, and treatment of human African trypanosomiasis (sleeping sickness). *Lancet Neurol, 12*, 186-194.

Kennedy, P. G. E. & Rodgers, J. (2019). Clinical and neuropathogenetic aspects of Human African Trypanosomiasis. *Front Immunol*, *10*, 39.

Kuepfer, I., Hhary, E. P., Allan, M., Edielu, A., Burri, C. & Blum, J. A. (2011). Clinical presentation of *T. b. rhodesiense* sleeping sickness in second stage patients from Tanzania and Uganda. *PLoS Negl Trop Dis, 5*(3), e968.

Kuepfer, I., Schmid, C., Allan, M., Edielu, A., Haary, E. P., Kakembo, A., Kibona, S., Blum, J. & Burri, C. (2012). Safety and efficacy of the 10-day melarsoprol schedule for the treatment of second stage Rhodesiense sleeping sickness. *PLoS Negl Trop Dis, 6*(8), e1695.

Kumar, A., Saha, B., and Singh, S. (2017). Dataset generated for dissection of mechanisms of trypanothione reductase and tryparedoxin peroxidase through dynamic network analysis and simulations in leishmaniasis. *Data Brief*. 15, 757–769.

Lai, A. F. E. J., Vrede, M. A, Soetosenojo, R. M. & Lai, A. F. R. F. (2002). Pentamidine, the drug of choice for the treatment of cutaneous leishmaniasis in Surinam. *Int J Dermatol*, *41*(11), 796–800.

Landfear, S. M. (2008). Drugs and transporters in kinetoplastid protozoa. *Adv Exp Med Biol*, *625*, 22-32.

Langousis, G. & Hill, K. L. (2014). Motility and more: the flagellum of *Trypanosoma brucei*. *Nat Rev Microbiol*, *12*(7), 505-518.

Langreth, S. G., Balber, A. E. (1975). Protein uptake and digestion in bloodstream and culture forms of Trypanosoma brucei. *J Protozool, 22*, 40–55.

Legros, D., Olivier, G., Gastellu-Etchegorry, M., Paquet, C., Burri, C., Jannin, J. & Buscher, P. (2002). Treatment of human African trypanosomiasis – present situation and needs for research and development. *Lancet Infect Dis*, 2(7), 437-440.

Lindner AK, Lejon V, Chappuis F, Seixas J, Kazumba L, Barrett M, Mwamba E, Erphas O, Akl E, Villanueva G, Bergman H, Simarro PP, Kadima Ebeja A, Gerardo Priotto G, Franco Minguell JR. (2020). New WHO guidelines for treatment of gambiense human African trypanosomiasis including fexinidazole: fundamental changes for clinical practice. *Lancet Infect Dis*, 20: e38–46.

Lira, R., Sundar, S., Makharia, A., Kenney, R., Gam, A., Saraiva, E. & Sacks, D. (1999). Evidence that the high incidence of treatment failures in Indian kala-azar is due to the emergence of antimony resistant strains of *Leishmania donovani*. *J Infect Dis*, *180*, 564-567.

Liu, D. & Uzonna, J. E. (2012). The early interaction of Leishmania with macrophages and dendritic cells and its influence on the host immune system. *Font Cell Infect Microbiol*, *2*, 83.

Lüscher, A., De Koning, H. P. & Mäser, P. (2007). Chemotherapeutic strategies against Trypanosoma brucei: Drug targets vs. drug targeting. *Curr Pharm Des*, *13*, 555–567.

Mackey, Z. B., Koupparis. K., Nishino, M. & McKerrow J. H. (2011). High-throughput analysis of an RNAi library identifies novel kinase targets in *Trypanosoma brucei*. *Chem Biol Drug Des, 78,* 454–463.

MacLean, LM., Odiit, M., Chisi, JE., Kennedy, PGE. & Sternberg, JM. (2010) Focus-specific clinical profiles in human African trypanosomiasis caused by Trypanosoma brucei rhodesiense. *PLoS Negl Trop Dis*. 4(12), e906.

Maharjan, M., Singh, S., Chatterjee, M. & Madhubala, R. (2008). Role of aquaglyceroporin (AQP1) gene and drug uptake in antimony-resistant clinical isolates of *Leishmania donovani*. *Am J Trop Med Hyg, 79*, 69–75.

Makaritsis, K. P., Gatselis, N. K., Iannou, M., Petinaki, E. & Dalekos, G. N. (2009). Polyclonal hypergammaglobulinemia and high smooth-muscle autoantibody titers with specificity against filamentous actin: consider viceral leishmaniasis, not just autoimmune hepatitis. *Int J Infect Dis*, *13*(4), e157-e160.

Mandal, G., Mandal, S., Sharma, M., Charret, K. S., Papadopoulou, B., Bhattacharjee, H. & Mukhopadhyay, R. (2015). Species-specific antimonial sensitivity in Leishmania is driven by post-transcriptional regulation of AQP1. *PLoS Negl Trop Dis, 9*, e0003500.

Mandal, G., Wyllie, S., Singh, N., Sundar, S., Fairlamb, A. H. & Chatterjee, M. (2007). Increased levels of thiols protect antimony unresponsive *Leishmania donovani* field isolates against reactive oxygen species generated by trivalent antimony. *Parasitology*, *134*, 1679-1687.

Mandal, S., Maharjan, M., Singh, S., Chatterjee, M. & Madhubala, R. (2010) Assessing aquaglyceroporin gene status and expression profile in antimony-susceptible and –resistant clinical isolates of *Leishmania donovani* in India. *J Antimicrob Chemother*. *65*, 496-507.

Marquis, N., Gourbal, B., Rosen, B.P., Mukhopadhyay, R. & Ouellette, M. (2005). Modulation in aquaglyceroporin AQP1 gene transcript levels in drug-resistant *Leishmania*. *Mol Microbiol, 57*, 1690–9.

Mäser, P., Sustterlin, Kralli, A. & Kaminsky, R. (1999). A nucleoside transporter from *Trypanosoma brucei* involved in drug resistance. *Science*, *285*(5425), 242-244.

Maslov, D.A., Podlipaev, S.A., Lukes, J., (2001). Phylogeny of the kinetoplastida: taxonomic problems and insights into the evolution of parasitism. *Memórias do Instituto Oswaldo Cruz 96*, 397-402.

Matovu, E., Stewart, M. L., Geiser, F., Brun, R., Mäser, P., Wallace, L. J. M., Burchmore, R. J., Enyaru, J. C. K., Barrett, M. P., Kaminsky, R., Seebeck, T. & De Koning, H. P. (2003). Mechanisms of arsenical and diamidine uptake and resistance in *Trypanosoma brucei*. *Eukaryot Cell*, *2*(5), 1003-1008.

Matthews, K. R. (2005). The development cell biology of *Trypanosoma brucei*. *J Cell Sci*, *118*, 283-290.

Maurel, C., Boursiac, Y., Luu, D. T., Santoni, V., Shahzad, Z., Verdoucq, L. Aquaporins in Plants. (2015). *Physiol Rev*, 95, 1321– 1358.

McCall, L., Zhang, W. & Matlashewski, G. (2013). Determinants for the development of visceral leishmaniasis disease. *PLoS Pathog*, *9*(1), e1003053.

McConville, M. J. & Naderer, T. (2011). Metabolic pathways required for the intracellular survival of *Leishmania*. *Ann Rev Microbiol, 6,* 543-561.

Migchelsen, S. J., Buscher, P., Hoepelman, A. I., Schallig, H. D. & Adams, E. R. (2011). Human African trypanosomiasis: a review of non-endemic cases in the past 20 years. *Int J Infect Dis*, *15*(8), e517-24.

Miranda-Versategui, C., Tuilliano, G., Gyorkos, T. W., Calderon, W., Rahme, E., Ward, B., Cruz, M., Llanos-Cuentas A. & Matlashewski, G. (2009). First-line therapy for human cutaneous leishmaniasis in Peru using the TLR7 against imiquimod in combination with pentavalent antimony. *PLoS Negl Trop Dis*, *3*(7), e491.

Mital, A. (2009). Synthetic nitroimidazoles: biological activities and mu- tagenicity relationships. *Sci Pharm 77*: 497-520.

Molla-Herman, A., Ghossoub, R., Blisnick, T., Meunier, A., Serres, C., Silbermann, F., Emmerson, C., Romeo, K., Bourdoncle, P., Schmitt, A., Saunier, S., Spassky, N., Bastin, P. & Benmerah, A. (2010). The ciliary pocket: an endocytic membrane domain at the base of primary and motile cilia. *J Cell Sci*, *123,* 1785-1795.

Monnerat, S., Almeida Costa, C. I., Forkert, A.C., Benz, C, Hamilton, A., Tetley, L., Burchmore, R., Novo, C., Mottram, J. C., Hammarton, T. C. (2013). Identification and functional characterisation of CRK12:CYC9, a novel cyclin-dependent kinase (CDK)-cyclin complex in Trypanosoma brucei. *PLoS One, 8,* e67327.

Montalvetti, A., Rohloff, P. & Docampo, R. (2004). A functional aquaporin co-localizes with the vacuolar proton pyrophosphatase to acidocalcisomes and the contractile vacuole complex of *Trypanosoma cruzi*. *J Biol Chem, 279*, 38673–38682.

Moore, E. M., & Lockwood, D. N. (2010). Treatment of visceral leishmaniasis. *J Glob Infect Dis*, *2*(2), 151-158.

Morgan, G. W., Hall, B. S., Denny, P. W., Field, M. C. & Carrington, M. C. (2002). The endocytic apparatus of the kinetoplastida II: Machinery and residents of the endocytic system. *Trends Parasitol, 18*, 540-546.

Mukhopadhyay, R., Bhattacharjee, H. & Rosen, B. P. (2014). Aquaglyceroporins: generalized metalloid channels. *Biochim Biophys Acta, 1840*(5), 1583–1591.

Müller-Lucks, A., Gena, P., Frascaria, D., Altamura, N., Svelto, M., Beitz, E. & Calamita, G. (2013). Preparative scale production and functional reconstitution of a human aquaglyceroporin (AQP3) using a cell free expression system. *New Biotechnol*, *30,* 545–551.

Munday, J. C., Eze, A. A., Baker, N., Glover, L., Clucas, C., Aguinaga Andrés, D., Natto, M. J., Teka, I. A., McDonald, J., Lee, R. S., Graf, F. E., Ludin, P., Burchmore, R. J., Turner, C. M., Tait, A., MacLeod, A., Mäser, P., Barrett, M. P., Horn, D., & De Koning, H. P. (2014). *Trypanosoma brucei* Aquaglyceroporin 2 is a high affinity transporter for pentamidine and melaminophenyl arsenic drugs and is the main genetic determinant of resistance to these drugs. *J Antimicrob Chemother, 69,* 651–663.

Munday, J. C., Settimo, L. & De Koning, H. P. (2015a). Transport proteins determine drug sensitivity and resistance in a protozoan parasite, Trypanosoma brucei. *Frontiers Pharmacol, 6,* 32.

Munday, J. C., Tagoe, D. N. A., Eze, A. A., Krezdorn, J. A., Rojas López, K. E., Alkhaldi, A. A. M., McDonald, F., Still, J., Alzahrani, K. J., Settimo, L. & De Koning, H. P. (2015b). Functional analysis of drug resistance-1 associated mutations in the Trypanosoma brucei Adenosine Transporter 1 (TbAT1) and the proposal of a structural model for the protein. *Mol Microbiol, 96,* 887–900.

Mwenechanya, R., Kovářová, J., Dickens, N. J., Mudaliar, M., Herzyk, P., Vincent, I. M., Weidt, S. K., Bugess, K. E., Burchmore, R. J. S., Pountain, A. W., Smith, T. K., Creek, D. J., Kim, D. H., Lepesheva, G. I. & Barrett, M. P. (2017). Sterol 14α-demethylase mutation leads to amphotericin B resistance in *Leishmania mexicana*. *PLoS Negl Trop Dis, 11*(6), e0005649.

Nerima, B., Matovu, E., Lubega, G. W. & Enyaru, J. C. K. (2007). Detection of mutant P2 adenosine transporter (TbAT1) gene in *Trypanosoma brucei gambiense* isolates from northwest Uganda using allele-specific polymerase chain reaction. *Trop Med Int Health, 12*(11), 1361-1368.

Nilsen, S. & Casini, A. (2016). Eds. Aquaporins in Health and Disease: new molecular targets for drug discovery. *New Molecular Targets for Drug Discovery*, CRC Press, Boca Raton, FL, p 321.

Nok, A. J. (2003). Arsenicals (melarsoprol), pentamidine and suramin in the treatment of human African trypanosomiasis. *Parasitol Res, 90,* 71-79.

Ogbadoyi, E. O., Robinson, D. R. & Gull, K. (2003). A high-order trans-membrane structural linkage is responsible for mitochondrial genome positioning and segregation by flagellar basal bodies in trypanosomes. *Mol Biol Cell, 14*(5), 1769-1779.

Okwor, I. & Uzonna, J. E. (2016). Social and economic burden of human leishmaniasis. *Am J Trop Med Hyg, 94*(3), 489-493.

Ooi, C. & Bastin, P. (2013) More than meets the eye: understand *Trypanosoma brucei* morphology in the tsetse. *Front Cell Infect Microbiol, 3,* 71.

Opperdoes, F. R., Borst, P. & Fonck, K. (1976). The potential use of inhibitors of glycerol-3- phosphate oxidase for chemotherapy of african trypanosomiasis. *FEBS Lett*, *62,* 169-172.

P. Srivastava, V.K. Prajapati, M. Rai, S. Sundar. (2011). Unusual case of resistance to amphotericin B in visceral leishmaniasis in a region in India where leishmaniasis is not endemic. *J. Clin. Microbiol,* 49, pp. 3088-3091.

Pal, A., Hall, B. S., & Field, M. C. (2002). Evidence for a non-LDL-mediated entry route for the typanocidal drug suramin in *Trypanosoma brucei*. *Mol Biochem Parasitol*, *122*(2), 217-221.

Pearson, R. D., Harcus, J. L., Roberts, D. & Donowitz, G. R. (1983). Differential survival of *Leishmania donovani* amastigotes in human monocytes. *J Immunol*, *131*, 1994-1999.

Pérez-Victoria, F. J., Castanys, S. & Gamarro, F. (2003). *Leishmania donovani* resistance to miltefosine involves a defective inward translocation of the drug. *Antimicrob Agents Chemother*, 47(8), 2397, 2403.

Pérez-Victoria, F. J., Sánchez-Canete, M. P., Castanys, S. & Gamarro, F. (2006). Phospholipid translocation and miltefosine potency require both *L. donovani* miltefosine transporter and the new protein *Ld*Ros3 in *Leishmania* parasites. *J Biol Chem, 281*(33), 23766-23775.

Perry, M., Wyllie, S., Prajapati, V., Menten, J., Raab, A., Feldmann, J., Chakrabarti, D., Sundar, S., Boelaert, M., Picado, A. & Fairlamb, A. (2015). Arsenic, antimony, and Leishmania: has arsenic contamination of drinking water in India led to treatment-resistant kala-azar? *Lancet, 385,* S80.

Perry, M., Wyllie, S., Raab, A., Feldmann, J. & Fairlamb, A. (2013). Chronic exposure to arsenic in drinking water can lead to resistance to antimonial drugs in a mouse model of visceral leishmaniasis. *Proc Natl Acad Sci USA, 110,* 19932.

Peters, N. & Sacks, D. (2006). Immune privilege in sites of chronic infection: Leishmania and regulatory T cells. *Immunological Reviews,* 213, 159-179.

Peters, N. C., Egen, J. G., Secundino, N., Debrabant, A., Kimblin, N., Kamhawi, S., Lawyer, P., Fay, M. P., Germain, R. N. & Sacks, D. (2008). *In vivo* imaging reveals an essential role for neutrophils in leishmaniasis transmitted by sand flies. *Science, 15*(5891), 970-974.

Philips, M. A. & Wang, C. C. (1987). A *Trypanosoma brucei* mutant resistant to alpha-difluoromethylornithine. *Mol Biochem Parasitol*, *22*(1), 9-17.

Pinger, J., Chowdhury, S. & Papavasiliou, F. N. (2017). Variant surface glycoprotein density defines an immune evasion threshold for African trypanosomes undergoing antigenic variation. *Nat Commun*, *8*(1), 828.

Plourde, M., Ubeda, J. M., Mandal, G., Lima do Monte-Neto, R., Mukhopadhyay, R., Ouellette, M. (2015) Generation of an aquaglyceroporin AQP1 null mutant in *Leishmania major*. *Mol Biochem Parasitol, 201*(2), 108-111.

Pogers, M. E. (2012). The role of Leishmania proteophosphoglycans in sand fly transmission and infection of the mammalian host. *Frontiers in Microbiology,* 3.

Ponte, Sucre, A., Gamarro, F., Dujardin, J. C., Barrett, M. P., López-Vélez, R., García-Hernández, R., Pountain, A. W., Mwenechanya, R. & Papadopoulou, B. (2017). Drug resistance and treatment failure in leishmaniasis: a 21st century challenge. *PLoS Negl Trop Dis*, *11*(12), e0006052.

Priotto, G., Kasparian, S., Mutombo, W., Ngouama, D., Ghorashian, S., Arnold, U., Ghabri, S., Baudin, E., Buard, V., Kazadi-Kyanza, S., Ilunga, M., Mutangala, W., Pohlig, G., Schmid, C., Karunakara, U., Torreele, E. & Kande, V. (2009). Nifurtimox-eflornithine combination therapy for second-stage African *Trypanosoma brucei gambiense* trypanosomiasis: a multicentre, randomised, phase III, non-inferiority trial. *Lancet*, *374*(9683), 56-64.

Priotto, G., Kasparian, S., Ngouama, D., Ghorashian, S., Arnold, U., Ghabri S. & Karunakara, U. (2007). Nifurtimox-eflornithine combination therapy for second-stage *Trypanosoma gambiense* sleeping sickness: a randomized clinical trial in Congo. *Clin Infect Dis*, *45*(11), 1435-1442.

Purkait, B., Kumar, A., Nandi, N., Sardar, A. H., Das, S., Kumar, S., Pandey, K., Ravidas, V., Kumar, M., De, T., Singh, D. & Das, P. (2012). Mechanism of amphotericin B resistance in clinical isolates of *Leishmania donovani*. *Antimicrob Agents Chemother*, *56*(2), 1031-1041.

Pyana Pati, P., Van Reet, N., Mumba Ngoyi, D., Ngay Lukusa, I., Karhemere Bin Shamamba, S., Büscher, P. (2014). Melarsoprol sensitivity profile of *Trypanosoma brucei gambiense* isolates from cured and relapsed sleeping sickness patients from the Democratic Republic of the Congo. *PLoS Negl Trop Dis*, *8*, e3212.

Quintana, J. F., Bueren-Calabuig, J., Zuccotto, F., Zoltner, M., De Koning, H. P., Horn, D., Field, M. C. (2020). Instability of aquaglyceroporin (AQP) 2 contributes to drug resistance in Trypanosoma brucei. *PLOS Negl Trop Dis*, in press.

Rahman, M., Ahmed, B. N., Faiz, M. A., Chowdhury, M. Z., Islam, Q. T., Sayeedur, R., Rahman, M. R., Hossain, M., Bangali, A. M., Ahmad, Z., Islam, M. N., Mascie-Taylor, C. G., Berman, J. & Arana, B. (2011). Phase IV trial of miltefosine in adults

and children for treatment of visceral leishmaniasis (kala-azar) in Bangladesh. *Am J Trop Med Hyg, 85*(1), 66-69.

Rai, S., Bhaskar., Goel, S.K., Nath Dwivedi, U., Sundar, S., Goyal, N. (2013). Role of efflux pumps and intracellular thiols in natural antimony resistant isolates of Leishmania donovani. *PLoS One*, *8*, e74862.

Ranjbarian, F., Vodnala, M., Alzahrani, K. J., Ebiloma, G. U., De Koning, H. P. & Hofer, A. (2017). 9-(2'-Deoxy-2'-fluoro-ß-d-arabinofuranosyl) adenine: a potent antitrypanosomal adenosine analogue that circumvents transport-related drug resistance. *Antimicrob Agents Chemother, 61*(6), e02719-16.

Ready, P. D. (2014). Epidemiology of visceral leishmaniasis. *Clin Epidemiol*, *6*, 147-154.

Reithinger, R., Brooker, S. & Kolaczinski, J. H. (2007). Visceral leishmaniasis in eastern Africa – current status. *Trans R Soc Trop Med Hyg*, *101*(12), 1169-1170.

Richard, D., Leprohon, P. , Drummelsmith , J. , and Ouellette , M. (2004) Growth phase regulation of the main folate transporter of *Leishmania infantum* and its role in methotrexate resistance . *J Biol Chem,* 279 : 54494 – 54501.

Rico, E., Rojas, F., Mony, B. M., Szoor, B., MacGregor, P. & Matthews, K. R. (2013). Bloodstream form pre-adaptation to the tsetse fly in *Trypanosoma brucei*. *Front Cell Infect Microbiol*, *3*, 78.

Rijal, S., Chappuis, F., Singh, R., Bovier, P. A., Acharya, P., Karki, B. M., Das, M. L., Desjeux, P., Loutan, L. & Koirala, S. (2003). Treatment of visceral leishmaniasis in south-eastern Nepal: decreasing efficacy of sodium stibogluconate and need for a policy to limit further decline. *Trans R Soc Trop Med Hyg*, *97*, 350–354.

Rijal, S., Ostyn, B., Uranw, S., Rai, K., Bhattarai, N. R., Dorlo, T. P., Beijnen, J. H., Vanaerschot, M., Decuypere, S., Dhakal, S. S., Das, M. L., Karki, P., Singh, R., Boelaert, M. & Dujardin, J. C. (2013). Increasing failure of miltefosine in the treatment of kala-azar in Nepal and the potential role of parasite drug resistance, refinection, or noncompliance. *Clin Infect Dis*, *56*(11), 1530-1538.

Ritter, U., Frischknecht, F. & Van Zandbergen, G. (2009). Are neutrophils important host cells for Leishmania parasites? *Trends Parasitol,* 25, 505-10.

Rittig, M. G. & Bogdan, C. (2000). *Leishmania*-host cell interaction: complexities and alternative views. *Parasitol Today*, *16*(7), 292-297.

Rodgers, J. (2009). Trypanosomiasis and the brain. *Parasitology*. 137(14):1995-2006

Rodrigues, J. C., Godinho, J. L. & de Souza, W. (2014). Biology of human pathogenic trypanosomatids: epidemiology, lifecycle and ultrastructure. *Subcell Biochem*, 74, 1-42.

Rogers, M.E., Chance, M. & Bates, P. (2002). The role of promastigote secretory gel in the origin and transmission of the infective stage of Leishmania mexicana by the sandfly Lutzomyia longipalpis. *Parasitology,* 124, 495-507.

Rohloff, P., Docampo, R. A. (2008). Contractile vacuole complex is involved in osmoregulation in *Trypanosoma cruzi*. *Exp Parasitol*, *118*, 17–24.

Rollo, I. M. & Williamson, J. (1951). Acquired resistance to 'Melarsen', tryparsamide and amidines in pathogenic trypanosomes after treatment with 'Melarsen' alone. *Nature, 167,* 147–148

Roque, A. L. R. & Jansen, A. M. (2014). Wild and synanthropic reservoirs of *Leishmania* species in the Americas. *Int J Parasitol Parasites Wildl*, *3*(3), 251-262.

Rotureau, B., Subota, I., Buisson, J. & Bastin, P. (2012). A new asymmetric division contributes to the continuous production of infective trypanosomes in the tsetse fly. *Development*. 139(10), 1842-1850.

S.R. Uliana, C.T. Trinconi, A.C. Coelho. (2017). Chemotherapy of leishmaniasis: present challenges Parasitology, 20 ,pp. 1-17.

Sacks, D., & Noben-Trauth, N. (2002). The immunology of susceptibility and resistance to Leishmania major in mice. *Nat Rev Immunol*, *2*, 845-858.

Sanderson, L., Dogruel, M., Rodgers, J., De Koning, H. P. & Thomas, S. A. (2009). Pentamidine movement across the murine blood-brain and blood-cerebrospinal fluid barriers: effect of trypanosome infection, combination therapy, p-glycoprotein, and multidrug resistant-associated protein. *J Pharmacol Exp Ther*, *329*(3), 967-977.

Sanderson, L., Khan, A. & Thomas, S. (2007). Distribution of suramin, an antitrypanosomal drug, across the blood-brain and blood-cerebrospinal fluid interfaces in wild-type and p-glycoprotein transporter-deficient mice. *Antimicrob Agents Chemother*, *51*(9), 3136-3146.

Schmidt, R. S., Macedo, J. P., Steinmann, M. E., Salgado, A. G., Butikofer, P., Sigel, E., Rentsch, D., Mäser, P. (2018) Transporters of *Trypanosoma brucei* – phylogeny, physiology, pharmacology. *FEBS J*, 285, 1012-1023.

Schuster, S., Kruger, T., Subota, I., Thusek, S., Rotureau, B., Beilhac, A. & Engstler, M. (2017). Development adaptations of trypanosome motility to the tsetse fly host environments unravel a multifaceted *in vivo* microswimmer system. *ELife*. 6, e27656.

Scott, A. G., Tait, A. & Turner, C. M. R. (1996). Characterisation of clones lines of *Trypanosoma brucei* expressing stable resistance to MelCy and suramin. *Acta Tropica*, *60*(4), 251-262.

Seed, J. R. & Wenck, M. A. (2003). Role of the long slender to short stumpy transition in the life cycle of the African trypanosomes. *Kinetoplastid Biol Dis, 2*(1), 3.

Serafim, T. D., Coutinho-Abreu, I. V., Oliveira, F., Meneses, C., Kamhawi, S. & Valenzuela, J. G. (2018). Sequential blood meals promote Leishmania replication and reverse metacyclogenesis augmenting vector infectivity. *Nat Microbiol,* 3, 548-555.

Shaked-Mishan, P., Ulrich, N., Ephros, M., Zilberstein, D. (2001). Novel Intracellular SbV reducing activity correlates with antimony susceptibility in *Leishmania donovani*. *J Biol Chem*, *276*, 3971–3976.

Sharma, R., Peacock, L., Gluenz, E., Gull, K., Gibson, W. & Carrington, M. (2008). Asymmetric cell division as a route to reduction in cell length and change in cell morphology in trypanosomes. *Protist*. 159(1), 137-151.

Sibley, L. D. (2011). Invasion and intracellular survival by protozoan parasites. *Immunol Rev*, *240*(1), 72-91.

Siegel, T. N., Hekstra, D. R., Wang, X., Dewell, S., Cross, G. A. (2010). Genome-wide analysis of mRNA abundance in two life-cycle stages of *Trypanosoma brucei* and identification of splicing and polyadenylation sites. *Nucleic Acids Res, 38*(15), 4946-4957.

Silvester, E., McWilliam, K. R. & Matthews, K. R. (2017). The cytological events and molecular control of life cycle development of *Trypanosoma brucei* in the mammalian bloodstream. *Pathogens, 6*(3), e29.

Singh, N., Chatterjee, M. & Sundar, S. (2014). The overexpression of genes of thiol metabolism contribute to drug resistance in clinical isolates of visceral leishmaniasis (kala azar) in India. *Parasit Vectors*, 7, 596.

Singh, O. P., Singh, B., Chakravarty, J. & Sundar, S. (2016). Current challenges in treatment options for visceral leishmaniasis in India: a public health perspective. *Infect Dis Poverty*, *5*, 19.

Singh, OP., Hasker, E., Sacks, D., Boelaert, M. & Sundar, S. (2014). Asymptomatic *Leishmania* infection: a new challenge for *Leishmania* control. *Clin Infect Dis*. 58(10), 1424-1429.

Song, J., Baker, N., Rothert, M., Henke, B., Jeacock, L., Horn, D., Beitz, E. (2016). Pentamidine is not a permeant but a nanomolar inhibitor of the Trypanosoma brucei Aquaglyceroporin-2. *PLoS Pathog, 12,* e1005436.

Soto, J., Buffet, P., Gorgl, M. & Berman, J. (1994). Successful treatment of Colombian cutaneous leishmaniasis with four injections of pentamidine. *Am J Trop Med Hyg*, *50*(1), 107-111.

Stanford University. (2008). Extacellular vs. Intracellular Parasitic Mechanisms of Immune Evasion: *Leishmania*. Available at: https://web.stanford.edu/class/humbio153/ImmuneEvasion/index.html (Accessed 19/04/2020).

Steinmann, P., Stone, C. M., Sutherland, C. S., Tanner, M. & Tediosi, F. (2015). Contemporary and emerging strategies for eliminating human African trypanosomiasis due to *Trypanosoma brucei gambiense*: review. *Trop Med Int Health*, *20*(6), 707-718.

Stevens, J. R., Noyes, H. A., Schofield, C. J. & Gibson, W. (2001) The molecular evolution of *Trypanosomatidae*. *Adv Parasitol*, 48, 1-56.

Steverding, D. (2010). The development of drugs for treatment of sleeping sickness: a historical review. *Parasit Vectors*, 3, 15.

Steverding, D. (2017). The history of leishmaniasis. *Parasit Vectors*, *10*(1), 82.

Stewart M. L., Krishna S., Burchmore R. J. S., Brun R., De Koning H. P., Boykin D. W., Tidwell R.R., Hall J. E., Barrett M. P. (2005). Detection of arsenical drug resistance in *Trypanosoma brucei* using a simple fluorescence test. *Lancet*, *366*, 486–487.

Stuart, K., Brun, R., Croft, S., Fairlamb, A., Gurtler, R. E., McKerrow, J., Reed, S. & Tarleton, R. (2008). Kinetoplastids: related protozoan pathogens, different diseases. *J Clin Invest*, 118(4), 1301-10.

Sui H, Han BG, Lee JK, Walian P, Jap BK. (2001). Structural basis of water-specific transport through the AQP1 water channel. *Nature,* 414:872–878.

Sundar, S, More, D. K., Singh, M. K., Singh, V. P., Sharma, S., Makharia, A., Kumar P. C. & Murray, H. W. (2000). Failure of pentavalent antimony in visceral leishmaniasis in India: report from the centre of the Indian epidemic. *Clin Infect Dis*, *31*, 1104-1107.

Sundar, S. & Chakravarty, J. (2008). Paromomycin in the treatment of leishmaniasis. *Expert Opin Investig Drugs*, *17*(5), 787-794.

Sundar, S. & Chakravarty, J. (2010). Liposomal amphotericin B and leishmaniasis: dose and response. *J Glob Infect Dis*, *2*(2), 159-166.

Sundar, S. & Chakravarty, J. (2012). Recent advances in the diagnosis and treatment of kala-azar. *Natl Med J India*, *25*, 85–89.

Sundar, S., & Chakravarty, J. (2015). An update on pharmacotherapy for leishmaniasis. *Expert Opin Pharmacother*, *16*(2), 237-252.

Sundar, S., Chakravarty, J. & Meena, L. P. (2019). Leishmaniasis: treatment, drug resistance and emerging therapies. *Expert Opin Orphan Drugs*, *7*(1), 1-10.

Sundar, S., Jha, T. K., Thakur, C. P., Engel, J., Sindermann, H., Fischer, C., Junge, K., Bryceson, A. & Berman, J. (2002). Oral miltefosine for Indian visceral leishmaniasis. *N Engl J Med*, *347*(22), 1739–1746.

Sundar, S., Jha, T. K., Thakur, C. P., Sinha, P. K. & Bhattacharya, S. K. (2007). Injectable paromomycin for visceral leishmaniasis in India. *N Engl J Med*, *356*(25), 2571-2581.

Sundar., S., Singh, A., Rai, M., Prajapati, V. K., Singh, A. K., Ostyn, B., Boelaert, M., Dujardin, J. C. & Chakravarty, J. (2012). Efficacy of miltefosine in the treatment of visceral leishmaniasis in India after a decade of use. *Clin Infect Dis*, *55*(4), 543-550.

Sunter, J. & Gull, K. (2017). Shape, form, function and *Leishmania* pathogenicity: from textbook descriptions to biology understanding. *Open Biol*, 7, 170165.

Sunter, J. D. & Gull, K. (2016). The flagellum attachment zone: 'the cellular ruler' of trypanosome morphology. *Trends Parasitol*, *32*(4), 309-324.

Sunyoto, T., Potet, J. & Boelaert, M. (2018). Why miltefosine—a life-saving drug for leishmaniasis—is unavailable to people who need it the most. *BMJ Glob Health, 3,* e000709.

Tadese, D., Hailu, A., Bekele, F., Bekele, F. & Belay, S. (2019). An epidemiological study of visceral leishmaniasis in North East Ethiopia using serological and leishmanin skin tests. *PLoS One*, *14*(12), e0225083.

Teka, I. A., Kazibwe, A., El-Sabbagh, N., Al-Salabi, M. I., Ward, C. P., Eze, A. A., Munday, J. C., Mäser, P., Matovu, E., Barrett, M. P., De Koning, H. P. (2011). The diamidine diminazene aceturate is a substrate for the High Affinity Pentamidine Transporter: implications for the development of high resistance levels. *Mol Pharmacol, 80,* 110–116.

Tetaud, E., Barrett, M. P., Bringaud, F. & Baltz, T. (1997). Kinetoplastid glucose transporters. *Biochem J*, *325*(Pt 3), 569-580.

Tetaud, E., Lecuix, I., Sheldrake, T., Baltz, T., & Fairlamb, A. H. (2002). A new expression vector for Crithidia fasciculata and Leishmania. *Mol Biochem Parasitol, 120*(2), 195–204.

Thakur, C. P., Pandey, A. K., Sinha, G. P., Roy, S., Behbehani, K. & Olliaro, P. (1996) Comparison of three treatment regimens with liposomal amphotericin B (AmBisome®) for visceral leishmaniasis in India: a randomized dose-finding study. *Trans R Soc Trop Med Hyg*, *90,* 319-322.

Thomas P. Jahn, Gerd P. Bienert. (2010). MIPs and their role in the exchange of metalloids. *Landes Bioscience*. Austin.

Thomas, J. A., Baker, N., Hutchinson, S., Dominicus, C., Trenaman, A., Glover, L., Alsford, S. & Horn, D. (2018). Insights into antitrypanosomal drug mode-of-action from cytology-based profiling. *PLoS Negl Trop Dis*, *12*(11), e0006980.

Torreele, E., Bourdin Trunz, B., Tweats, D., Kaiser, M., Brun, R., Mazué, G., Bray, MA; Pécoul, B (2010). Fexinidazole--a new oral nitroimidazole drug candidate entering clinical development for the treatment of sleeping sickness. *PLOS Neglected Tropical Diseases*. 4 (12): e923.

Torres-Guerrero, E., Quintanilla-Cedillo, M., Ruiz-Esmenjaud, J. & Arenas, R. (2017). Leishmaniasis: a review. *F1000 Res*, *6*(750), 1-15.

Trindade, S., Rijo-Ferreira, F., Carvalho, T., Pinto-Neves, D., Guegan, F., Aresta-Branco, F., Bento, F., Young, SA., Pinto, A., Abbeele, JVD., Ribeiro, RM., Dias, S., Smith, TK. & Figueiredo, LM. 2016. Trypanosoma brucei parasites occupy and functionally adapt to the adipose tissue in mice. *Cell Host Microbe*. 19(6), 837-848.

Uliana, S. R. B., Trinconi, C. T. & Coelho, A. C. (2018). Chemotherapy of leishmaniasis: present challenges. *Parasitology*, *145*(4), 464-480.

Unciti-Broceta, J. D., Arias, J. L., Maceira, J., Soriano, M., Ortiz-González, M., Hernández-Quero, J., Muñóz-Torres, M., De Koning, H. P., Magez S, Garcia-Salcedo, J. A. (2015). Specific cell targeting therapy bypasses drug resistance mechanisms in African trypanosomiasis. *PloS Pathog, 11*, e1004942.

Uzcátegui, N. L., Figarella, K., Bassarak, B., Meza, N. W., Mukhopadhyay, R., Ramirez, J. L., Duszenko, M. (2013). *Trypanosoma brucei* aquaglyceroporins facilitate the uptake of arsenite and antimonite in a pH dependent way. *Cell Physiol Biochem, 32*(4), 880-888.

Uzcátegui, N. L., Szallies, A., Pavlovic-Djuranovic, S., Palmada, M., Figarella, K., Boehmer, C., Lang, F., Beitz, E., Duszenko, M. (2004). Cloning, heterologous expression, and characterization of three aquaglyceroporins from *Trypanosoma brucei*. *J Biol Chem, 279,* 42669–42676.

Uzcategui, NL., Szallies, A., Pavlovic-Djuranovic, S., Palmada, M., Figarella, K., Boehmer, C., *et al*. (2004). Cloning, heterologous expression, and characterisation of three aquaglyceroporins from *Trypanosoma brucei*. *J Biol Chem*. 279:42669-42676.

Van den Abbeele, J., Claes, Y., van Bockstaele, D., Le Ray, D. & Coosemans, M. (1999). *Trypanosoma brucei* spp. Development in the tsetse fly: characterization of the post-mesocyclic stages in the foregut and proboscis. *Parasitology*, *118,* 469–478.

Vassella, E., Reuner, B., Yutzy, B. & Boshart, M. (1997). Differentiation of African trypanosomes is controlled by a density sensing mechanism which signals cell cycle arrest via the cAMP pathway. *J Cell Sci, 110*(Pt 21), 2661-2671.

Vélez, I., López, L., Sánchez, X., Mestra, L., Rojas, C. & Rodgríguez, E. (2010). Efficacy of miltefosine for the treatment of American cutaneous leishmaniasis. *Am J Trop Med Hyg, 83*(2), 351-356.

Verkman, A. S. (2013). Aquaporins. *Curr. Biol*. 23, R52–R55.

Verkman, A. S., Anderson, M. O. & Papadopoulos, M. C. (2014). Aquaporins: Important but elusive drug targets. *Nat Rev Drug Discovery, 13*, 259–277.

Vincent, I. M., Creek, D., Watson, D. G., Kamleh, M. A., Woods, D. J., Wong, P. E., Burchmore, R. J. S. & Barrett, M. P. (2010). A molecular mechanism for eflornithine resistance in African trypanosomes. *PLoS Pathog, 6*(11), e1001204.

Walker, D. M., Oghumu, S., Gupta, G., McGwire, B. S., Drew, M. E. & Satoskar, A. R. (2014). Mechanisms of cellular invasion by intracellular parasites. *Cell Mol Life Sci, 71*(7), 1245-1263.

Wallace, L. J. M., Candlish, D. & De Koning, H. P. (2002). Different substrate recognition motifs of human and trypanosome nucleobase transporters: selective uptake of purine antimetabolites. *J Biol Chem, 277*, 26149–26156.

Ward, C. P., Wong, P. E., Burchmore, R. J., De Koning, H. P. & Barrett, M. P. (2011). Trypanocidal furamidine analogues: influence of pyridine nitrogens on trypanocidal activity, transport kinetics and resistance patterns. *Antimicrob Agents Chemother, 55*, 2352–2361.

Wastling, S, L. & Welburn, S. C. (2011). diagnosis of human sleeping sickness: sense and sensitivity. *Trends Parasitol*, *27*, 394-402.

Wasunna, M., Njenga, S., Balasegaram, M., Alexander, N., Omollo, R., Edwards, T., Dorlo, T. P., Musa, B., Ali, M. H., Elamin, M. Y., Kirigi, G., Juma, R., Kip, A. E., Schoone, G. J., Hailu, A., Olobo, J., Ellis, S., Kimutai, R., Wells, S., Khalil, E. A., Strub, Wourgaft, N., Alves, F. & Musa, A. (2016). Efficacy and safety of AmBisome in combination with sodium stibogluconate or miltefosine and miltefosine monotherapy for African visceral leishmaniasis: phase II randomized trial. *PLoS Negl Trop Dis*, *10*(9), e0004880.

Waterhouse, A., Bertoni, M., Bienert, S., Studer, G., Tauriello, G., Gumienny, R., Heer, F.T., De Beer, T.A.P., Rempfer, C., Bordoli, L., Lepore, R. & Schwede, T. (2018). SWISS-MODEL: Homology modelling of protein structures and complexes. *Nucleic Acids Research*, 46(W1): W296-W303.

Weiss, F., Vogenthaler, N., Franco-Paredes, C. & Parker, S. R. (2009). *Leishmania tropica*-induced cutaneous and presumptive concomitant viscerotropic leishmaniasis with prolonged incubation. *Arch Dermatol*, *145*(9), 1023-1026.

Wiedemar, N., Graf, F. E., Zwyer, M., Ndomba, E., Renggli, C. K., Cal, M., Schmidt, R. S., Wenzler, T. & Mäser, P. (2018). Beyond immune escape: a variant surface glycoprotein causes suramin resistance in *Trypanosoma brucei*. *Mol Microbiol*, *107*(1), 57-67.

World Health Organisation. (2020a). Leishmaniasis factsheet. Available at: https://www.who.int/news-room/fact-sheets/detail/leishmaniasis (Accessed 14/04/2020).

World Health Organisation. (2020b). Leishmaniasis epidemiological situation. Available at: https://www.who.int/leishmaniasis/burden/en/ (Accessed 14/04/2020).

World Health Organisation. (2020c). Cutaneous leishmaniasis factsheet. Available at: http://www.emro.who.int/neglected-tropical-diseases/information-resources-leishmaniasis/cl-factsheet.html (Accessed 20/04/2020).

World Health Organisation. (2020d). Human African trypanosomiasis epidemiological situation. Available at: https://www.who.int/trypanosomiasis_african/country/en/ (Accessed 26/04/2020).

Wree, D., Wu, B., Zeuthen, T., Beitz, E. (2011). Requirement for asparagine in the aquaporin NPA signature motifs for cation exclusion. *FEBS J, 278,* 740–748.

Wu, B., Steinbronn, C., Alsterfjord, M., Zeuthen, T. & Beitz, E. (2009). Concerted action of two cation filters in the aquaporin water channel. *EMBO J, 28*, 2188–2194.

Yang, G., Choi, G. & No, J. H. (2016). Antileishmanial mechanism of diamidines Involves targeting kinetoplasts. *Antimicrob Agents Chemother*, *60*(11), 6828-6836.

Zijlstra, E. E., Musa, A. M., Khalil, E. A. G., Hassan, I. E. & El-Hassan, A. M. (2003). Post-kala-azar dermal leishmaniasis. *Lancet Infect Dis*, *3*(2), 87-98.

Zoltner, M., Campagnaro, G. D., Taleva, G., Burrell, A., Cerone, M., Leung, K-F, Achcar, F., Horn, D., Vaughan, S., Gadelha, C., Zíková A, Barrett M. P., De Koning, H. P., Field, M. C. (2020). Suramin exposure alters cellular metabolism and mitochondrial energy production in African trypanosomes. *J Biol Chem, in press.*

Zoltner, M., Horn, D., De Koning, H. P., Field, M. C. (2016). Exploiting the Achilles' heel of membrane trafficking in trypanosomes. *Curr Opin Microbiol, 34*, 97–103.

Zoltner, M., Leung, K. F., Alsford, S., Horn, D., Field, M. C. (2015). Modulation of the surface proteome through multiple ubiquitylation pathways in African trypanosomes. *PLoS Pathog, 11*, e1005236.